2018 URSI Commission B School for Young Scientists

Multiscale Computational Electromagnetics in Time Domain

Lecture Notes

May 27, 2018

ExpoMeloneras Convention Centre

Gran Canaria, Spain

2018 URSI Commission B School for Young Scientists

Multiscale Computational Electromagnetics in Time Domain*

Lecture Notes

May 27, 2018

ExpoMeloneras Convention Centre

Gran Canaria, Spain

* This School is organized during the "2018 URSI Atlantic Radio Science Conference" (URSI AT-RASC 2018), May 28 - June 1, 2018, Gran Canaria, Spain.

Table of Contents

Preface

The “2018 URSI Commission B School for Young Scientists” is organized by URSI Commission B and is arranged on the occasion of the “2018 URSI Atlantic Radio Science Conference” (URSI AT-RASC 2018), May 28 - June 1, 2018, Gran Canaria, Spain. This School is a one-day event held during URSI AT-RASC 2018, and is sponsored jointly by URSI Commission B and the URSI AT-RASC 2018 Organizing Committee. The School offers a short, intensive course, where a series of lectures will be delivered by a leading scientist in the Commission B community. Young scientists are encouraged to learn the fundamentals and future directions in the area of electromagnetic theory from these lectures.

Program

1. Course Title

Multiscale Computational Electromagnetics in Time Domain

2. Course Instructor

Prof. Qing Huo Liu
Department of Electrical and Computer Engineering, Duke University, USA

3. Course Program

Lecture 1

- Date and Time: 9:00-13:00, Sunday, May 27, 2018
- Venue: ExpoMeloneras Convention Centre, Gran Canaria, Spain
- Lecture Topics:

  1D Time Domain Methods
  The Finite Difference Time Domain (FDTD) Method
  The Finite Element Time Domain (FETD) Method
  The Fourier Pseudospectral Time Domain (PSTD) Method
  The Chebyshev PSTD Method
  The Frequency Domain Spectral Element Method (SEM)
  The Spectral Element Time Domain (SETD) Method

Lecture 2

- Date and Time: 14:00-18:00, Sunday, May 27, 2018
- Venue: ExpoMeloneras Convention Centre, Gran Canaria, Spain
- Lecture Topics:

  1D Multiscale DGTD Method
  3D DGTD Methods
  Nodal DGTD Methods
  Vector (Subdomain) DGTD Method with EH Fields
  Vector (Subdomain) DGTD Method with EB Fields
  Vector DGTD Method with the Wave Equation
  Vector DGTD Method for Coupling SE, FE and FDTD Methods

Lecture Abstract

Multiscale Computational Electromagnetics in Time Domain

Prof. Qing Huo Liu, PhD, FIEEE, FASA, FEMA, FOSA
Department of Electrical and Computer Engineering, Duke University, USA
www.ee.duke.edu/~qhliu
Email: qhliu@duke.edu

2018 edition of the *URSI Commission B School for Young Scientists* lectures by Prof. Qing Huo Liu focuses on the multiscale computational electromagnetics. The objective of this short course is to introduce the multiscale time-domain computational electromagnetics to address realistic electromagnetic sensing and system-level design problems. Such problems are often multiscale and contain three electrical scales, i.e., the fine scale (geometrical feature size much smaller than a wavelength), the coarse scale (geometrical feature size greater than a wavelength), and the intermediate scale between the two extremes. Most existing commercial solvers are based on single methodologies (such as finite element method or finite-difference time-domain method), and are unable to solve large multiscale problems. In this short course, we will present the discontinuous Galerkin time-domain (DGTD) framework to combine the spectral element, finite difference, and finite element time domain methods, using both explicit and implicit time integration techniques. Numerical results show significant advantages of the multiscale method. Time permitting, we will also overview some recent techniques in solving multiscale problems in the frequency domain.

Biographical Sketch of Course Instructor

Qing Huo Liu received his B.S. and M.S. degrees in physics from Xiamen University, China, and Ph.D. degree in electrical engineering from the University of Illinois at Urbana-Champaign. His research interests include computational electromagnetics and acoustics, inverse problems, and their application in nanophotonics, geophysics, biomedical imaging, and electronic packaging. He has published over 400 papers in refereed journals and 500 papers in conference proceedings. He was with the Electromagnetics Laboratory at the University of Illinois at Urbana-Champaign as a Research Assistant from September 1986 to December 1988, and as a Postdoctoral Research Associate from January 1989 to February 1990. He was a Research Scientist and Program Leader with Schlumberger-Doll Research, Ridgefield, CT from 1990 to 1995. From 1996 to May 1999 he was an Associate Professor with New Mexico State University. Since June 1999 he has been with Duke University where he is now a Professor of Electrical and Computer Engineering.

Dr. Liu is a Fellow of the IEEE, the Acoustical Society of America, the Electromagnetics Academy, and the Optical Society of America. Currently he serves as the founding Editor-in-Chief of the new *IEEE Journal on Multiscale and Multiphysics Computational Techniques*, the Deputy Editor in Chief of *Progress in Electromagnetics Research*, an Associate Editor for *IEEE Transactions on Geoscience and Remote Sensing*, and an Editor of *Journal of Computational Acoustics*. He received the 1996 Presidential Early Career Award for Scientists and Engineers (PECASE) from the White House, the 1996 Early Career Research Award from the Environmental Protection Agency, and the 1997 CAREER Award from the National Science Foundation. He serves as an IEEE Antennas and Propagation Society Distinguished Lecturer for 2014-2016. He received the ACES technical achievement award in 2017.

Multiscale Computational Electromagnetics in Time Domain

May 27, 2018

Prof. Qing Huo Liu

Department of Electrical and Computer Engineering,

Duke University, USA

Duke University

Multiscale Computational Electromagnetics in Time Domain

Professor Qing Huo Liu
Department of Electrical and Computer Engineering
Duke University
www.ee.duke.edu/~qhliu

May 27, 2018

Chapter 1. 1-D Time Domain Methods

This chapter review the finite difference, finite element, pseudospectral and spectral time domain methods for 1D problems. In particular, large scale problems are of interest where objects and domains are larger than the typical wavelength.

Topics:

- The Finite Difference Time Domain (FDTD) Method
- The Finite Element Time Domain (FETD) Method
- The Fourier pseudospectral time domain (PSTD) method
- The Chebyshev PSTD method
- The frequency domain spectral element method (SEM)
- The spectral element time domain (SETD) method

1.1 Finite-Difference Time-Domain Method

In one-dimensional problems, the medium and fields

- depend only on one coordinate direction (say x),
- and independent of all other directions.

In this case, Maxwell's equation can be decoupled into two **decoupled** sets of problems:

Set 1: (E_y, H_z) produced by (J_y, M_z)

Set 2: (E_z, H_y) produced by (J_z, M_y).

Our objective in this section is to develop methods for Set 1. The solution of Set 2 is similar.

Set 1: (E_y, H_z) are governed by

$$\frac{\partial E_y}{\partial x} = -\mu\frac{\partial H_z}{\partial t} - \sigma_m H_z - M_z \tag{1.1}$$

$$\frac{\partial H_z}{\partial x} = -\epsilon\frac{\partial E_y}{\partial t} - \sigma_e E_y - J_y \tag{1.2}$$

* J_y is the y component of the electric current density.

Set 2: (E_z, H_y) are similarly governed by

$$\frac{\partial E_z}{\partial x} = \mu\frac{\partial H_y}{\partial t} + \sigma_m H_y + M_y \tag{1.3}$$

$$\frac{\partial H_y}{\partial x} = \epsilon\frac{\partial E_z}{\partial t} + \sigma_e E_z + J_z \tag{1.4}$$

1.1.1 Finite-Difference Schemes

Common finite-difference schemes are

- Forward differencing scheme:

$$\frac{\partial f(x,t)}{\partial x} = \frac{f(x+\Delta x,t) - f(x,t)}{\Delta x} + O(\Delta x) \tag{1.5}$$

- Backward differencing scheme:

$$\frac{\partial f(x,t)}{\partial x} = \frac{f(x,t) - f(x-\Delta x,t)}{\Delta x} + O(\Delta x) \tag{1.6}$$

- Central differencing scheme as in Yee's FDTD Method:

$$\frac{\partial f(x,t)}{\partial x} = \frac{f(x+\frac{\Delta x}{2},t) - f(x-\frac{\Delta x}{2},t)}{\Delta x} + O(\Delta x^2) \tag{1.7}$$

The order of the error terms can be easily verified by Taylor expansions.

1.1.2 The Finite-Difference Time-Domain Method

We first discretize the electric and magnetic fields at staggered spatial points and temporal points.
The domain $a \le x \le b = a + L$ is uniformly divided into I cells with $\Delta x = \frac{b-a}{I}$. The grid points for E_y are at $x_i^e = a + (i-1)\Delta x$, $i = 1, \cdots, I+1$. The magnetic field H_z is located at $x_i^h = x_i^e + \frac{1}{2}\Delta x$, $i = 1, \cdots, I$.

$$E_i^n \equiv E_y(x_i^e, n\Delta t), \quad H_{i+\frac{1}{2}}^{n+\frac{1}{2}} \equiv H_z(x_i^h, (n+\frac{1}{2})\Delta t) \tag{1.8}$$

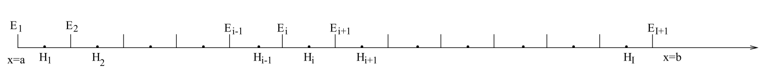

Figure: 1.1 1-D FDTD grid with **E** field located at the boundaries $x = a$ and $x = b$ and at integer grid points, while **H** field located at half-integer grid points. Note that the half integer index of **H** is rounded down to integers for programming. The indexing for **E** and **H** can be reversed.

The staggered grid FDTD method (Yee scheme)

$$\begin{aligned}
\frac{E_{i+1}^n - E_i^n}{\Delta x} &= -\mu_{i+\frac{1}{2}} \frac{H_{i+\frac{1}{2}}^{n+\frac{1}{2}} - H_{i+\frac{1}{2}}^{n-\frac{1}{2}}}{\Delta t} - \sigma_{m,i+\frac{1}{2}} \frac{H_{i+\frac{1}{2}}^{n+\frac{1}{2}} + H_{i+\frac{1}{2}}^{n-\frac{1}{2}}}{2} \\
&\quad -M_{i+\frac{1}{2}}^n \qquad (1.9) \\
\frac{H_{i+\frac{1}{2}}^{n+\frac{1}{2}} - H_{i-\frac{1}{2}}^{n+\frac{1}{2}}}{\Delta x} &= -\epsilon_i \frac{E_i^{n+1} - E_i^n}{\Delta t} - \sigma_{e,i} \frac{E_i^{n+1} + E_i^n}{2} - J_i^{n+\frac{1}{2}} \qquad (1.10)
\end{aligned}$$

The source terms

$$J_i^{n+\frac{1}{2}} = \frac{1}{\Delta x} \int_{x_i^e - \frac{\Delta x}{2}}^{x_i^e + \frac{\Delta x}{2}} J_y(x, (n+\frac{1}{2})\Delta t) dx \approx J_y(x_i^e, (n+\frac{1}{2})\Delta t),$$

$$M_{i+\frac{1}{2}}^n = \frac{1}{\Delta x} \int_{x_i^h - \frac{\Delta x}{2}}^{x_i^h + \frac{\Delta x}{2}} M_z(x, n\Delta t) dx \approx M_z(x_i^h, n\Delta t),$$

The averaged μ and σ_m at $x = x_i^h$

$$\mu_{i+\frac{1}{2}} = \frac{1}{\Delta x} \int_{x_i^h - \frac{\Delta x}{2}}^{x_i^h + \frac{\Delta x}{2}} \mu(x) dx, \quad \sigma_{m,i+\frac{1}{2}} = \frac{1}{\Delta x} \int_{x_i^h - \frac{\Delta x}{2}}^{x_i^h + \frac{\Delta x}{2}} \sigma_m(x) dx$$

And the averaged ϵ and σ_e at $x = x_i^e$

$$\epsilon_i = \frac{1}{\Delta x} \int_{x_i^e - \frac{\Delta x}{2}}^{x_i^e + \frac{\Delta x}{2}} \epsilon(x) dx, \quad \sigma_{e,i} = \frac{1}{\Delta x} \int_{x_i^e - \frac{\Delta x}{2}}^{x_i^e + \frac{\Delta x}{2}} \sigma(x) dx,$$

From these equations, it is easy to obtain a leap-frog scheme

$$H_{i+\frac{1}{2}}^{n+\frac{1}{2}} = B_0 H_{i+\frac{1}{2}}^{n-\frac{1}{2}} - B_1(E_{i+1}^n - E_i^n) - B_2 M_{i+\frac{1}{2}}^n \quad (1.11)$$

$$E_i^{n+1} = A_0 E_i^n - A_1(H_i^{n+\frac{1}{2}} - H_{i-1}^{n+\frac{1}{2}}) - A_2 J_i^{n+\frac{1}{2}} \quad (1.12)$$

The FD coefficients are given by

$$A_0 = \frac{2\epsilon_i - \sigma_{e,i}\Delta t}{2\epsilon_i + \sigma_{e,i}\Delta t}, A_1 = \frac{2\Delta t}{(2\epsilon_i + \sigma_{e,i}\Delta t)\Delta x}, A_2 = A_1\Delta x$$

$$B_0 = \frac{2\mu_{i+\frac{1}{2}} - \sigma_{m,i+\frac{1}{2}}\Delta t}{2\mu_{i+\frac{1}{2}} + \sigma_{m,i+\frac{1}{2}}\Delta t}, B_1 = \frac{2\Delta t}{(2\mu_{i+\frac{1}{2}} + \sigma_{m,i+\frac{1}{2}}\Delta t)\Delta x}, B_2 = B_1\Delta x$$

Proper initial and boundary conditions are needed to obtain unique solutions.

1.1.3 Initial Conditions

The initial conditions usually refer to field values at $t = 0$. However, since we discretize E and H at staggered temporal points, we will use the initial value of

$$E_i^0 = E_y(x_i^e, 0) \quad (1.13)$$

$$H_{i+\frac{1}{2}}^{-\frac{1}{2}} = H_z(x_i^h, -\frac{1}{2}\Delta t) \quad (1.14)$$

for all integer values of i.

1.1.4 Boundary Conditions

A. PEC Boundary Conditions

$$E_1^n = E_{I+1}^n = 0 \tag{1.15}$$

B. PMC Boundary Conditions

PMC Implementation 1: Let H_z locate at PMC boundaries.

H_z at integer points $x_i^h = a + (i-1)\Delta x$, and E_y nodes at $x_i^e = x_i^h + \frac{1}{2}\Delta x$.

The PMC boundary conditions can be treated easily

$$H_1^{n+\frac{1}{2}} = H_{I+1}^{n+\frac{1}{2}} = 0 \tag{1.16}$$

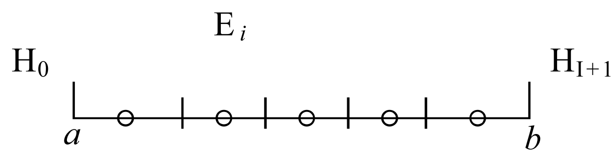

Figure § 1.02 First implementation of PMC boundary

PMC Implementation 2: Let E_y locate at PMC boundaries.

The PMC boundary condition

$$H_z(x=a) = 0 \quad \text{or} \quad \frac{\partial E_y(x=a)}{\partial x} = 0$$

H_z is an odd function at $x = a$, so at the virtual node $H_{-\frac{1}{2}}^{n+\frac{1}{2}} = -H_{\frac{1}{2}}^{n+\frac{1}{2}}$

The update equation for E_1 is modified as

$$E_1^{n+1} = E_1^n - \frac{2\Delta t}{\epsilon_i \Delta x} H_1^{n+\frac{1}{2}} \tag{1.17}$$

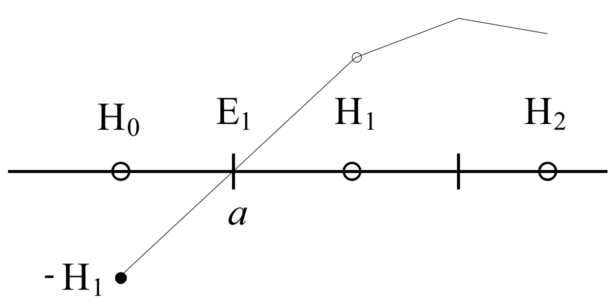

C. Radiation Boundary Conditions

Incident field $\mathbf{E}^{\mathrm{inc}}$ from outside, and the scattered field $\mathbf{E}^{\mathrm{sct}} = \mathbf{E} - \mathbf{E}^{\mathrm{inc}}$.

- The radiation condition at the left boundary $x = a$

$$\frac{\partial E_y^{sct}}{\partial x} = \frac{1}{c_L}\frac{\partial E_y^{sct}}{\partial t} \tag{1.18}$$

where c_L is the speed of light for $x \leq a$.
Similarly, at the right boundary $x = b$, the radiation condition is

$$\frac{\partial E_y^{sct}}{\partial x} = -\frac{1}{c_R}\frac{\partial E_y^{sct}}{\partial t} \tag{1.19}$$

where c_R is the speed of light for $x \geq b$.
These conditions are exact as long as the medium is homogeneous for $x \leq a$ and for $x \geq b$.

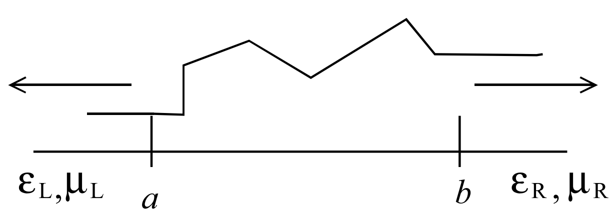

Figure § 1.04 Radiation boundary conditions for the 1D problem where the scattered field travels outward. The material discontinuities can occur as close as $1.5\Delta x$ from the boundaries $x = a$ and $x = b$.

The above radiation conditions can be written explicitly

$$E_y^{sct}(x,t) = f_-(t + x/c_L) \text{ at } x = a \tag{1.20}$$

$$E_y^{sct}(x,t) = f_+(t - x/c_R) \text{ at } x = b \tag{1.21}$$

$f_-(t) \sim$ the time function of the waves propagating to the left

$f_+(t) \sim$ the time function of the waves propagating to the right

Therefore, with linear interpolation, one has

$$\begin{aligned} E_y^{sct}(a, t+\Delta t) &= f_-(t+\Delta t + x_1/c_L) = E_y^{sct}(a + c_L\Delta t, t) \\ &\approx E_y^{sct}(a,t)(1 - \frac{c_L\Delta t}{\Delta x}) + E_y^{sct}(a+\Delta x, t)\frac{c_L\Delta t}{\Delta x} \end{aligned} \tag{1.22}$$

$$\begin{aligned} E_y^{sct}(b, t+\Delta t) &= f_+(t+\Delta t - x_{I+1}/c_R) = E_y^{sct}(b - c_R\Delta t, t) \\ &\approx E_y^{sct}(b,t)(1 - \frac{c_R\Delta t}{\Delta x}) + E_y^{sct}(b-\Delta x, t)\frac{c_R\Delta t}{\Delta x} \end{aligned} \tag{1.23}$$

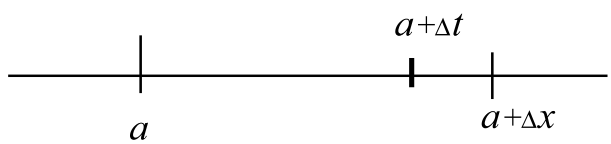

Figure § 1.06 Scattered field at $x = a + \Delta t c_L$ at the previous time step can be interpolated from the values at two adjacent grid points $x = a$ and $x = a + \Delta x$.

Remark: One important thing about 1D incident waves:

Unlike in 2D and 3D, the incident wave in 1D cannot be *distinguished* from an internal source for the opposite boundary that is NOT impinged by the wave.

For example, if the incident wave comes from left, $\mathbf{E}^{inc}$ is not zero for $x = a$; but to the boundary at $x = b$, this incident wave cannot be distinguished from an internal source at $a < x < b$. Hence the incident field is treated as zero for the boundary at $x = b$, and vise versa.

Now if the incident electric field are

$E_{yL}^{\text{inc}}(x,t)$ from the left, and

$E_{yR}^{\text{inc}}(x,t)$ from the right,

the updating equations for E_1^{n+1} and E_{I+1}^{n+1} are

$$\begin{aligned} E_1^{n+1} = {} & E_{yL}^{\text{inc}}(x_1^e, t+\Delta t) + [E_1^n - E_{yL}^{\text{inc}}(x_1^e, t)](1 - \frac{c_L \Delta t}{\Delta x}) \\ & +[E_2^n - E_{yL}^{\text{inc}}(x_2^e, t)]\frac{c_L \Delta t}{\Delta x} \end{aligned} \tag{1.24}$$

$$\begin{aligned} E_{I+1}^{n+1} = {} & E_{yR}^{\text{inc}}(x_{I+1}^e, t+\Delta t) + [E_{I+1}^n - E_{yR}^{\text{inc}}(x_{I+1}^e, t)](1 - \frac{c_R \Delta t}{\Delta x}) \\ & +[E_I^n - E_{yR}^{\text{inc}}(x_I^e, t)]\frac{c_R \Delta t}{\Delta x} \end{aligned} \tag{1.25}$$

Equations (1.24) and (1.25)

- together with (1.11) and (1.12) for $i = 2, \cdots, I$
- complete the time stepping process.

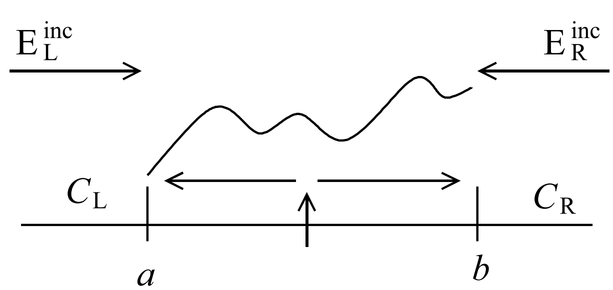

Figure § 1.07 Incident electric field from the left side and from the right side.

1.1.5 Accuracy and Stability Conditions

In order for the FDTD method to produce accurate results,
the spatial discretization must be fine enough.
If the maximum frequency of the pulse excitation is f_{max}
(for example, f_{max} is the frequency where the spectrum decays to -40 dB of the peak value),
the minimum wavelength inside the domain is

$$\lambda_{min} = \frac{c_{\min}}{f_{max}} \tag{1.26}$$

* $c_{\min} = \min\{1/\sqrt{\mu\epsilon}\}$ is the minimum speed of light in the material inside the domain.

For a moderate size of problem of several wavelengths,

- to obtain accuracy of the order of 1%,
- empirically the sampling density S_D should be chosen such that the number of points per wavelength (PPWs)

$$\text{Sampling Density } S_D \equiv \frac{\lambda_{min}}{\Delta x} \geq 10 \text{ (PPWs)} \tag{1.27}$$

If the problem size becomes large with respect to the minimum wavelength,
this sampling density has to be increased.
In other words, the numerical dispersion error of the FDTD method
increases with the problem size.

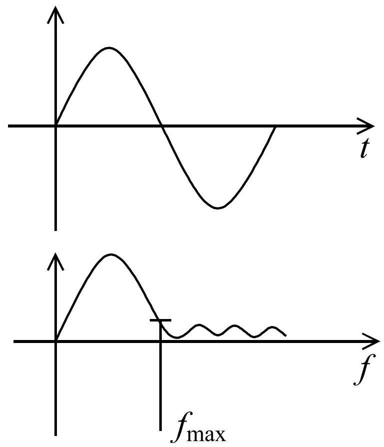

Figure § 1.08 Pulse (top) and its spectrum magnitude. A maximum frequency f_{max} is defined as one beyond which the magnitude is negligible (for example -40 dB below the peak magnitude).

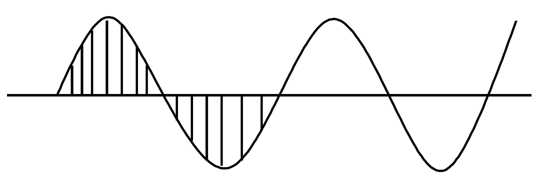

Figure § 1.09 The spatial sampling density is defined as the number of points per wavelength (PPW) at f_{max}.

The stability condition for the FDTD method is

$$\Delta t \le \frac{\Delta x}{\sqrt{D} c_{\max}} \tag{1.28}$$

where $c_{\max} = \max\{1/\sqrt{\mu\epsilon}\}$ is the maximum speed of light, D is the dimensionality of the problem (in the 1D case, $D = 1$).

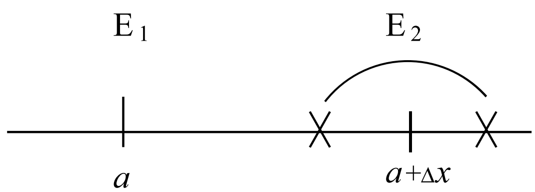

Figure § 1.10 The stability condition will ensure that within one time step the wave will propagate a distance within one cell rather than over one cell.

1.1.6 Sources and Their Time Functions

Electromagnetic sources can be (a) internal electric and magnetic sources; (b) E_{yL}^{inc} incident from the left, and (c) E_{yR}^{inc} incident from the right.
The time function of the source can be written as $s(t)$. For example, if the incident wave is from the left

$$E_{yL}^{\text{inc}}(x,t) = E_0 s(t - (x - x_0)/c_L) \tag{1.29}$$

where $x_0 \le a$ is the initial location of the incident wave.

If the incident wave is from the right,

$$E_{yR}^{\text{inc}}(x,t) = E_0 s(t + (x - x_0)/c_R) \tag{1.30}$$

where $x_0 \ge b$ is the initial location of the incident wave.

Similarly, for an internal point source located inside the domain at $a < x = x_s < b$

$$J_y(x,t) = J_0 \delta(x - x_s) s(t) \tag{1.31}$$

where $s(t)$ is the time function of the pulse.
In this case, in the updating equation (1.12) the discrete current source term is

$$\begin{aligned} J_i^{n+\frac{1}{2}} &\approx \frac{1}{\Delta x} \int\limits_{x_i^e - \frac{1}{2}\Delta x}^{x_i^e + \frac{1}{2}\Delta x} \delta(x - x_s) s(t = (n + \frac{1}{2})\Delta t) dx \\ &= \begin{cases} \frac{1}{\Delta x} s((n + \frac{1}{2})\Delta t) & \text{if } x_i^e - \frac{1}{2}\Delta x \le x_s < x_i^e + \frac{1}{2}\Delta x \\ 0 & \text{otherwise} \end{cases} \end{aligned} \tag{1.32}$$

There are several commonly used time functions, including
(a) Gaussian pulse and its derivatives;
(b) Blackman-Harris window (BHW) function and its derivatives:

$$s(t) = \begin{cases} \sum\limits_{n=0}^{n=3} a_n \cos(2n\pi t/T) & \text{if } 0 \le t \le T \\ 0 & \text{otherwise} \end{cases} \tag{1.33}$$

$$\begin{cases} a_0 = 0.35322222, a_1 = -0.488, \\ a_2 = 0.145, a_3 = -0.01022222 \end{cases}$$

The characteristic frequency of BHW function is defined as $f_{ch} = 1/T$.
The maximum frequency of this BHW-1 pulse is

$$f_{max} \approx 3.351 f_{ch}$$

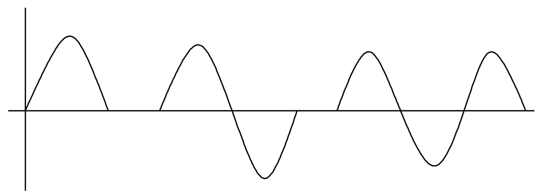

Figure § 1.11 Gaussian pulse (left), its first derivation (center) and second derivative (right). All three have infinite tails.

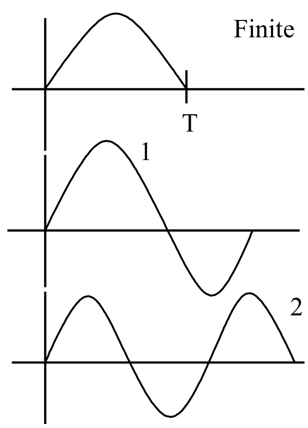

Figure § 1.12 Blackman-Harris window (BHW) function (top), its first derivative (BHW-1, center) and second derivative (BHW-2, bottom). All three have a finite duration $T = 1/f_{ch}$.

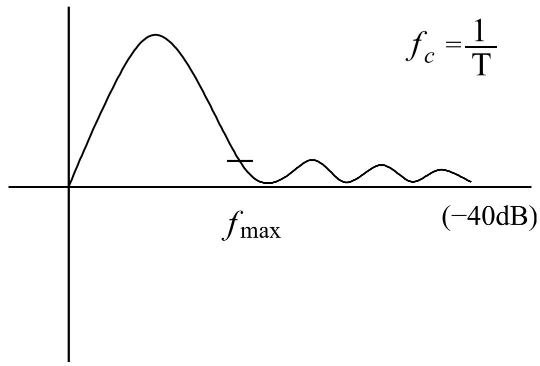

Figure § 1.13 The -40 dB truncation frequency f_{max} is related to the characteristic frequency of BHW-1 function as $f_{max} \approx 3.351 f_{ch}$.

1.2 The Finite Element Time Domain (FETD) Method

1.2.1 1-D Wave Equation for the Electric Field

$$\frac{\partial}{\partial x}\mu_r^{-1}\frac{\partial E_y}{\partial x} - \frac{\epsilon_r(x)}{c^2}\frac{\partial^2 E_y}{\partial t^2} = -S_y, \quad x \in [a, b] \tag{1.34}$$

* the source term $S_y(x,t) = -\mu_0 \frac{\partial J_y}{\partial t} + \frac{\partial(\mu_r^{-1} M_z)}{\partial x}$
* $J_y \sim$ the electric current densities of the source
* $M_z \sim$ the magnetic current densities of the source

This equation is the strong form of the wave equation.

The **weak form** of the wave equation can be obtained by

- multiplying (1.34) with a testing function $w_m(x)$
- integrating over the interval $[a, b]$:

$$\int_a^b dx w_m(x) \left[\frac{\partial}{\partial x} \mu_r^{-1}(x) \frac{\partial E_y}{\partial x} - \frac{\epsilon_r(x)}{c^2} \frac{\partial^2 E_y}{\partial t^2} \right] = - \int_a^b dx w_m(x) S_y(x,t) \qquad (1.35)$$

Integrating by parts, we obtain the weak form equation

$$\begin{aligned} &\int_a^b dx \left[-\frac{\partial w_m}{\partial x} \cdot \mu_r^{-1}(x) \frac{\partial E_y}{\partial x} - \frac{\epsilon_r(x)}{c^2} w_m(x) E_y \right] \\ &= - \left[\mu_r^{-1}(x) w_m(x) \frac{\partial E_y}{\partial x} \right]_a^b - \int_a^b dx w_m(x) S_y(x,t) \\ &= \mu_0 \left[w_m(x) \frac{\partial H_z(x,t)}{\partial t} \right]_a^b - \int_a^b dx w_m(x) S_y(x,t) \qquad (1.36) \end{aligned}$$

* $\frac{\partial E_y}{\partial x} = -\mu \frac{\partial H_z}{\partial t}$ has been used.

Initial and boundary conditions must be applied to obtain unique solutions.

1.2.2 Perfect Electric-Conductor (PEC) Boundaries

As $E_y = 0$ is known at the outer boundaries, only the internal field need to be expanded in terms of basis functions $\{f_n(x)\}$:

$$E_y(x,t) = \sum_{n=1}^{N} e_n(t) f_n(x) \tag{1.37}$$

where $N = N_e - 1$ for the first-order basis functions.

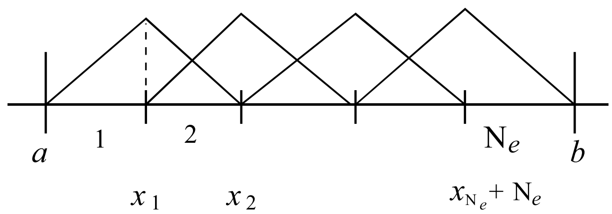

Figure § 1.23 Perfect electric-conductor (PEC) boundaries.

The surface term vanishes, and the boundary unknowns are removed from the system.

With the Galerkin method, the semi-discretized equation

$$\mathbf{M}\frac{d^2\mathbf{e}}{dt^2} = \mathbf{S}\mathbf{e} + \mathbf{v} \tag{1.38}$$

The elements of the mass matrix and stiffness matrix are

$$M_{mn} = \int_a^b dx \epsilon_r(x) f_m(x) f_n(x) \equiv \langle f_m(x), \epsilon_r(x) f_n(x)\rangle_\Omega$$

$$S_{mn} = -c^2 \int_a^b dx \frac{df_m}{dx}\mu_r^{-1}\frac{df_n}{dx} \equiv -c^2\langle f_m'(x), \mu_r^{-1} f_n'(x)\rangle_\Omega$$

$$\begin{aligned} v_m &= -c^2 \int_a^b dx f_m[\mu_0 \frac{\partial J_y}{\partial t} + \frac{\partial(\mu_r^{-1}M_z)}{\partial x}] \\ &\equiv -c^2\langle f_m, \mu_0\frac{\partial J_y}{\partial t} + \frac{\partial(\mu_r^{-1}M_z)}{\partial x}\rangle_\Omega \end{aligned}$$

If there are N_e elements, the number of DoFs is $N = N_e - 1$. This is the **essential boundary condition**.

1.2.3 Perfect Magnetic-Conductor (PMC) Boundaries

Boundary E_y values remain unknowns, so $N = N_e + 1$ for first-order basis functions.
The surface term in (1.36) is zero as $H_z = 0$ at PMC boundaries.

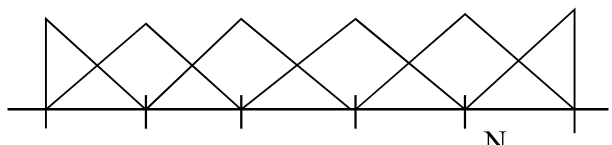

Figure § 1.24 Perfect magnetic-conductor (PMC) boundaries.

The discretized equation remains the same as the PEC case except $N = N_e + 1$.
This PMC boundary condition is known as a **natural boundary condition** for E_y: Basis and testing functions do not explicitly satisfy the boundary condition.

1.2.4 Radiation Boundary Conditions

Radiation boundary conditions for an unbounded domain:

$$\frac{1}{\mu_L}\frac{\partial E_y^{sct}}{\partial x}|_{x=a} = -\frac{\partial H_z^{sct}}{\partial t}|_{x=a} = \frac{1}{\eta_L}\frac{\partial E_y^{sct}}{\partial t}|_{x=a} \tag{1.39}$$

$$\frac{1}{\mu_R}\frac{\partial E_y^{sct}}{\partial x}|_{x=b} = -\frac{\partial H_z^{sct}}{\partial t}|_{x=b} = -\frac{1}{\eta_R}\frac{\partial E_y^{sct}}{\partial t}|_{x=b} \tag{1.40}$$

where $\eta_{L,R} = \sqrt{\frac{\mu_{L,R}}{\epsilon_{L,R}}}$ are the wave impedance to the left and to the right of the domain, respectively, and are assumed real.

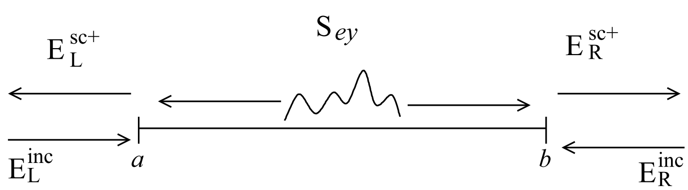

Figure § 1.25 Radiation Boundary Conditions.

The RBC for the total field $H_z = H_z^{inc} + H_z^{sct}$:

$$\dot{H}_z|_{x=a} = -\frac{1}{\eta_L}\dot{E}_y|_{x=a} + \frac{2}{\eta_L}\dot{E}_{yL}^{inc}|_{x=a} \tag{1.41}$$

$$\dot{H}_z|_{x=b} = \frac{1}{\eta_R}\dot{E}_y|_{x=b} - \frac{2}{\eta_R}\dot{E}_{yR}^{inc}|_{x=b} \tag{1.42}$$

where E_{yL}^{inc} and E_{yR}^{inc} are the incident electric field from left and from right sides, respectively.

Substituting the RBCs into (1.36) yields

$$\begin{aligned}
&\int_a^b dx \left[-\frac{\partial w_m}{\partial x} \cdot \mu_r^{-1}(x)\frac{\partial E_y}{\partial x} - \frac{\epsilon_r(x)}{c^2} w_m(x)\ddot{E}_y\right] \\
&\quad -\mu_0[\eta_R^{-1} w_m(b)\dot{E}_y(b,t) + \eta_L^{-1} w_m(a)\dot{E}_y(a,t)] \\
&= -2\mu_0 \left[\eta_R^{-1} w_m(b)\dot{E}_{yR}^{inc}(b,t) + \eta_L^{-1} w_m(a) E_{yL}^{inc}(a,t)\right] \\
&\quad - \int_a^b dx w_m(x) S_y(x,t)
\end{aligned} \tag{1.43}$$

If there are N_e elements inside the domain, the number of DoFs is $N = N_e + 1$.

1.2.5 Galerkin's method with triangular functions

Testing and basis functions are both triangular (piecewise linear) functions.

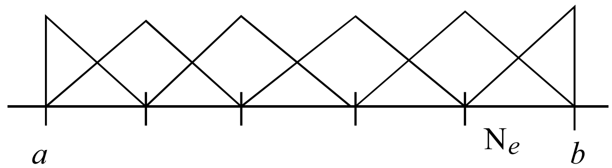

$$
\begin{aligned}
S_{mn} &= -\int_{x_{m-1}}^{x_{m+1}} \frac{dt_m}{dx} \cdot \mu_r^{-1}(x) \frac{dt_n}{dx} dx \\
&= \begin{cases}
-\frac{(1-\delta_{m,1})}{\mu_{r,m-1}\Delta x_{m-1}} - \frac{(1-\delta_{m,N})}{\mu_{r,m}\Delta x_m} & \text{if } n = m \\
\frac{(1-\delta_{m,N})}{\mu_{r,m}\Delta x_m} & \text{if } n = m+1 \\
\frac{(1-\delta_{m,1})}{\mu_{r,m-1}\Delta x_{m-1}} & \text{if } n = m-1 \\
0 & \text{otherwise}
\end{cases}
\end{aligned}
$$

$$
\begin{aligned}
M_{mn} &= \int_{x_{m-1}}^{x_{m+1}} \epsilon_r(x) t_m(x) t_n(x) dx \\
&= \begin{cases}
\frac{(1-\delta_{m,1})\epsilon_{r,m-1}\Delta x_{m-1}}{3} + \frac{(1-\delta_{m,N})k_0^2\epsilon_{r,m}\Delta x_m}{3} & \text{if } n = m \\
\frac{(1-\delta_{m,N})\epsilon_{r,m}\Delta x_m}{6} & \text{if } n = m+1 \\
\frac{(1-\delta_{m,1})\epsilon_{r,m-1}\Delta x_{m-1}}{6} & \text{if } n = m-1 \\
0 & \text{otherwise}
\end{cases}
\end{aligned}
$$

$$
\begin{aligned}
v_m &= -c_0^2 \int_{x_{m-1}}^{x_{m+1}} dx t_m(x) S_y(x,t) \\
&\quad -2\mu_0 c_0^2 \left[\frac{\delta_{m,1}\dot{E}_{yL}^{inc}(a,t)}{\eta_L} + \frac{\delta_{m,N} E_{yR}^{inc}(b,t)}{\eta_R} \right]
\end{aligned}
$$

For a point electric current source $J_y = J_0\delta(x - x_s)$ at x_s, we have $S_y = -\mu_0 J_0 \delta(x - x_s)\dot{s}(t)$, and

$$v_m = \mu_0 c_0^2 J_0 t_m(x_s)\dot{s}(t) - 2c_0^2 \left[\frac{\delta_{m,1}\dot{E}_{yL}^{inc}(a,t)}{\eta_L} + \frac{\delta_{m,N}\dot{E}_{yR}^{inc}(b,t)}{\eta_R}\right]$$

1.2.6 Elemental Matrices and Assembly

The above is the node-based approach to obtain FETD matrices.
An alternative way is the element-by-element approach, which is often preferred in multidimensions. The FETD matrices are first calculated element by element, then assembled globally.

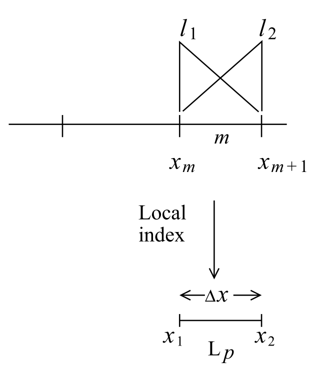

Figure § 1.27 Element-by-element approach.

The m-th element in 1D has two nodal points,x_m and x_{m+1}. We use $p, q = 1, 2$ as their local node indices in the e-th element.

* Local elemental matrices $M_{pq}^{(e)}$, $S_{pq}^{(e)}$, and $v_p^{(e)}$.
* Corresponding global indices when assembling the matrices

$$M_{mn} = \sum_{e}^{N_e} M_{pq}^{(e)}$$

$$S_{mn} = \sum_{e}^{N_e} S_{pq}^{(e)}$$

$$v_m = \sum_{e}^{N_e} v_p^{(e)}$$

The basis function written compactly with simplex coordinates,

$$t_p(x) \equiv \ell_p(x) = \frac{L_p}{L^{(e)}} = \frac{x_{p+1} - x}{x_{p+1} - x_p}, \quad p = 1, 2 \tag{1.44}$$

* $L_p = x_{p+1} - x$ is the "distance" of x to x_{p+1}.
* $L^{(e)} = x_{p+1} - x_p$ is the "distance" from x_p to x_{p+1}.
* $\Delta x^{(e)} = |L^{(e)}| = |x_{p+1} - x_p|$ is the positive element length.

The simplex coordinate ℓ_p is thus the relative length from the nodal point $p + 1$. Indices $(p, q) = (1, 2)$ are cyclic with a period of 2:

- In other words, $p + 2k = p$ for any integer k.

The elemental matrices

$$M_{mn} = \sum_{e=1}^{e=N_e} M_{pq}^{(1,e)}, \quad S_{mn} = \sum_{e=1}^{e=N_e} S_{pq}^{(2,e)}]$$

$$C_{mn} = -\mu_0 c_0^2 \left[\frac{\delta_{m,1}\delta_{n,1}}{\eta_L} + \frac{\delta_{m,N}\delta_{n,N}}{\eta_R} \right]$$

The local indices (p, q) are mapped to the global indices (m, n).

$$\begin{aligned} S_{pq}^{(e)} &= -c_0^2 \int_{x_p}^{x_{p+1}} \frac{d\ell_p}{dx} \cdot \mu_r^{-1}(x) \frac{d\ell_q}{dx} dx = -\frac{c_0^2}{L^{(e)}} \int_0^1 \frac{d\ell_p}{d\ell_p} \cdot \mu_r^{-1}(x) \frac{d\ell_q}{d\ell_p} d\ell_p \\ &= \begin{cases} -\frac{c_0^2}{\mu_r^{(e)} \Delta x^{(e)}} & \text{if } q = p \\ \frac{c_0^2}{\mu_r^{(e)} \Delta x^{(e)}} & \text{if } q = p \pm 1 \\ 0 & \text{otherwise} \end{cases} \end{aligned}$$

$$\begin{aligned} M_{pq}^{(e)} &= \int_{x_p}^{x_{p+1}} \epsilon_r(x)\ell_p(x)\ell_q(x)dx = L^{(e)} \int_0^1 \epsilon_r(x)\ell_p(x)\ell_q(x)d\ell_p \\ &= \begin{cases} \frac{\epsilon_r^{(e)} \Delta x^{(e)}}{3} & \text{if } q = p \\ \frac{\epsilon_r^{(e)} \Delta x^{(e)}}{6} & \text{if } q = p \pm 1 \\ 0 & \text{otherwise} \end{cases} \end{aligned}$$

The excitation vector for a point electric source is

$$v_m = \sum_{e=1}^{N_e} v_p^{(e)} - 2\mu_0 c_0^2 \left[\frac{\delta_{m,1}\dot{E}_{yL}^{inc}(a,t)}{\eta_L} + \frac{\delta_{m,N}\dot{E}_{yR}^{inc}(b,t)}{\eta_R} \right]$$

$$v_p^{(e)} = \mu_0 c_0^2 J_0 t_p(x_s) \dot{s}(t)$$

1.2.7. Solution of Semi-Discrete Equation

$$\mathbf{M}\frac{d^2\mathbf{e}}{dt^2} + \mathbf{C}\frac{d\mathbf{e}}{dt} = \mathbf{S}\mathbf{e} + \mathbf{v} \tag{1.45}$$

We can rewrite this as a set of coupled first order ODEs

$$\begin{aligned} \mathbf{M}\frac{d\dot{\mathbf{e}}}{dt} + \mathbf{C}\dot{\mathbf{e}} &= \mathbf{S}\mathbf{e} + \mathbf{v} \\ \dot{\mathbf{e}} &= \frac{d\mathbf{e}}{dt} \end{aligned} \tag{1.46}$$

Using a 2nd-order (instead of the better 4th-order) time integration yields

$$\begin{aligned} \dot{\mathbf{e}}^{n+\frac{1}{2}} &= (\mathbf{M} + \frac{\Delta t}{2}\mathbf{C})^{-1}[(\mathbf{M} - \frac{\Delta t}{2}\mathbf{C})\dot{\mathbf{e}}^{n-\frac{1}{2}} + \mathbf{S}\mathbf{e}^n + \mathbf{v}^n] \\ \mathbf{e}^{n+1} &= \mathbf{e}^n + \Delta t\dot{\mathbf{e}}^{n+\frac{1}{2}} \end{aligned}$$

Note the diagonal mass matrix inversion is trivial and efficient.

Limitations of the low-order FETD method:

* Low-order convergence - error decreases slowly with the sampling density (SD)
* A high SD is necessary: typically 20 points per wavelength (PPW) for $\text{Error}_2 \leq 1\%$
* Expensive and not very suitable for large-scale problems

Stability condition: Depending on the time integration scheme and properties of system matrices.

For a PDE time-domain solver, the numerical dispersion error is linearly proportional to the length of time integration.

* To maintain an acceptable accuracy, the sampling rate must be increased accordingly if a longer time window is needed.

The required SD is determined by

1. the problem spatial size in terms of the wavelength, and
2. the length of time window in terms of the period.

Therefore, for a large-scale problem,the SD should be increased

* from the SD of a small-scale problem,
* thus making large-scale problems even more challenging.

1.3 One-Dimensional PSTD Methods

The single-domain pseudospectral time-domain (PSTD) methods use

- (a) trigonometric functions
- (b) Chebyshev/Legendre polynomials

to approximate spatial derivatives with high accuracy.

The Fourier and Chebyshev PSTD methods have the spectral accuracy if the medium is very smooth.

1.3.1 Periodic 1D Problems

The spatial derivative can be found through a matrix notation.

A. Derivative Matrix for the 2nd-Order FD Method
The central differencing scheme

$$u_m = \frac{df(x_m)}{dx} \approx \frac{f(x_{m+1}) - f(x_{m-1})}{2\Delta x} \tag{1.47}$$

has a 2nd-order accuracy, i.e., the error is $O(\Delta x^2)$.
This can be verified by Taylor expansion.

Now let's assume a set of periodic data, $\{f_m, m = 1, \cdots, N\}$
where $f_{m+N} = f_m$, for all integer m.
Written in terms of a differentiation matrix D

$$\mathbf{u} = D\mathbf{f} \tag{1.48}$$

$$\mathbf{u} = [u_1, \cdots, u_N]^T, \quad \mathbf{f} = [f_1, \cdots, f_N]^T \tag{1.49}$$

$$D = \frac{1}{2\Delta x}\begin{pmatrix} 0 & 1 & 0 & \cdots & 0 & -1 \\ -1 & 0 & 1 & \cdots & 0 & 0 \\ \vdots & \vdots & \vdots & \ddots & \vdots & \vdots \\ 1 & 0 & 0 & \cdots & -1 & 0 \end{pmatrix} \tag{1.50}$$

Note $D_{mn} = a_{m-n}$ is a Toeplitz matrix.

Another view: Interpolation with 2nd-order polynomials $p^{(2)}(x)$

$$
\begin{aligned}
f(x) &\approx f_{m-1}\phi_{-1}^{(2)}(x) + f_m\phi_0^{(2)}(x) + f_{m+1}\phi_1^{(2)}(X) \\
&= \sum_{\ell=-1}^{1} f_{m+\ell}\phi_\ell^{(2)}(x), \quad x_{m-1} \le x < x_{m+1} \qquad (1.51)
\end{aligned}
$$

where $\phi_m^{(2)}(x)$ are the Lagrange interpolation polynomials:

$$
\begin{aligned}
\phi_{-1}^{(2)}(x) &= \frac{(x-x_m)(x-x_{m+1})}{2\Delta x^2} \\
\phi_0^{(2)}(x) &= -\frac{(x-x_{m-1})(x-x_{m+1})}{\Delta x^2} \\
\phi_1^{(2)}(x) &= \frac{(x-x_{m-1})(x-x_m)}{2\Delta x^2} \qquad (1.52)
\end{aligned}
$$

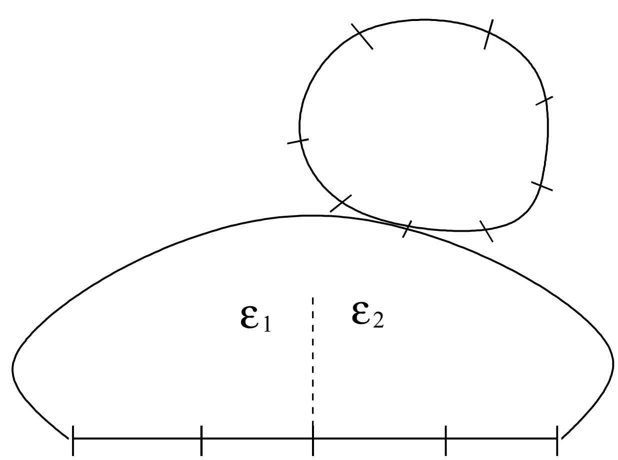

Figure § 3.01 Derivative matrix for the 2nd-Order FD method.

Hence the derivative at node x_m is given by

$$u_m = \frac{df(x_m)}{dx} = \sum_{\ell=-1}^{1} f_{m+\ell} \frac{d\phi_\ell^{(2)}(x_m)}{dx} \equiv D_{mn} f_n \tag{1.53}$$

The matrix is given by

$$D_{mn} = \frac{1}{2\Delta x}[\delta_{n,m+1} - \delta_{n,m-1}] \equiv \frac{1}{2\Delta x}[\delta_{m-n+1,0} - \delta_{m-n-1,0}]$$
$$\equiv a_{m-n} = \begin{cases} \frac{1}{2\Delta x}, & n = m+1 \\ -\frac{1}{2\Delta x}, & n = m-1 \\ 0, & \text{otherwise} \end{cases} \tag{1.54}$$

Again D is a Toeplitz matrix with

$$a_k = \frac{1}{2\Delta x}[\delta_{k-1,0} - \delta_{k+1,0}]$$

B. The 4th-Order FD Method

Similarly, for the fourth-order FD scheme, we have

$$f(x) \approx p^{(4)}(x) = \sum_{\ell=-2}^{2} f_{m+\ell}\phi_\ell^{(4)}(x), \quad x_{m-2} \le x < x_{m+2} \tag{1.55}$$

The derivative matrix is given by

$$\begin{aligned} D_{mn} &\equiv a_{m-n} \\ &= \frac{1}{12\Delta x}[8\delta_{m-n+1,0} - 8\delta_{m-n-1,0} - \delta_{m-n+2,0} + \delta_{m-n-2,0}] \\ &= \begin{cases} \frac{1}{12\Delta x}, & n = m-2 \\ -\frac{2}{3\Delta x}, & n = m-1 \\ \frac{2}{3\Delta x}, & n = m+1 \\ \frac{-1}{12\Delta x}, & n = m+2 \\ 0, & \text{otherwise} \end{cases} \end{aligned}$$

C. The Nth-Order FD Method

Similarly, for the N-th order FD scheme with all N points

$$D_{mn} = \frac{d\phi_{n-m}^{(N)}(x_m)}{dx} \tag{1.56}$$

where $\phi_{n-m}^{(N)}(x)$ are the N-th order Lagrange polynomials.

The required $N+1$ data points are provided by

- the N points in the domain, and
- the additional point from the periodic boundary condition.

D. Trigonometric Interpolation and FFT Method

The period of the computational domain: $L = x_{max} - x_{min}$.

* Sampling points: $x_m = x_{min} + (m-1)\Delta x$
  for $m = 0, \cdots, N-1$ and $\Delta x = L/N$.

The periodic function is written as a truncated Fourier series

$$f(x) \approx \frac{1}{N} \sum_{p=-N/2}^{N/2-1} \hat{f}_p e^{j2\pi p(x-x_0)/N\Delta x} \tag{1.57}$$

The Fourier series coefficients are

$$
\begin{aligned}
\hat{f}_p &= \frac{N}{L}\int_{x_{min}}^{x_{max}} f(x)e^{-j2\pi p(x-x_0)/N\Delta x}dx \\
&\approx \sum_{m=0}^{N-1} f(x_m)e^{-j2\pi mp/N} \\
&\equiv \{\mathrm{DFT}[\mathbf{f}]\}_p \qquad (1.58)
\end{aligned}
$$

Thus, from (1.57), we have the spatial derivative

$$
\begin{aligned}
\frac{df(x_m)}{dx} &\approx \frac{1}{N^2}\sum_{p=-N/2}^{N/2-1} \frac{j2\pi p}{\Delta x}\hat{f}_p e^{j2\pi mp/N} \\
&\equiv \frac{2\pi}{N\Delta x}\left\{\mathrm{DFT}^{-1}[jp\hat{f}_p]\right\}_m \\
&= \frac{2\pi}{N\Delta x}\{\mathrm{DFT}^{-1}[jp\{\mathrm{DFT}(\mathbf{f})\}_p]\}_m \qquad (1.59)
\end{aligned}
$$

When substituting the Fourier series coefficients $\hat{f}_n$ into (1.57), one can obtain the explicit derivative matrix

$$
\begin{aligned}
\frac{df(x_m)}{dx} &\approx \frac{2\pi}{N^2\Delta x}\sum_{n=0}^{N-1} f(x_n)\sum_{p=-N/2}^{N/2-1} jpe^{j2\pi(m-n)p/N} \\
&= \sum_{n=0}^{N-1} f(x_n)D_{mn} \qquad (1.60)
\end{aligned}
$$

$$
\begin{aligned}
D_{mn} &= \frac{2\pi}{N^2\Delta x}\sum_{p=-N/2}^{N/2-1} jpe^{j2\pi(m-n)p/N} \\
&= \frac{\pi}{N\Delta x}(-1)^{m-n}\cot\left(\frac{(m-n)\pi}{N}\right)(1-\delta_{m-n,0}) \\
&\equiv a_{m-n} \qquad (1.61)
\end{aligned}
$$

Therefore, the derivative matrix again is Toeplitz.

The derivative vector is given by

$$\frac{d\mathbf{f}}{dx} = \mathbf{Df} = \mathrm{DFT}^{-1}\left\{\mathrm{DFT}[\mathbf{f}] \cdot \mathrm{DFT}[\mathbf{a}]\right\} \tag{1.62}$$

This derivative costs $O(N \log N)$ operations by FFT.

The accuracy of this algorithm is “spectral” for an analytic function.

* The error decreases as $O(\alpha^N)$ where $0 < \alpha < 1$.

E. The Fourier PS Method

1-D time domain EM problem for $x \in [x_{min}, x_{max}]$

$$\frac{\partial E_y}{\partial x} = -\mu \frac{\partial H_z}{\partial t} - \sigma_m H_z - M_z \tag{1.63}$$

$$\frac{\partial H_z}{\partial x} = -\epsilon \frac{\partial E_y}{\partial t} - \sigma_e E_y - J_y \tag{1.64}$$

with **periodic boundary conditions**

$$E_y(x+L,t) = E_y(x,t), \quad H_z(x+L,t) = H_z(x,t) \tag{1.65}$$

where $L = x_{max} - x_{min}$, and appropriate initial conditions.

Spatial and Temporal Grids

In contrast to the FDTD method which uses a staggered grid,

- the Fourier PS method uses a collocated centered grid
- where all field components are located at the cell centers.

$$E_i^n \equiv E_y((i+\frac{1}{2})\Delta x, n\Delta t)$$
$$H_i^{n+\frac{1}{2}} \equiv H_z((i+\frac{1}{2})\Delta x, (n+\frac{1}{2})\Delta t) \qquad (1.66)$$

where $\Delta x = \frac{L}{N}$. This centered grid provides an important advantage over FDTD

* No need for material averaging in a staggered grid.
* No need for field averaging in anisotropic media.

Note that the time step is still staggered for E and H.

Time Integration Scheme

For an isotropic medium, the central time differencing yields

$$\mathbf{H}^{n+\frac{1}{2}} = C_{h1}\mathbf{H}^{n-\frac{1}{2}} - C_{h2}\{D_x[\mathbf{E}^n] + \mathbf{M}^n\} \qquad (1.67)$$

$$\mathbf{E}^{n+1} = C_{e1}\mathbf{E}^n + C_{e2}\{D_x[\mathbf{H}^{n+\frac{1}{2}}] - \mathbf{J}^{n+\frac{1}{2}}\} \qquad (1.68)$$

• Here D_x denotes the derivative operator

$$D_x[\mathbf{f}] \equiv \frac{2\pi}{L}\left\{\mathrm{DFT_x}^{-1}[jp\{\mathrm{DFT_x}[\mathbf{f}]\}_p]\right\} \qquad (1.69)$$

The coefficients

$$C_{h1} = \frac{\mu - \Delta t\sigma_m/2}{\mu + \Delta t\sigma_m/2}, \quad C_{h2} = \frac{\Delta t}{\mu + \Delta t\sigma_m/2}$$
$$C_{e1} = \frac{\epsilon - \Delta t\sigma_e/2}{\epsilon + \Delta t\sigma_e/2}, \quad C_{e2} = \frac{\Delta t}{\epsilon + \Delta t\sigma_e/2} \qquad (1.70)$$

The 4th-order Runge-Kutta method can also be used for better accuracy.

Source Implementation is the PSTD Method

A point source is a discrete Delta function, so it will suffer from the well-known Gibbs phenomenon.

* A point source is approximated as a smoothed source over a few (4-6) cells.

  Example: $s(x) = S_0 \cdot \mathrm{BHW}_0(x - x_s)$ where $x = x_s$ is the point source location.
* An alternative method is to solve for the scattered field.

1.3.2 A Bounded 1-D Problem

Many problems in practice are bounded and thus not periodic (for example, a PEC cavity). The Fourier PSTD method has following issues:

* The discontinuity at boundaries will create the Gibbs phenomena.

Furthermore, the wave field will "wrap around" (the wrap-around effect)

- because of the periodicity,
- thus corrupting the fields inside the computational domain.

In addition, the uniform interpolation points will cause the Runge phenomenon.

A. Gibbs' Phenomenon and Wrap-Around Effect

When the trigonometric interpolation

- is used to approximate a discontinuous function,
- it will introduce a large error near the discontinuities.

• This error is called the Gibbs' phenomenon.

Furthermore, when a non-periodic function

- is interpolated by the trigonometric interpolation method,
- it will create the wrap-around effect
  * when the wavefield from other periods will propagate into the interested domain.

B. The Runge Phenomenon

If a uniform grid is used in the Lagrange interpolation method to interpolate a non-periodic function,

- as one increases the order of the interpolation polynomials,
- the numerical error near the edges actually grows exponentially.

• This is the so-called Runge phenomenon for a uniform grid.

For uniform interpolation points

$$f(x) \approx \sum_{i=1}^{N+1} f_i \phi^{(N)}_{i-[N/2-1]}(x), \qquad |x| \leq 1 \tag{1.71}$$

Runge phenomenon: The error increases exponentially with N near $x = \pm 1$.
To avoid this Runge phenomenon, the grid points are clustered near the edge.

A. Chebyshev Interpolation
The Chebyshev points:

- The grid density per unit length should change with N
- so that the density is proportional to

$$\frac{N}{\pi\sqrt{1-\xi^2}}, \qquad \xi \in [-1, 1]$$

An example is the Gauss-Chebyshev-Lobatto (GCL) points

$$\xi_m = -\cos(m\pi/N), \qquad m = 0, \cdots, N \tag{1.72}$$

If $x_{min} \leq x \leq x_{max}$, we can first transform x into ξ by

$$x = J_x \xi + \frac{1}{2}(x_{min} + x_{max})$$

$J_x = (x_{max} - x_{min})/2$ is the Jacobian of the transformation.

Given $\{f_m = f(x_m) = f(\xi_m)\}$ $(m = 0, \cdots, N)$,

- the function can be interpolated by Lagrange polynomials

$$\begin{aligned}
\phi_m^{(N)}(x) &= \prod_{n=0,n\neq m}^{N} \frac{(x - x_n)}{(x_m - x_n)} \\
&= \prod_{n=0,n\neq m}^{N} \frac{(\xi - \xi_n)}{(\xi_m - \xi_n)} = \phi_m^{(N)}(\xi), \quad m = 0, \cdots, N
\end{aligned}$$

The interpolation polynomial can be written into a closed form

$$\phi_m^{(N)}(\xi) = \frac{(1 - \xi^2)T_N'(\xi)(-1)^{m+1+N}}{c_m N^2(\xi - \xi_m)} \tag{1.73}$$

$$c_m = 1 + \delta_{m,0} + \delta_{m,N}$$

Example: $N = 1$, then $\xi_0 = -1$, $\xi_1 = 1$

$$f(\xi) \approx \frac{1}{2}(1 - \xi)f_0 + \frac{1}{2}(1 + \xi)f_1$$

$$\frac{df}{dx} = \frac{1}{J_x}[-\frac{1}{2}f_0 + \frac{1}{2}f_1]$$

At the grid points, the derivatives are

$$\begin{pmatrix} u_0 \\ u_1 \end{pmatrix} = D^{(1)} \begin{pmatrix} f_0 \\ f_1 \end{pmatrix} \tag{1.74}$$

The derivative matrix

$$D^{(1)} = \frac{1}{2J_x} \begin{pmatrix} -1 & 1 \\ -1 & 1 \end{pmatrix} \tag{1.75}$$

Similarly, if $N = 2$, then $\xi_0 = -1$, $\xi_1 = 0$, $\xi_2 = 1$, we have

$$f(\xi) = \frac{1}{2}\xi(\xi - 1)f_0 + (1 - \xi^2)f_1 + \frac{1}{2}\xi(1 + \xi)f_2$$

$$\frac{df}{dx} = \frac{1}{J_x}\left[(\xi - \frac{1}{2})f_0 - 2\xi f_1 + (\xi + \frac{1}{2})f_2\right]$$

The derivative matrix

$$D^{(2)} = \frac{1}{2J_x}\begin{pmatrix} -3 & 4 & -1 \\ -1 & 0 & 1 \\ 1 & -4 & 3 \end{pmatrix} \tag{1.76}$$

The general formula for an arbitrary positive integer N

$$D^{(N)}_{mn} = \frac{1}{J_x} \cdot \begin{cases} \dfrac{c_m}{c_n}\dfrac{(-1)^{m+n}}{\xi_m - \xi_n} & m \neq n \\ -\dfrac{\xi_n}{2(1-\xi_n^2)} & 1 \leq m = n \leq N-1 \\ -\dfrac{2N^2+1}{6} & m = n = 0 \\ \dfrac{2N^2+1}{6} & m = n = N \end{cases}$$

$$c_m = 1 + \delta_{m,0} + \delta_{m,N}$$

The straightforward way to find the derivative needs to multiple this dense matrix $D_{mn}^{(N)}$ with the vector $\mathbf{f}$

* It requires $O(N^2)$ operations.

This can be circumvented by the fast cosine transform.
Since the Lagrange polynomials used above are of order N,

* we can represent function $f(x)$ equivalently by Chebyshev polynomials up to order N.

Function $f(x)$ can be expanded with Chebyshev polynomials $T_n(\xi) = \cos[n \cos^{-1}(\xi)]$:

$$f(\xi) = \sum_{n=0}^{N} a_n T_n(\xi) \tag{1.77}$$

a_n are the expansion coefficients.

Examples of Chebyshev polynomials

$$\begin{aligned} T_0(\xi) &= 1 \\ T_1(\xi) &= \xi \\ T_2(\xi) &= 2\xi^2 - 1 \\ T_3(\xi) &= 4\xi^3 - 3\xi \end{aligned} \tag{1.78}$$

For Chebyshev polynomials, some recursion relations are

$$\begin{aligned}T_{n+1}(\xi) &= 2\xi T_n(\xi) - T_{n-1}(\xi)\\ \frac{T'_{n+1}(\xi)}{n+1} - \frac{T'_{n-1}(\xi)}{n-1} &= 2T_n(\xi)\\ (1-\xi^2)T'_n(\xi) &= -n\xi T_n(\xi) + nT_{n-1}(\xi)\\ 2T_m(\xi)T_n(\xi) &= T_{n+m}(\xi) + T_{|n-m|}(\xi)\end{aligned} \tag{1.79}$$

Therefore, from $T_0(\xi)$ and $T_1(\xi)$,

one can obtain all higher-order Chebyshev polynomials.

Then, using (1.77), one can obtain the derivative of $f(\xi)$

$$\frac{df(\xi)}{d\xi} = \sum_{n=0}^{N} a_n \frac{dT_n(\xi)}{d\xi} = \sum_{n=0}^{N} b_n T_n(\xi) \tag{1.80}$$

The coefficients $\{b_n\}$ can be derived through

the recursion relations of the Chebyshev polynomials.

With these relations, and by comparing (1.80) and derivative of (1.77), we have

$$\begin{cases} b_N = 0 \\ b_{N-1} = 2Na_N \\ b_{N-2} = 2(N-1)a_{N-1} \\ b_{n-1} = b_{n+1} + 2na_n, \quad n = N-2, N-3, \cdots, 2 \\ b_0 = a_1 + \frac{1}{2}b_2 \end{cases} \tag{1.81}$$

With the choice of the grid points in (1.72),

- we can obtain the coefficients $\{a_n\}$ and $\{b_n\}$
- using the fast cosine transform (FCT) algorithm.

First, a_n can be obtained by the inverse fast cosine transform since

$$\begin{aligned} f(\xi_m) = \sum_{n=0}^{N} a_n T_n(\xi_m) = & \sum_{n=0}^{N} a_n \cos[n \cos^{-1}(-\cos\frac{m\pi}{N})] \\ = & \sum_{n=0}^{N} a_n \cos n(\pi - \frac{m\pi}{N}) \end{aligned} \tag{1.82}$$

Step 1: Coefficients

$$\{a_n\} = \mathrm{FCT}^{-1}[f(\xi_m)] \tag{1.83}$$

Step 2: $\{b_n\}$ can be obtained by $\{a_n\}$ from (1.81)

$$\{b_n\} = B[a_n] \tag{1.84}$$

Step 3: Derivative at the grid points

$$\{\frac{df(\xi_m)}{d\xi}\} = -\mathrm{FCT}[b_n] = \sum_{n=0}^{N} b_n \cos n(\pi - \frac{m\pi}{N}) \tag{1.85}$$

Symbolically, we can finally write the spatial derivative as

$$\{\frac{df(x_m)}{dx}\} \equiv D_{GCL}[\mathbf{f}] = -\frac{2}{L} \cdot \mathrm{FCT}[B\{\mathrm{FCT}^{-1}[f(\xi_m)]\}] \tag{1.86}$$

Thus, the cost of finding the derivative is $O(N \log N)$.

B. Legendre Interpolation

A similar approach can be

- developed for Legendre interpolation method.

However, in this case,

- the cost is in general $O(N^2)$
- as one cannot use the fast cosine transform algorithm
- to speed up the derivative computation.

Nevertheless, this is not a problem if $N \leq 16$ as it is usually faster to do the direct matrix-vector multiply than FCT for smaller N values.

C. 1-D Chebyshev PSTD Method

We can also use the collocated grid points for E_y and H_z. For an isotropic medium, the central time differencing yields

$$\mathbf{H}^{n+\frac{1}{2}} = C_{h1}\mathbf{H}^{n-\frac{1}{2}} - C_{h2}\{D_{GCL}[\mathbf{E}^n] + \mathbf{M}^n\} \tag{1.87}$$

$$\mathbf{E}^{n+1} = C_{e1}\mathbf{E}^n + C_{e2}\{D_{GCL}[\mathbf{H}^{n+\frac{1}{2}}] - \mathbf{J}^{n+\frac{1}{2}}\} \tag{1.88}$$

• Here D_{GCL} denotes the derivative operator in (1.86)

$$D_{GCL}[\mathbf{f}] = -\frac{2}{L} \cdot \text{FCT}[B\{\text{FCT}^{-1}[\mathbf{f}]\}] \tag{1.89}$$

The coefficients

$$\begin{aligned} C_{h1} &= \frac{\mu - \Delta t\sigma_m/2}{\mu + \Delta t\sigma_m/2}, \quad C_{h2} = \frac{\Delta t}{\mu + \Delta t\sigma_m/2} \\ C_{e1} &= \frac{\epsilon - \Delta t\sigma_e/2}{\epsilon + \Delta t\sigma_e/2}, \quad C_{e2} = \frac{\Delta t}{\epsilon + \Delta t\sigma_e/2} \end{aligned} \tag{1.90}$$

The 4th-order Runge-Kutta method can also be used for better accuracy.

1.3.3 The PSTD Method for an Unbounded Domain

For an unbounded domain, waves will propagate to outside the domain. **Wrap-around effect:**

* The Fourier PS method makes waves travel periodically to the domain to corrupt the late time solutions.

Fortunately, the perfectly matched layer (PML) saves the day.

* PML at one or both end attenuate waves without reflecting.
* PML attenuation can be adjusted to make the wrap-around negligible.
* Thus the Fourier PSTD can completely model unbounded media.

1-D time domain EM problem for $x \in [x_{min}, x_{max}]$ with the well-posed PML (GX Fan & QH Liu, 2001/2004)

$$
\begin{aligned}
\mu \frac{\partial \tilde{H}_z}{\partial t} &= -\frac{\partial \tilde{E}_y}{\partial x} - (\sigma_m + \omega_x \mu)\tilde{H}_z - \sigma_m \omega_x H_z^{(1)} - M_z \\
\epsilon \frac{\partial \tilde{E}_y}{\partial t} &= -\frac{\partial \tilde{H}_z}{\partial x} - (\sigma_e + \omega_x \epsilon)\tilde{E}_y - \sigma_e \omega_x E_y^{(1)} - J_y \\
\frac{\partial E_y^{(1)}}{\partial t} &= \tilde{E}_y - \omega_x E_y^{(1)} \\
\frac{\partial H_z^{(1)}}{\partial t} &= \tilde{H}_z - \omega_x H_z^{(1)}
\end{aligned} \tag{1.91}
$$

with **periodic boundary conditions**

$$\tilde{E}_y(x+L,t) = \tilde{E}_y(x,t), \quad \tilde{H}_z(x+L,t) = \tilde{H}_z(x,t) \tag{1.92}$$

where $L = x_{max} - x_{min}$, $\tilde{E}_y = E_y + \omega_x E_y^{(1)}$, $\tilde{H}_z = H_z + \omega_x H_z^{(1)}$.

Collocated Spatial Grid and Staggered Temporal Grid

$$\begin{aligned}
\tilde{E}_i^n &\equiv \tilde{E}_y((i+\frac{1}{2})\Delta x, n\Delta t) \\
\tilde{H}_i^{n+\frac{1}{2}} &\equiv \tilde{H}_z((i+\frac{1}{2})\Delta x, (n+\frac{1}{2})\Delta t)
\end{aligned} \tag{1.93}$$

Time Integration Scheme

$$\begin{aligned}
&\mathbf{H}^{(1),n} = A_1\mathbf{H}^{(1),n-1} + A_2\tilde{\mathbf{H}}^{n-\frac{1}{2}} \\
&\mathbf{E}^{(1),n+\frac{1}{2}} = A_1\mathbf{E}^{(1),n-\frac{1}{2}} + A_2\tilde{\mathbf{E}}^{n} \\
&\tilde{\mathbf{H}}^{n+\frac{1}{2}} = C_{h1}\tilde{\mathbf{H}}^{n-\frac{1}{2}} - C_{h2}\{D_x[\tilde{\mathbf{E}}^n] + \sigma_m\omega_x\mathbf{H}^{(1),n} + \mathbf{M}^n\} \\
&\tilde{\mathbf{E}}^{n+1} = C_{e1}\tilde{\mathbf{E}}^{n} + C_{e2}\{D_x[\tilde{\mathbf{H}}^{n+\frac{1}{2}}] + \sigma_e\omega_x\mathbf{E}^{(1),n+\frac{1}{2}} - \mathbf{J}^{n+\frac{1}{2}}\}
\end{aligned} \tag{1.94}$$

- Here D_x denotes the derivative operator

$$D_x[\mathbf{f}] \equiv \frac{2\pi}{L}\left\{\mathrm{DFT_x}^{-1}[jp\{\mathrm{DFT_x}[\mathbf{f}]\}_p]\right\} \tag{1.95}$$

The coefficients

$$\begin{aligned}
A_1 &= \frac{1-\omega_x\Delta t/2}{1+\omega_x\Delta t/2}, \quad A_2 = \frac{\Delta t}{1+\omega_x\Delta t/2} \\
C_{h1} &= \frac{\mu - \Delta t(\sigma_m+\omega_x\mu)/2}{\mu + \Delta t(\sigma_m+\omega_x\mu)/2}, \quad C_{h2} = \frac{\Delta t}{\mu + \Delta t(\sigma_m+\omega_x\mu)/2} \\
C_{e1} &= \frac{\epsilon - \Delta t(\sigma_e+\omega_x\epsilon)/2}{\epsilon + \Delta t(\sigma_e+\omega_x\epsilon)/2}, \quad C_{e2} = \frac{\Delta t}{\epsilon + \Delta t(\sigma_e+\omega_x\epsilon)/2}
\end{aligned}$$

The 4th-order Runge-Kutta method can also be used for better accuracy.

1.3.4 Dispersion Analysis and Stability Condition

Sample wave equation for $x \in [0, L]$

$$\frac{\partial u(x,t)}{\partial x} + \frac{1}{c}\frac{\partial u(x,t)}{\partial t} = 0, \quad x \in [0, L], \quad t \geq 0 \tag{1.96}$$

with a periodic boundary condition $u(0,t) = u(L,t)$ and an initial condition $u(x,0) = e^{i\omega x/c}$. This PDE has an exact solution

$$u(x,t) = e^{i\omega(x/c - t)} \tag{1.97}$$

In FD and PS methods, there can be numerical dispersion errors in spatial and temporal discretization.

A. Approximations of Spatial Derivatives

$$\frac{\partial u(x,t)}{\partial x} \approx \mathcal{D}_x\{u(x,t)\}$$

where the derivative operator is given by

$$\mathcal{D}_x f(x) = \begin{cases} \dfrac{2\pi}{L}\mathcal{F}^{-1}\Big\{jp[\mathcal{F}(f)]_p\Big\}, & \mathrm{P}S \\ \displaystyle\sum_{p=1}^{P/2} \frac{a_p}{\Delta x}[f(x + (p - \frac{1}{2})\Delta x) - f(x - (p - \frac{1}{2})\Delta x)], & \mathrm{F}D \end{cases} \tag{1.98}$$

The 2nd-order FD method: $P = 2$ and $a_1 = 1$;
The 4th-order FD method: $P = 4$, $a_1 = 27/24$, and $a_2 = -1/24$.

For the PS method, $\mathcal{F}$ and $\mathcal{F}^{-1}$ denote the forward and inverse discrete Fourier transforms through an FFT algorithm.

B. Phase Dispersion Errors

Nyquist theorem for a smooth band-limited signal: D_x is exact in PS as long as $\omega \leq \pi c/\Delta x$ (i.e., $\Delta x \leq \lambda/2$ where λ is the wavelength). The phase error is zero.

The FD method gives a solution $u_{FD}(x,t) = e^{i\omega(x/c-\beta t)}$ with

$$\beta(\omega) = \frac{\sum_{j=1}^{P/2} a_j \sin[(j-1/2)\omega\Delta x/c]}{(\omega\Delta x/2c)}$$

The phase (or dispersion) error is

$$e(\omega,t) = \omega t[1-\beta(\omega)]$$

This dispersion error is linearly proportional to time.

The FD method requires a large SD for a long time window.

Dispersion Analysis and Stability Condition

The dispersion relations for the FDTD and PSTD methods in a homogeneous lossless medium are

$$\sin\frac{\omega\Delta t}{2} = \begin{cases} \dfrac{c\Delta t}{2}\sqrt{k_x^2+k_y^2+k_z^2}, & \text{PSTD} \\[2ex] \dfrac{c\Delta t}{\Delta x}\sqrt{\displaystyle\sum_{\eta=x,y,z}\left\{\sum_{j=1}^{P/2} a_j \sin^2[k_\eta\Delta\eta(j-1/2)]\right\}^2}, & \text{FDTD} \end{cases} \tag{1.99}$$

The corresponding CFL stability conditions can also be written compactly as

$$\frac{c\Delta t}{\Delta x} \leq \frac{1}{\alpha\sqrt{D}}$$

for a problem of dimensionality D, where $\alpha = 1$ for FDTD, and $\alpha = \pi/2 \approx 1.5708$ for PSTD.

The stability condition for the PSTD method is a factor of $\pi/2 \approx 1.57$ more stringent than the FDTD method for the same Δx.
However, because of much larger Δx afforded by the PSTD method, Δt in the Fourier PSTD method

- need not be smaller than the FDTD method
- for the same accuracy.

In practice, for large-scale problems without small geometrical features finer than a quarter wavelength, the choice of Δt in the Fourier PSTD method

* is usually dictated by the accuracy
  rather than the stability consideration.

1.4 The Spectral Element Method in Frequency Domain

The above PSTD methods are for smooth media. For large-scale highly discontinuous media, the spectral element method in time domain will be used. But we will first consider the **SEM in frequency domain**.

1.4.1. Gauss-Legendre-Lobatto (GLL) Polynomials

* A special set of Lagrangian interpolation polynomials with the nodal points located at the Gauss-Legendre-Lobatto (GLL) points.

In a 1-D standard reference element $\xi \in [-1, 1]$

The N-th order GLL basis functions are defined by

$$\phi_j^{(N)}(\xi) = \frac{-1}{N(N+1)L_N(\xi_j)} \frac{(1-\xi^2)L'_N(\xi)}{(\xi - \xi_j)}, \quad j = 0, \cdots, N \tag{1.100}$$

where $L_N(\xi)$ is the N-th order Legendre polynomial, and $L'_N(\xi)$ is its derivative.

Within the element $\xi \in [-1, 1]$ the nodal points $\{\xi_j\}$ are the **GLL points**: The $(N + 1)$ roots of equation

$$(1 - \xi_j^2) L'_N(\xi_j) = 0 \tag{1.101}$$

Note that $\xi_0 = -1$, $\xi_N = 1$.
Legendre polynomials satisfy the Legendre differential equation

$$\frac{d}{d\xi}[(1 - \xi^2)\frac{L_N(\xi)}{d\xi}] + N(N + 1)L_N(\xi) = 0 \tag{1.102}$$

These polynomials can be written as

$$L_N(\xi) = \frac{1}{2^N N} \frac{d^N}{d\xi^N}[(\xi^2 - 1)^N] \tag{1.103}$$

Orthogonal relation

$$\int_{-1}^{1} L_m(\xi) L_n(\xi) d\xi = \frac{2}{2n + 1}\delta_{mn} \tag{1.104}$$

Examples of Legendre polynomials

$$\begin{aligned}
L_0(\xi) &= 1 \\
L_1(\xi) &= \xi \\
L_2(\xi) &= \frac{1}{2}(3\xi^2 - 1) \\
L_3(\xi) &= \frac{1}{2}(5\xi^3 - 3\xi)
\end{aligned}$$

The derivative matrix with the GLL points is (Canuto et al., 1988)

$$D_{mn}^{(N)} = \frac{1}{J_x} \cdot \begin{cases} \dfrac{L_N(\xi_m)}{L_N(\xi_n)(\xi_m - \xi_n)} & \text{if} \quad m \neq n \\ -\dfrac{N(N+1)}{4} & \text{if} \quad m = n = 0 \\ \dfrac{N(N+1)}{4} & \text{if} \quad m = n = N \\ 0 & \text{otherwise} \end{cases}$$

GLL Quadrature

The integration of a smooth function $f(x)$ by GLL quadrature:

$$I = \int_{x_{min}}^{x_{max}} f(x)dx = |J_x| \int_{-1}^{1} f(x(\xi))d\xi \approx |J_x| \sum_{p=1}^{N} w_p f(x(\xi_p)) \quad (1.105)$$

where $\{w_n\}$ are the weights of the GLL quadrature.
This is exact if $f(x)$ is a polynomial of degree $2N-1$ or smaller.

Special Case: For $f(x) = \phi_m^{(N)}(\xi)\phi_n^{(N)}(\xi)$

$$I_{m,n} = \int_{x_{min}}^{x_{max}} f(x)dx = |J_x| \int_{-1}^{1} \phi_m^{(N)}(\xi)\phi_n^{(N)}(\xi)d\xi$$

$$\approx |J_x| \sum_{p=0}^{N} w_p \phi_m^{(N)}(\xi_p)\phi_n^{(N)}(\xi_p) = |J_x| w_m \delta_{m,n} \quad (1.106)$$

since for a Lagrange interpolation function $\phi_m^{(N)}(\xi_p) = \delta_{m,p}$.

1.4.2. The SEM in Frequency Domain

1-D Helmholtz equation for a domain with complex $\mu_r(x)$ and $\epsilon_r(x)$

$$\frac{d}{dx}\mu_r^{-1}\frac{dE_y}{dx} + k_0^2\epsilon_r E_y = -S_e \tag{1.107}$$

where $S_e = \frac{d(\mu_r^{-1}M_{iz})}{dx} - j\omega\mu_0 J_y$.
Spectral element expansion within each element (note the continuity between elements)

$$E_y(x) = \sum_{n=0}^{N_E} e_n\phi_n(x), \quad x \in [x_{min}^{(e)}, x_{max}^{(e)}] \tag{1.108}$$

The basis and testing functions will use the GLL polynomials.

Weak form Helmholtz equation

$$\begin{aligned}
&\int_a^b dx\left[-\frac{dw_m}{dx}\cdot\mu_r^{-1}(x)\frac{dE_y}{dx} + k_0^2\epsilon_r(x)w_m(x)E_y(x)\right] \\
= \quad & -\left[\mu_r^{-1}(x)w_m(x)\frac{dE_y}{dx}\right]_a^b - \int_a^b dx w_m(x)S_y(x) \\
= \quad & j\omega\mu_0\left[w_m(x)H_z(x)\right]_a^b - \int_a^b dx w_m(x)S_y(x)
\end{aligned} \tag{1.109}$$

Radiation boundary conditions

$$\begin{aligned}
H_z(x=a) &= [H_{zL}^{inc} + H_{zL}^{sct}]_{x=a} = \frac{1}{\eta_L}[2E_{zL}^{inc} - E_z]_{x=a} \\
H_z(x=b) &= [H_{zR}^{inc} + H_{zR}^{sct}]_{x=b} = \frac{1}{\eta_R}[-2E_{zR}^{inc} + E_z]_{x=b}
\end{aligned} \tag{1.110}$$

where $\eta_{L,R} = \sqrt{\mu/\epsilon}|_{x=a^-,b^+}$ are impedances for $x < a$ and $x > b$.

Weak form Helmholtz equation with radiation BCs

$$\begin{aligned}
&\int_a^b dx\left[-\frac{dw_m}{dx}\cdot\mu_r^{-1}(x)\frac{dE_y}{dx}+k_0^2\epsilon_r(x)w_m(x)E_y(x)\right] \\
&\qquad -j\omega[\eta_L^{-1}w_m(a)E_y(a)+\eta_R^{-1}w_m(b)E_y(b)] \\
&= -j2\omega\left[\eta_L^{-1}w_m(a)E_{yL}^{inc}(a)+\eta_R^{-1}w_m(b)E_{yR}^{inc}(b)\right] \\
&\qquad -\int_a^b dx w_m(x)S_y(x) \qquad (1.111)
\end{aligned}$$

We choose both testing and basis functions as the GLL polynomials ϕ_n.

SEM Impedance Matrix and Excitation Vector

$$\begin{aligned}
Z_{mn} &= \int_a^b dx\left[-\frac{d\phi_m}{dx}\cdot\mu_r^{-1}(x)\frac{d\phi_n}{dx}+k_0^2\epsilon_r(x)\phi_m(x)\phi_n(x)\right] \\
&\quad -j\omega[\eta_R^{-1}\phi_m(b)\phi_n(b)+\eta_L^{-1}\phi_m(a)\phi_n(a)] \\
&= Z_{mn}^{(1)}+Z_{mn}^{(2)}-j\omega\left[\frac{\delta_{m,1}\delta_{n,1}}{\eta_L}+\frac{\delta_{m,N}\delta_{n,N}}{\eta_R}\right]
\end{aligned}$$

$$\begin{aligned}
V_m &= -\int_a^b dx\phi_m(x)S_y(x) \\
&\quad -j2\omega\left[\eta_R^{-1}\phi_m(b)E_{yR}^{inc}(b)+\eta_L^{-1}\phi_m(a)E_{yL}^{inc}(a)\right] \\
&= -\int_a^b dx\phi_m(x)S_y(x)-j2\omega\left[\frac{\delta_{m,1}E_{yL}^{inc}(a)}{\eta_L}+\frac{\delta_{m,N}E_{yR}^{inc}(b)}{\eta_R}\right]
\end{aligned}$$

The elemental SEM impedance matrix

$$Z_{mn} = \sum_{e=1}^{e=N_e} [Z_{pq}^{(1,e)} + Z_{pq}^{(2,e)}] - j\omega \left[\frac{\delta_{m,1}\delta_{n,1}}{\eta_L} + \frac{\delta_{m,N}\delta_{n,N}}{\eta_R} \right]$$

Local indices (p, q) are mapped to the global indices (m, n).

$$\begin{aligned} Z_{pq}^{(1,e)} &= -\int_{x_{min}^{(e)}}^{x_{max}^{(e)}} \frac{d\phi_p}{dx} \cdot \mu_r^{-1}(x) \frac{d\phi_q}{dx} dx = -\frac{2}{L^{(e)}} \int_{-1}^{1} \frac{d\phi_p}{d\xi} \cdot \mu_r^{-1}(x) \frac{d\phi_q}{d\xi} d\xi \\ &= -\frac{2}{L^{(e)}} \sum_{n=0}^{N_E} \frac{w_n}{\mu_r(x(\xi_n))} \frac{d\phi_p(\xi_n)}{d\xi} \frac{d\phi_q(\xi_n)}{d\xi} \end{aligned}$$

$$\begin{aligned} Z_{pq}^{(2,e)} &= k_0^2 \int_{x_{min}^{(e)}}^{x_{max}^{(e)}} \epsilon_r(x)\phi_p(x)\phi_q(x)dx \\ &= k_0^2 \frac{L^{(e)}}{2} \int_{-1}^{1} \epsilon_r(x(\xi))\phi_p(\xi)\phi_q(\xi)d\xi \\ &= k_0^2 \frac{L^{(e)}}{2} \sum_{n=0}^{N_E} w_n \epsilon_r(x(\xi_n))\phi_p(\xi_n)\phi_q(\xi_n) \\ &= k_0^2 \frac{L^{(e)}}{2} w_p \epsilon_r(x(\xi_p))\delta_{p,q} \end{aligned}$$

This gives a diagonal elemental mass matrix.

The excitation vector for sources is

$$V_m = \sum_{e=1}^{N_e} V_p^{(e)} - j2\omega \left[\frac{\delta_{m,1} E_{yL}^{inc}(a)}{\eta_L} + \frac{\delta_{m,N} E_{yR}^{inc}(b)}{\eta_R} \right]$$

$$\begin{aligned} V_p^{(e)} &= \frac{L^{(e)}}{2} \sum_{n=0}^{N_E} w_n [j\omega\mu_0 J_y(x(\xi_n))\phi_p(\xi_n) + \frac{2M_z(x(\xi_n))}{\mu_r(x(\xi_n))L^{(e)}} \frac{d\phi_p(\xi_n)}{d\xi}] \\ &= \frac{j\omega\mu_0 L^{(e)}}{2} J_y(x(\xi_p)) w_p + \sum_{n=0}^{N_E} w_n \frac{M_z(x(\xi_n))}{\mu_r(x(\xi_n))} \frac{d\phi_p(\xi_n)}{d\xi} \end{aligned}$$

for smooth sources, where the M_z has been evaluated by integration by parts, assuming that the magnetic current at the element boundaries are zero. **For point sources** $J_y = J_0\delta(x - x_J)$ **and** $M_z = M_0\delta(x - x_M)$**,**

$$V_p^{(e)} = j\omega\mu_0 J_0 \phi_p(\xi(x_J)) + \frac{M_0}{\mu_r(x_M)} \frac{d\phi_p(\xi(x_M))}{d\xi}$$

A Note on the Source Implementation

To preserve the high-order convergence, the source excitation implementation should be careful when the source is a nonsmooth function inside an element. In that case, it is better to solve for the scattered field instead of total field in the source element (or even including the adjacent elements). The other elements can still use the total field. This is the total-field/scattered-field (TF/SF) formulation.
Alternative way: Approximate the singular source by a smoothed source.

Once these matrix and vector are assembled, the solution can be easily obtained by

$$\mathbf{I} = \mathbf{Z}^{-1}\mathbf{V}$$

1.5. The Spectral Element Time Domain Method

1.5.1. The SETD Method for 1-D Wave Equation

To avoid basis functions for both fields, we consider the 1-D wave equation for the special case where $\sigma_m = 0$:

$$\frac{\partial}{\partial x}\mu_r^{-1}\frac{\partial E_y}{\partial x} - \frac{1}{c^2}\epsilon_r\frac{\partial^2 E_y}{\partial t^2} - \mu_0\sigma_e\frac{\partial E_y}{\partial t} = -S_e \tag{1.112}$$

where $c = 1/\sqrt{\mu_0\epsilon_0}$ and $S_e = \frac{\partial(\mu_r^{-1}M_{iz})}{\partial x} - \mu_0\frac{\partial J_{iy}}{\partial t}$.
Spectral element expansion within each element (note the continuity between elements)

$$E_y(x,t) = \sum_{n=0}^{N_E} e_n(t)\phi_n(x) \tag{1.113}$$

$$H_z(x,t) = \sum_{n=0}^{N_H} h_n(t)\psi_n(x) \tag{1.114}$$

The choice of basis functions should be carefully considered.

The Weak Form Helmholtz Equation in Time Domain

Weak form Helmholtz equation with radiation BCs

$$\begin{aligned}
&\int_a^b dx\Big[-\frac{dw_m}{dx}\cdot\mu_r^{-1}(x)\frac{dE_y}{dx} \\
&\qquad -w_m(x)\{\frac{1}{c^2}\epsilon_r(x)\frac{\partial^2 E_y(x,t)}{\partial t^2} + \mu_0\sigma_e\frac{\partial E_y(x,t)}{\partial t}\}\Big] \\
&\qquad -[\eta_L^{-1}w_m(a)\frac{\partial E_y(a,t)}{\partial t} + \eta_R^{-1}w_m(b)\frac{\partial E_y(b,t)}{\partial t}] \\
&= -2\frac{\partial}{\partial t}\left[\eta_L^{-1}w_m(a)E_{yL}^{inc}(a,t) + \eta_R^{-1}w_m(b)E_{yR}^{inc}(b,t)\right] \\
&\qquad -\int_a^b dx w_m(x)S_y(x,t)
\end{aligned} \tag{1.115}$$

Both testing and basis functions will be the GLL polynomials.

Radiation Boundary Conditions in Time Domain

$$\mu_r^{-1}(a)\frac{\partial E_y(a,t)}{\partial x} = \frac{\partial H_z(a,t)}{\partial t} = \frac{1}{\eta_L}[2\dot{E}_{yL}^{inc} - \dot{E}_y]_{x=a} \quad (1.116)$$

$$\mu_r^{-1}(b)\frac{\partial E_y(b,t)}{\partial x} = \frac{\partial H_z(b,t)}{\partial t} = \frac{1}{\eta_R}[-2\dot{E}_{yR}^{inc} + \dot{E}_y]_{x=b} \quad (1.117)$$

where a dot over a variable denotes its time derivative.

The elemental SETD matrices:

$$S_{pq}^{(e)} = -\int_{x_{min}^{(e)}}^{x_{max}^{(e)}} \frac{d\phi_p}{dx}\cdot\mu_r^{-1}(x)\frac{d\phi_q}{dx}dx = -\frac{2}{L^{(e)}}\sum_{n=0}^{N_E}\frac{w_n\phi_p'(\xi_n)\phi_q'(\xi_n)}{\mu_r(x(\xi_n))}$$

$$M_{e,pq}^{(e)} = \frac{1}{c^2}\int_{x_{min}^{(e)}}^{x_{max}^{(e)}} \epsilon_r(x)\phi_p(x)\phi_q(x)dx = \frac{L^{(e)}}{2c^2}w_p\epsilon_r(x(\xi_p))\delta_{p,q}$$

$$\begin{aligned} C_{e,pq}^{(e)} &= \mu_0\int_{x_{min}^{(e)}}^{x_{max}^{(e)}} \sigma_e(x)\phi_p(x)\phi_q(x)dx + \frac{\phi_p(\xi)\phi_q(\xi)|_a}{\eta_L} + \frac{\phi_p(\xi)\phi_q(\xi)|_b}{\eta_R} \\ &= \left[\frac{\mu_0 L^{(e)}}{2}w_p\sigma_e(x(\xi_p)) + \frac{\delta_{e,1}\delta_{p,0}}{\eta_L} + \frac{\delta_{e,N_e}\delta_{p,N_E}}{\eta_R}\right]\delta_{p,q} \end{aligned}$$

Note the diagonal elemental mass matrices for ϵ_r and σ_e.

The excitation vector for sources is

$$v_p = \sum_{e=1}^{N_e} v_p^{(e)} - 2\frac{\partial}{\partial t}\left[\frac{\delta_{p,1}E_{yL}^{inc}(a,t)}{\eta_L} + \frac{\delta_{p,N}E_{yR}^{inc}(b,t)}{\eta_R}\right]$$

$$\begin{aligned} v_p^{(e)} &= \frac{L^{(e)}}{2}\sum_{n=0}^{N_E} w_n[\mu_0 \dot{J}_y(x(\xi_n),t)\phi_p(\xi_n) + \frac{2\dot{M}_z(x(\xi_n),t)}{\mu_r(x(\xi_n))L^{(e)}}\frac{d\phi_p(\xi_n)}{d\xi}] \\ &= \frac{\mu_0 L^{(e)}}{2}\dot{J}_y(x(\xi_p),t)w_p + \sum_{n=0}^{N_E} w_n \frac{\dot{M}_z(x(\xi_n),t)}{\mu_r(x(\xi_n))}\frac{d\phi_p(\xi_n)}{d\xi} \end{aligned}$$

for smooth sources, where the M_z term has been evaluated by integration by parts, assuming that the magnetic current at the element boundaries are zero. **For point sources** $J_y = J_0(t)\delta(x - x_J)$ **and** $M_z = M_0(t)\delta(x - x_M)$**,**

$$v_p^{(e)} = \mu_0 \dot{J}_0(t)\phi_p(\xi(x_J)) + \frac{\dot{M}_0(t)}{\mu_r(x_M)}\frac{d\phi_p(\xi(x_M))}{d\xi}$$

The System Equation in Time Domain

$$\mathbf{M}\frac{d^2\mathbf{e}}{dt^2} + \mathbf{C}\frac{d\mathbf{e}}{dt} = \mathbf{S}\mathbf{e} + \mathbf{v} \tag{1.118}$$

We can rewrite this as a set of coupled first order ODEs

$$\begin{aligned} \mathbf{M}\frac{d\dot{\mathbf{e}}}{dt} + \mathbf{C}\dot{\mathbf{e}} &= \mathbf{S}\mathbf{e} + \mathbf{v} \\ \dot{\mathbf{e}} &= \frac{d\mathbf{e}}{dt} \end{aligned} \tag{1.119}$$

Using a 2nd-order (instead of the better 4th-order) time integration yields

$$\begin{aligned} \dot{\mathbf{e}}^{n+\frac{1}{2}} &= (\mathbf{M} + \frac{\Delta t}{2}\mathbf{C})^{-1}[(\mathbf{M} - \frac{\Delta t}{2}\mathbf{C})\dot{\mathbf{e}}^{n-\frac{1}{2}} + \mathbf{S}\mathbf{e}^n + \mathbf{v}^n] \\ \mathbf{e}^{n+1} &= \mathbf{e}^n + \Delta t\dot{\mathbf{e}}^{n+\frac{1}{2}} \end{aligned}$$

Note the diagonal mass matrix inversion is trivial and efficient.

Magnetic field from electric field

Once the electric field is solved, **H** can be obtained by Faraday's law

$$\frac{\partial B_z}{\partial t} = -\frac{\partial E_y}{\partial x} \quad -M_z \tag{1.120}$$

By central time differencing, we have

$$\mathbf{b}_z^{n+\frac{1}{2}} = \mathbf{b}_z^{n-\frac{1}{2}} - \Delta t(\mathbf{D}\mathbf{e}^n + \mathbf{m}_z^n) \tag{1.121}$$

where **D** is the derivative matrix.
B_z is in general **not continuous** between adjacent elements.

1.5.2. The SETD Method for 1st-Order EH Equations

1-D time domain EM problem for $x \in [a, b]$

$$\frac{\partial E_y}{\partial x} = -\mu\frac{\partial H_z}{\partial t} - \sigma_m H_z - M_z \tag{1.122}$$

$$\frac{\partial H_z}{\partial x} = -\epsilon\frac{\partial E_y}{\partial t} - \sigma_e E_y - J_y \tag{1.123}$$

Spectral element expansion within each element (note the continuity between elements)

$$E_y(x,t) = \sum_{n=0}^{N_E} e_n(t)\phi_n(x), \quad H_z(x,t) = \sum_{n=0}^{N_H} h_n(t)\psi_n(x) \tag{1.124}$$

The choice of basis functions should be carefully considered.

Weak Form Equations

Integration by parts for the magnetic field

$$\langle \phi_m, \frac{\partial H_z}{\partial x} \rangle_\Omega = -\langle \frac{\partial \phi_m}{\partial x}, H_z \rangle_\Omega + [\phi_m H_z]_a^b = -\langle \frac{\partial \phi_m}{\partial x}, H_z \rangle_\Omega + \frac{[\phi_m(-2E_{yR}^{inc} + E_y)]_b}{\eta_R} - \frac{[\phi_m(2E_{yL}^{inc} - E_y)]_a}{\eta_L}$$

Weak form equations

$$\langle \psi_m, \mu \frac{\partial H_z}{\partial t} \rangle_\Omega = -\langle \psi_m, \frac{\partial E_y}{\partial x} - \sigma_m H_z - M_z \rangle_\Omega \quad (1.125)$$

$$\langle \phi_m, \epsilon \frac{\partial E_y}{\partial t} \rangle_\Omega = \langle \frac{\partial \phi_m}{\partial x}, H_z \rangle_\Omega - \langle \phi_m, \sigma_e E_y + J_y \rangle_\Omega - \frac{[\phi_m(-2E_{yR}^{inc} + E_y)]_b}{\eta_R} + \frac{[\phi_m(2E_{yL}^{inc} - E_y)]_a}{\eta_L} \quad (1.126)$$

The above boundary terms are zero for PEC and PMC outer boundaries. Furthermore, removal of the corresponding E unknowns on the PEC boundary is needed.

The System Equation in Time Domain

$$\mathbf{M}_e \dot{\mathbf{e}} = \mathbf{S}_h \mathbf{h} - \mathbf{C}_e \mathbf{e} - \mathbf{j} \quad (1.127)$$

$$\mathbf{M}_h \dot{\mathbf{h}} = -\mathbf{S}_e \mathbf{e} - \mathbf{C}_h \mathbf{h} - \mathbf{m} \quad (1.128)$$

The elemental SETD matrices are:

$$M_{e,pq}^{(e)} = \langle \phi_p, \epsilon \phi_q \rangle_{\Omega_e} = \frac{1}{2} w_p^{(N_E)} L^{(e)} \epsilon(x_p) \delta_{p,q}$$

$$M_{h,pq}^{(e)} = \langle \psi_p, \mu \psi_q \rangle_{\Omega_e} = \frac{1}{2} w_p^{(N_H)} L^{(e)} \mu(x_p) \delta_{p,q}$$

$$C_{e,pq}^{(e)} = \langle \phi_p, \sigma_e \phi_q \rangle_{\Omega_e} + \delta_{e,1} \left[\phi_p \cdot \frac{\phi_0}{\eta_L} \right]_{x=a} + \delta_{e,N_e} \left[\phi_p \cdot \frac{\phi_{N_E}}{\eta_L} \right]_{x=b}$$

$$= \frac{1}{2} w_p^{(N_E)} L^{(e)} \sigma_e(x_p) \delta_{p,q} + \delta_{e,1} \delta_{p,0} / \eta_L + \delta_{e,N_e} \delta_{p,N_E} / \eta_R$$

$$C_{h,pq}^{(e)} = \langle \psi_p, \sigma_m \psi_q \rangle_{\Omega_e} = \frac{1}{2} w_p^{(N_H)} L^{(e)} \sigma_m(x_p) \delta_{p,q}$$

$$S_{e,pq}^{(e)} = \langle \psi_p, \phi_q' \rangle_{\Omega_e} = w_p^{(N_H)} \phi_q'(\xi_p)$$

$$S_{h,pq}^{(e)} = \langle \phi_p', \psi_q \rangle_{\Omega_e} = \sum_{n=0}^{N_E} w_n^{(N_E)} \phi_p'(\xi_n) \psi_q(\xi_n) \approx w_p^{(N_H)} \phi_q'(\xi_p)$$

The elemental excitation vectors for smooth sources are

$$\begin{aligned}
j_p^{(e)} &= \langle \phi_p, J_y \rangle + \frac{2E_{yL}^{inc}(a,t)}{\eta_L}\delta_{p,0}\delta_{e,1} + \frac{2E_{yR}^{inc}(a,t)}{\eta_R}\delta_{p,N_E}\delta_{e,N_e} \\
&= \frac{L^{(e)}}{2}\sum_{n=0}^{N_E} w_n^{(N_E)} J_y(x_n,t)\phi_p(\xi_n) \\
&\quad + \frac{2E_{yL}^{inc}(a,t)}{\eta_L}\delta_{p,0}\delta_{e,1} + \frac{2E_{yR}^{inc}(b,t)}{\eta_R}\delta_{p,N_E}\delta_{e,N_e}
\end{aligned}$$

$$= \frac{L^{(e)} w_p^{(N_E)} J_y(x_p,t)}{2} + \frac{2E_{yL}^{inc}(a,t)}{\eta_L}\delta_{p,0}\delta_{e,1} + \frac{2E_{yR}^{inc}(b,t)}{\eta_R}\delta_{p,N_E}\delta_{e,N_e}$$

$$m_p^{(e)} = \langle \psi_p, M_z \rangle = \frac{L^{(e)}}{2}\sum_{n=0}^{N_H} w_n^{(N_H)} M_z(x_n,t)\psi_p(\xi_n) = \frac{L^{(e)} w_p^{(N_H)} M_z(x_p,t)}{2}$$

for smooth sources, where the M_z term has been evaluated by integration by parts, assuming that the magnetic current at the element boundaries are zero.

For point sources $J_y = J_0(t)\delta(x - x_J)$ and $M_z = M_0(t)\delta(x - x_M)$,

$$\begin{aligned}
j_p^{(e)} &= J_0(t)\phi_p(\xi(x_J)) + \frac{2E_{yL}^{inc}(a,t)}{\eta_L}\delta_{p,0}\delta_{e,1} + \frac{2E_{yR}^{inc}(b,t)}{\eta_R}\delta_{p,N_E}\delta_{e,N_e} \\
m_p^{(e)} &= M_0(t)\psi_p(\xi(x_M))
\end{aligned}$$

But again it's better to used TF/SF formulation or smoothed sources in this case.

The Time Integration for **E** and **H**

By using central differencing we can obtain

$$\begin{aligned}\mathbf{h}^{n+\frac{1}{2}} &= (\mathbf{M}_h + \frac{\Delta t}{2}\mathbf{C}_h)^{-1}[(\mathbf{M}_h - \frac{\Delta t}{2}\mathbf{C}_h)\mathbf{h}^{n-\frac{1}{2}} - \Delta t(\mathbf{S}_e\mathbf{e}^n + \mathbf{m}^n)] \\ \mathbf{e}^{n+1} &= (\mathbf{M}_e + \frac{\Delta t}{2}\mathbf{C}_e)^{-1}[(\mathbf{M}_e - \frac{\Delta t}{2}\mathbf{C}_e)\mathbf{e}^n + \Delta t(\mathbf{S}_h\mathbf{h}^{n+\frac{1}{2}} - \mathbf{j}^{n+\frac{1}{2}})]\end{aligned}$$

Note the diagonal elemental matrices for $\mathbf{M}_e$, $\mathbf{M}_h$, $\mathbf{C}_e$ and $\mathbf{C}_h$, so the above matrix inversion is trivial and efficient.

Remarks: Higher order (such as the 4th-order) Runge-Kutta methods can be used to improve time integration accuracy.

1.5.3. The SETD Method for 1st-Order EB Equations

The above discussions hint a better 1-D time domain EM system based on EB (or similarly DH) fields

$$\frac{\partial B_z}{\partial t} = -\frac{\partial E_y}{\partial x} - \sigma_m \mu^{-1} B_z - M_z \tag{1.129}$$

$$\epsilon\frac{\partial E_y}{\partial t} = -\frac{\partial \mu^{-1} B_z}{\partial x} - \sigma_e E_y - J_y \tag{1.130}$$

Spectral element expansion within each element (note the continuity between elements)

$$E_y(x,t) = \sum_{n=0}^{N_E} e_n(t)\phi_n(x), \quad B_z(x,t) = \sum_{n=0}^{N_B} b_n(t)\psi_n(x) \tag{1.131}$$

where in fact B_z does not need to be continuous between elements in 1D, so here $\psi_n(x)$ is only defined within each element.

Weak Form Equations

Integration by parts for the magnetic field yields the weak form equations

$$\langle \psi_m, \frac{\partial B_z}{\partial t} \rangle_\Omega = -\langle \psi_m, \frac{\partial E_y}{\partial x} - \sigma_m \mu^{-1} B_z - M_z \rangle_\Omega \quad (1.132)$$

$$\langle \phi_m, \epsilon \frac{\partial E_y}{\partial t} \rangle_\Omega = \langle \frac{\partial \phi_m}{\partial x}, \mu^{-1} B_z \rangle_\Omega + \langle \phi_m, \sigma_e E_y + J_y \rangle_\Omega - \frac{[\phi_m(-2E_{yR}^{inc} + E_y)]_b}{\eta_R} - \frac{[\phi_m(2E_{yL}^{inc} - E_y)]_a}{\eta_L} \quad (1.133)$$

The above boundary terms are zero for PEC and PMC outer boundaries. Furthermore, removal of the corresponding E unknowns on the PEC boundary is needed.

The System Equation in Time Domain

$$\mathbf{M}_e \dot{\mathbf{e}} = \mathbf{S}_b \mathbf{b} - \mathbf{C}_e \mathbf{e} - \mathbf{j} \quad (1.134)$$

$$\mathbf{M}_b \dot{\mathbf{b}} = -\mathbf{S}_e \mathbf{e} - \mathbf{C}_b \mathbf{b} - \mathbf{m} \quad (1.135)$$

The elemental SETD matrices are:

$$M_{e,pq}^{(e)} = \langle \phi_p, \epsilon \phi_q \rangle_{\Omega_e} = \frac{1}{2} w_p^{(N_E)} L^{(e)} \epsilon(x_p) \delta_{p,q}$$

$$M_{b,pq}^{(e)} = \langle \psi_p, \psi_q \rangle_{\Omega_e} = \frac{1}{2} w_p^{(N_B)} L^{(e)} \delta_{p,q}$$

$$C_{e,pq}^{(e)} = \langle \phi_p, \sigma_e \phi_q \rangle_{\Omega_e} + \delta_{e,1} \left[\phi_p \cdot \frac{\phi_0}{\eta_L} \right]_{x=a} + \delta_{e,N_e} \left[\phi_p \cdot \frac{\phi_{N_E}}{\eta_L} \right]_{x=b}$$

$$= \frac{1}{2} w_p^{(N_E)} L^{(e)} \sigma_e(x_p) \delta_{p,q} + \delta_{e,1} \delta_{p,0} / \eta_L + \delta_{e,N_e} \delta_{p,N_E} / \eta_R$$

$$C_{b,p}^{(e)} \langle \psi_p, \sigma_m \mu^{-1} \psi_q \rangle_{\Omega_e} = \frac{\sigma_m(x_p)}{2\mu(x_p)} w_p^{(N_B)} L^{(e)} \delta_{p,q}$$

$$S_{e,pq}^{(e)} = \langle \psi_p, \phi_q' \rangle_{\Omega_e} = w_p^{(N_B)} \phi_q'(\xi_p)$$

$$S_{b,pq}^{(e)} = \langle \phi_p', \mu^{-1} \psi_q \rangle_{\Omega_e} = \sum_{n=0}^{N_E} \frac{w_n^{(N_E)}}{\mu(x_n^{(N_E)})} \phi_p'(\xi_n) \psi_q(\xi_n) \approx \frac{w_p^{(N_B)}}{\mu(x_n^{(N_B)})} \phi_q'(\xi_p)$$

The elemental excitation vectors for smooth sources are

$$\begin{aligned}
j_p^{(e)} &= \langle \phi_p, J_y \rangle + \frac{2E_{yL}^{inc}(a,t)}{\eta_L}\delta_{p,0}\delta_{e,1} + \frac{2E_{yR}^{inc}(a,t)}{\eta_R}\delta_{p,N_E}\delta_{e,N_e} \\
&= \frac{L^{(e)}}{2}\sum_{n=0}^{N_E} w_n^{(N_E)} J_y(x_n,t)\phi_p(\xi_n) \\
&\quad + \frac{2E_{yL}^{inc}(a,t)}{\eta_L}\delta_{p,0}\delta_{e,1} + \frac{2E_{yR}^{inc}(b,t)}{\eta_R}\delta_{p,N_E}\delta_{e,N_e} \\
&= \frac{L^{(e)} w_p^{(N_E)} J_y(x_p,t)}{2} + \frac{2E_{yL}^{inc}(a,t)}{\eta_L}\delta_{p,0}\delta_{e,1} + \frac{2E_{yR}^{inc}(b,t)}{\eta_R}\delta_{p,N_E}\delta_{e,N_e}
\end{aligned}$$

$$m_p^{(e)} = \langle \psi_p, M_z \rangle = \frac{L^{(e)}}{2}\sum_{n=0}^{N_B} w_n^{(N_B)} M_z(x_n,t)\psi_p(\xi_n) = \frac{L^{(e)} w_p^{(N_B)} M_z(x_p,t)}{2}$$

for smooth sources, where the M_z term has been evaluated by integration by parts, assuming that the magnetic current at the element boundaries are zero.

For point sources $J_y = J_0(t)\delta(x - x_J)$ and $M_z = M_0(t)\delta(x - x_M)$,

$$\begin{aligned}
j_p^{(e)} &= J_0(t)\phi_p(\xi(x_J)) + \frac{2E_{yL}^{inc}(a,t)}{\eta_L}\delta_{p,0}\delta_{e,1} + \frac{2E_{yR}^{inc}(b,t)}{\eta_R}\delta_{p,N_E}\delta_{e,N_e} \\
m_p^{(e)} &= M_0(t)\psi_p(\xi(x_M))
\end{aligned}$$

But again it's better to used TF/SF formulation or smoothed sources in this case.

The Time Integration for $\mathbf{E}$ and $\mathbf{B}$

By using central differencing we can obtain

$$\begin{aligned}
\mathbf{b}^{n+\frac{1}{2}} &= (\mathbf{M}_b + \frac{\Delta t}{2}\mathbf{C}_b)^{-1}[(\mathbf{M}_b - \frac{\Delta t}{2}\mathbf{C}_b)\mathbf{b}^{n-\frac{1}{2}} - \Delta t(\mathbf{S}_e\mathbf{e}^n + \mathbf{m}^n)] \\
\mathbf{e}^{n+1} &= (\mathbf{M}_e + \frac{\Delta t}{2}\mathbf{C}_e)^{-1}[(\mathbf{M}_e - \frac{\Delta t}{2}\mathbf{C}_e)\mathbf{e}^n + \Delta t(\mathbf{S}_b\mathbf{b}^{n+\frac{1}{2}} - \mathbf{j}^{n+\frac{1}{2}})]
\end{aligned}$$

Note the diagonal elemental matrices for $\mathbf{M}_e$, $\mathbf{M}_b$, $\mathbf{C}_e$ and $\mathbf{C}_b$, so the above matrix inversion is trivial and efficient.

Remarks: Higher order (such as the 4th-order) Runge-Kutta methods can be used to improve time integration accuracy.

EB Formulation Versus EH Formulation

The EH Formulation

- Basis functions for H_z and E_y both continuous across elements.
- Spurious modes in 3D if $N_H = N_E$ - compatibility issue. How about 1D?
- More unknowns to obtain the N_E-order accuracy, as $N_H = N_E + 1$.
- The $\mathrm{E}_n\mathrm{H}_{n+1}$ scheme.

The EB (or DH) formulation

- Basis functions for B_z discontinuous across elements.
- No spurious modes.
- $N_B = N_E - 1$ produces the N_E-order accuracy.
- Fewer unknowns than the EH formulation.

Thus, the EB formulation is favored.

QHL/DGTD

DUKE EDMUND T. PRATT, JR. SCHOOL OF ENGINEERING

URSI AT-RASC Short Course

Multiscale Computational Electromagnetics in Time Domain

Qing Huo Liu
Department of Electrical and Computer Engineering
Duke University

May 27, 2018

QHL/DGTD

DUKE EDMUND T. PRATT, JR. SCHOOL OF ENGINEERING

Chapter 2
1D Multiscale DGTD Method

- Typical multiscale problems
- Why DGTD method for multiscale problems?
- Conservation form of wave equations
- Subdomain-based DGTD method
- Fluxes at the subdomain interfaces
- Hybrid time integration methods

QHL/DGTD

DUKE EDMUND T. PRATT, JR. SCHOOL OF ENGINEERING

Typical Multiscale Problems

- Wavelength (λ) as the reference scale (in frequency domain, skin depth may be also a scale)
- Coarse scale: $L_c \gg \lambda$
- Fine scale: $L_f \ll \lambda$
- Intermediate scale (L_m) between coarse and fine scales

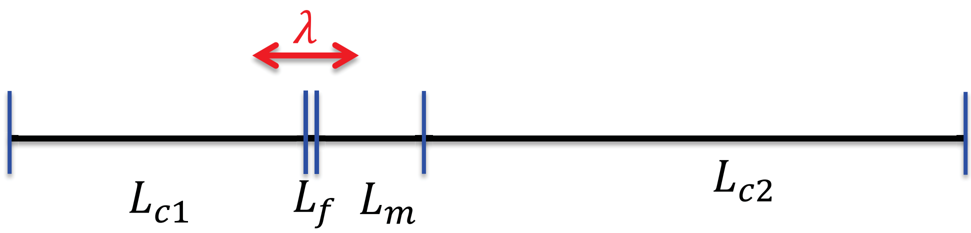

QHL/DGTD

DUKE EDMUND T. PRATT, JR. SCHOOL OF ENGINEERING

Why DGTD method for multiscale problems?

- SETD method efficient for coarse scale, but not fine scale. Why?
- Explicit FETD and FDTD methods are good for intermediate scale, but not fine scale or coarse scale. Why?
- Stability condition of SETD, FETD, and FDTD methods

FDTD: $\Delta t \le \frac{\Delta x}{\sqrt{D} c_{max}}$ Tiny Δt for electrically fine cells

QHL/DGTD

Approach: Multiscale DGTD: Hybridization of SETD and FETD (and/or FDTD)

- Use SETD for the coarse and intermediate scale subdomains
- Use FETD for the fine-scale subdomains

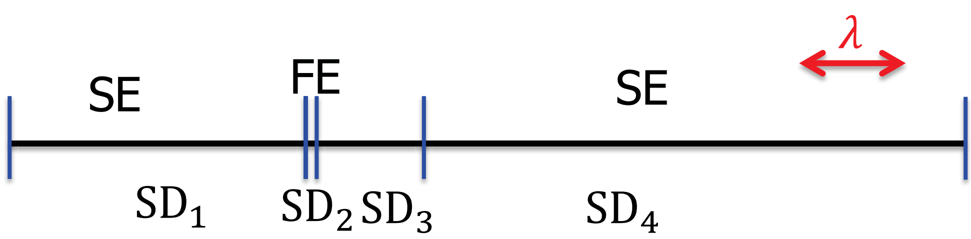

QHL/DGTD

DGTD Method with SETD and FETD

- 1D Maxwell's equations

$$\epsilon \frac{\partial E_y}{\partial t} + \frac{\partial \mu^{-1} B_z}{\partial x} = -\sigma_e E_y - J_y$$

$$\frac{\partial B_z}{\partial t} + \frac{\partial E_y}{\partial x} = -\frac{\sigma_m}{\mu} B_z - M_z$$

- Expansion in the i-th subdomain

$$E_y^i = \sum_n e_n^i \phi_n^i(x),\ B_z^i = \sum_n b_n^i \psi_n^i(x)\ ,\ \psi_n^i\ \mathit{discontinuous}$$

Use Galerkin's method for testing the above equations

QHL/DGTD

Numerical Flux for Interfaces Between Subdomains

- Testing and integration by parts

$$\left\langle \phi_m^i, \epsilon \frac{\partial E_y}{\partial t} + \sigma_e E_y + J_y \right\rangle_{\Omega^\mathrm{i}} = \left\langle \partial_x \phi_m^i, H_z \right\rangle_{\Omega^\mathrm{i}} - \left\langle \phi_m^i, H_z^* \right\rangle_{\partial\Omega^\mathrm{i}}$$

$$\left\langle \psi_m^i, \frac{\partial B_z}{\partial t} + \frac{\sigma_m}{\mu} B_z + M_z \right\rangle_{\Omega^\mathrm{i}} = -\left\langle \psi_m^i, \partial_x E_y \right\rangle_{\Omega^\mathrm{i}} + \left\langle \psi_m^i, (E_y - E_y^*) \right\rangle_{\partial\Omega^\mathrm{i}}$$

Note that twice integration by parts yields the second equation

- (E_y^*, H_z^*) is the numerical flux at subdomain interfaces between adjacent subdomains

DUKE EDMUND T. PRATT, JR. SCHOOL OF ENGINEERING

QHL/DGTD

Numerical Flux 1: Central Flux

- The simplest numerical flux is the central flux by averaging the tangential fields as the tangential E and H should be continuous

$$E_y^* = \frac{1}{2}[E_y^i + E_y^j]$$

$$H_z^* = \frac{1}{2}[H_z^i + H_z^j]$$

- For 3D problems, the central

$$\hat{n}^i \times \mathbf{E}^* = \frac{1}{2}[\hat{n}^i \times \mathbf{E}^i + \hat{n}^i \times \mathbf{E}^j]$$

$$\hat{n}^i \times \mathbf{H}^* = \frac{1}{2}[\hat{n}^i \times \mathbf{H}^i + \hat{n}^i \times \mathbf{H}^j]$$

$$\hat{n}^i \times (\mu^{-1}\mathbf{B})^* = \frac{1}{2}[\hat{n}^i \times \frac{\mathbf{B}^i}{\mu^{(i)}} + \hat{n}^i \times \frac{\mathbf{B}^j}{\mu^{(j)}}]$$

DUKE EDMUND T. PRATT, JR. SCHOOL OF ENGINEERING

QHL/DGTD

Numerical Flux 2: Upwind Flux

- Characteristics in 1D Maxwell's equations

$$\frac{\partial D_y}{\partial t} + \frac{\partial \mu^{-1} B_z}{\partial x} = -\sigma_e E_y - J_y$$
$$\frac{\partial B_z}{\partial t} + \frac{\partial \epsilon^{-1} D_y}{\partial x} = -\frac{\sigma_m}{\mu} B_z - M_z$$

Ignore the losses and source terms

$$\frac{\partial \mathbf{u}}{\partial t} + \frac{\partial (\mathbf{Au})}{\partial x} = 0$$

where $\mathbf{u} = \begin{bmatrix} D_y \\ B_z \end{bmatrix}, \mathbf{A} = \begin{bmatrix} 0 & \epsilon^{-1} \\ \mu^{-1} & 0 \end{bmatrix}$

QHL/DGTD

Eigenvalue Problem of A

- Eigenpair λ and $\mathbf{v}$

$$\mathbf{Av} = \lambda \mathbf{v}$$

- Eigenvalues and eigen vectors

$$\lambda_{1,2} = \pm c \equiv \pm \frac{c_0}{\sqrt{\mu_r \epsilon_r}}, \qquad \Lambda = \begin{bmatrix} \lambda_1 & 0 \\ 0 & \lambda_2 \end{bmatrix}$$
$$v_1 = \begin{bmatrix} \eta \\ 1 \end{bmatrix}, \mathrm{v}_2 = \begin{bmatrix} -\eta \\ 1 \end{bmatrix}$$

- Transformation matrix

$$\mathbf{V} = [v_1 \; v_2\,] = \begin{bmatrix} \eta & -\eta \\ 1 & 1 \end{bmatrix}, \qquad \mathbf{V}^{-1} = \frac{1}{2\eta} \begin{bmatrix} 1 & \eta \\ -1 & \eta \end{bmatrix}$$

QHL/DGTD

Eigenvalue Problem of A (continued)

- Transformation of A by Λ and $\mathbf{V}$

$$\mathbf{AV} = \mathbf{V}\Lambda, \qquad \mathrm{A} = \mathbf{V}\Lambda\mathbf{V}^{-1}$$

- Wave equation

$$\frac{\partial \mathbf{u}}{\partial t} + \frac{\partial(\mathbf{Au})}{\partial x} = 0$$

$$\frac{\partial \tilde{\mathbf{u}}}{\partial t} + \frac{\partial(\boldsymbol{\Lambda}\tilde{\mathbf{u}})}{\partial x} = 0$$

- Characteristics for $\lambda_{1,2} = \pm c$

$$\tilde{\mathbf{u}}_{1,2} = \mathbf{V}^{-1}\mathbf{u} = \tilde{\mathbf{u}}\left(t - \frac{x}{\lambda_{1,2}}\right) = \tilde{\mathbf{u}}\left(t \mp \frac{x}{c}\right)$$

QHL/DGTD

Alternative Derivation

- Characteristics in 1D Maxwell's equations

$$\epsilon\frac{\partial E_y}{\partial t} + \frac{\partial H_z}{\partial x} = -\sigma_e E_y - J_y$$
$$\mu\frac{\partial H_z}{\partial t} + \frac{\partial E_y}{\partial x} = -\frac{\sigma_m}{\mu} B_z - M_z$$

Ignore the losses and source terms

$$\mathbf{M}\frac{\partial \mathbf{u}}{\partial t} + \mathbf{A}\frac{\partial \mathbf{u}}{\partial x} = 0$$

where $\mathbf{u} = \begin{bmatrix} E_y \\ H_z \end{bmatrix}, \mathbf{M} = \begin{bmatrix} \epsilon & 0 \\ 0 & \mu \end{bmatrix}, \mathbf{A} = \begin{bmatrix} 0 & 1 \\ 1 & 0 \end{bmatrix}$

QHL/DGTD

Eigenvalue Problem of A

- Eigenpair λ and $\mathbf{v}$

$$\mathbf{M}^{-1}\mathbf{A}\mathbf{v} = \lambda\mathbf{v}$$

- Eigenvalues and eigen vectors

$$\lambda_{1,2} = \pm c \equiv \pm\frac{c_0}{\sqrt{\mu_r \epsilon_r}}, \qquad \Lambda = \begin{bmatrix}\lambda_1 & 0\\ 0 & \lambda_2\end{bmatrix}$$

$$v_1 = \begin{bmatrix}\eta\\ 1\end{bmatrix}, \mathrm{v}_2 = \begin{bmatrix}-\eta\\ 1\end{bmatrix}$$

- Transformation matrix

$$\mathbf{V} = [v_1\ v_2\ ] = \begin{bmatrix}\eta & -\eta\\ 1 & 1\end{bmatrix}, \qquad \mathbf{V}^{-1} = \frac{1}{2\eta}\begin{bmatrix}1 & \eta\\ -1 & \eta\end{bmatrix}$$

QHL/DGTD

Eigenvalue Problem of A (continued)

- Transformation of A by Λ and $\mathbf{V}$

$$\mathbf{AV} = \mathbf{V}\Lambda, \qquad \mathrm{A} = \mathbf{V}\Lambda\mathbf{V}^{-1}$$

- Wave equation

$$\frac{\partial\mathbf{u}}{\partial t} + \mathbf{A}\frac{\partial\mathbf{u}}{\partial x} = 0$$

$$\frac{\partial\tilde{\mathbf{u}}}{\partial t} + \frac{\partial(\boldsymbol{\Lambda}\tilde{\mathbf{u}})}{\partial x} = 0$$

- Characteristics for $\lambda_{1,2} = \pm c$

$$\tilde{\mathbf{u}}_{1,2} = \mathbf{V}^{-1}\mathbf{u} = \tilde{\mathbf{u}}\left(t - \frac{x}{\lambda_{1,2}}\right) = \tilde{\mathbf{u}}\left(t \mp \frac{x}{c}\right)$$

Characteristics and Riemann Solver

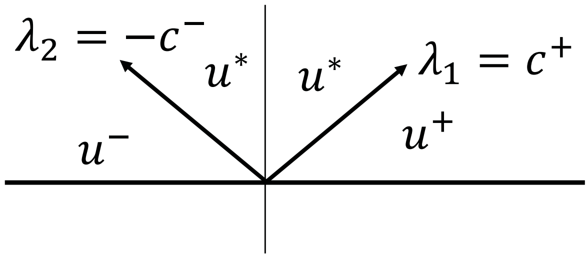

- Riemann Solver: For all characteristic i

$$-\lambda_i \mathbf{M}[\mathbf{u}^- - \mathbf{u}^+] + [(\mathbf{Au})^- - (\mathbf{Au})^+] = 0$$

Applying this to $i = 1,2$ yields

$$c^-\mathbf{M}^-[\mathbf{u}^* - \mathbf{u}^-] + [(\mathbf{Au})^* - (\mathbf{Au})^-] = 0$$
$$-c^+\mathbf{M}^+[\mathbf{u}^* - \mathbf{u}^+] + [(\mathbf{Au})^* - (\mathbf{Au})^+] = 0$$

Upwind Flux

Combining the two yields

$$(c^-\mathbf{M}^- + c^+\mathbf{M}^+)(\mathbf{Au})^*$$
$$= c^-\mathbf{M}^-(\mathbf{Au})^+ + c^+\mathbf{M}^+(\mathbf{Au})^- + c^-c^+\mathbf{M}^-\mathbf{M}^+[\mathbf{u}^- - \mathbf{u}^+]$$

Upwind Flux

$$E_y^* = \frac{Y^-E_y^- + Y^+E_y^+}{Y^- + Y^+} + \frac{H_z^+ - H_z^-}{Y^- + Y^+}$$

$$H_z^* = \frac{Z^-H_z^- + Z^+H_z^+}{Z^- + Z^+} + \frac{E_y^+ - E_y^-}{Z^- + Z^+}$$

QHL/DGTD

Upwind Flux in 3D

$$\hat{\boldsymbol{n}}_i \times \mathbf{E}^* = \frac{\hat{\boldsymbol{n}}_i \times (Y^i\mathbf{E}^i + Y^j\mathbf{E}^j)}{Y^i + Y^j} + \frac{\hat{\boldsymbol{n}}_i \times \hat{\boldsymbol{n}}_i \times (\mu^i\mathbf{B}^j - \mu^j\mathbf{B}^i)}{\mu^i\,\mu^j(Y^i+Y^j)}$$

$$\hat{\boldsymbol{n}}_i \times \mathbf{H}^* = \frac{\hat{\boldsymbol{n}}_i \times (\mu^j Z^i\mathbf{B}^i + \mu^i Z^j\mathbf{B}^j)}{\mu^i\,\mu^j(Z^i+Z^j)} + \frac{\hat{\boldsymbol{n}}_i \times \hat{\boldsymbol{n}}_i \times (\mathbf{E}^j - \mathbf{E}^i)}{(Z^i+Z^j)}$$

QHL/DGTD

Solution of 1D Equations with DGTD

- Testing and integration by parts

$$\left\langle \phi_m^i, \epsilon\frac{\partial E_y^i}{\partial t} + \sigma_e E_y^i + J_y \right\rangle_{\Omega^i} = \langle \partial_x\phi_m^i, H_z\rangle_{\Omega^i} - \langle \phi_m^i, H_z^*\rangle_{\partial\Omega^i}$$

$$\left\langle \psi_m^i, \frac{\partial B_z^i}{\partial t} + \frac{\sigma_m}{\mu} B_z^i + M_z \right\rangle_{\Omega^i} = -\langle \psi_m^i, \partial_x E_y^i\rangle_{\Omega^i} - \langle \psi_m^i, E_y^* - E_y^i\rangle_{\partial\Omega^i}$$

- (E_y^*, H_z^*) are now replaced by the numerical flux

$$E_y^* = \frac{Y^iE_y^i + Y^jE_y^j}{Y^i+Y^j} + \frac{H_z^j - H_z^i}{Y^i+Y^j} \equiv (a_{ee}^{ii}+1)E_y^i + a_{eb}^{ii}B_z^i + a_{ee}^{ij}B_y^j + a_{eb}^{ij}\,B_z^j$$

$$H_z^* = \frac{Z^iH_z^i + Z^jH_z^j}{Z^i+Z^j} + \frac{E_y^j - E_y^i}{Z^i+Z^j} \equiv a_{bb}^{ii}B_z^i + a_{be}^{ii}E_y^i + a_{be}^{ij}E_y^j + a_{bb}^{ij}\,B_z^j$$

QHL/DGTD

- Coefficients

$$a_{ee}^{ii} = \frac{Y^i}{Y^i + Y^j} - 1, \qquad a_{eb}^{ii} = -\frac{1}{\mu^i(Y^i + Y^j)}$$

$$a_{ee}^{ij} = \frac{Y^j}{Y^i + Y^j}, \qquad a_{eb}^{ij} = \frac{1}{\mu^j(Y^i + Y^j)}$$

$$a_{bb}^{ii} = \frac{Z^i/\mu^i}{Z^i + Z^j}, \qquad a_{be}^{ii} = -\frac{1}{(Z^i + Z^j)}$$

$$a_{bb}^{ij} = \frac{Z^j/\mu^j}{Z^i + Z^j}, \qquad a_{be}^{ij} = \frac{1}{(Z^i + Z^j)}$$

QHL/DGTD

- Final weak form equations

$$\left\langle \phi_m^i, \epsilon \frac{\partial E_y^i}{\partial t} + \sigma_e E_y^i + J_y \right\rangle_{\Omega^i}$$

$$= \left\langle \partial_x \phi_m^i, \left(\mu^i\right)^{-1} B_z \right\rangle_{\Omega^i} - \left\langle \phi_m^i, a_{bb}^{ii} B_z^i + a_{be}^{ij} E_y^i + a_{be}^{ij} E_y^j + a_{bb}^{ij} B_z^j \right\rangle_{\partial\Omega^i}$$

$$\left\langle \psi_m^i, \frac{\partial B_z^i}{\partial t} + \frac{\sigma_m}{\mu} B_z^i + M_z \right\rangle_{\Omega^i}$$

$$= -\left\langle \psi_m^i, \partial_x E_y^i \right\rangle_{\Omega^i} - \left\langle \psi_m^i, a_{ee}^{ii} E_y^i + a_{eb}^{ii} B_z^i + a_{ee}^{ij} E_y^j + a_{eb}^{ij} B_z^j \right\rangle_{\partial\Omega^i}$$

QHL/DGTD

- (E_y, H_z) are expanded in terms basis functions

$$E_y^{i,j} = \sum_{n=0}^{N_E^{i,j}} e_n^{i,j}(t)\phi_m^i(x),\ B_z^{i,j} = \sum_{n=0}^{N_B^{i,j}} b_n^{i,j}(t)\psi_m^i(x)$$

- Then we obtain the system equations

$$\mathbf{M}_{ee}^i \frac{\partial \mathbf{e}^i}{\partial t} = \mathbf{S}_{eb}^i \mathbf{b}^i - \mathbf{C}_{ee}^i \mathbf{e}^i - \mathbf{j}^i - \sum_j (\mathbf{A}_{be}^{ij} \mathbf{e}^j + \mathbf{A}_{bb}^{ij} \mathbf{b}^j)$$

$$\mathbf{M}_{bb}^i \frac{\partial \mathbf{b}^i}{\partial t} = -\mathbf{S}_{be}^i \mathbf{e}^i - \mathbf{C}_{bb}^i \mathbf{b}^i - \mathbf{m}^i - \sum_j (\mathbf{A}_{ee}^{ij} \mathbf{e}^j + \mathbf{A}_{eb}^{ij} \mathbf{b}^j)$$

QHL/DGTD

- Then we obtain the system equations for all subdomains $i = 1, \cdots, N_{sub}$

$$\mathbf{M}^i \frac{\partial \mathbf{v}^i}{\partial t} = -\sum_j \mathbf{L}^{ij} \mathbf{v}^j - \mathbf{f}^i$$

- Here the matrices are

$$\mathbf{v}^i = \begin{bmatrix} \mathbf{e}^i \\ \mathbf{b}^i \end{bmatrix}, \mathbf{f}^i = \begin{bmatrix} \mathbf{j}^i \\ \mathbf{m}^i \end{bmatrix}$$

$$\mathbf{M}^i = \begin{bmatrix} \mathbf{M}_{ee}^i & 0 \\ 0 & \mathbf{M}_{bb}^i \end{bmatrix}, \mathbf{L}^{ij} = \begin{bmatrix} \mathbf{A}_{be}^{ij} + \delta_{ij} \mathbf{C}_{ee}^i & \mathbf{A}_{bb}^{ij} - \delta_{ij} \mathbf{S}_{eb}^i \\ \mathbf{A}_{ee}^{ij} + \delta_{ij} \mathbf{S}_{be}^i & \mathbf{A}_{eb}^{ij} + \delta_{ij} \mathbf{C}_{bb}^i \end{bmatrix}$$

Hybrid Time Integration: s-Stage Explicit + Implicit

- Explicit Runge-Kutta Method for Coarse Subdomains

$$\mathbf{v}_{n+1}^{i} = \mathbf{v}_{n}^{i} + \Delta t \sum_{k=1}^{s} b_k \mathbf{u}_k^{i}$$

$$\mathbf{M}^{i}\mathbf{u}_k^{i} = -\sum_{j=1}^{N_{sub}} \mathbf{L}^{ij}\left(\mathbf{v}_n^{j} + \Delta \mathbf{t} \sum_{\ell=1}^{k-1} a_{k,\ell}\mathbf{u}_\ell^{j}\right) - \mathbf{f}^{i}(t_n + c_k \Delta t)$$

- Butcher Tableau

$$\begin{array}{c|cccccc}
0 & 0 & 0 & \dots & \dots & 0 \\
c_2 & a_{2,1} & 0 & \ddots & \ddots & \vdots \\
c_3 & a_{3,1} & a_{3,2} & 0 & \ddots & \vdots \\
\vdots & \vdots & \vdots & \vdots & \ddots & 0 \\
c_s & a_{s,1} & a_{s,2} & \dots & a_{s,s-1} & 0 \\
\hline
 & b_1 & b_2 & b_3 & \dots & b_s
\end{array}$$

- Explicit Singly Diagonally Implicit RK (ESDIRK) Butcher Tableau

$$\begin{array}{c|cccccc}
0 & a_{1,1}^{\text{im}} & 0 & \dots & \dots & 0 \\
c_2 & a_{2,1}^{\text{im}} & a_{2,2}^{\text{im}} & 0 & \ddots & \vdots \\
c_3 & a_{3,1}^{\text{im}} & a_{3,2}^{\text{im}} & a_{3,3}^{\text{im}} & \ddots & \vdots \\
\vdots & \vdots & \vdots & \vdots & \ddots & 0 \\
c_s & a_{s,1}^{\text{im}} & a_{s,2}^{\text{im}} & \dots & a_{s,s-1}^{\text{im}} & a_{s,s}^{\text{im}} \\
\hline
 & b_1 & b_2 & b_3 & \dots & b_s
\end{array}$$

- Coefficients *b* and *c* are exactly the same for Ex-RK and ESDIRK

QHL/DGTD

IMEX Time Integration

- Implicit Runge-Kutta Method for Fine Subdomains

$$\mathbf{v}_{n+1}^{i} = \mathbf{v}_{n}^{i} + \Delta t \sum_{k=1}^{s} b_k \mathbf{u}_k^i\,, \qquad i = 1, \cdots, N_{sub} = N_{im} + N_{ex}$$

$$\mathbf{M}^i \mathbf{u}_k^i = -\sum_{j=1}^{N_{im}} \mathbf{L}^{ij} \left(\mathbf{v}_n^j + \Delta t \sum_{\ell=1}^{k} a_{k,\ell}^{im} \mathbf{u}_\ell^j \right) - \mathbf{f}^i \left(t_n + c_k \Delta t\right)$$

$$- \sum_{j=N_{im}+1}^{N_{sub}} \mathbf{L}^{ij} \left(\mathbf{v}_n^j + \Delta t \sum_{\ell=1}^{k-1} a_{k,\ell}^{ex} \mathbf{u}_\ell^j \right)$$

- Need to invert a system matrix for the IM part

QHL/DGTD

Popular Explicit Time Integration Schemes

$$\dot{y} = f(t, y), \qquad y(t_0) = y_0$$

1. Second-Order RK Methods

$$\begin{array}{c|cc} 0 & & \\ \alpha & \alpha & \\ \hline & (1-\frac{1}{2\alpha}) & \frac{1}{2\alpha} \end{array}$$

$$y_{n+1} = y_n + h[(1 - \frac{1}{2\alpha}) f(t_n, y_n) + \frac{1}{2\alpha} f\big(t_n + \alpha h, y_n + \alpha h f(t_n, y_n)\big)]$$

2. The mid-point method is a special case with $\alpha = \frac{1}{2}$

$$\begin{array}{c|cc} 0 & & \\ 1/2 & 1/2 & \\ \hline & 0 & 1 \end{array}$$

$$y_{n+1} = y_n + hf\left(t_n + \frac{h}{2}, y_n + \frac{h}{2} f(t_n, y_n)\right)$$

QHL/DGTD

3. Fourth-Order 4-Stage RK Method

0				
1/2	1/2			
1/2	0	1/2		
1	0	0	1	
	1/6	1/3	1/3	1/6

$$k_1 = f(t_n, y_n)$$

$$k_2 = f\left(t_n + \frac{h}{2}, y_n + \frac{h}{2}k_1\right)$$

$$k_3 = f\left(t_n + \frac{h}{2}, y_n + \frac{h}{2}k_2\right)$$

$$k_4 = f(t_n + h, y_n + hk_3)$$

$$y_{n+1} = y_n + h\sum_{i=1}^{4} b_i k_i = y_n + \frac{h}{6}(k_1 + 2k_2 + 2k_3 + k_4)$$

QHL/DGTD

Popular Implicit Time Integration Schemes

$$\dot{y} = f(t, y), \qquad y(t_0) = y_0$$

1. Second-Order Implicit RK Method – Trapezoidal Rule

0	**0**	**0**
1	1/2	1/2
	1/2	1/2

$$k_1 = f(t_n, y_n)$$

$$k_2 = f\left(t_n + \frac{h}{2}, y_n + \frac{h}{2}(k_1 + k_2)\right)$$

$$y_{n+1} = y_n + \frac{h}{2}(k_1 + k_2)$$

QHL/DGTD

Popular Hybrid IMEX Time Integration Schemes

$$\dot{y} = f(t, y), \qquad y(t_0) = y_0$$

DUKE EDMUND T. PRATT, JR. SCHOOL OF ENGINEERING

1. Second-Order IMEX RK Method

First perform time integration in explicit subdomains $(\alpha = 1)$

0	**0**	**0**
1	1	0
EX	1/2	1/2

$$k_1^{ex} = f^{ex}(t_n, y_n)$$

$$k_2^{ex} = f^{ex}(t_n + h, y_n^{ex} + hk_1^{ex})$$

$$y_{n+1}^{ex} = y_n^{ex} + \frac{h}{2}(k_1^{ex} + k_2^{ex})$$

Then in implicit subdomains

0	**0**	**0**
1	1/2	1/2
IM	1/2	1/2

$$k_1^{im} = f^{im}(t_n, y_n)$$

$$k_2^{im} = f^{im}\left(t_n + h, y_n^{im} + \frac{h}{2}(k_1^{im} + k_2^{im})\right)$$

$$y_{n+1}^{im} = y_n^{im} + \frac{h}{2}(k_1^{im} + k_2^{im})$$

QHL/DGTD

Popular Hybrid IMEX Time Integration Schemes

$$\dot{y} = f(t, y), \qquad y(t_0) = y_0$$

DUKE EDMUND T. PRATT, JR. SCHOOL OF ENGINEERING

2. Fourth-Order IMEX RK Method

First perform time integration in explicit subdomains

$$k_1^{ex} = f^{ex}(t_n, y_n)$$

$$k_i^{ex} = f^{ex}\left(t_n + c_i h, y_n^{ex} + h\sum_{j=1}^{i-1} a_{ij}^{ex} k_j^{ex}\right), i = 2,3,4$$

$$y_{n+1}^{ex} = y_n^{ex} + h(b_1 k_1^{ex} + b_2 k_2^{ex} + b_3 k_3^{ex} + b_4 k_4^{ex})$$

Then in implicit subdomains

$$k_1^{im} = f^{im}(t_n, y_n)$$

$$k_i^{im} = f^{im}\left(t_n + c_i h, y_n^{im} + h\sum_{j=1}^{i-1} a_{ij}^{im} k_j^{im} + h a_{ii}^{im} k_i^{im}\right), i = 2,3,4$$

$$y_{n+1}^{im} = y_n^{im} + h\left(b_1 k_1^{im} + b_2 k_2^{im} + b_3 k_3^{im} + b_4 k_4^{im}\right)$$

QHL/DGTD

DUKE
EDMUND T. PRATT, JR. SCHOOL OF ENGINEERING

Butcher Tableau for the Fourth-Order Hybrid IMEX Time Integration Scheme

$c_1 = 0$				
$c_2 = 1767732205903/2027836641118$	$a_{21} = 1767732205903/4055673282236$	$a_{22} = 1767732205903/4055673282236$		
$c_3 = 3/5$	$a_{31} = 2746238789719/10658868560708$	$a_{32} = -640167445237/6845629431997$	$a_{33} = 1767732205903/4055673282236$	
$c_4 = 1$	$a_{41} = 1471266399579/7840856788654$	$a_{42} = -4482444167858/7529755066697$	$a_{43} = 11266239266428/11593286722821$	$a_{44} = 1767732205903/4055673282236$
IM	$b_1 = 1471266399579/7840856788654$	$b_2 = -4482444167858/7529755066697$	$b_3 = 11266239266428/11593286722821$	$b_4 = 1767732205903/4055673282236$

$c_1 = 0$				
$c_2 = 1767732205903/2027836641118$	$a_{21} = 1767732205903/2027836641118$			
$c_3 = 3/5$	$a_{31} = 5535828885825/10492691773637$	$a_{32} = 788022342437/10882634858940$		
$c_4 = 1$	$a_{41} = 6485989280629/16251701735622$	$a_{42} = -4246266847089/9704473918619$	$a_{43} = 10755448449292/10357097424841$	
EX	$b_1 = 1471266399579/7840856788654$	$b_2 = -4482444167858/7529755066697$	$b_3 = 11266239266428/11593286722821$	$b_4 = 1767732205903/4055673282236$

QHL/DGTD

DUKE
EDMUND T. PRATT, JR. SCHOOL OF ENGINEERING

Summary

- 1D DGTD methods include “element-based DGTD” and “subdomain-based DGTD” methods
- Element-based DGTD method has one element per subdomain.
- Subdomain-based DGTD method has multiple elements per subdomain, thus can have fewer DoFs than the element-based DGTD method.
- Element-based DGTD can be considered a special case of subdomain-based DGTD method when the number of elements becomes one.

QHL/DGTD

URSI AT-RASC Short Course

Multiscale Computational Electromagnetics in Time Domain

Qing Huo Liu

Department of Electrical and Computer Engineering

Duke University

May 27, 2018

QHL/DGTD

Chapter 3. 3D DGTD Methods

- References: Duke Ph.D. dissertations and related papers (Q. H. Liu Group)
  - Tian Xiao (Ph.D. 2004)
  - Gang Zhao (Ph.D. 2005)
  - Jiefu Chen (Ph.D. 2010)
  - Luis Tobon (Ph.D. 2013)
  - Qiang Ren (Ph.D. 2015)
  - Qingtao Sun (Ph.D. 2017)
- Following slides are adapted from the slides in these Ph.D. defenses.

QHL/DGTD

Outline

- Nodal DGTD Methods
  - DGTD and DG-PSTD Methods
- Subdomain DGTD Method with EH Fields
- Subdomain DGTD Method with EB Fields
- Comparison of Various DGTD Methods

QHL/DGTD

Governing Equations

Maxwell's Equations

Topological Laws

$$\boxed{\begin{aligned} \frac{\partial \mathbf{D}}{\partial t} &= \nabla \times \mathbf{H} - \mathbf{J}_c - \mathbf{J}_s \\ -\frac{\partial \mathbf{B}}{\partial t} &= \nabla \times \mathbf{E} + \mathbf{M}_c + \mathbf{M}_s \end{aligned}}$$

$$\nabla \cdot \mathbf{D} = \rho_e$$

$$\nabla \cdot \mathbf{B} = \rho_m$$

Constitutive Relations

$$\mathbf{D} = \epsilon \mathbf{E}$$

$$\mathbf{B} = \mu \mathbf{H}$$

$$\mathbf{J}_c = \sigma_e \mathbf{E}$$

$$\mathbf{M}_c = \sigma_m \mathbf{H}$$

QHL/DGTD

3.1 Nodal DGTD Methods

- Nodal DGTD Methods with Tetrahedron Elements
  - Tian Xiao, High-order/Spectral Methods For Transient Wave Equations, Ph.D. Dissertation, Duke University, 2004.
  - T. Xiao, and Q. H. Liu, "Three-dimensional unstructured-grid discontinuous Galerkin method for Maxwell's equations with well-posed perfectly matched layer," Microwave Opt. Technol. Lett., vol. 46, no. 5, pp. 459-463, 2005.
- Nodal DGTD Methods with Hexahedron Elements
  - Gang Zhao, The 3-D Multi-Domain Pseudospectral Time-domain Method For Electromagnetic Modeling, Ph.D. Dissertation, Duke University, 2005.
  - Q. H. Liu, and G. Zhao, "Advances in PSTD Techniques." Chapter 17, Computational Electromagnetics: The Finite-Difference Time-Domain Method, A. Taflove, and S. Hagness, Artech House, Inc., 2005.

QHL/DGTD

FEM and Spectral-Based DGTD Methods

- Nodal Discontinuous Galerkin Time Domain Method
  - FEM basis and testing functions
  - Spectral nodal basis and testing functions
- Discontinuous approximation across element interfaces
  - Face-based communication between adjacent elements
  - Support *hp* adaptivity
    - Spectral accuracy with *p*
    - High-order accuracy with *h*
  - Amenable to parallel computation
  - Weakly enforcement of differential equations and B.C.s

Nodal DGTD Method

- Domain Decomposition
- General Formulation

Maxwell

$$\frac{\partial(\mu\mathbf{H})}{\partial t} = -\nabla \times \mathbf{E},$$

$$\frac{\partial(\epsilon\mathbf{E})}{\partial t} = \nabla \times \mathbf{H} - \sigma\mathbf{E}.$$

Nodal Basis

$$\mathbf{E}(\mathbf{x},t) \approx \sum_{j=1}^{N} \mathbf{E}_j(t)L_j(\mathbf{x}),$$

$$\mathbf{H}(\mathbf{x},t) \approx \sum_{j=1}^{N} \mathbf{H}_j(t)L_j(\mathbf{x}),$$

Testing

$$\int_D \left(\frac{\partial(\mu\mathbf{H})}{\partial t} + \nabla \times \mathbf{E}\right) L_i(\mathbf{x})dv = 0,$$

$$\int_D \left(\frac{\partial(\epsilon\mathbf{E})}{\partial t} - \nabla \times \mathbf{H} + \sigma\mathbf{E}\right) L_i(\mathbf{x})dv = 0.$$

Nodal DGTD Methods

- Each element is one subdomain
- Scalar basis functions can be used
- At an interface between two elements, the DoFs are redundant (thus more DoFs than continuous Galerkin)

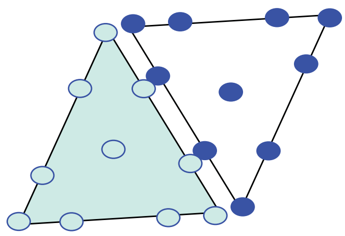

QHL/DGTD

$$\int_D L_i \nabla \times \mathbf{E} dv = \int_D \nabla \times (L_i \mathbf{E}) dv - \int_D \nabla L_i \times \mathbf{E} dv.$$

$$\int_D \nabla \times (L_i \mathbf{E}) dv = \oint_{\delta D} L_i \hat{\mathbf{n}} \times \mathbf{E}^* |ds|,$$

$$\int_D L_i \nabla \times \mathbf{E} dv = \oint_{\delta D} L_i \hat{\mathbf{n}} \times \mathbf{E}^* |ds| - \int_D \nabla L_i \times \mathbf{E} dv.$$

Integrate by parts

$$\hat{\mathbf{n}} \times \mathbf{E}^*|_{\delta D} = \hat{\mathbf{n}} \times \frac{(Y\mathbf{E} - \hat{\mathbf{n}} \times \mathbf{H})^- + (Y\mathbf{E} + \hat{\mathbf{n}} \times \mathbf{H})^+}{Y^- + Y^+},$$

$$\hat{\mathbf{n}} \times \mathbf{H}^*|_{\delta D} = \hat{\mathbf{n}} \times \frac{(Z\mathbf{H} + \hat{\mathbf{n}} \times \mathbf{E})^- + (Z\mathbf{H} - \hat{\mathbf{n}} \times \mathbf{E})^+}{Z^- + Z^+},$$

Upwind Flux

QHL/DGTD

Upwind Flux for 2D (Similar for 3D)

$$\begin{pmatrix} H^n \\ H^\tau \\ E^z \end{pmatrix} = \begin{pmatrix} \cos\theta & \sin\theta & 0 \\ -\sin\theta & \cos\theta & 0 \\ 0 & 0 & 1 \end{pmatrix} \begin{pmatrix} H^x \\ H^y \\ E^z \end{pmatrix}$$

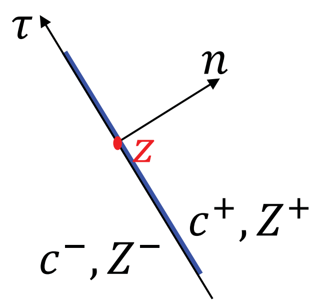

$$\mu \frac{\partial H^n}{\partial t} = -\frac{\partial E^z}{\partial \tau}, \qquad \mu \frac{\partial H^\tau}{\partial t} = \frac{\partial E^z}{\partial n}, \qquad \varepsilon \frac{\partial E^z}{\partial t} = \frac{\partial H^\tau}{\partial n} - \frac{\partial H^n}{\partial \tau}$$

$$\mathbf{M}\frac{\partial \mathbf{u}}{\partial t} + \mathbf{A}\frac{\partial \mathbf{u}}{\partial n} + \mathbf{B}\frac{\partial \mathbf{u}}{\partial \tau} = 0$$

$$\begin{pmatrix} W_1 \\ W_2 \\ W_3 \end{pmatrix} = \mathbf{S}^{-1} \begin{pmatrix} H^\tau \\ E^z \\ H^n \end{pmatrix} \qquad \mathbf{S} = \begin{pmatrix} -\eta & \eta & 0 \\ 1 & 1 & 0 \\ 0 & 0 & 1 \end{pmatrix}$$

$\lambda_{1,2,3} = c, -c, 0$ for $\mathrm{M}^{-1}\mathrm{A}$

Upwind components W_{1-} and W_{2+} are not affected by interface.
W_{2-} and W_{1+} are modified by the interface through BCs

$$\begin{pmatrix} E^z_- \\ H^\tau_- \end{pmatrix} = \begin{pmatrix} E^z_+ \\ H^\tau_+ \end{pmatrix}$$

$$\begin{pmatrix} -\eta_- & \eta_- \\ 1 & 1 \end{pmatrix} \begin{pmatrix} W_{1-} \\ W^c_{2-} \end{pmatrix} = \begin{pmatrix} -\eta_+ & \eta_+ \\ 1 & 1 \end{pmatrix} \begin{pmatrix} W^c_{1+} \\ W_{2+} \end{pmatrix}$$

QHL/DGTD

$$\begin{pmatrix} E_c^z \\ H_c^\tau \end{pmatrix} = \begin{pmatrix} E_\pm^z \\ H_\pm^\tau \end{pmatrix} = \begin{pmatrix} -\eta_\pm & \eta_\pm \\ 1 & 1 \end{pmatrix} \begin{pmatrix} W_{1\pm}^c \\ W_{2\pm}^c \end{pmatrix},$$

where $W_{1-}^c = W_{1-}$ and $W_{2+}^c = W_{2+}$.

$W_3 = H^n$ is a non-propagating wave and does not need to be corrected.

$$E_z^* = \frac{Y^- E_z^- + Y^+ E_z^+}{Y^- + Y^+} + \frac{H_\tau^+ - H_\tau^-}{Y^- + Y^+}$$

$$H_\tau^* = \frac{Z^- H_\tau^- + Z^+ H_\tau^+}{Z^- + Z^+} + \frac{E_z^+ - E_z^-}{Z^- + Z^+}$$

$$\begin{pmatrix} H_{\pm,c}^x \\ H_{\pm,c}^y \\ E_{\pm,c}^z \end{pmatrix} = \begin{pmatrix} \cos\theta & -\sin\theta & 0 \\ \sin\theta & \cos\theta & 0 \\ 0 & 0 & 1 \end{pmatrix} \begin{pmatrix} H_c^\tau \\ H_\pm^n \\ E_c^z \end{pmatrix}$$

QHL/DGTD

Upwind Flux for 3D

$$\boxed{\begin{aligned} \hat{\mathbf{n}} \times \mathbf{E}^*|_{\delta D} &= \hat{\mathbf{n}} \times \frac{(Y\mathbf{E} - \hat{\mathbf{n}} \times \mathbf{H})^- + (Y\mathbf{E} + \hat{\mathbf{n}} \times \mathbf{H})^+}{Y^- + Y^+}, \\ \hat{\mathbf{n}} \times \mathbf{H}^*|_{\delta D} &= \hat{\mathbf{n}} \times \frac{(Z\mathbf{H} + \hat{\mathbf{n}} \times \mathbf{E})^- + (Z\mathbf{H} - \hat{\mathbf{n}} \times \mathbf{E})^+}{Z^- + Z^+}, \end{aligned}}$$

Upwind Flux

- PEC boundary condition

$$[\hat{n} \times \mathbf{E}] = -2\hat{n} \times \mathbf{E}_-, [\hat{n} \times \mathbf{H}] = 0$$

- PMC boundary condition

$$[\hat{n} \times \mathbf{H}] = -2\hat{n} \times \mathbf{H}_-, [\hat{n} \times \mathbf{E}] = 0$$

QHL/DGTD

Semi-discrete form

$$\frac{d\mathbf{E}}{dt} = (M^{\epsilon})^{-1}\,\mathbf{S}\times\mathbf{H} - \sigma\,(M^{\epsilon})^{-1}\,M\mathbf{E} + (M^{\epsilon})^{-1}\,F\left(\hat{\mathbf{n}}\times\frac{Z^{+}[\mathbf{H}]-\hat{\mathbf{n}}\times[\mathbf{E}]}{Z^{+}+Z^{-}}\right)\Bigg|_{\delta D}$$

$$\frac{d\mathbf{H}}{dt} = (M^{\mu})^{-1}\,\mathbf{S}\times\mathbf{E} - (M^{\mu})^{-1}\,F\left(\hat{\mathbf{n}}\times\frac{Y^{+}[\mathbf{E}]+\hat{\mathbf{n}}\times[\mathbf{H}]}{Y^{+}+Y^{-}}\right)\Bigg|_{\delta D}$$

$$M_{ij} = (L_i(\mathbf{x}), L_j(\mathbf{x}))_D\,,$$

$$M^{\epsilon}_{ij} = (L_i(\mathbf{x}), \epsilon(\mathbf{x})L_j(\mathbf{x}))_D\,,\quad M^{\mu}_{ij} = (L_i(\mathbf{x}), \mu(\mathbf{x})L_j(\mathbf{x}))_D\,,$$

$$S_{ij} = (L_i(\mathbf{x}), \nabla L_j(\mathbf{x}))_D\,,\quad F_{ij} = (L_i(\mathbf{x}), L_l(\mathbf{x}))_{\delta\mathbf{D}}\,.$$

Runge-Kutta schemes for time stepping

QHL/DGTD

DGTD Method on a Unstructured Mesh

- Nodal distribution
  - Denser when closer to boundary
  - N = (M+1)(M+2)(M+3)/6 nodes in each element.
  - L = (M+1)(M+2)/2 nodes on each face.
- Reference Tetrahedron

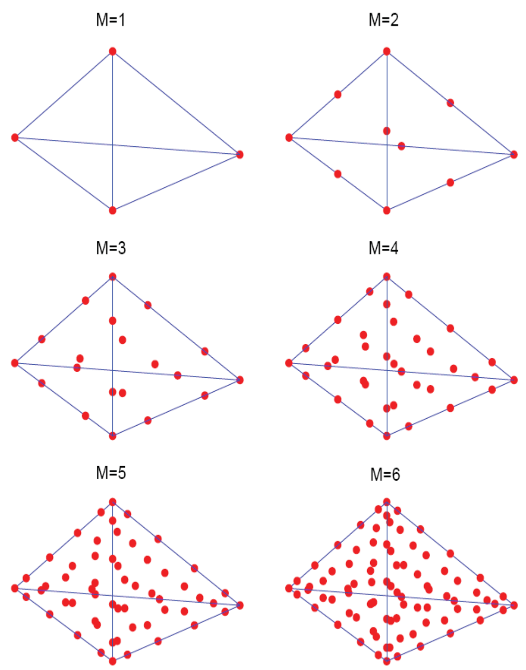

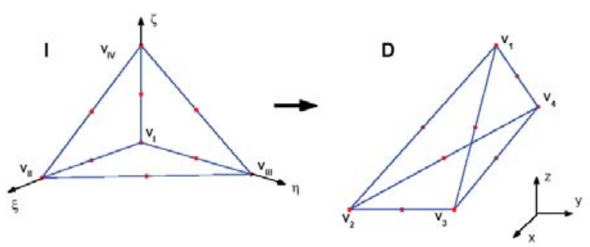

QHL/DGTD

Examples

- Accuracy Validation – by a cube cavity

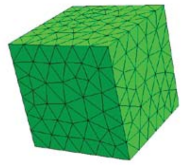

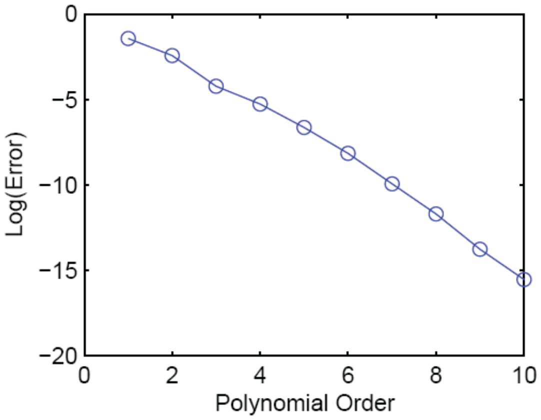

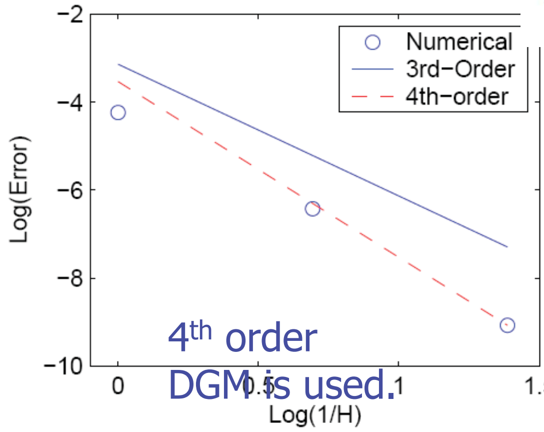

4^{th} order DGM is used.

Spectral Accuracy with *p*

High-order Accuracy with *h*

QHL/DGTD

A Dipole at center of a dielectric sphere

A 6^{th} order DGTD with 4^{th} order RK time stepping are used.

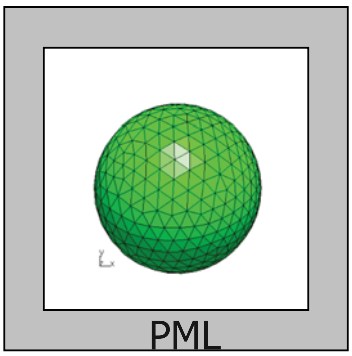

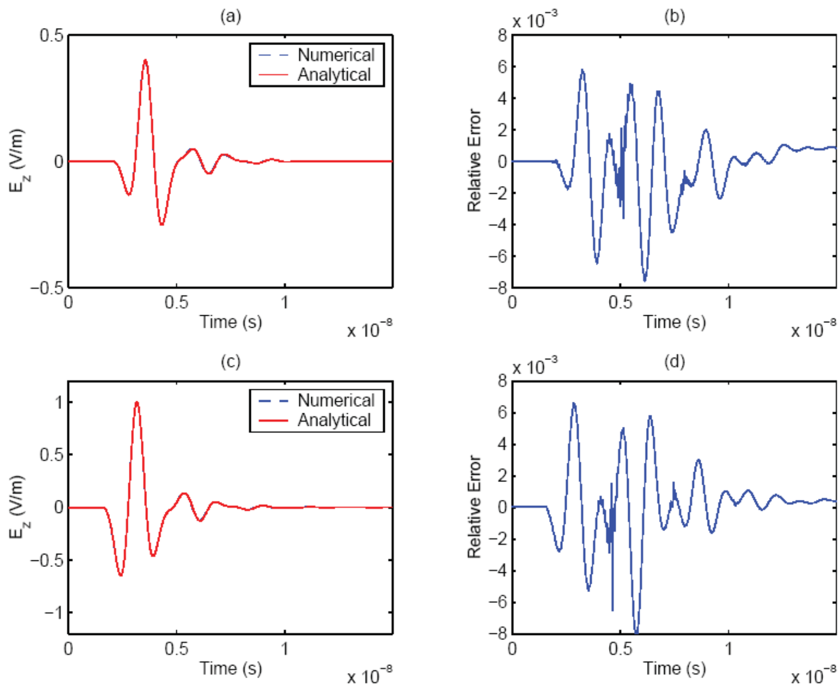

QHL/DGTD

Acoustic Plane wave incident on a rigid sphere

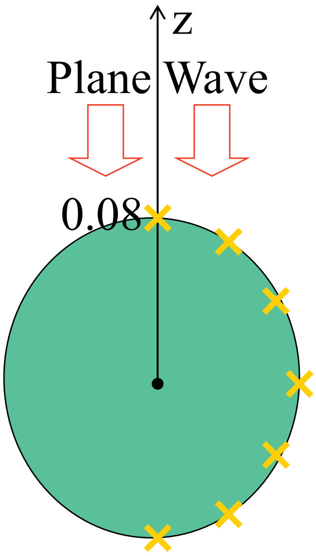

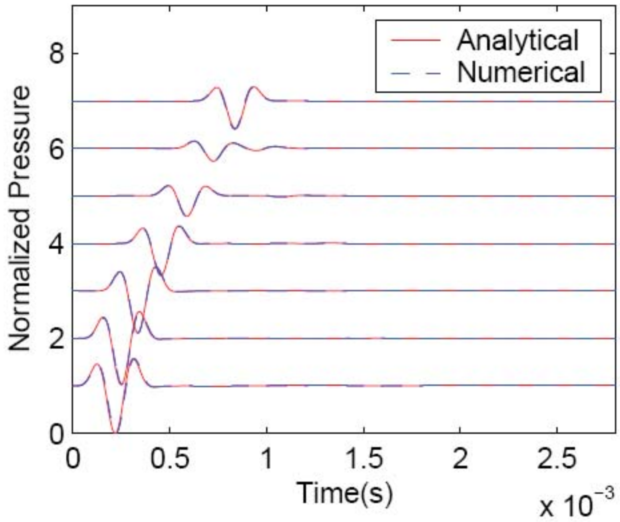

A 5th order DGTD is used.

QHL/DGTD

Staggered Time Stepping for Unstructured DGTD

- Unstructured DGTD is at best 2nd order accurate for curved objects due to linear geometry approximation.
- Higher-order RK time stepping is a waste of time since it require more stages per time step without achieving higher-order accurate solution.

  e.g. Though 4th order 5 stage RK allows a about 1.4 times bigger maximal stable time step, it is still 5/1.4/2=1.78 times slower than 2nd order 2 stage RK.
- Second-order time stepping is sufficient.
- Staggered time stepping is optimal among second-order time stepping.

QHL/DGTD

Formulation

- E and H at different time levels.
- Predictor-Corrector Method
  - Predictor

$$\mathbf{E}^{n+1/2} = \mathbf{E}^{n} + \frac{\Delta t}{2}\Big[(\mathrm{M}^{\epsilon})^{-1}\,\mathbf{V}\times\mathbf{H}^{n+1/2} + (\mathrm{M}^{\epsilon})^{-1}\,\mathrm{M}\sigma\mathbf{E}^{n}$$

$$+ (\mathrm{M}^{\epsilon})^{-1}\,\mathrm{F}\left(\hat{\mathbf{n}}\times\frac{Z^{+}[\mathbf{H}]^{n+1/2} - \hat{\mathbf{n}}\times[\mathbf{E}]^{n}}{Z^{+}+Z^{-}}\right)\Big|_{\delta\mathbf{D}}\Big].$$

  - Corrector

$$\mathbf{E}^{n+1} = \mathbf{E}^{n} + \Delta t\Big[(\mathrm{M}^{\epsilon})^{-1}\,\mathbf{V}\times\mathbf{H}^{n+1/2} + (\mathrm{M}^{\epsilon})^{-1}\,\mathrm{M}\sigma\mathbf{E}^{n+1/2}$$

$$+ (\mathrm{M}^{\epsilon})^{-1}\,\mathrm{F}\left(\hat{\mathbf{n}}\times\frac{Z^{+}[\mathbf{H}]^{n+1/2} - \hat{\mathbf{n}}\times[\mathbf{E}]^{n+1/2}}{Z^{+}+Z^{-}}\right)\Big|_{\delta\mathbf{D}}\Big].$$

- More efficient than 2nd order 2 stage RK.

QHL/DGTD

A Dipole in a Dielectric Cylinder

A 3rd order DGTD is applied.

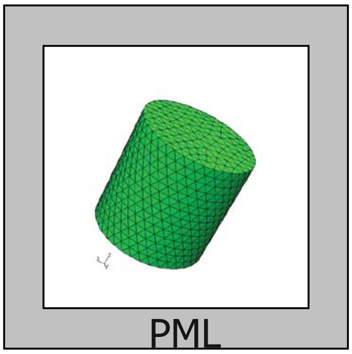

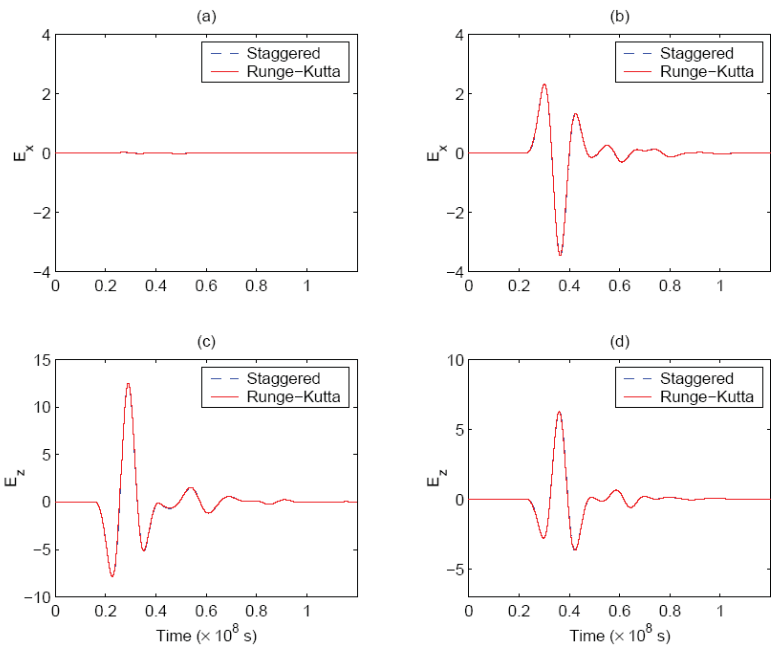

QHL/DGTD

Scaffold Photonic Structure

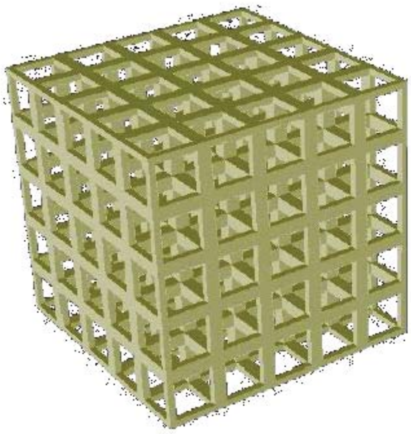

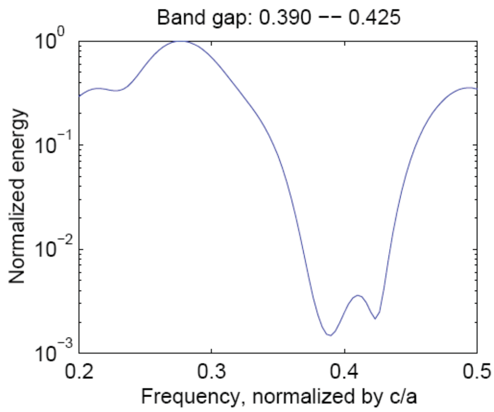

Scaffold:
Dielectric Constant 13
Thickness 1/8 a.

Background:
Dielectric Constant 1

A 3rd order DGM is applied.

QHL/DGTD

DGTD on Quadratic Simplex Grids

- Use quadratic curvilinear elements instead of straight-sided tetrahedrons
- Can achieve 3rd order accuracy for curved geometries.

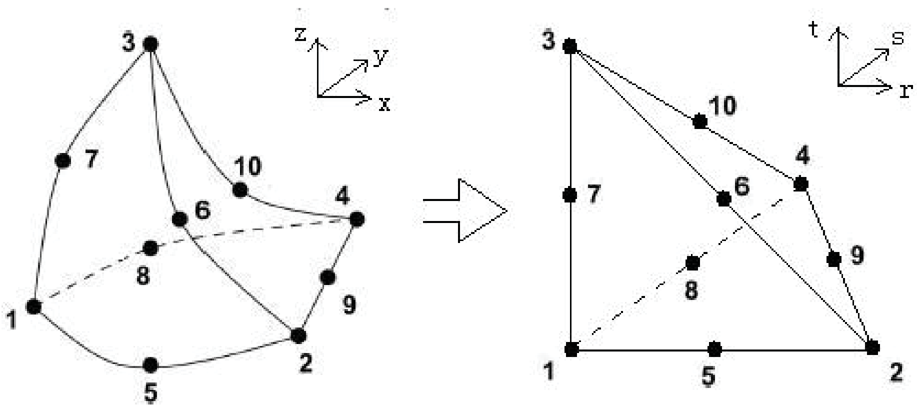

QHL/DGTD

Electric dipole in a sphere PEC Cavity

Straight-sided elements | Quadratic elements

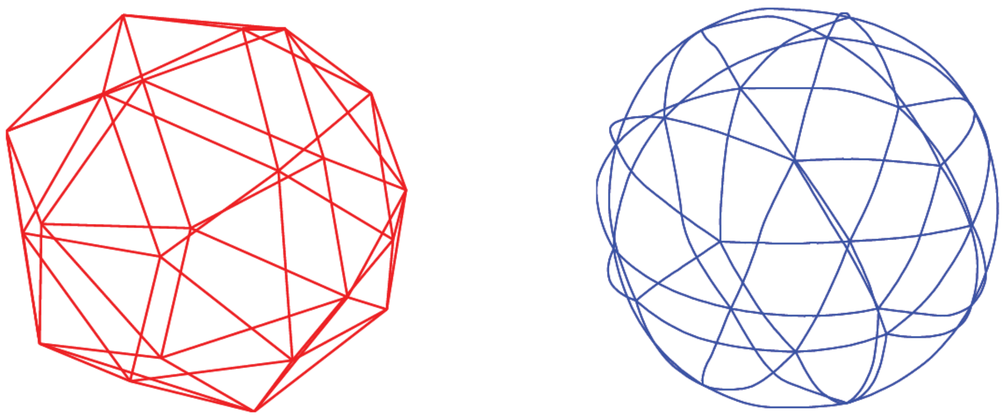

QHL/DGTD

A 3rd order DGTD is used

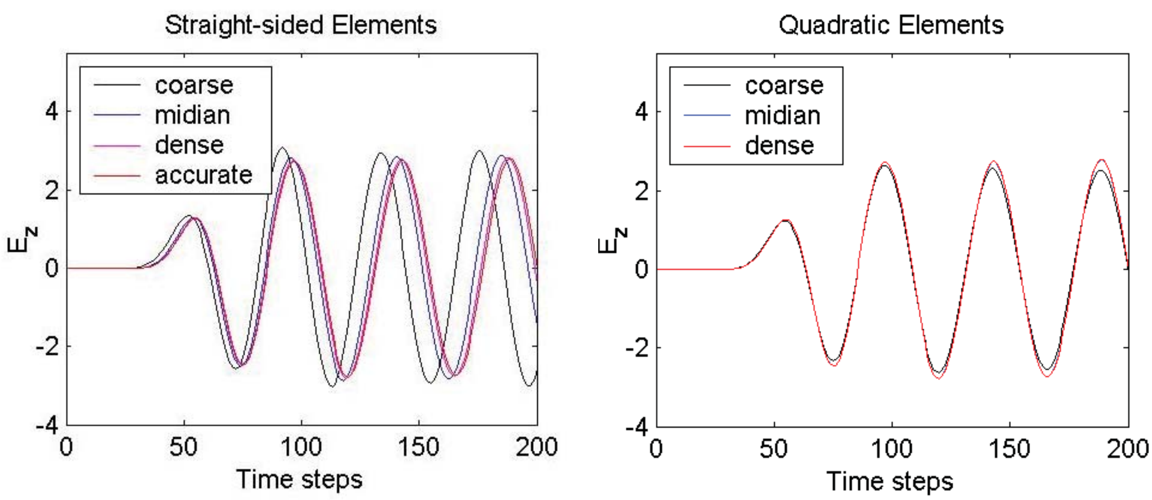

Quadratic mesh converges much faster than straight-sided.

QHL/DGTD

Accuracy Order

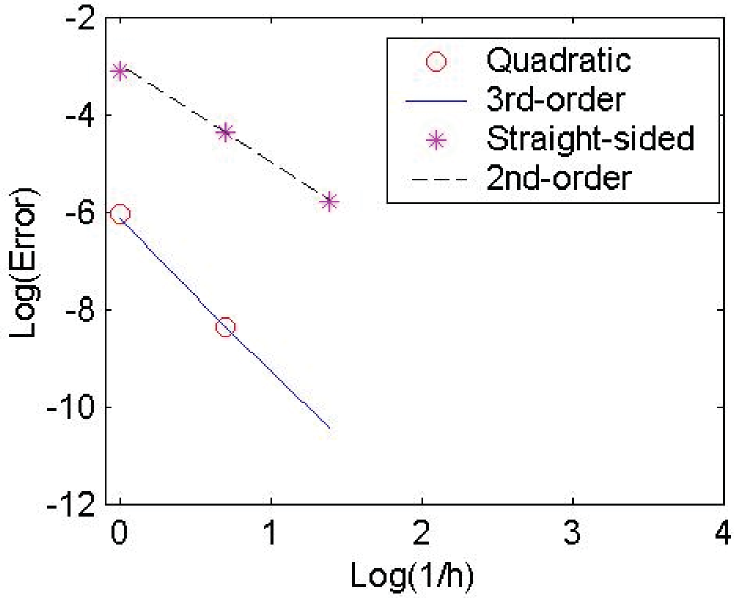

QHL/DGTD

Hybrid DGTD with Different Orders

- Hybrid Element
  - Tetrahedrons
  - Regular Prisms
  - Cubes
- Mixed Order
  - High Order
  - Low Order
  - Different order in different domain

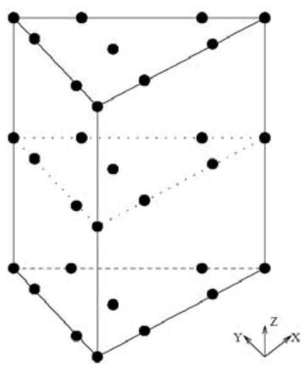

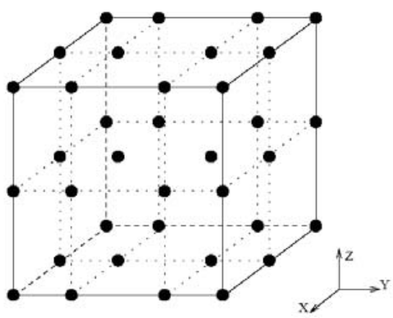

QHL/DGTD

- Flexible Hybridization
  - Non-matching nodes across interfaces
  - Non-matching faces between adjacent elements which make the mesh generation very easy

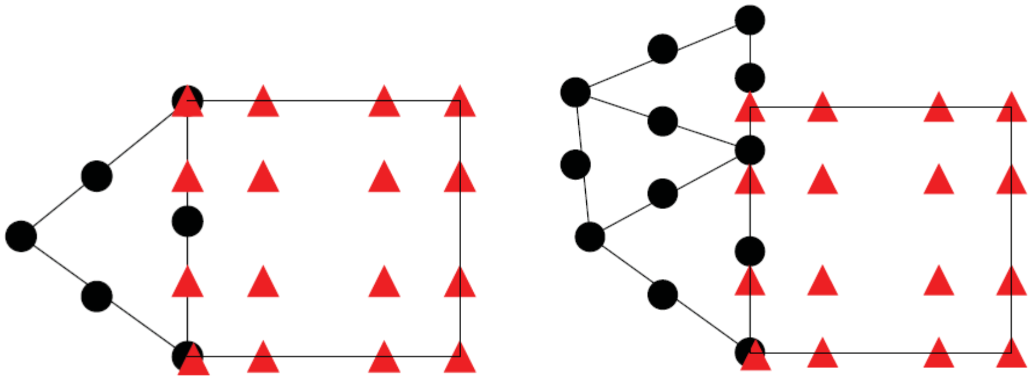

QHL/DGTD

- Face-Based Communication by interpolation
- Domain Decomposition Strategies
  - Use large cubes as much as possible
  - Use tetrahedrons or prisms to capture boundary curvature
  - Use methods with proper orders
    - For large cubes, use high-order method
    - For fine details, use low-order method
    - For tetrahedrons for curved objects, use low-order order method
    - Try to avoid a wide rage of time steps

2D Examples – Cavity with 2 Materials

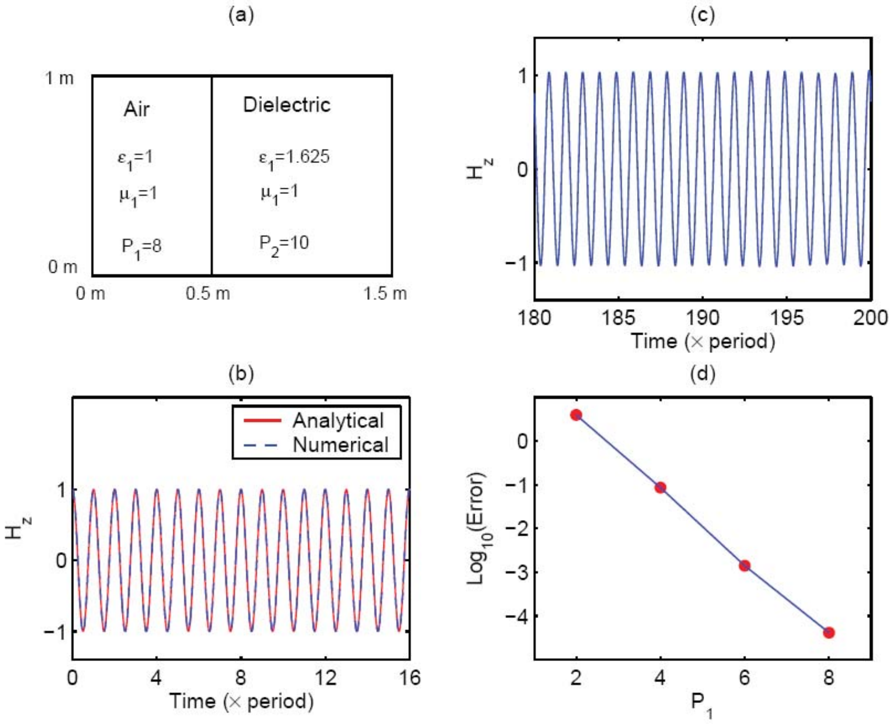

2D Examples – Cavity with 3 Materials

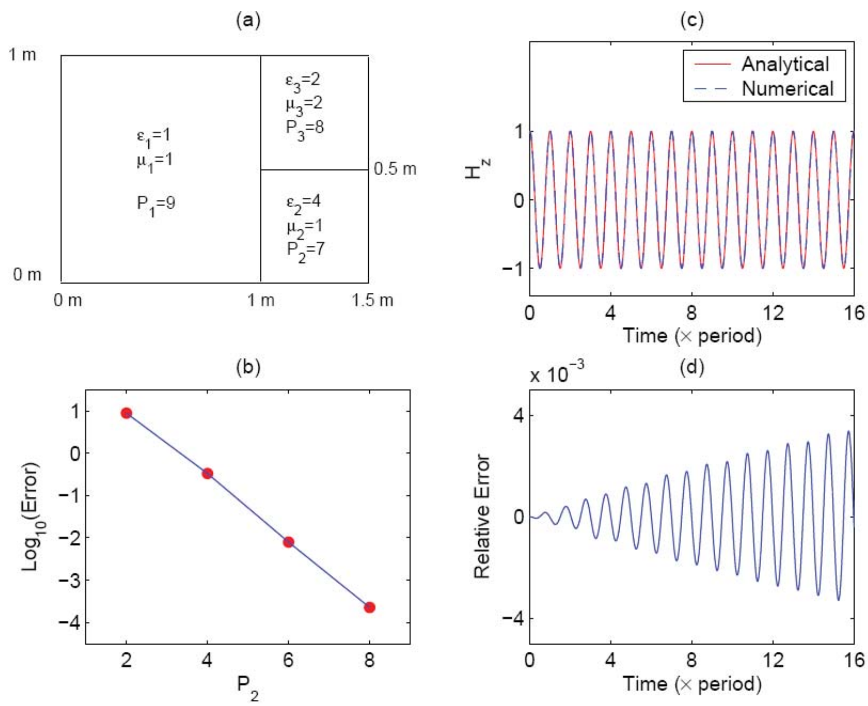

QHL/DGTD

The Grid Applied

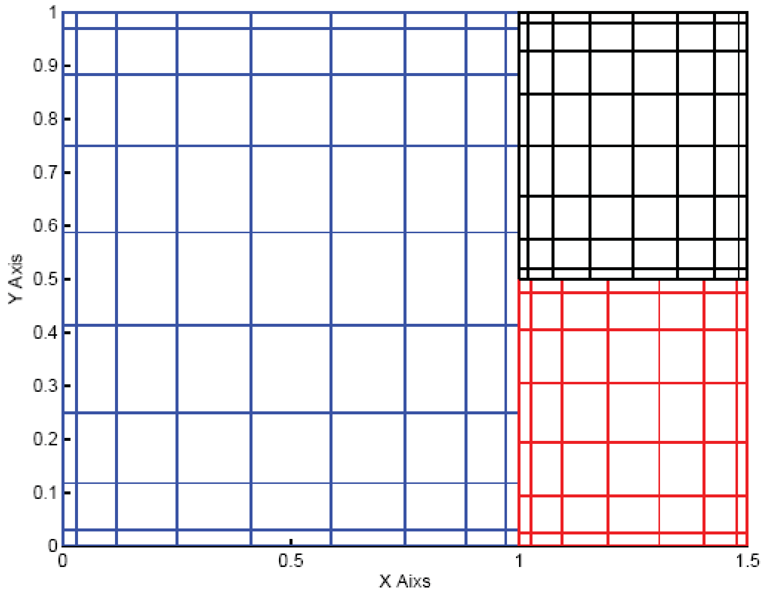

QHL/DGTD

3D Examples

- Efficient Implementation for PML Regions
  - High-Order DGTD for cubes on PML region
  - DGTD for tetrahedrons on inner computational domain

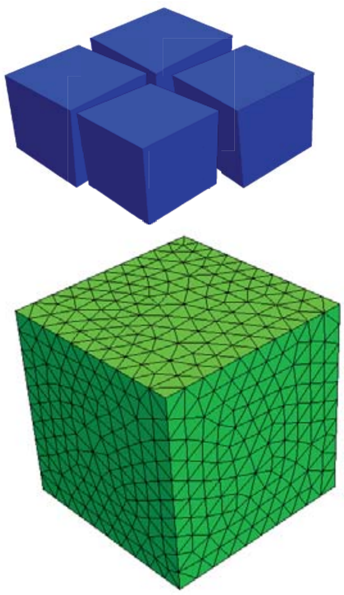

QHL/DGTD

Homogeneous Case – A Dipole Source

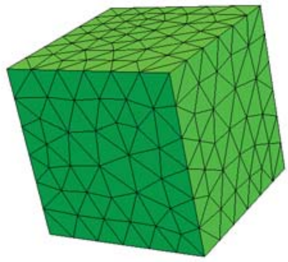

- 7^{th} order DGTD for tetrahedrons in inner computational domain.
- 7^{th} order DGTD for cubes in PML region.

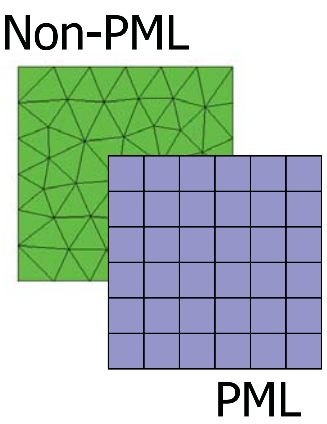

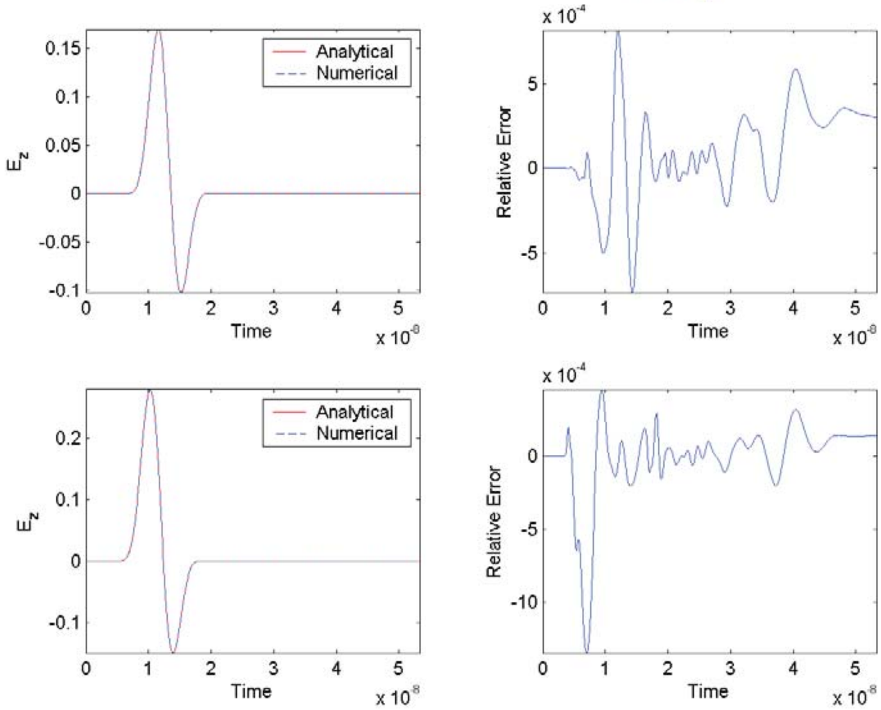

QHL/DGTD

Inhomogeneous Case – A Dielectric Sphere

- 4^{th} order DGTD for tetrahedrons in inner computational domain.
- 7^{th} order DGTD for cubes in PML region.

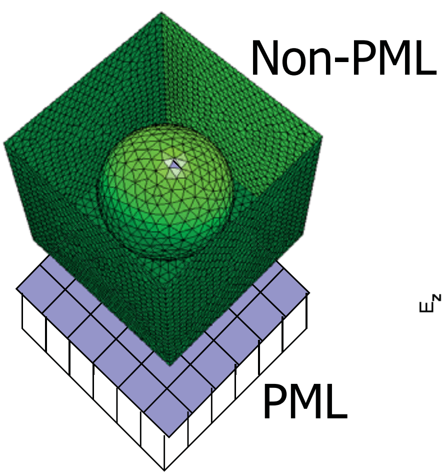

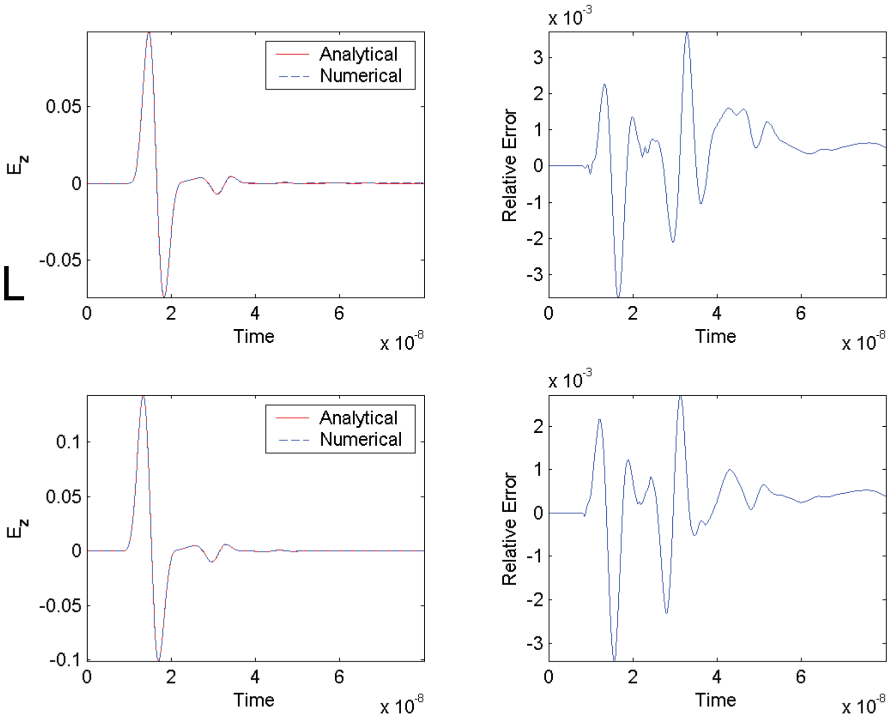

QHL/DGTD

Summary

- Spectral-Based DGTD Methods
  - ***Discontinuous Galerkin Time Domain Method*** has several good features: face-based communication, weakly enforcement of BC, support *hp* adaptivity, easiness for parallel computation.
  - ***Staggered Time Stepping*** for unstructured DGTD is introduced to avoid the waste of high-order RK schemes for curved objects.
  - ***Quadratic Simplex Elements*** can achieve 3rd order accuracy for curved objects.
  - ***Hybrid DGTD*** is powerful for complex problems. It allows hybrid elements, mixed order, and flexible hybridization.
  - DGTD can be combined with PSTD to perform fast spatial derivatives (stiffness matrices). [G. Zhao, 2005; Q. H. Liu and G. Zhao, 2005)]

QHL/DGTD

Potential Drawbacks of the Nodal DGTD Method

- Each subdomain must be one element, so the boundary DoFs are always redundant. For lower order methods, this can produce much more DoFs than the CGTD method.
- For implicit regions, the redundant DoFs do not bring noticeable benefits.
- Numerical experiments show that long term instability may be an issue, although filtering can reduce this problem.

3.2 Vector (Subdomain) DGTD Method with EH Fields

- Vector (Subdomain) DGTD Methods with Tetrahedron Elements and Hexahedron Elements
  - J. Chen, A Hybrid Spectral-Element / Finite-Element Time-Domain Method for Multiscale Electromagnetic Simulations, Ph.D. Dissertation, Duke University, 2010.
  - J. Chen, and Q. H. Liu, "A non-spurious vector spectral element method for Maxwell's equations," Progress Electromag. Res., PIER 96, pp. 205-215, 2009.
  - J. Chen, Q. H. Liu, M. Chai, and J. A. Mix, "A non-spurious 3-D vector discontinuous Galerkin finite-element time-domain method," IEEE Microwave Wireless Compon. Lett., vol. 20, no. 1, pp. 1-3, Jan. 2010.
  - J. Chen, and Q. H. Liu, "Discontinuous Galerkin time-domain methods for multiscale electromagnetic simulations: A review," invited review paper, Proc. IEEE, vol. 101, no. 2, pp. 242-253, Feb. 2013.
  - L. Tobon, J. Chen, and Q. H. Liu, "Spurious solutions in mixed finite element method for Maxwell's equations: Dispersion analysis and new basis functions," *J. Computat. Phys.*, vol. 30, 7300-7310, 2011.

Outline

- Multiscale electromagnetic problems
- A non-spurious mixed finite element method (FEM)
- A non-spurious mixed spectral element method (SEM)
- The hybrid FEM/SEM spatial discretization
- The hybrid implicit-explicit (IMEX) time stepping
- Numerical examples
- Conclusion and future work

QHL/DGTD

Introduction and Motivation: Multiscale Electromagnetic Problems

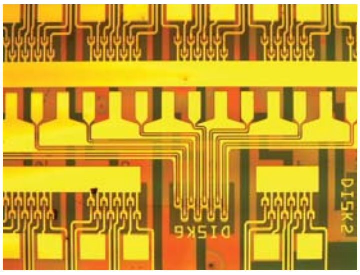

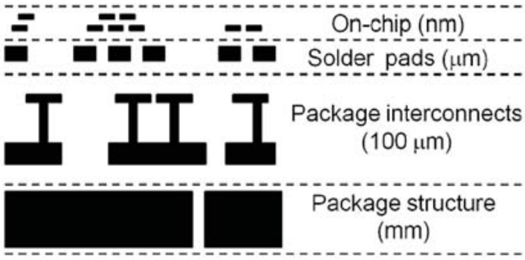

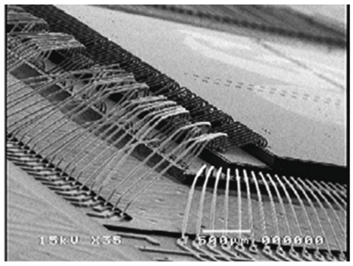

(online source)

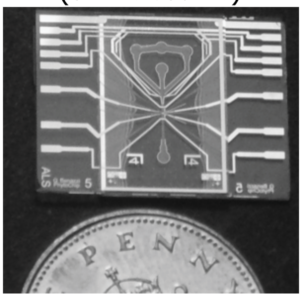

Small structures

Package

Conductor traces

Dimension ≈ 0.01 λ_{min} ≈ 1 mm

Very small structures

Solder pads

On-Chip traces

Dimension ≈ 0.00001 λ_{min} ≈ 10 nm

Multiscale Factor = **Largest Δ /Smallest δ** *~100000*

QHL/DGTD

A multiscale case: reverberation chamber

multiscale factor ≥ 1000

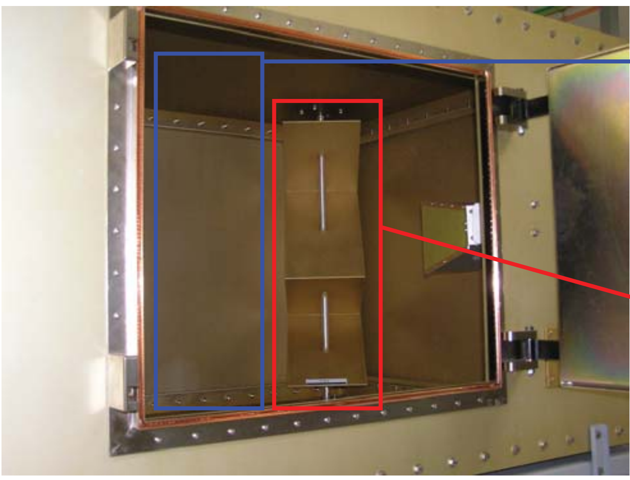

empty space in cavity

largest dimension ≥ 10 λ

stirers, device under test

smallest dimension ≤ 1/100 λ

QHL/DGTD

Conventional Time-Domain Methods

- Finite-difference time-domain (FDTD)
- Finite-element time-domain (FETD) with E&B
- Solve 1st-order Maxwell's equations with PML
  - Require a sampling density >20 points per wavelength; inefficient for electrically large regions
- Challenges both in spatial and temporal discretization

QHL/DGTD

Challenges for conventional methods

- Spatial discretization
  - finite difference: too many unknowns
  - finite element: inversion of matrices
- Time integration
  - explicit scheme: very small Δt
  - implicit scheme: inversion of matrices

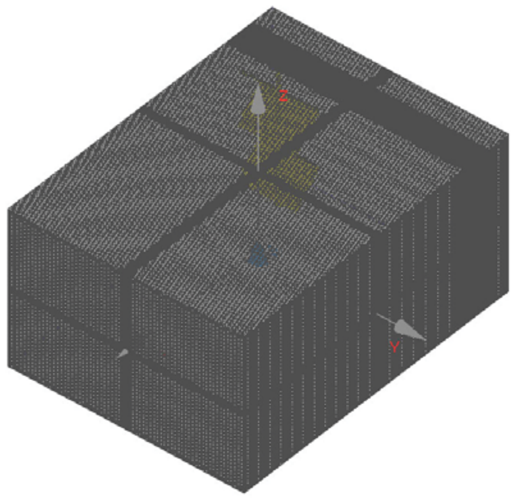

FDTD grid

QHL/DGTD

Hybrid method based on domain decomposition

- Spatial discretization
  - finite element for fine parts
  - spectral element for coarse parts
- Time integration
  - explicit schemes for coarse mesh
  - implicit schemes for dense mesh

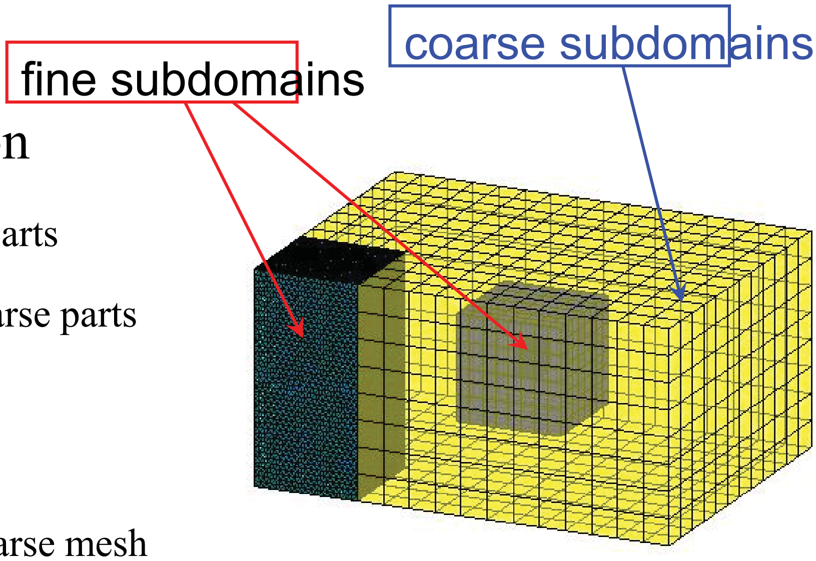

hybrid mesh

QHL/DGTD

Governing equations for electromagnetics

wave equation

$$\nabla \times (\frac{1}{\mu}\nabla \times \mathbf{E}) + \epsilon\frac{\partial^2 \mathbf{E}}{\partial t^2} + \sigma\frac{\partial \mathbf{E}}{\partial t} = -\frac{\partial \mathbf{J}_s}{\partial t}$$

conventional FEM

Maxwell's equations

$$\mu\frac{\partial \mathbf{H}}{\partial t} + \nabla \times \mathbf{E} = 0$$

$$\epsilon\frac{\partial \mathbf{E}}{\partial t} + \sigma\mathbf{E} - \nabla \times \mathbf{H} = -\mathbf{J}_s$$

mixed FEM

desirable for hybrid method

QHL/DGTD

DUKE
EDMUND T. PRATT, JR. SCHOOL OF ENGINEERING

Flux communication between subdomains

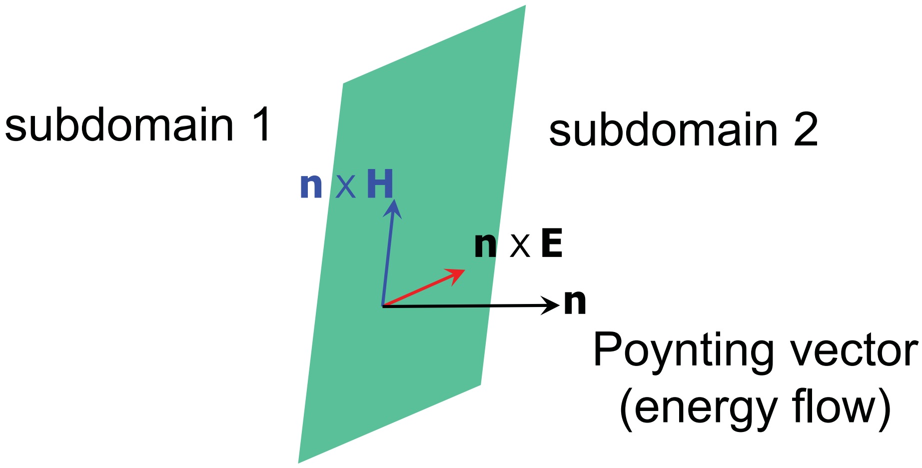

Energy flow on interface is based on both **E** and **H**

QHL/DGTD

DUKE
EDMUND T. PRATT, JR. SCHOOL OF ENGINEERING

The hybrid SETD/FETD method

SETD for electrically coarse structure

FETD for electrically fine structure

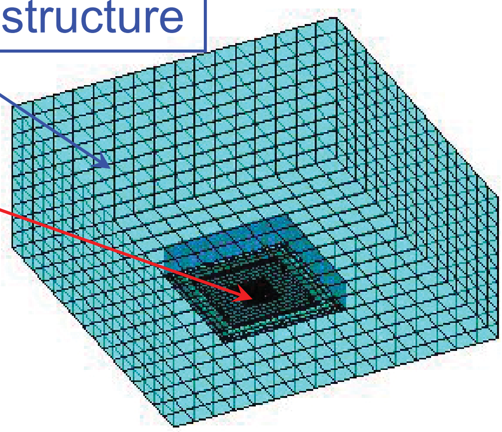

SETD/FETD meshes
divide into 4 subdomains
coarsest PPW $\approx$ 10
total unknowns: $\approx$ 50,000
$\Delta t \approx 1/10$ period

- Spatial discretization
  - Domain decomposition
  - Spectral element + finite element
- Time integration
  - Explicit schemes for coarse subdomains
  - Implicit schemes for fine subdomains

QHL/DGTD

Non-spurious elements for Maxwell's equations

$$\mathbf{E}^i = \sum_n e_n^i \boldsymbol{\phi}_n^i(\mathbf{r}), \mathbf{H}^i = \sum_n h_n^i \boldsymbol{\psi}_n^i(\mathbf{r})$$

FETD

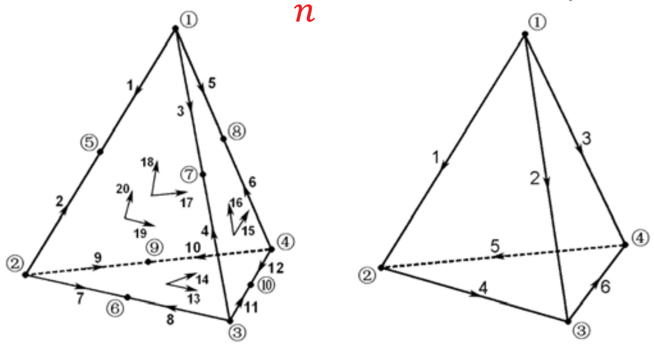

E **H**

SETD

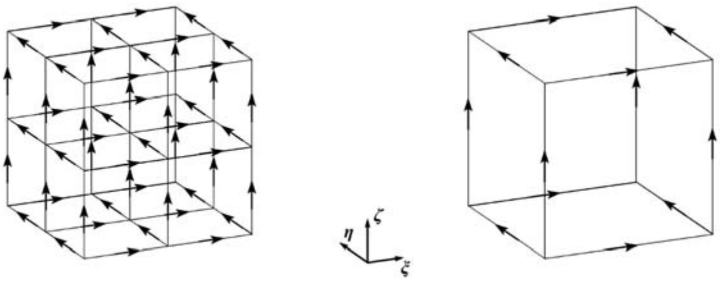

- **If E and H are used, $E_{n+1}H_n$ or $E_{n+1}H_n$ are required to avoid spurious modes.**
- **E_nH_n will produce spurious modes.**

QHL/DGTD

Frequency domain results

$$\mu\frac{\partial \mathbf{H}}{\partial t} + \nabla \times \mathbf{E} = 0$$

$$\epsilon\frac{\partial \mathbf{E}}{\partial t} + \sigma\mathbf{E} - \nabla \times \mathbf{H} = -\mathbf{J}_s$$

$$j\omega \mathbf{M}_{ee}^i \mathbf{e}^i = \mathbf{S}_{eh}\mathbf{h}^i$$

$$j\omega \mathbf{M}_{hh}^i \mathbf{h}^i = -\mathbf{S}_{he}\mathbf{e}^i$$

Eigenvalue problem

$$\mathbf{S}_{eh}\left(\mathbf{M}_{hh}^i\right)^{-1}\mathbf{S}_{he}\ \mathbf{e}^i = \omega^2 \mathbf{M}_{ee}^i \mathbf{e}^i$$

No spurious modes Many spurious modes

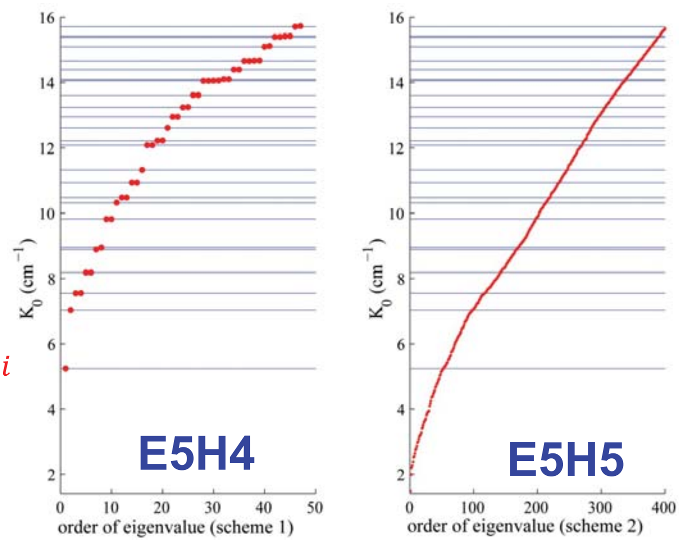

Eigenvalues of the cavity by (left) SEM scheme 1 and (right) SEM scheme 2.

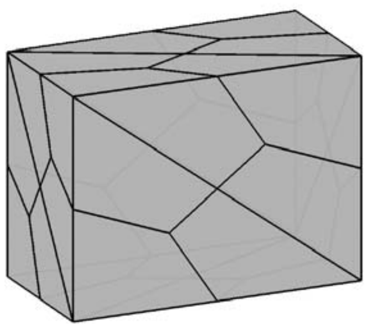

Example I: Spurious modes in mixed FEM

broadband source

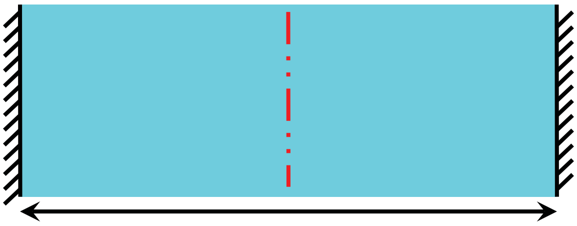

6 λ w.r.t. the highest mode

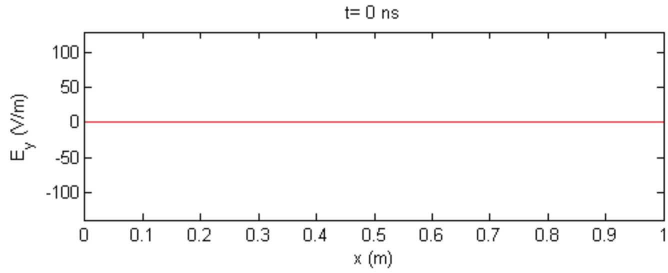

analytical solution

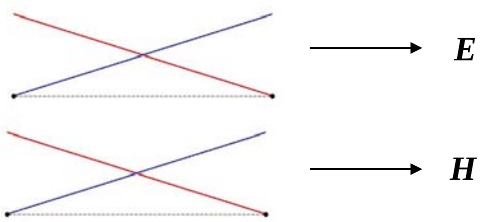

common interpolation

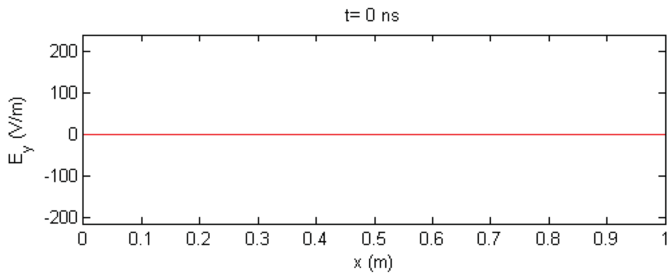

mixed FEM

Mixed interpolation is free of spurious modes

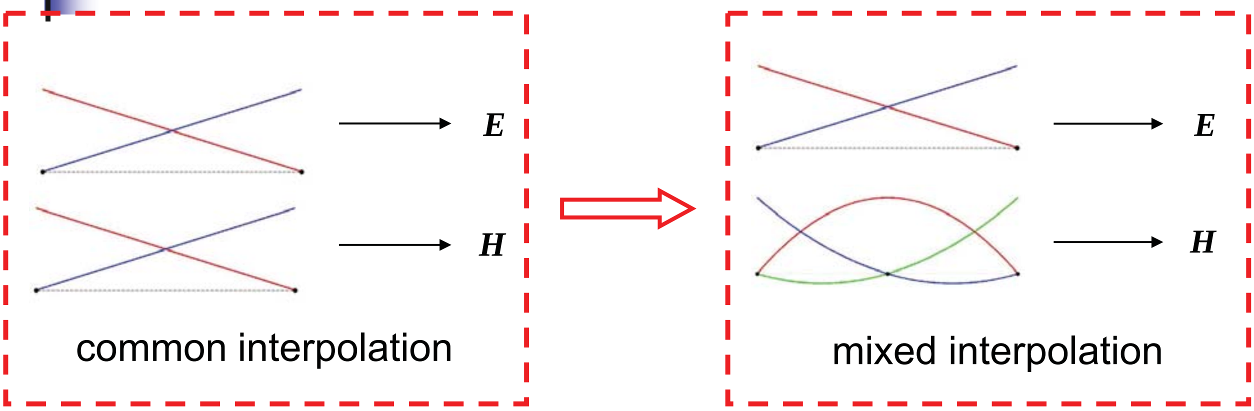

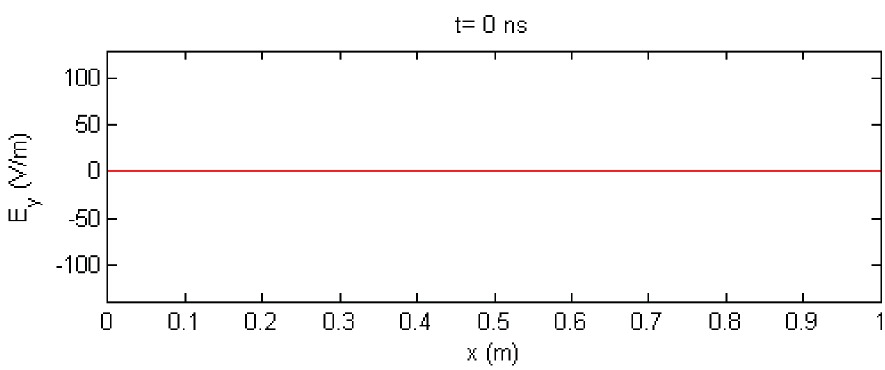

time-varying results

QHL/DGTD

Dispersion analysis for mixed FEM

For common interpolation (E1H1)

$$\tilde{k}d = 3\sin(kd)/(2+\cos(kd))$$

For mixed interpolation (E2H1)

$$\tilde{k}d = \sqrt{\frac{5(3-\cos(kd))(1-\cos(kd)) + \sin^2(kd)}{(3-\cos(kd))(2+\cos(kd))}}$$

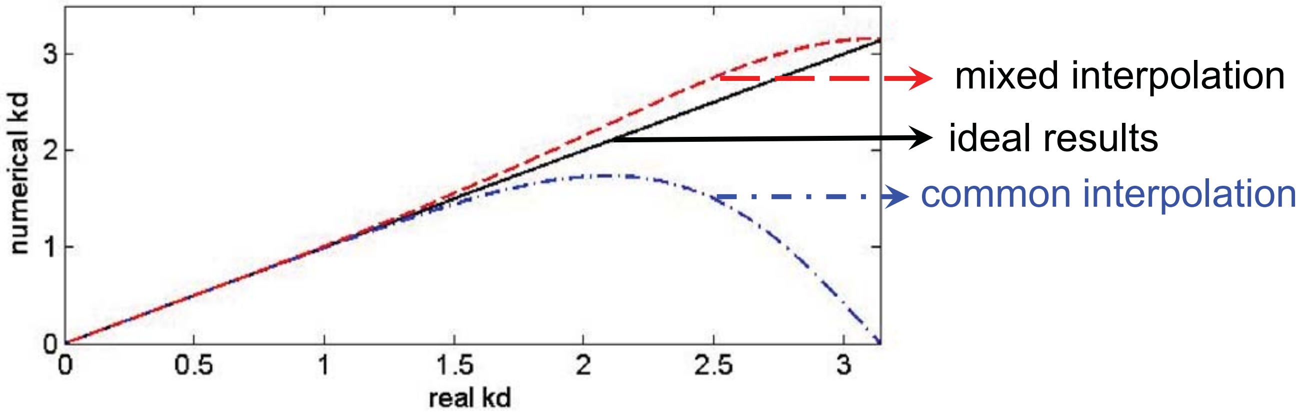

QHL/DGTD

3D non-spurious mixed vector FEM

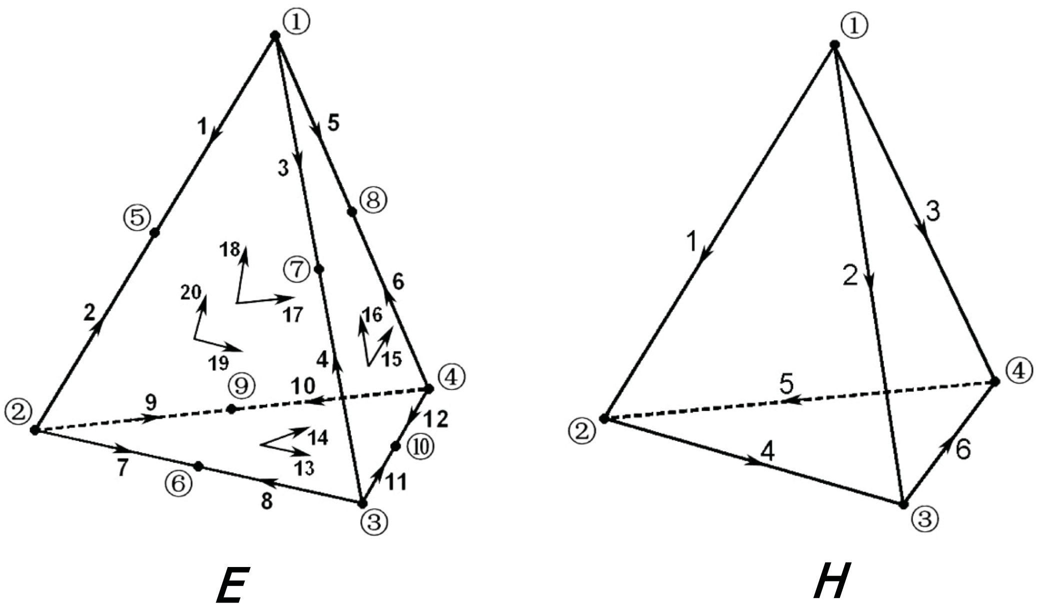

2nd order edge element   1st order edge element

SEM is a special kind of higher order FEM

uniform sampling points   non-uniform sampling points

4th Order FEM

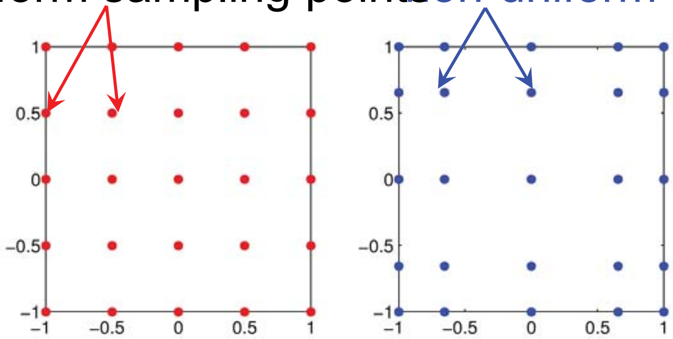

4th Order SEM

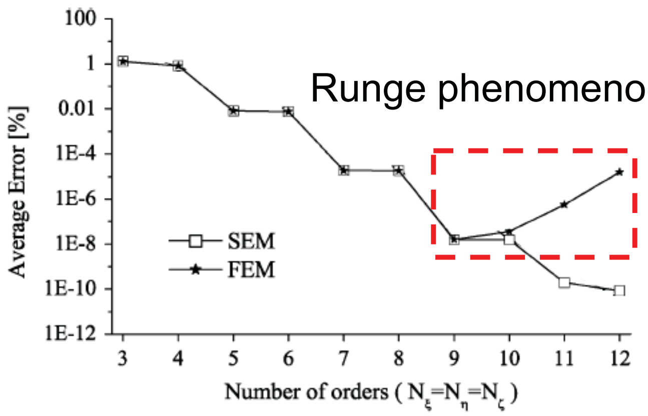

FEM v.s. SEM (3D cavity)

Higher order SEM is efficient for coarse structure

$1\lambda \times 1\lambda \times 1\lambda$ homogeneous space

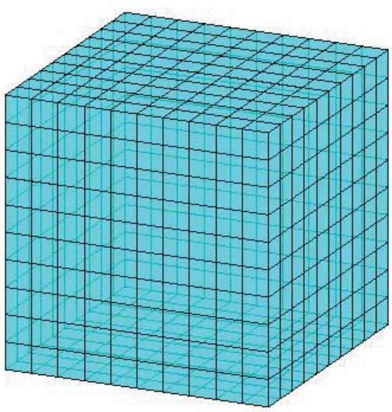

$\approx$

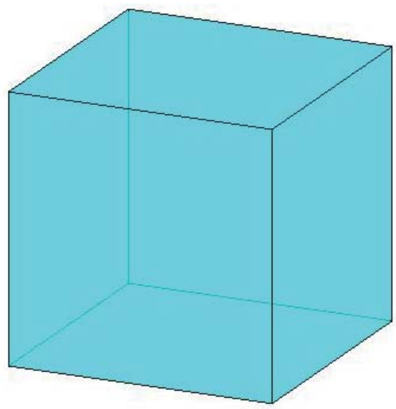

$10 \times 10 \times 10$ 1st order FEM
total number of unknowns: 6000

$1 \times 1 \times 1$ 5th order SEM
total number of unknowns: 750

about 90% of unknowns are saved by higher order SEM

3D Non-spurious mixed vector SEM

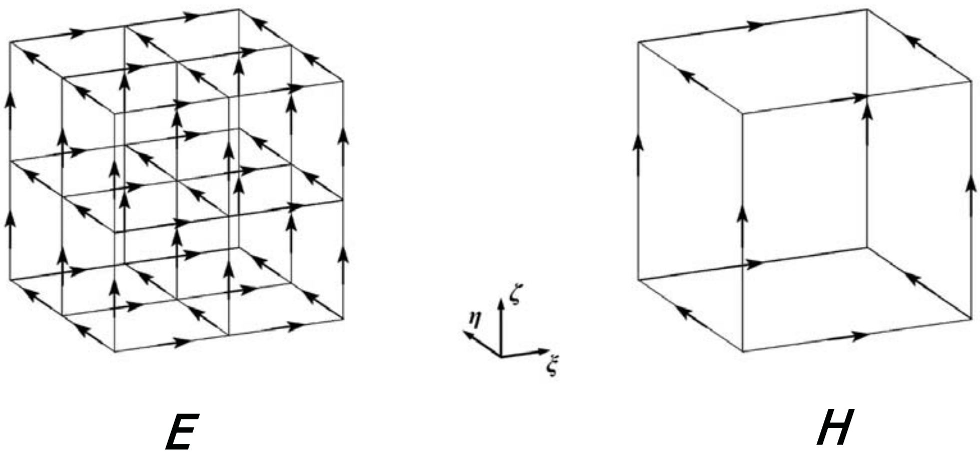

2nd order spectral element 1st order spectral element

Example II: 3D PEC cavity

SEM scheme 1: E5H4
SEM scheme 2: E5H5

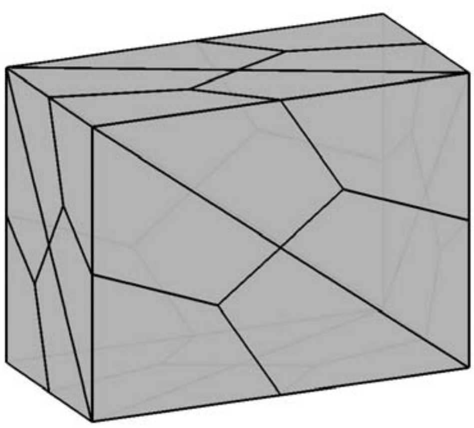

Dipole position: (-0.014, -0.236, 0.011) cm
Dipole polarization: $-0.62\hat{x} + 0.62\hat{y} + 0.47\hat{z}$
time function: BHW pulse with $f_c = 9.4$ GHz
Time-stepping: RK4 with $\Delta t = 0.5$ ps

A 1 cm $\times$ 0.5 cm $\times$ 0.75 cm metallic cavity filled with air.

QHL/DGTD

Time domain results

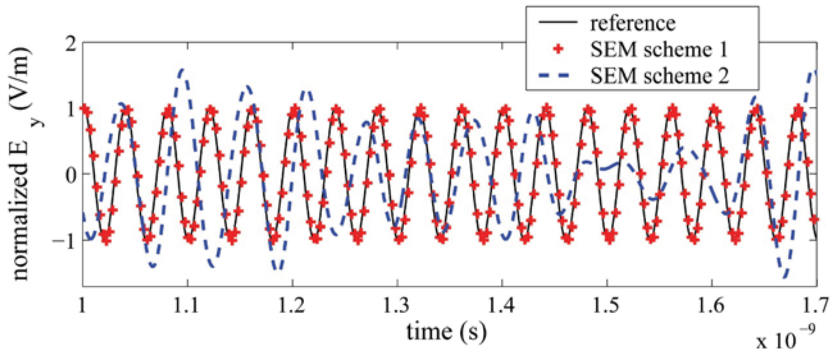

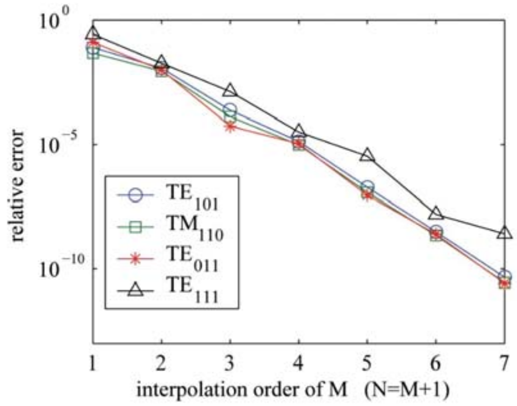

Spectral accuracy by non-spurious SEM

QHL/DGTD

The hybrid SEM/FEM spatial discretization

- Electrically fine structures: lower order tetrahedral FEM
- Electrically coarse structures: higher order hexahedral SEM
- Interface between different subdomains: Riemann solver

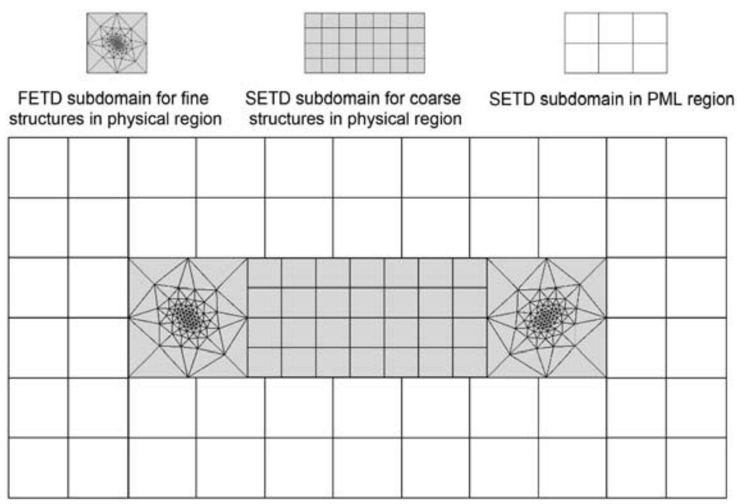

A schematic mesh for the hybrid SEM/FEM discretization

QHL/DGTD

Galerkin's weak form and surface integration

Maxwell's equations

$$\epsilon\frac{\partial \mathbf{E}}{\partial t} + \sigma_e\mathbf{E} - \nabla\times\mathbf{H} = -\mathbf{J}_s$$

$$\mu\frac{\partial \mathbf{H}}{\partial t} + \sigma_m\mathbf{H} + \nabla\times\mathbf{E} = -\mathbf{M}_s$$

Galerkin's weak form

$$\int_V \mathbf{\Phi}\cdot\left(\epsilon\frac{\partial \mathbf{E}}{\partial t} + \sigma_e\mathbf{E} - \nabla\times\mathbf{H} + \mathbf{J}_s\right)dV = 0$$

$$\int_V \mathbf{\Psi}\cdot\left(\mu\frac{\partial \mathbf{H}}{\partial t} + \sigma_m\mathbf{H} + \nabla\times\mathbf{E} + \mathbf{M}_s\right)dV = 0$$

perform integration by parts

$$\int_V \mathbf{\Phi}\cdot\left(\epsilon\frac{\partial \mathbf{E}}{\partial t} + \sigma_e\mathbf{E} + \mathbf{J}_s\right)dV = \int_V \nabla\times\mathbf{\Phi}\cdot\mathbf{H}dV + \boxed{\int_S \mathbf{\Phi}\cdot(\mathbf{n}\times\mathbf{H})dS}$$

$$\int_V \mathbf{\Psi}\cdot\left(\mu\frac{\partial \mathbf{H}}{\partial t} + \sigma_m\mathbf{H} + \mathbf{M}_s\right)dV = -\int_V \nabla\times\mathbf{\Psi}\cdot\mathbf{E}dV \boxed{- \int_S \mathbf{\Psi}\cdot(\mathbf{n}\times\mathbf{E})dS}$$

surface integration

QHL/DGTD

Riemann solver for surface integration

Galerkin's weak form with integration by parts

$$\int_V \mathbf{\Phi}\cdot\left(\epsilon\frac{\partial \mathbf{E}}{\partial t} + \sigma_e\mathbf{E} + \mathbf{J}_s\right)dV = \int_V \nabla\times\mathbf{\Phi}\cdot\mathbf{H}dV + \boxed{\int_S \mathbf{\Phi}\cdot(\mathbf{n}\times\mathbf{H})dS}$$

$$\int_V \mathbf{\Psi}\cdot\left(\mu\frac{\partial \mathbf{H}}{\partial t} + \sigma_m\mathbf{H} + \mathbf{M}_s\right)dV = -\int_V \nabla\times\mathbf{\Psi}\cdot\mathbf{E}dV \boxed{- \int_S \mathbf{\Psi}\cdot(\mathbf{n}\times\mathbf{E})dS}$$

surface integration

Riemann solver for interface between adjacent subdomains

$$(\mathbf{n}\times\mathbf{H}) = \frac{\mathbf{n}\times\left(Z^{(i)}\mathbf{H}^{(i)} + Z^{(j)}\mathbf{H}^{(j)}\right) + \mathbf{n}\times\mathbf{n}\times\left(\mathbf{E}^{(i)} - \mathbf{E}^{(j)}\right)}{Z^{(i)} + Z^{(j)}}$$

$$(\mathbf{n}\times\mathbf{E}) = \frac{\mathbf{n}\times\left(Y^{(i)}\mathbf{E}^{(i)} + Y^{(j)}\mathbf{E}^{(j)}\right) - \mathbf{n}\times\mathbf{n}\times\left(\mathbf{H}^{(i)} - \mathbf{H}^{(j)}\right)}{Y^{(i)} + Y^{(j)}}$$

QHL/DGTD

Non-conforming interface between subdomains

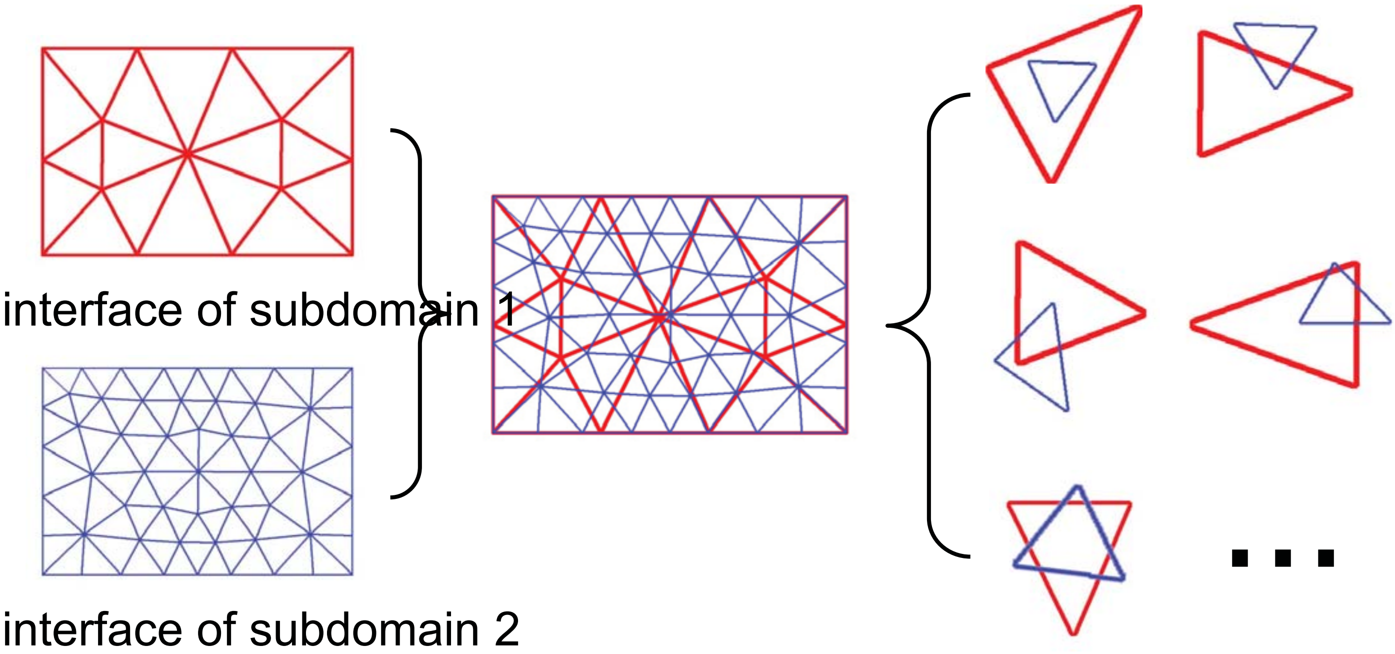

QHL/DGTD

Integration on non-conforming interface

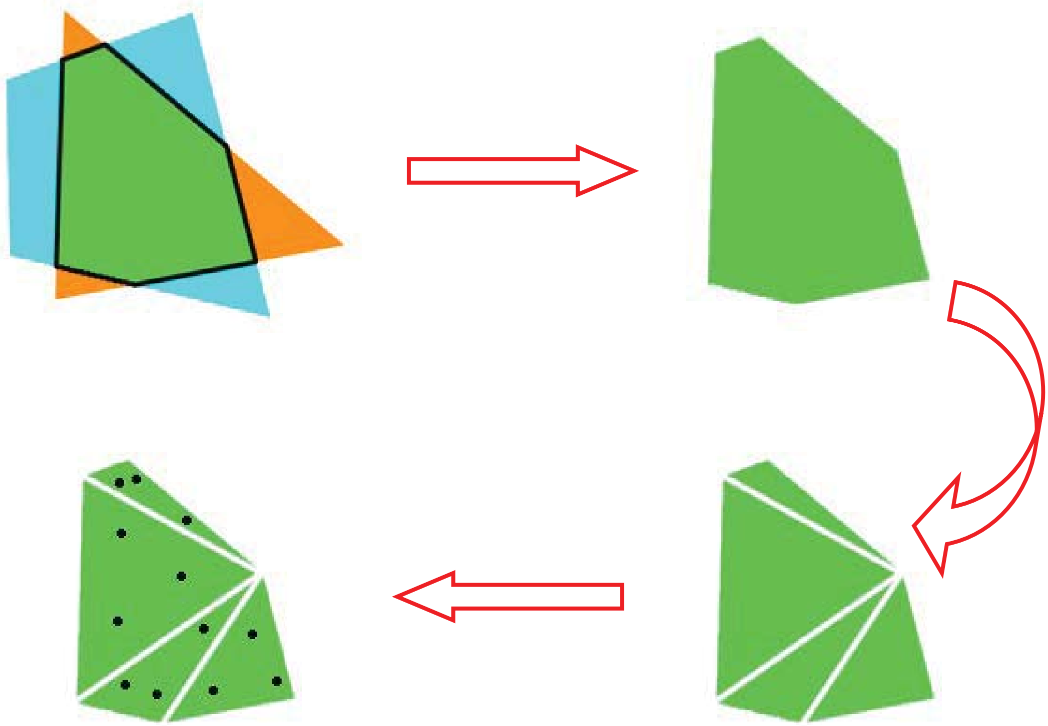

QHL/DGTD

Discretized system of equations

The discretized SETD/FETD system with N subdomains is

$$\mathbf{M}^{(i)}\frac{d\mathbf{v}^{(i)}}{dt} = \sum_{j=1}^{N}\mathbf{L}^{(ij)}\mathbf{v}^{(j)} + \mathbf{f}^{(i)}, \quad i = 1, \cdots, N$$

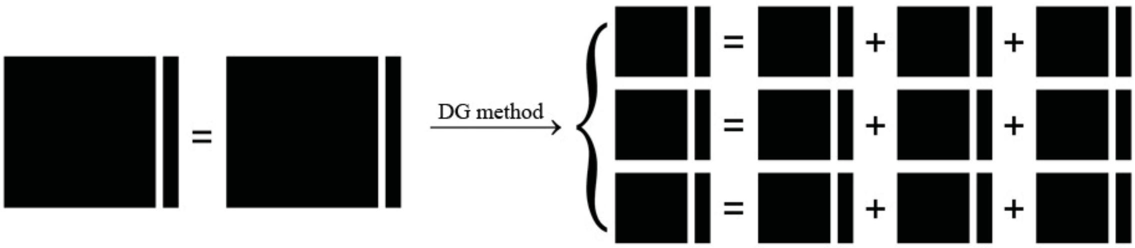

QHL/DGTD

The hybrid implicit-explicit time stepping

- Electrically coarse subdomains: explicit Runge-Kutta scheme
- Electrically fine subdomains: implicit Runge-Kutta scheme
- Adjacent explicit and implicit subdomains: IMEX-RK scheme

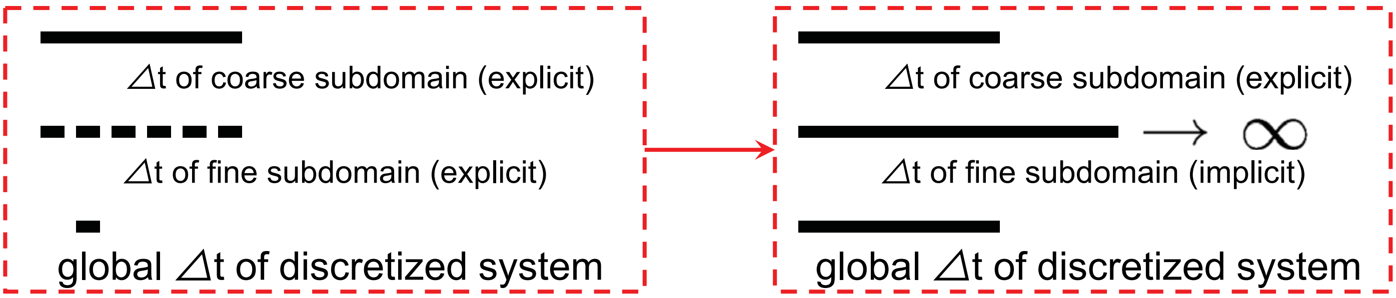

conventional explicit scheme   hybrid explicit-implicit scheme

QHL/DGTD

Three time stepping scenarios

1.

coarse mesh	coarse mesh

Local explicit RK scheme

2.

coarse mesh	dense mesh

Implicit-explicit RK scheme

3.

dense mesh	dense mesh

Local implicit RK scheme
subdomain-based iterative algorithm

QHL/DGTD

Local explicit Runge-Kutta scheme

coarse mesh	coarse mesh

$$
\begin{array}{c|cccccc}
0 & 0 & 0 & \cdots & \cdots & 0 \\
c_2 & a^{\mathrm{ex}}_{2,1} & 0 & \ddots & \ddots & \vdots \\
c_3 & a^{\mathrm{ex}}_{3,1} & a^{\mathrm{ex}}_{3,2} & 0 & \ddots & \vdots \\
\vdots & \vdots & \vdots & \vdots & \ddots & 0 \\
c_s & a^{\mathrm{ex}}_{s,1} & a^{\mathrm{ex}}_{s,2} & \cdots & a^{\mathrm{ex}}_{s,s-1} & 0 \\
\hline
 & b_1 & b_2 & b_3 & \cdots & b_s
\end{array}
$$

explicit RK

$$\mathbf{M}_1\mathbf{u}_1^{\mathrm{new}} = \Delta t a^{\mathrm{ex}} \left(\mathbf{L}_{(1,1)}\mathbf{u}_1^{\mathrm{old}} + \mathbf{L}_{(1,2)}\mathbf{u}_2^{\mathrm{old}}\right) + \mathbf{q}_1$$

$$\mathbf{M}_2\mathbf{u}_2^{\mathrm{new}} = \Delta t a^{\mathrm{ex}} \left(\mathbf{L}_{(2,1)}\mathbf{u}_1^{\mathrm{old}} + \mathbf{L}_{(2,2)}\mathbf{u}_2^{\mathrm{old}}\right) + \mathbf{q}_2$$

QHL/DGTD

Implicit-explcit Runge-Kutta scheme

$$
\begin{array}{c|cccccc}
0 & 0 & 0 & \cdots & \cdots & 0 \\
c_2 & a^{\mathrm{ex}}_{2,1} & 0 & \ddots & \ddots & \vdots \\
c_3 & a^{\mathrm{ex}}_{3,1} & a^{\mathrm{ex}}_{3,2} & 0 & \ddots & \vdots \\
\vdots & \vdots & \vdots & \vdots & \ddots & 0 \\
c_s & a^{\mathrm{ex}}_{s,1} & a^{\mathrm{ex}}_{s,2} & \cdots & a^{\mathrm{ex}}_{s,s-1} & 0 \\
\hline
 & b_1 & b_2 & b_3 & \cdots & b_s
\end{array}
$$

explicit RK

coarse mesh	dense mesh

$$
\begin{array}{c|cccccc}
0 & a^{\mathrm{im}}_{1,1} & 0 & \cdots & \cdots & 0 \\
c_2 & a^{\mathrm{im}}_{2,1} & a^{\mathrm{im}}_{2,2} & 0 & \ddots & \vdots \\
c_3 & a^{\mathrm{im}}_{3,1} & a^{\mathrm{im}}_{3,2} & a^{\mathrm{im}}_{3,3} & \ddots & \vdots \\
\vdots & \vdots & \vdots & \vdots & \ddots & 0 \\
c_s & a^{\mathrm{im}}_{s,1} & a^{\mathrm{im}}_{s,2} & \cdots & a^{\mathrm{im}}_{s,s-1} & a^{\mathrm{im}}_{s,s} \\
\hline
 & b_1 & b_2 & b_3 & \cdots & b_s
\end{array}
$$

implicit RK

$$\mathbf{M}_1 \mathbf{u}_1^{\mathrm{new}} = \Delta t a^{\mathrm{ex}} \mathbf{L}_{(1,1)} \mathbf{u}_1^{\mathrm{old}} + \Delta t a^{\mathrm{im}} \mathbf{L}_{(1,2)} \mathbf{u}_2^{\mathrm{old}} + \mathbf{q}_1$$

$$\left(\mathbf{M}_2 - \Delta t a^{\mathrm{im}} \mathbf{L}_{(2,2)}\right) \mathbf{u}_2^{\mathrm{new}} = \Delta t a^{\mathrm{ex}} \mathbf{L}_{(2,1)} \mathbf{u}_1^{\mathrm{old}} + \mathbf{q}_2$$

QHL/DGTD

Local implicit Runge-Kutta scheme

dense mesh	dense mesh

$$
\begin{array}{c|cccccc}
0 & a^{\mathrm{im}}_{1,1} & 0 & \cdots & \cdots & 0 \\
c_2 & a^{\mathrm{im}}_{2,1} & a^{\mathrm{im}}_{2,2} & 0 & \ddots & \vdots \\
c_3 & a^{\mathrm{im}}_{3,1} & a^{\mathrm{im}}_{3,2} & a^{\mathrm{im}}_{3,3} & \ddots & \vdots \\
\vdots & \vdots & \vdots & \vdots & \ddots & 0 \\
c_s & a^{\mathrm{im}}_{s,1} & a^{\mathrm{im}}_{s,2} & \cdots & a^{\mathrm{im}}_{s,s-1} & a^{\mathrm{im}}_{s,s} \\
\hline
 & b_1 & b_2 & b_3 & \cdots & b_s
\end{array}
$$

implicit RK

$$\left(\begin{bmatrix} \mathbf{M}_1 & \mathbf{0} \\ \mathbf{0} & \mathbf{M}_2 \end{bmatrix} - \Delta t a^{\mathrm{im}}_{k,k} \begin{bmatrix} \mathbf{L}_{(1,1)} & \mathbf{L}_{(1,2)} \\ \mathbf{L}_{(2,1)} & \mathbf{L}_{(2,2)} \end{bmatrix} \right) \begin{bmatrix} \mathbf{u}_1 \\ \mathbf{u}_2 \end{bmatrix} = \begin{bmatrix} \mathbf{q}_1 \\ \mathbf{q}_2 \end{bmatrix}$$

(subdomain-based) block Jacobian iteration

$$\begin{bmatrix} \mathbf{M}_1 - \Delta t a^{\mathrm{im}}_{k,k} \mathbf{L}_{(1,1)} & \mathbf{0} \\ \mathbf{0} & \mathbf{M}_2 - \Delta t a^{\mathrm{im}}_{k,k} \mathbf{L}_{(2,2)} \end{bmatrix} \begin{bmatrix} \mathbf{u}_1 \\ \mathbf{u}_2 \end{bmatrix}^{i+1} = \Delta t a^{\mathrm{im}}_{k,k} \begin{bmatrix} \mathbf{0} & \mathbf{L}_{(1,2)} \\ \mathbf{L}_{(2,1)} & \mathbf{0} \end{bmatrix} \begin{bmatrix} \mathbf{u}_1 \\ \mathbf{u}_2 \end{bmatrix}^{i} + \begin{bmatrix} \mathbf{q}_1 \\ \mathbf{q}_2 \end{bmatrix}$$

block Gauss-Seidel, SOR, CG, BiCG, etc. can also be employed here

QHL/DGTD

Block Thomas algorithm for layered structures

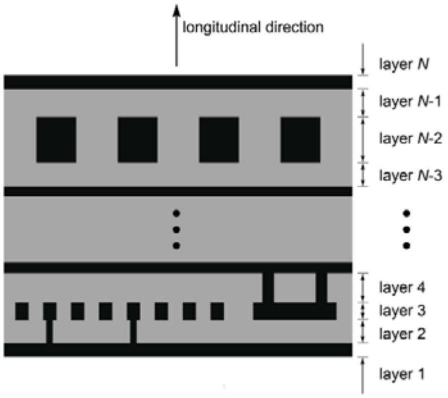

$$\begin{bmatrix} \mathbf{B}_1 & \mathbf{C}_1 & \mathbf{0} & \cdots & \mathbf{0} \\ \mathbf{A}_2 & \mathbf{B}_2 & \mathbf{C}_2 & \ddots & \vdots \\ \mathbf{0} & \mathbf{A}_3 & \mathbf{B}_3 & \ddots & \mathbf{0} \\ \vdots & \ddots & \ddots & \ddots & \mathbf{C}_{N-1} \\ \mathbf{0} & \cdots & \mathbf{0} & \mathbf{A}_N & \mathbf{B}_N \end{bmatrix} \begin{bmatrix} \mathbf{u}_1 \\ \mathbf{u}_2 \\ \vdots \\ \vdots \\ \mathbf{u}_N \end{bmatrix} = \begin{bmatrix} \mathbf{q}_1 \\ \mathbf{q}_2 \\ \vdots \\ \vdots \\ \mathbf{q}_N \end{bmatrix}$$

block tri-diagonal system

$$\left\{\begin{array}{l} \mathbf{C}'_1 = \mathbf{B}_1^{-1}\mathbf{C}_1 \\ \text{for } i = 2 : N-1 \\ \quad \mathbf{C}'_i = \left(\mathbf{B}_i - \mathbf{A}_i\mathbf{C}'_{i-1}\right)^{-1}\mathbf{C}_i, \\ \text{end} \\ \mathbf{f}'_1 = \mathbf{B}_1^{-1}\mathbf{f}_1 \\ \text{for } i = 2 : N \\ \quad \mathbf{f}'_i = \left(\mathbf{B}_i - \mathbf{A}_i\mathbf{C}'_{i-1}\right)^{-1}\left(\mathbf{f}_i - \mathbf{A}_i\mathbf{f}'_{i-1}\right) \\ \text{end} \\ \mathbf{q}_N = \mathbf{f}'_N \\ \text{for } i = N-1 : -1 : 1 \\ \quad \mathbf{q}_i = \mathbf{f}'_i - \mathbf{C}'_i\mathbf{q}_{i+1} \\ \text{end} \end{array}\right.$$

The block Thomas algorithm will eliminate iterations during time stepping

QHL/DGTD

Example III: reverberation chamber

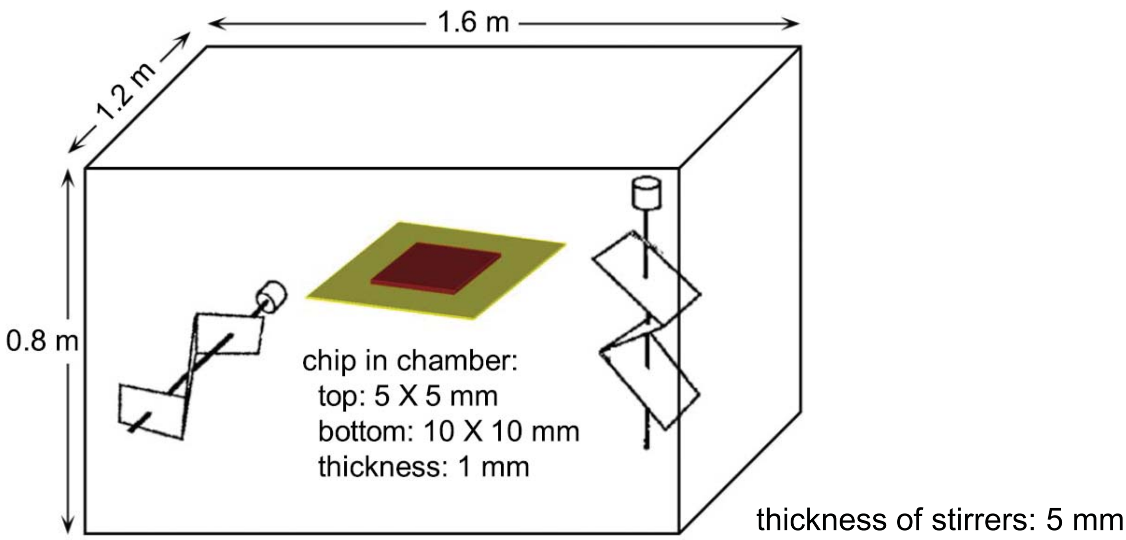

multiscale factor = 1600

QHL/DGTD

Numerical results by SETD/FETD and FDTD

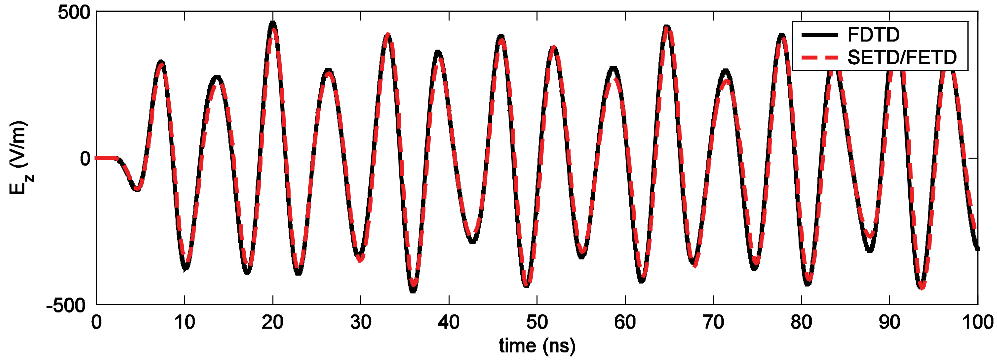

receiver @ (-0.5 m , 0.3 m, 0.1 m)

Computational costs of FDTD and hybrid SETD/FETD methods

	FDTD	hybrid SETD/FETD
number of unknowns	16,692,480	103,240
Δt (ps)	1	100
number of time steps	100,000	1,000
memory (MB)	501	315
CPU time (minutes)	156.6	11.3

QHL/DGTD

Example IV: antenna array

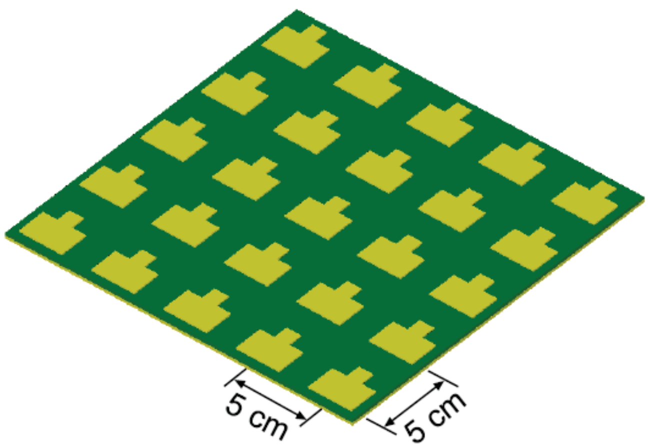

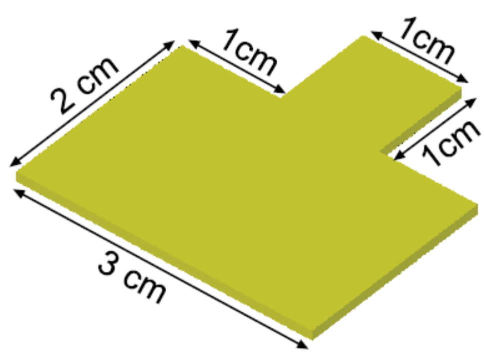

thickness of patch antenna: 1 mm

multiscale factor = 250

QHL/DGTD

Numerical results by SETD/FETD and FDTD

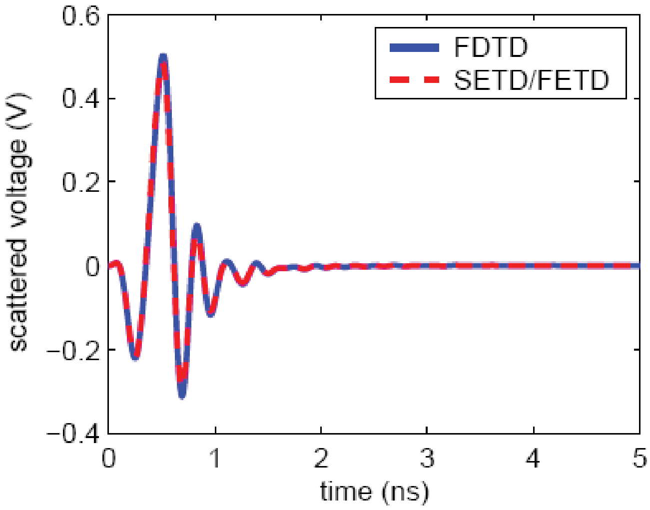

	hybrid SETD/FETD	FDTD
$\Delta t(ps)$	10	0.1
number of time steps	500	50,000
memory (MB)	277	438
CPU time (hours)	2.2	3.4

QHL/DGTD

Domain decomposition can save memory

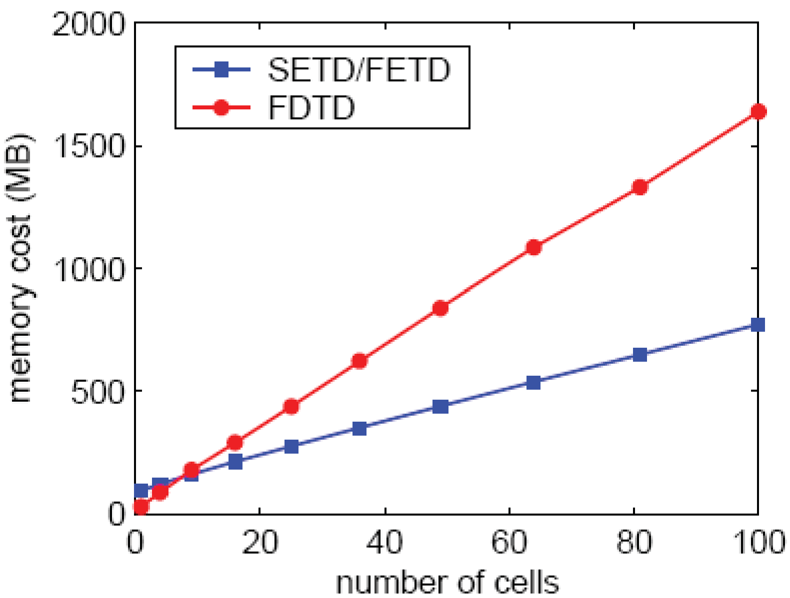

QHL/DGTD

Example V: interconnect package

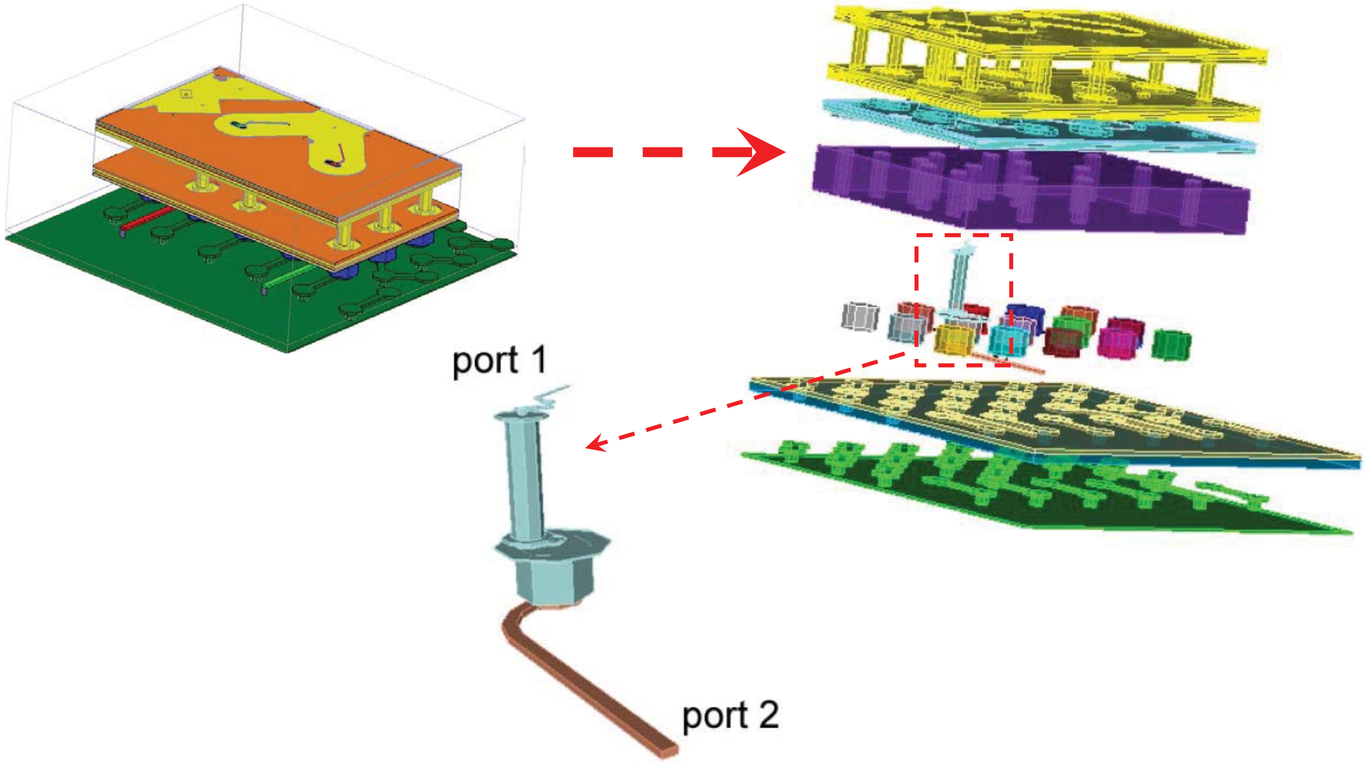

QHL/DGTD

FDTD grid and SETD/FETD mesh

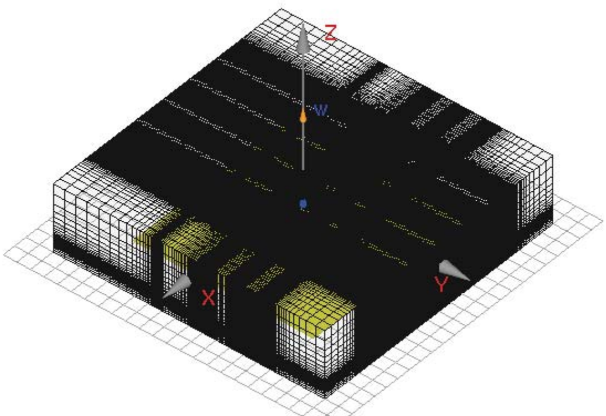

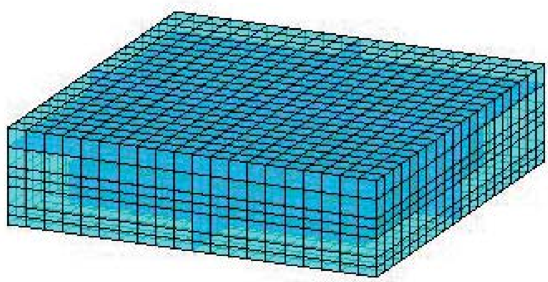

FDTD grid
PPW=40
cells: 511 X 323 X 60
total DoF: > 50 million
Δt = 3.98 fs
nt = 125,628

SETD / FETD mesh
PPW=40
44 subdomains
total DoF: 152,356
Δt = 500 fs
nt = 1,000

QHL/DGTD

DUKE EDMUND T. PRATT, JR. SCHOOL OF ENGINEERING

Numerical results by three methods

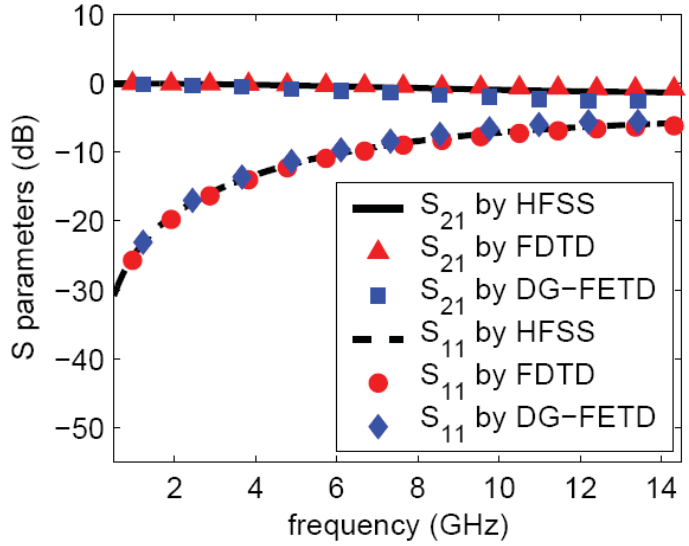

Comparison of computational costs by different methods

	hybrid SETD/FETD	FDTD	HFSS
memory (MB)	371	1,627	1,433
CPU time (minutes)	13.1	522	319

QHL/DGTD

DUKE EDMUND T. PRATT, JR. SCHOOL OF ENGINEERING

Summary

- The 3D FETD method with E_nH_{n+1} bases for Maxwell's equations. This method is used to discretize electrically fine structures.
- The 3D SETD method with E_nH_{n+1} bases for Maxwell's equations. This method is used to discretize electrically coarse structures.
- The hybrid SEM/FEM DGTD method for multiscale structures.
- Integrated the hybrid implicit-explicit time stepping scheme into the hybrid SETD/FETD method
- Applied the block Thomas algorithm to speed up the hybrid SETD/FETD method for layered structures

3.3 Vector (Subdomain) DGTD Method with EB Fields

- Vector (Subdomain) DGTD Methods with the EB Fields and Tetrahedron Elements and Hexahedron Elements

  - L. E. Tobon, Numerical Solution of Multiscale Electromagnetic Systems, Ph.D. Dissertation, Duke University, 2013.
  - L. E. Tobon, Q. Ren, and Q. H. Liu, “A new efficient 3D Discontinuous Galerkin Time Domain (DGTD) method for large and multiscale electromagnetic simulations,” *J. Computat. Phys.*, vol. 283, pp. 374-387, Feb. 2015.
  - Q. Ren, Compatible Subdomain Level Isotropic/Anisotropic Discontinuous Galerkin Time Domain (DGTD) Method for Multiscale Simulation, Ph.D. Dissertation, Duke University, 2015.
  - Q. Ren, L. E. Tobon, Q. T. Sun, and Q. H. Liu, “A New 3-D Nonspurious Discontinuous Galerkin Spectral Element Time-Domain (DG-SETD) Method for Maxwell’s Equations,” *IEEE Trans. Antennas Propagat.*, vol.63, no. 6, pp. 2585-2594, 2015.
  - Q. T. Sun, L. E. Tobon, Q. Ren, Y. Hu, and Q. H. Liu, “Efficient Noniterative Implicit Time-Stepping Scheme Based On E And B Fields For Sequential DG-FETD Systems,” *IEEE Trans. Components Packaging And Manufacturing Technology*, vol. 5, no. 12, pp. 1839-1849, Dec. 2015.
  - Q. Ren, Q. Sun, L. Tobón, Q. Zhan, and Q. H. Liu, "EB Scheme-Based Hybrid SE-FE DGTD Method for Multiscale EM Simulations," *IEEE Trans. Antennas Propagat.*, vol. 64, no. 9, pp. 4088-4091, Sep. 2016.
  - Q. Ren, Q. Zhan, Q. H. Liu, “An Improved Subdomain Level Nonconformal Discontinuous Galerkin Time Domain (DGTD) Method for Materials With Full-Tensor Constitutive Parameters”, *IEEE Photonics J.*, vol. 9, no. 2, p. 2600113, Apr. 2017.

Challenges

The FDTD method: high discretization density required to capture the geometric characteristics of electrically fine structures.

The FETD method: requires solving matrix equations, huge matrix for multiscale problems, either directly or iteratively.

Explicit time stepping: very small time steps → large number of steps.

Implicit time stepping: solution of large dense matrix each step.

Domain Decomposition Method

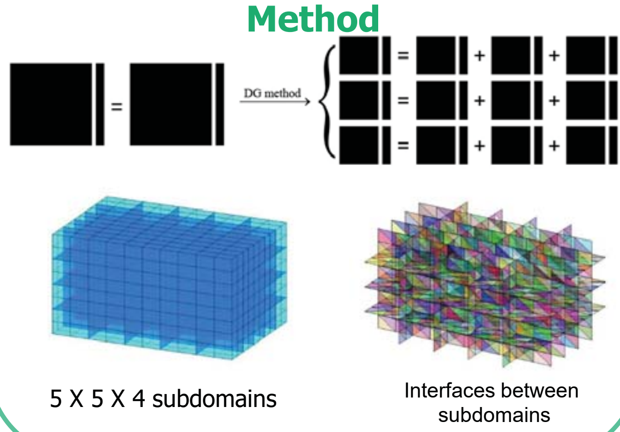

QHL/DGTD

Spatial Discretization and Time Integration

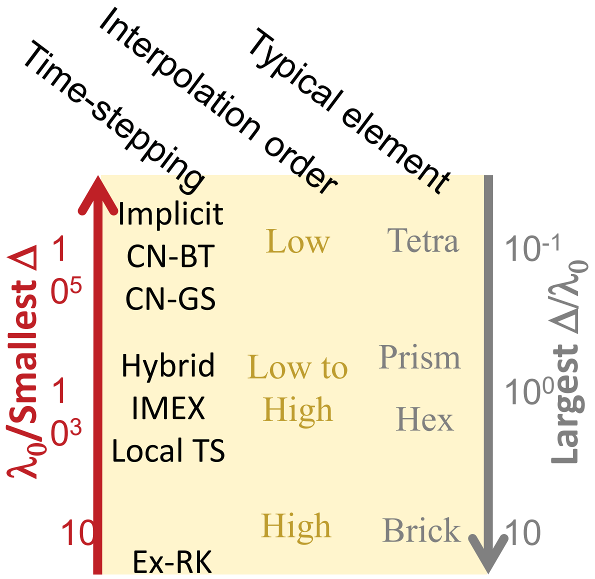

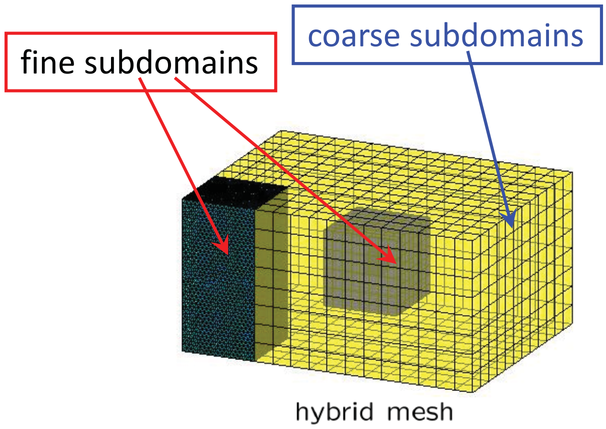

Multiscale Factor = Largest Δ /Smallest δ

QHL/DGTD

Summary (L. Tobon & Q. Ren)

1. *A unified framework based on the theory of differential forms and the finite element method.* It is used to analyze the discretization of the Maxwell's equations.
2. *Numerical analysis based on modal analysis for one- and two- dimensional spectral elements*. Comparison with analytical formulas of numerical dispersion based on semidiscrete analysis.
3. *Study of dispersive Hodge Operator.* Phase velocity analysis provides same conclusion as previous dispersion analysis.
4. *Implementation, analysis and application of Spectral-Prism element for EH DGTD;* including single domain performance analysis, and applications to multiple domain and multi-layered EM cases.
5. *Formulation, implementation and application of new LDU algorithm for highly multiscale EM cases decomposed in sequential order.*
6. *Implementation of first and second order divergence-conforming tetrahedral element for EB DGTD;* including single domain performance analysis, and applications to multiple domain and multiscale EM cases.
7. DGTD for anisotropic media.

QHL/DGTD

Maxwell's Equations

	Topological Laws	Constitutive Laws
Ampere-Maxwell's law	$\frac{\partial \mathbf{D}}{\partial t} = \nabla \times \mathbf{H} - \mathbf{J}_c - \mathbf{J}_s$	$\mathbf{D} = \epsilon \mathbf{E}$
Faraday-Lenz' law	$-\frac{\partial \mathbf{B}}{\partial t} = \nabla \times \mathbf{E} + \mathbf{M}_c + \mathbf{M}_s$	$\mathbf{B} = \mu \mathbf{H}$
Electric Gauss' law	$\nabla \cdot \mathbf{D} = \rho_e$	$\mathbf{J}_c = \sigma_e \mathbf{E}$
Magnetic Gauss' law	$\nabla \cdot \mathbf{B} = \rho_m$	$\mathbf{M}_c = \sigma_m \mathbf{H}$

$$\begin{array}{ccccccc} & & \mathbf{E} & \overset{\nabla\times}{\rightarrow} & \mathbf{B} & \overset{\nabla\cdot}{\rightarrow} & \rho_m \\ & & \epsilon \downarrow & & \mu \uparrow & & \\ \rho_e & \overset{\nabla\cdot}{\leftarrow} & \mathbf{D} & \overset{\nabla\times}{\leftarrow} & \mathbf{H} & & \end{array}$$

Tonti diagram for electromagnetics

QHL/DGTD

Maxwell Equations

Physics

$$\begin{array}{ccccccc} & & \mathbf{E} & \overset{\nabla\times}{\rightarrow} & \mathbf{B} & \overset{\nabla\cdot}{\rightarrow} & \rho_m \\ & & \epsilon \downarrow & & \mu \uparrow & & \\ \rho_e & \overset{\nabla\cdot}{\leftarrow} & \mathbf{D} & \overset{\nabla\times}{\leftarrow} & \mathbf{H} & & \end{array}$$

Tonti diagram

FEM

$$H^1 \overset{\nabla}{\rightarrow} \mathbf{H}(curl) \overset{\nabla\times}{\rightarrow} \mathbf{H}(div) \overset{\nabla\cdot}{\rightarrow} L^2$$

De Rham sequence

Differential Forms

$$\begin{array}{ccccccc} C^0 & \overset{d}{\rightarrow} & C^1 & \overset{d}{\rightarrow} & C^2 & \overset{d}{\rightarrow} & C^3 \\ \updownarrow\star & & \updownarrow\star & & \updownarrow\star & & \updownarrow\star \\ C^3 & \overset{d}{\leftarrow} & C^2 & \overset{d}{\leftarrow} & C^1 & \overset{d}{\leftarrow} & C^0 \end{array}$$

Cochain complex

$$\begin{array}{ccccccc} 0-\text{form} & \overset{d}{\rightarrow} & 1-\text{form} & \overset{d}{\rightarrow} & 2-\text{form} & \overset{d}{\rightarrow} & 3-\text{form} \\ \text{(Scalar Potentials)} & & \text{(Intensity fields)} & & \text{(Flux densities)} & & \text{(Charge densities)} \\ H^1 & & \mathbf{H}(curl) & & \mathbf{H}(div) & & L^2 \\ \Phi_E & \overset{\nabla}{\rightarrow} & \mathbf{E} & \overset{\nabla\times}{\rightarrow} & \mathbf{B} & \overset{\nabla\cdot}{\rightarrow} & \rho_m \\ & & \star_\epsilon \downarrow\uparrow \star_{\epsilon^{-1}} & & \star_{\mu^{-1}} \downarrow\uparrow \star_\mu & & \\ \rho_e & \overset{\nabla\cdot}{\leftarrow} & \mathbf{D} & \overset{\nabla\times}{\leftarrow} & \mathbf{H} & \overset{\nabla}{\leftarrow} & \Phi_M \\ L^2 & & \mathbf{H}(div) & & \mathbf{H}(curl) & & H^1 \\ 3-\text{form} & \overset{d}{\leftarrow} & 2-\text{form} & \overset{d}{\leftarrow} & 1-\text{form} & \overset{d}{\leftarrow} & 0-\text{form} \end{array}$$

QHL/DGTD

The Weak Form

DUKE
EDMUND T. PRATT, JR. SCHOOL OF ENGINEERING

Discrete Representation

$$\mathbf{E} \approx \sum_{j=1}^{N_E} e_j \mathbf{\Phi}_j^E \qquad \mathbf{D} \approx \sum_{j=1}^{N_D} d_j \mathbf{\Psi}_j^D$$

$$\mathbf{H} \approx \sum_{j=1}^{N_H} h_j \mathbf{\Phi}_j^H \qquad \mathbf{B} \approx \sum_{j=1}^{N_B} b_j \mathbf{\Psi}_j^B$$

Curl-Conforming   Div-Conforming

The weak form

$$\int_\Omega \mathbf{\Theta}_p \cdot \left(\frac{\partial \mathbf{D}}{\partial t} = \nabla \times \mathbf{H} - \mathbf{J} \right) dV = 0$$

$$\int_\Omega \mathbf{\Upsilon}_q \cdot \left(\frac{\partial \mathbf{B}}{\partial t} = -\nabla \times \mathbf{E} - \mathbf{M} \right) dV = 0$$

QHL/DGTD

Linear Systems

DUKE
EDMUND T. PRATT, JR. SCHOOL OF ENGINEERING

EH

$$\mathbf{M}_{ee} \frac{d\mathbf{e}}{dt} = \mathbf{K}_{eh}\mathbf{h} + \mathbf{C}_{ee}\mathbf{e} + \mathbf{j}$$
$$\mathbf{M}_{hh} \frac{d\mathbf{h}}{dt} = \mathbf{K}_{he}\mathbf{e} + \mathbf{C}_{hh}\mathbf{h} + \mathbf{m}$$

EB

$$\mathbf{M}_{ee} \frac{d\mathbf{e}}{dt} = \mathbf{K}_{eb}\mathbf{b} + \mathbf{C}_{ee}\mathbf{e} + \mathbf{j}$$
$$\mathbf{M}_{bb} \frac{d\mathbf{b}}{dt} = \mathbf{K}_{be}\mathbf{e} + \mathbf{C}_{bb}\mathbf{b} + \mathbf{m}$$

EHDB

$$\mathbf{M}_{dd} \frac{d\mathbf{d}}{dt} = \mathbf{K}_{dh}\mathbf{h} + \mathbf{C}_{ee}\mathbf{e} + \mathbf{j}$$
$$\mathbf{M}_{bb} \frac{d\mathbf{b}}{dt} = \mathbf{K}_{be}\mathbf{e} + \mathbf{C}_{hh}\mathbf{h} + \mathbf{m}$$

Mass matrices

$$(\mathbf{M}_{ee})_{kl}^e = \langle \mathbf{\Phi}_k^E, \epsilon \mathbf{\Phi}_l^E \rangle_{V_e}$$
$$(\mathbf{M}_{hh})_{kl}^e = \langle \mathbf{\Phi}_k^H, \mu \mathbf{\Phi}_l^H \rangle_{V_e}$$
$$(\mathbf{M}_{bb})_{kl}^e = \langle \mathbf{\Psi}_k^B, \mathbf{\Psi}_l^B \rangle_{V_e}$$
$$(\mathbf{M}_{dd})_{kl}^e = \langle \mathbf{\Psi}_k^D, \mathbf{\Psi}_l^D \rangle_{V_e}$$

Damping matrices

$$(\mathbf{C}_{ee})_{kl}^e = \langle \mathbf{\Phi}_k^E, \sigma_e \mathbf{\Phi}_l^E \rangle_{V_e}$$
$$(\mathbf{C}_{hh})_{kl}^e = \langle \mathbf{\Phi}_k^H, \sigma_m \mathbf{\Phi}_l^H \rangle_{V_e}$$
$$(\mathbf{C}_{bb})_{kl}^e = \langle \mathbf{\Psi}_k^B, \sigma_m \mu^{-1} \mathbf{\Psi}_l^B \rangle_{V_e}$$

Stiffness matrices

$$(\mathbf{K}_{eh})_{kl}^e = \langle \mathbf{\Phi}_k^E, \nabla \times \mathbf{\Phi}_l^H \rangle_{V_e}$$
$$(\mathbf{K}_{he})_{kl}^e = -\langle \mathbf{\Phi}_k^H, \nabla \times \mathbf{\Phi}_l^E \rangle_{V_e}$$
$$(\mathbf{K}_{eb})_{kl}^e = \langle \nabla \times \mathbf{\Phi}_k^E, \mu^{-1} \mathbf{\Psi}_l^B \rangle_{V_e}$$
$$(\mathbf{K}_{be})_{kl}^e = -\langle \mathbf{\Psi}_k^B, \nabla \times \mathbf{\Phi}_l^E \rangle_{V_e}$$

where

$$\langle \mathbf{f}, \mathbf{g} \rangle_{V_e} = \int_{V_e} \mathbf{f}^T \cdot \mathbf{g} dV$$

Hodge operators

$$\mathbf{d} = \star_\epsilon \mathbf{e} = \epsilon_0 \mathbf{M}_{dd}^{-1} \mathbf{M}_{de} \mathbf{e}$$
$$\mathbf{b} = \star_\mu \mathbf{h} = \mu_0 \mathbf{M}_{bb}^{-1} \mathbf{M}_{bh} \mathbf{h}$$
$$\mathbf{e} = \star_{1/\epsilon} \mathbf{d} = \frac{1}{\epsilon_0} \mathbf{M}_{ee}^{-1} \mathbf{M}_{ed} \mathbf{d}$$
$$\mathbf{h} = \star_{1/\mu} \mathbf{b} = \frac{1}{\mu_0} \mathbf{M}_{hh}^{-1} \mathbf{M}_{hb} \mathbf{b}$$

QHL/DGTD

Curl-conforming basis functions in SETD (hexahedron element)

DUKE EDMUND T. PRATT, JR. SCHOOL OF ENGINEERING

(E)

$$\hat{\mathbf{\Phi}}_{ijk}^{(\xi,M)} = \hat{\xi}\phi_i^{(M-1)}(\xi)\phi_j^{(M)}(\eta)\phi_k^{(M)}(\zeta), i=0,\cdots,M-1; (j,k)=0,\cdots,M$$
$$\hat{\mathbf{\Phi}}_{ijk}^{(\eta,M)} = \hat{\eta}\phi_i^{(M)}(\xi)\phi_j^{(M-1)}(\eta)\phi_k^{(M)}(\zeta), j=0,\cdots,M-1; (i,k)=0,\cdots,M$$
$$\hat{\mathbf{\Phi}}_{ijk}^{(\zeta,M)} = \hat{\zeta}\phi_i^{(M)}(\xi)\phi_j^{(M)}(\eta)\phi_k^{(M-1)}(\zeta), k=0,\cdots,M-1; (i,j)=0,\cdots,M$$

$$\phi_m^{(M)}(x) = \frac{-(1-x^2)L_N'(x)}{N(N+1)L_N(x_m)(x-x_m)}, m=0,\cdots,M$$

GLL polynomials

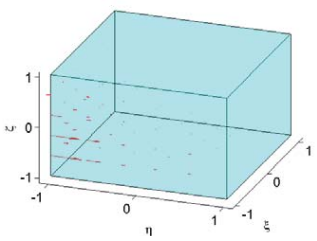

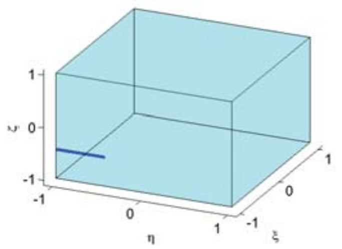

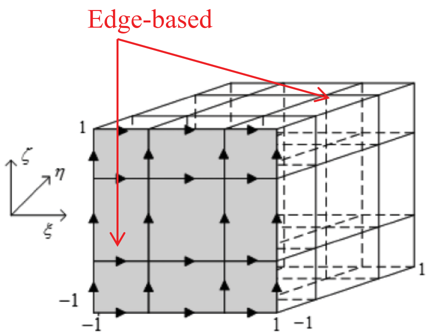

3rd order reference element

QHL/DGTD

Divergence-conforming basis functions in SETD (hexahedron element)

DUKE EDMUND T. PRATT, JR. SCHOOL OF ENGINEERING

(B)

$$\hat{\mathbf{\Psi}}_{ijk}^{(\xi,M)} = \hat{\xi}\phi_i^{(M)}(\xi)\phi_j^{(M-1)}(\eta)\phi_k^{(M-1)}(\zeta), i=0,\cdots,M; (j,k)=0,\cdots,M-1$$
$$\hat{\mathbf{\Psi}}_{ijk}^{(\eta,M)} = \hat{\eta}\phi_i^{(M-1)}(\xi)\phi_j^{(M)}(\eta)\phi_k^{(M-1)}(\zeta), j=0,\cdots,M; (i,k)=0,\cdots,M-1$$
$$\hat{\mathbf{\Psi}}_{ijk}^{(\zeta,M)} = \hat{\zeta}\phi_i^{(M-1)}(\xi)\phi_j^{(M-1)}(\eta)\phi_k^{(M)}(\zeta), k=0,\cdots,M; (i,j)=0,\cdots,M-1$$

$$\phi_m^{(M)}(x) = \frac{-(1-x^2)L_N'(x)}{N(N+1)L_N(x_m)(x-x_m)}, m=0,\cdots,M$$

GLL polynomials

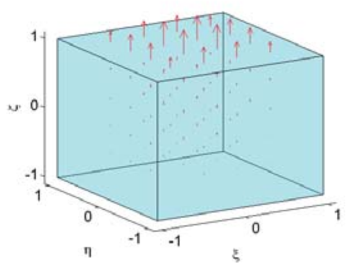

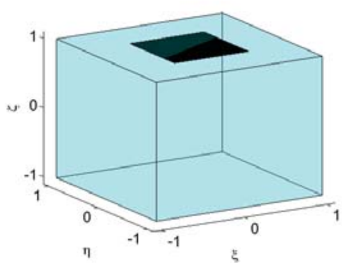

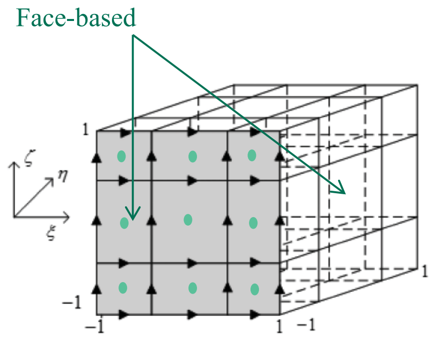

3rd order reference element

Curl-conforming basis functions in FETD (tetrahedron element)

Constant Tangential- Linear Normal (Ct/Ln) (E1)

$$\Phi_{ij}^{CtLn} = s_i \nabla s_j - s_j \nabla s_i$$ 6

s_p is the barycentric coordinate of the p-th vertex.

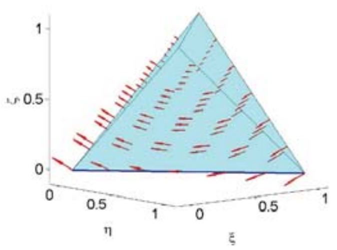

Linear Tangential- Quadratic Normal (Lt/Qn) (E2)

$$\Phi_{ij}^{LtQn} = s_i \nabla s_j$$ 12

$$\Phi_{ijk}^{LtQn} = s_i s_k \nabla s_j - s_j s_k \nabla s_i$$ 8

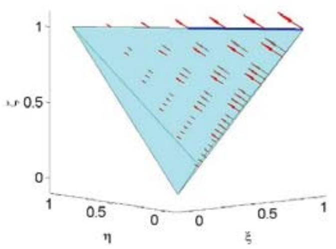

reference element

$$V = \frac{\sqrt{2}}{12}$$

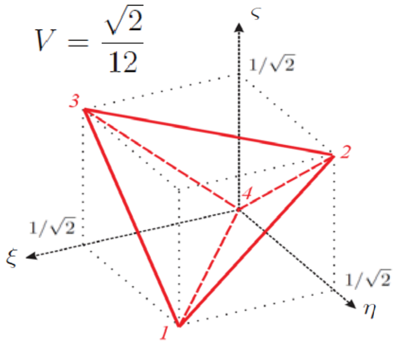

Divergence-conforming basis functions (tetrahedron element)

Constant Normal - Linear Tangential (Cn/Lt) (B1)

$$\Psi_{ijk}^{CnLt} = 2\left(s_i \vec{v}_{jk} + s_j \vec{v}_{ki} + s_k \vec{v}_{ij}\right)$$ 4

where $\vec{v}_{ij} = \nabla s_i \times \nabla s_j.$

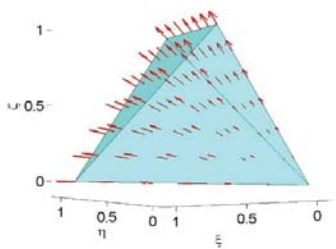

Linear Normal - Quadratic Tangential (Ln/Qt) (B2)

$$\Psi_{ijk}^{LnQt} = s_i \vec{v}_{jk}$$ 12

$$\Psi_{ijkl}^{LnQt} = 2 s_l \left(s_i \vec{v}_{jk} + s_j \vec{v}_{ki} + s_k \vec{v}_{ij}\right)$$ 3

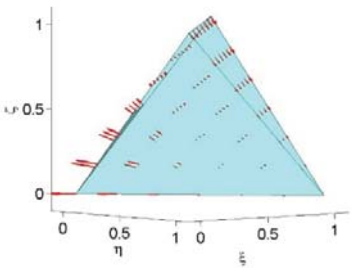

reference element

$$V = \frac{\sqrt{2}}{12}$$

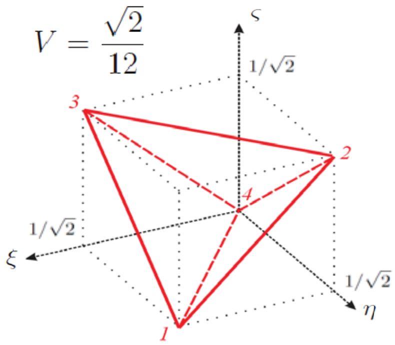

QHL/DGTD

Curl-conforming basis functions in prism element

Low order (E1n or H1n)

$$\hat{\Omega}_{1\,ik}^{(1,N)}(\xi,\eta,\varsigma)=\Theta_i^{(1)}(\xi,\eta)\,\phi_k^{(N)}(\varsigma)$$ Horizontal

$$\hat{\Omega}_{2\,ik}^{(1,N)}(\xi,\eta,\varsigma)=\hat{\varsigma}s_i(\xi,\eta)\,\phi_k^{(N-1)}(\varsigma)$$ Vertical

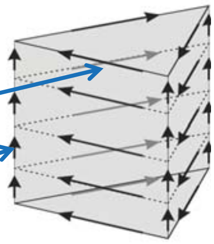

reference element

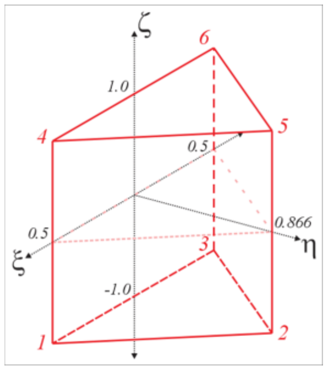

where

$$\Theta_i^{(1)}(\xi,\eta)=(s_{i+1}\nabla s_{i+2}-s_{i+2}\nabla s_{i+1})$$

$$\phi_m^{(M)}(x)=\frac{-(1-x^2)L_N'(x)}{N(N+1)L_N(x_m)(x-x_m)},m=0,\cdots,M$$

Name rule of basis functions in prism element:
1st digit is the order of triangles
2nd digit is the order of PLL polynomials in z direction

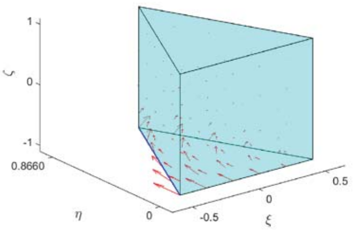

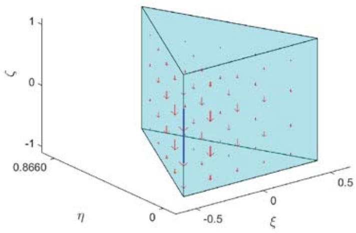

QHL/DGTD

High Order (E2n or H2n)

$$\hat{\Omega}_{1\,ijk}^{(2,N)}(\xi,\eta,\varsigma)=\Theta_{ij}^{(2)}(\xi,\eta)\,\phi_k^{(N)}(\varsigma)$$ Horizontal

$$\hat{\Omega}_{2\,ijk}^{(2,N)}(\xi,\eta,\varsigma)=\hat{\varsigma}L_{ij}(\xi,\eta)\,\phi_k^{(N-1)}(\varsigma)$$ Vertical

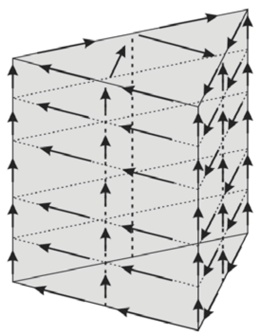

where

$$\phi_m^{(M)}(x)=\frac{-(1-x^2)L_N'(x)}{N(N+1)L_N(x_m)(x-x_m)},m=0,\cdots,M$$

$$\Theta_{ij}^{(2)}(\xi,\eta)=s_i\nabla s_j,\quad i=1,2,3;\quad j=1,2,3;\quad i\neq j$$

$$\Theta_{ij}^{(2)}(\xi,\eta)=(1-s_i-s_j)s_j\nabla s_i-(1-s_i-s_j)s_i\nabla s_j,\quad i=1,2;\quad j=1,2;\quad i\neq j$$

$$L_{ij}(\xi,\eta)=(2s_i-1)s_i,\quad i=1,2,3$$

$$L_{ij}(\xi,\eta)=s_is_j,\quad i,j=1,2,3;\quad i\neq j$$

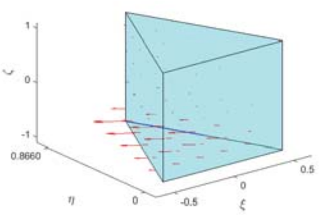

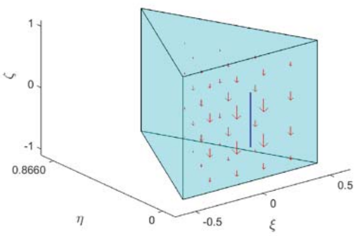

QHL/DGTD

Divergence-conforming basis functions in prism element

Low order (B1n or D1n)

$$\hat{\Xi}_{1k}^{(1,N)}(\xi,\eta,\varsigma)=\Upsilon_i^{(1)}(\xi,\eta)\,\phi_k^{(N-1)}(\varsigma)$$ Horizontal

$$\hat{\Xi}_{2ik}^{(1,N)}(\xi,\eta,\varsigma)=\hat{\varsigma}C\phi_k^{(N)}(\varsigma)$$ Vertical

where

$$\Upsilon_i^{(1)}(\xi,\eta)=\hat{\varsigma}\times(s_{i+1}\nabla s_{i+2}-s_{i+2}\nabla s_{i+1})$$

$$\phi_m^{(M)}(x)=\frac{-(1-x^2)L_N'(x)}{N(N+1)L_N(x_m)(x-x_m)},m=0,\cdots,M$$

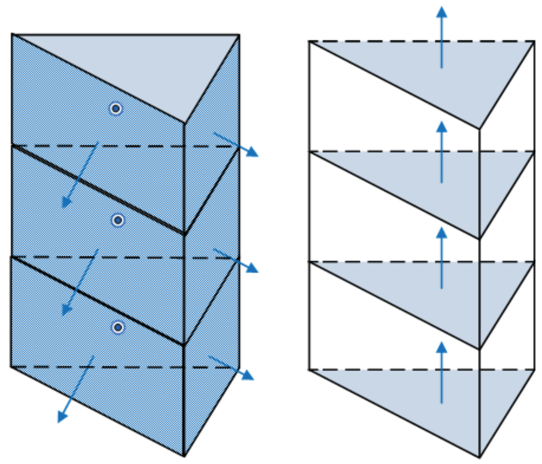

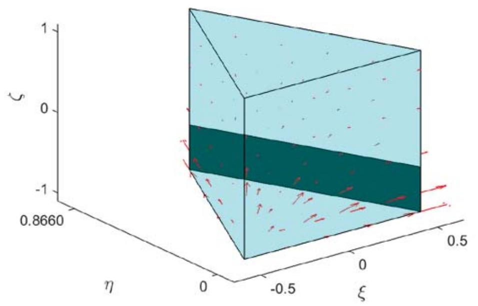

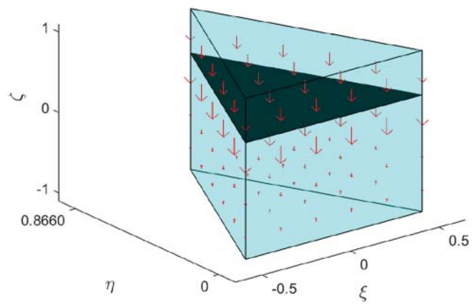

QHL/DGTD

High order (B2n or D2n)

$$\hat{\Xi}_{1ijk}^{(2,N)}(\xi,\eta,\varsigma)=\hat{\varsigma}\times\Theta_{ij}^{(2)}(\xi,\eta)\,\phi_k^{(N-1)}(\varsigma)$$ Horizontal

$$\hat{\Xi}_{2ik}^{(2,N)}(\xi,\eta,\varsigma)=\hat{\varsigma}s_i\phi_k^{(N)}(\varsigma)$$ Vertical

where

$$\Theta_{ij}^{(2)}(\xi,\eta)=s_i\nabla s_j,\quad i=1,2,3;\quad j=1,2,3;\quad i\neq j$$

$$\Theta_{ij}^{(2)}(\xi,\eta)=(1-s_i-s_j)s_j\nabla s_i-(1-s_i-s_j)s_i\nabla s_j,\quad i=1,2;\quad j=1,2;\quad i\neq j$$

$$\phi_m^{(M)}(x)=\frac{-(1-x^2)L_N'(x)}{N(N+1)L_N(x_m)(x-x_m)},m=0,\cdots,M$$

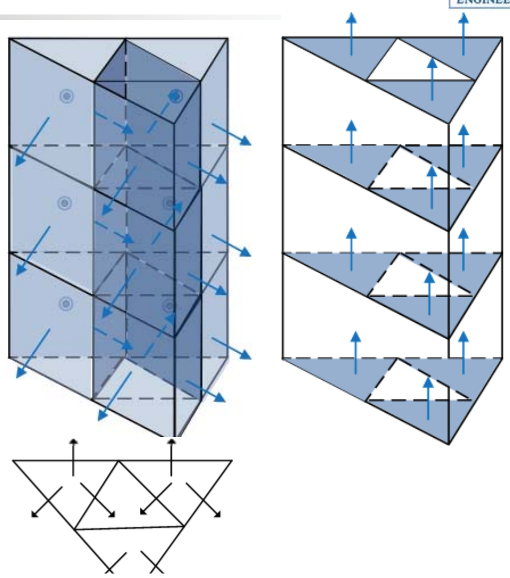

Total DoF in one prism element for divergence-conforming B2n or D2n: 8N+ 3(N+1)

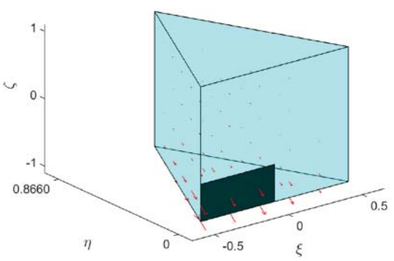

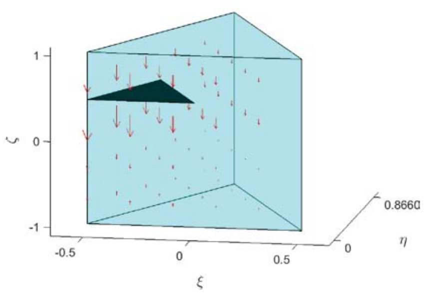

QHL/DGTD

Comparison of EH and EB Basis Functions

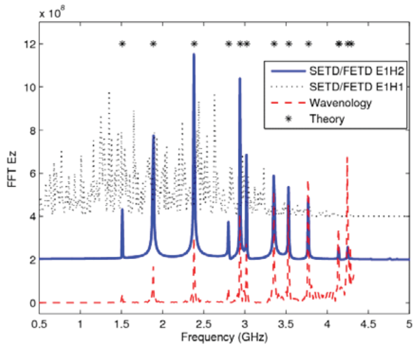

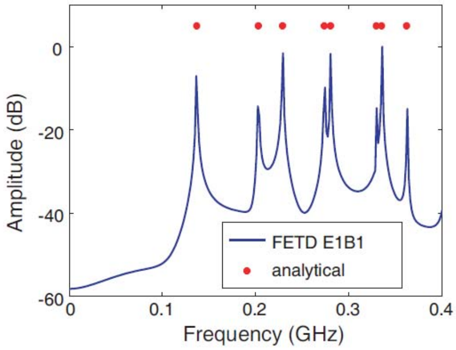

DoFs comparison

	Tetrahedron	Hexahedron
E_1H_2	26	66
E_1B_1	10	18
E_2H_3	92	180
E_2B_2	35	90
E_3H_4		408
E_3B_3		252

EB Scheme has much less DoFs

QHL/DGTD

Eigenvalue Problem for Analysis of Spurious Modes

Assuming harmonic variation $\frac{d}{dt} \to j\omega$

$$\boxed{\mathbf{Yv} = \chi \mathbf{Xv}}$$

$$\mathbf{Y} = -\mathbf{K}_{\alpha\beta}\left[\mathbf{M}_{\beta\beta}\right]\mathbf{K}_{\beta\alpha}$$

$$\mathbf{X} = \mathbf{M}_{\alpha\alpha}$$

$$\chi = \left(\frac{\omega}{c_0}\right)^2$$

Ref.: L. Tobon, J. Chen, and Q. H. Liu, "Spurious solutions in mixed finite element method for Maxwell's equations: Dispersion analysis and new basis functions," *J. Computat. Phys.*, vol. 30, 7300-7310, 2011.

QHL/DGTD

Eigenvalues, 1D periodic domain

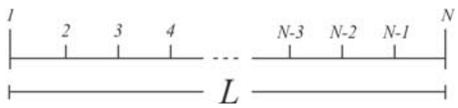

$L=1m$

Periodic Boundary Condition

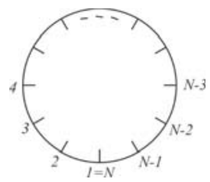

$k_{an} = 2\pi i \quad i = 1...N$

Eigenvalues with N=100:

Analytical	Mode E1H1	Numerical E1H1	Mode E2H1	Numerical E2H1
...	2	0.00000125	1	0.00000441
6.28318531	4	6.28318476	3	6.28318646
12.56637061	6	12.56635317	5	12.56640743
...	8	18.80005824		...
18.84955592	10	18.84942316	7	18.84983387
25.13274123	12	25.13217993	9	25.13390293
31.41592654	14	31.41420634	11	31.41943484
...	16	37.30580267		...

Spurious Modes !!

No spurious modes in E2H1

$EmHn$ represents $m-th$ order in E, and $n-th$ order in H

QHL/DGTD

Analytical	Mode E1H1	Numerical E1H1
...	2	0.00000125
6.28318531	4	6.28318476
12.56637061	6	12.56635317
...	8	18.80005824
18.84955592	10	18.84942316
25.13274123	12	25.13217993
31.41592654	14	31.41420634
...	16	37.30580267

Eigenvectors of E1H1:

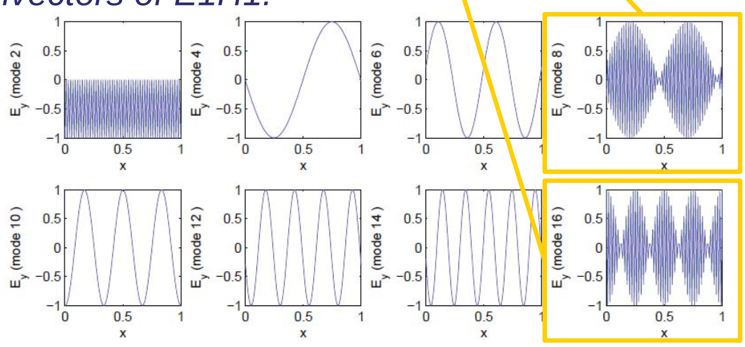

Spurious! 2nd kind

QHL/DGTD

Eigenvalues, 1D transient problem

Source:
1st derivative of BHW
fc=1.29GHz
Located in 0.35 m

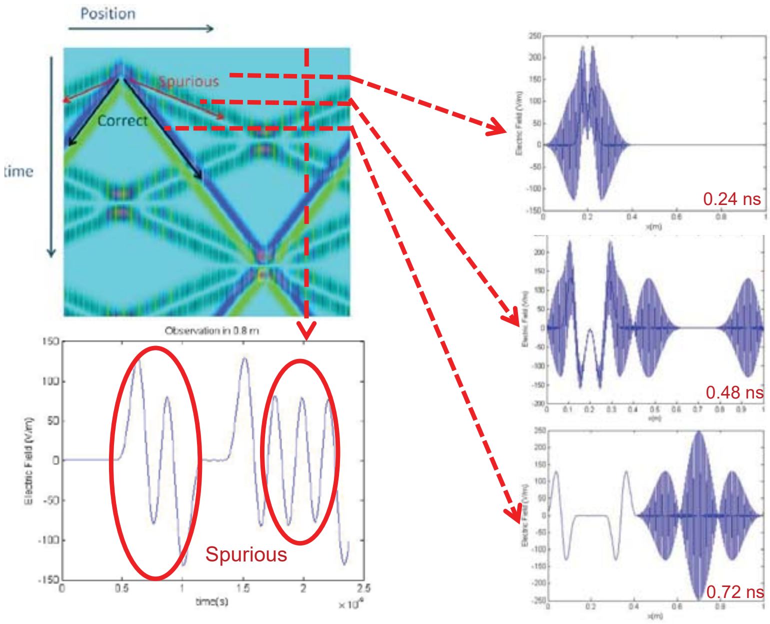

Observations

- Spurious with faster group velocities.
- Rapid change in space.
- Slow and difficult to found in time variation.

QHL/DGTD

Eigenvalues, 3D cavity

Dipole Source
Loc. (0.1,0.1,0.03)
Pol. (1,1,1)
Fc=2GHz

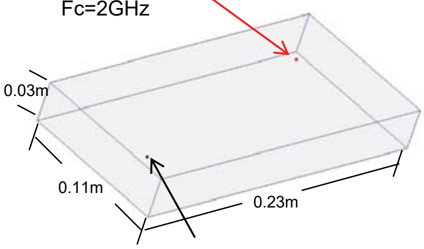

Dipole Receiver
Loc.
(0.20,0.07,0.013)

Mesh:
Brick elements
Δ=0.01x0.01x0.01

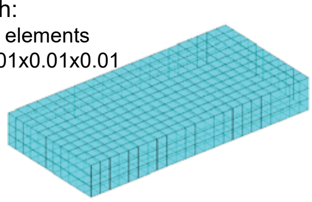

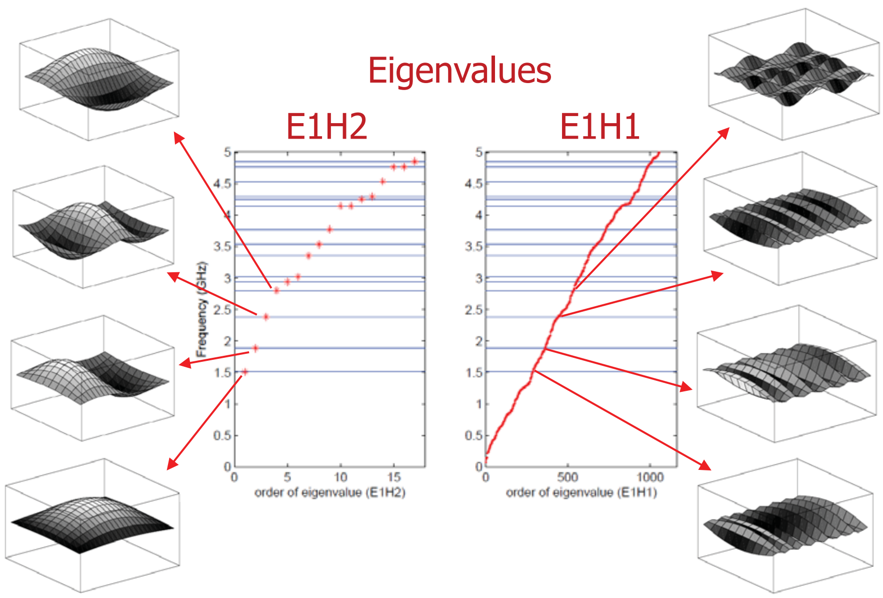

Eigenvectors E1H2

Eigenvectors E1H1

QHL/DGTD

Eigenvalues, 3D cavity

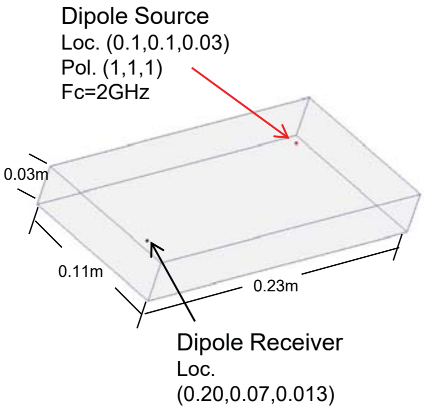

Mesh:
Brick elements
Δ=0.01x0.01x0.01

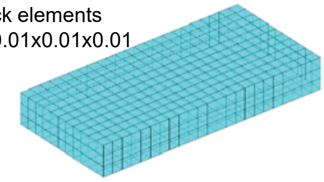

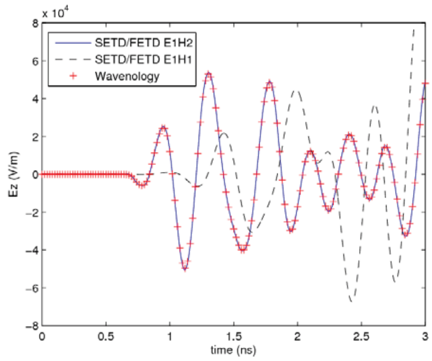

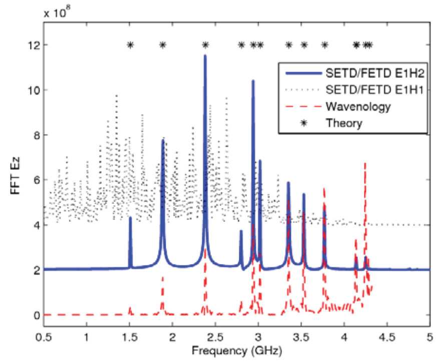

QHL/DGTD

Dispersion analysis, 1D semidiscrete analysis

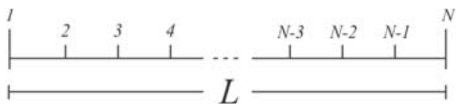

Periodic Boundary Condition

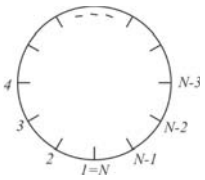

$k_{an} = 2\pi i \quad i = 1\ldots N$

Ampere-Maxwell's law

$$j\epsilon\omega E_y + \frac{dH_z}{dx} = 0$$

Weak form:

$$j\omega \sum_{p=1}^{n_e} E_p \int_0^L \epsilon \phi_q^{(M)} \phi_p^{(M)} dx + \sum_{p=1}^{n_h} H_p \int_0^L \phi_q^{(M)} \frac{d\psi_p^{(N)}}{dx} dx = 0$$

Faraday-Lenz' law

$$j\mu\omega H_z + \frac{dE_y}{dx} = 0$$

$$\sum_{p=1}^{n_e} E_p \int_0^L \psi_q^{(N)} \frac{d\phi_p^{(M)}}{dx} dx + j\omega \sum_{p=1}^{n_h} H_p \int_0^L \mu \psi_q^{(N)} \psi_p^{(N)} dx = 0$$

Discretization

$$E_y(x) = \sum_{p=1}^{n_e} E_p \phi_p^{(M)}(x) \qquad H_z(x) = \sum_{q=1}^{n_h} H_q \psi_q^{(N)}(x)$$

$$\boxed{\begin{Bmatrix} E_q \\ H_q \end{Bmatrix} = \begin{Bmatrix} E_p \\ H_p \end{Bmatrix} e^{jkx_{qp}}}$$

QHL/DGTD

Dispersion analysis, 1D semidiscrete analysis

$$\Omega^{1D}_{n,E1H1} = \frac{3\sin(\Omega_R)}{\cos(\Omega_R)+2}$$

Similarly,

$$\Omega^{1D}_{n,E2H1} = \sqrt{\frac{5(3-\cos(\Omega_R))(1-\cos(\Omega_R))+\sin^2(\Omega_R)}{(3-\cos(\Omega_R))(2+\cos(\Omega_R))}}$$

$$\Omega = \frac{\kappa L}{P\min(M_E, M_H)}$$

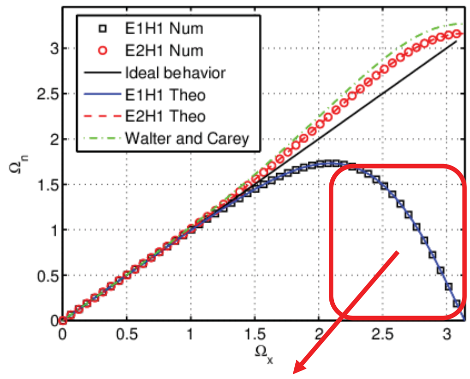

Non monotonic behavior using elements with common interpolation

Spurious Modes

QHL/DGTD

Dispersion analysis, 2D semidiscrete analysis

$$\Omega^{2D}_{n,E1H1} = \sqrt{\frac{27}{2}}\left[\sum_{\alpha,\beta=x,y}\frac{\sin^2\Omega_\alpha(1+\cos\Omega_\beta)}{(2+\cos\Omega_\alpha)^2(2+\cos\Omega_\beta)}\right]^{1/2}$$

$$\Omega^{2D}_{n,E1H2} = \sqrt{\frac{25}{3}}\left[\sum_{\alpha,\beta=x,y}\frac{\sin\frac{\Omega_\alpha}{2}\left(4+\cos\frac{\Omega_\beta}{2}\right)\left(\sin\Omega_\alpha+4\sin\frac{\Omega_\alpha}{2}\right)}{(2+\cos\Omega_\alpha)\left[\left(2+\cos\frac{\Omega_\alpha}{2}\right)\left(2+\cos\frac{\Omega_\beta}{2}\right)+12\right]}\right]^{1/2}$$

$$\Omega_n^{ideal} = \sqrt{\Omega_x^2+\Omega_y^2}$$

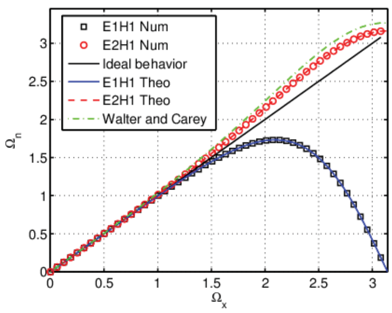

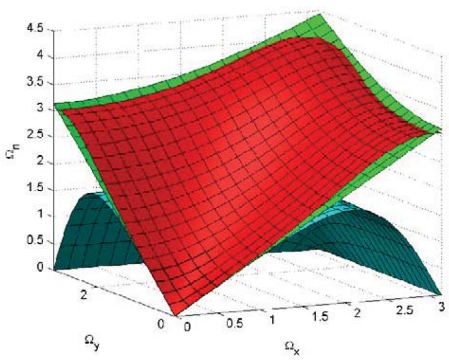

Blue→ E1H1
Red → E1H2
Green → Ideal

This approach becomes cumbersome for higher orders basis functions.

QHL/DGTD

Dispersion analysis, modal analysis

DUKE
EDMUND T. PRATT, JR. SCHOOL OF ENGINEERING

0. Periodic Boundary Condition

1. Assume harmonic plane wave solution

$$\mathbf{E}_a(\mathbf{r}, t, \kappa, \theta) = \mathbf{E}_0(\theta) \exp(\boldsymbol{\kappa} \cdot \mathbf{r} - i\omega t)$$

$$|\boldsymbol{\kappa}| = \kappa = \frac{\omega}{c_0} = \frac{2\pi}{\lambda_0}$$

2. Approx. discrete harmonic plane wave

$$\mathbf{e_a} = \mathbf{M_{ee}^{-1}} \mathbf{e}^*$$

q^{th} element: $e_q^* = \int_V \boldsymbol{\Phi}_q^{(M_E)} \cdot \mathbf{E}_0(\theta) \exp(\boldsymbol{\kappa} \cdot \mathbf{r})\, dV$

$$\boxed{\mathbf{Yv} = \chi \mathbf{Xv}} \Rightarrow \boxed{\tilde{\chi} = \tilde{\kappa}^2 = \frac{\mathbf{e_a}^T \mathbf{Y} \mathbf{e_a}}{\mathbf{e_a}^T \mathbf{X} \mathbf{e_a}}} \qquad \boxed{\Omega = \frac{\kappa L}{P \min(M_E, M_H)}}$$

3. Approx. eigenvalue

Rayleigh quotient

Normalized wavenumber

QHL/DGTD

Dispersion modal analysis, Quadrilateral TE_z

DUKE
EDMUND T. PRATT, JR. SCHOOL OF ENGINEERING

E1 H1 B1 D1

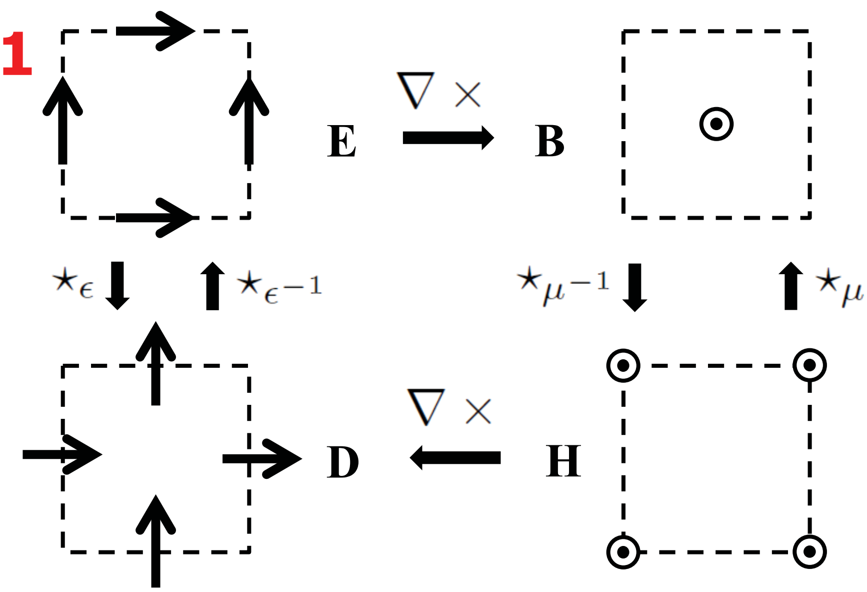

QHL/DGTD

Dispersion modal analysis, E1H1

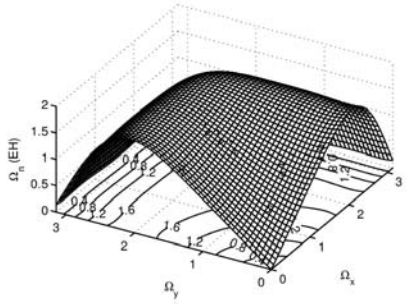

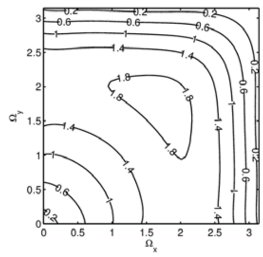

Phase velocity

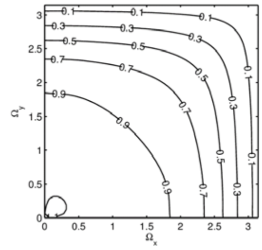

Phase velocity goes to zero for large wavenumbers

Small error, less that 4% for large wavenumbers

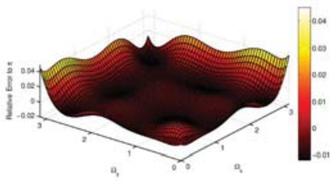

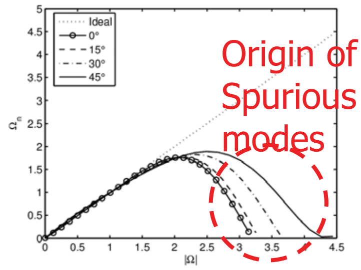

Group velocity

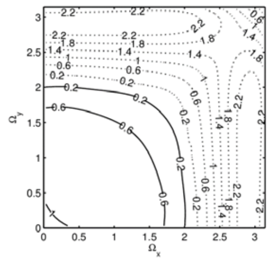

Negative Group velocity for large wavenumbers

Spurious solutions

QHL/DGTD

Dispersion modal analysis, E1B1

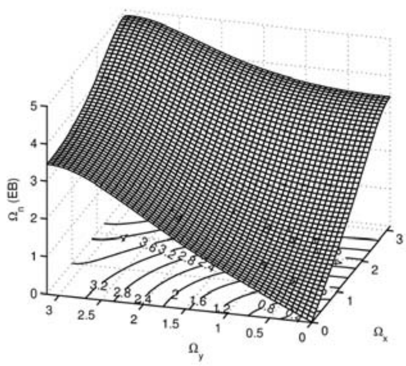

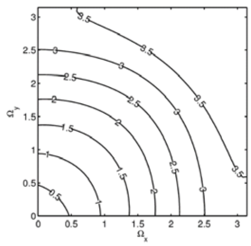

Good behavior

Phase velocity

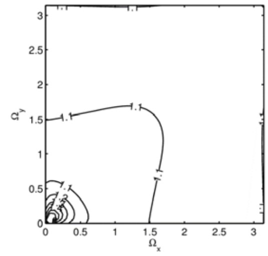

Phase velocity a Little bit faster than one

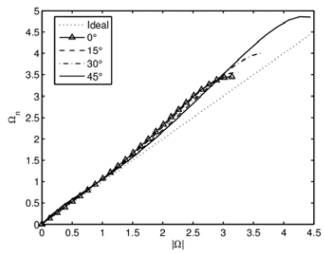

No spurious solutions

Group velocity

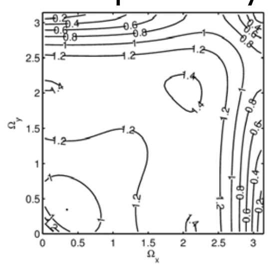

Positive group velocity for all wavenum bers

Dispersion modal analysis, Quadrilateral TE_z

E1 H2 B1 D2

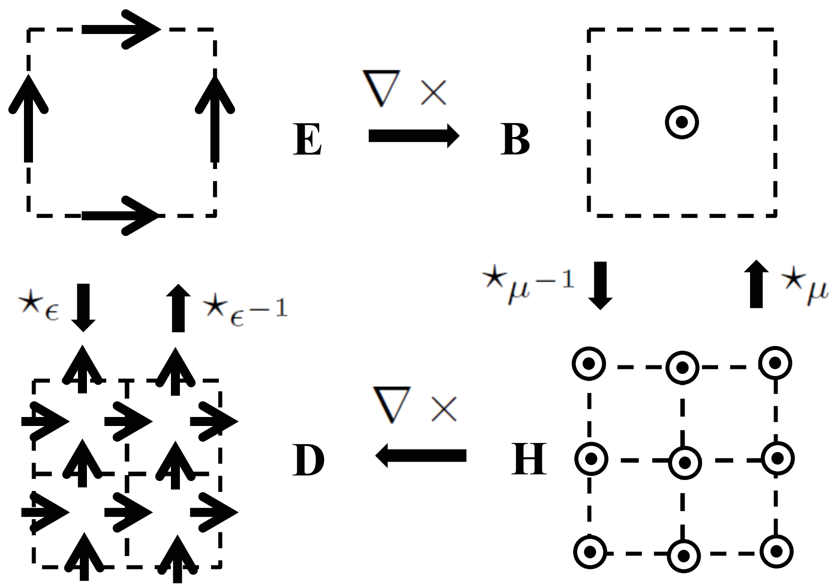

Dispersion modal analysis, Quadrilateral TE_z

E2 H2 B2 D2

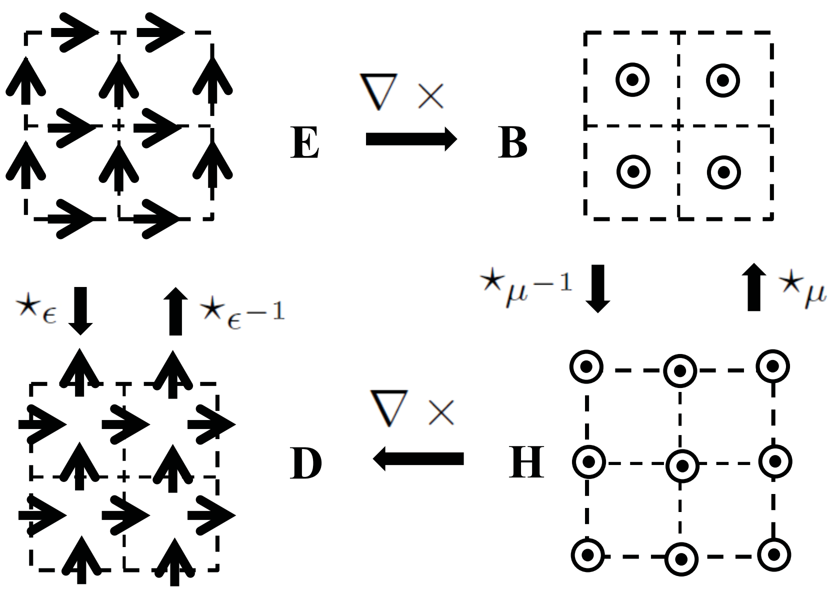

QHL/DGTD

Dispersion modal analysis, E2H2

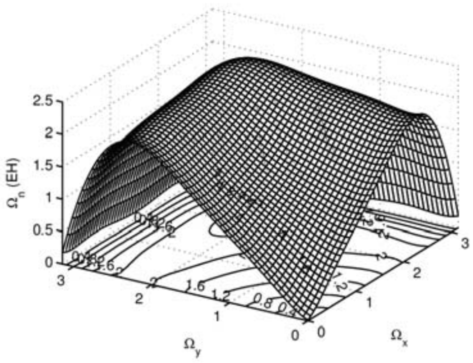

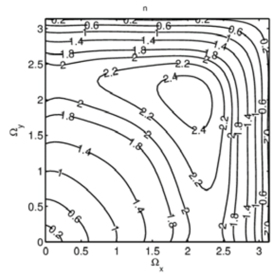

Phase velocity

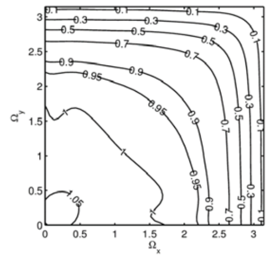

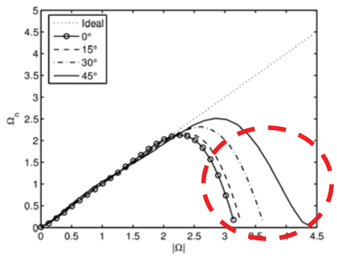

Group velocity

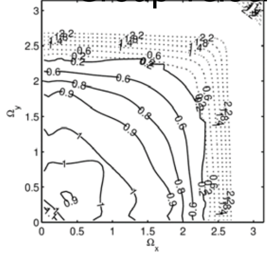

Negative and fast group velocities

Spurious solutions

QHL/DGTD

Dispersion modal analysis, E2B2

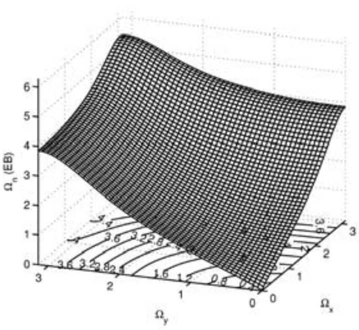

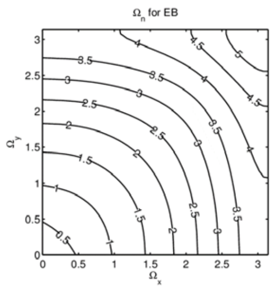

Phase velocity

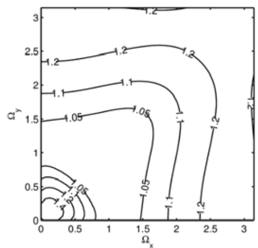

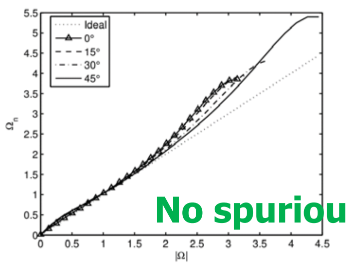

No spurious modes

Group velocity

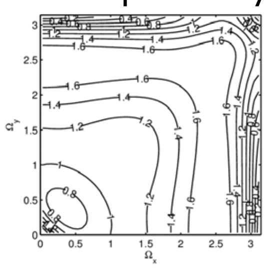

QHL/DGTD

Study of tetrahedral element

E1 H2 B1 D2

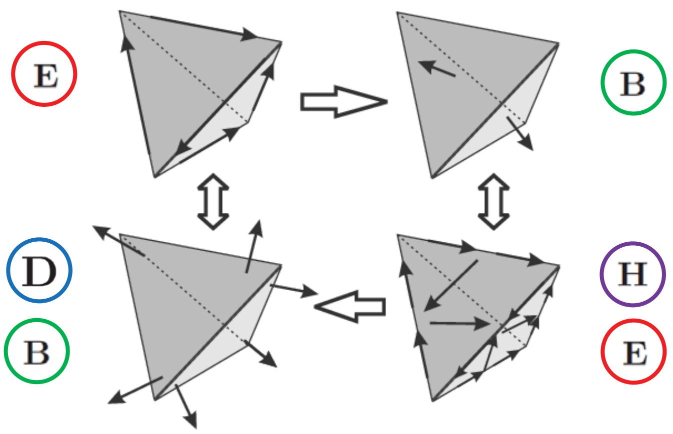

E2 B2

QHL/DGTD

Eigenvalue analysis, tetrahedral element

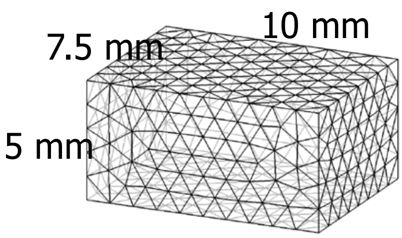

Source: $(\sqrt{2}\,\mathrm{mm}, \sqrt{2}\,\mathrm{mm}, \sqrt{2}\,\mathrm{mm})$

Receiver: $(6\sqrt{2}\,\mathrm{mm}, 4\sqrt{2}\,\mathrm{mm}, 2\sqrt{2}\,\mathrm{mm})$

Time function: 1st d. BHW

f_{max}=30 GHz λ_{min}=10 mm

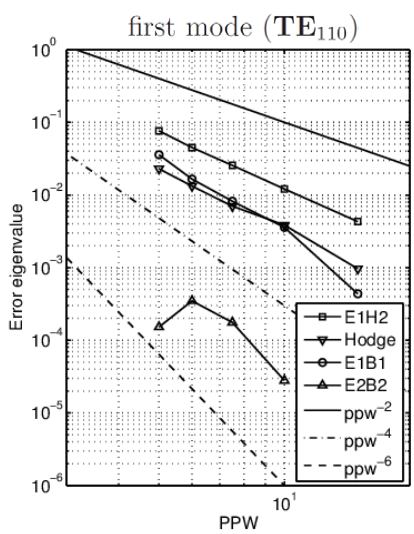

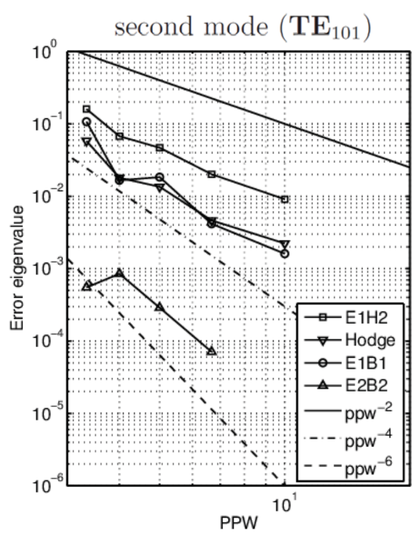

QHL/DGTD

DUKE EDMUND T. PRATT, JR. SCHOOL OF ENGINEERING

Eigenvector analysis, tetrahedral element

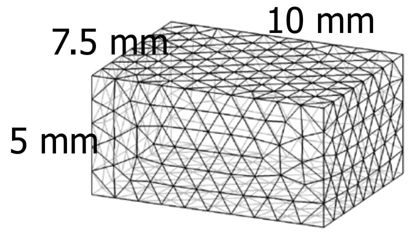

Source: $(\sqrt{2}\,\mathrm{mm}, \sqrt{2}\,\mathrm{mm}, \sqrt{2}\,\mathrm{mm})$

Receiver: $(6\sqrt{2}\,\mathrm{mm}, 4\sqrt{2}\,\mathrm{mm}, 2\sqrt{2}\,\mathrm{mm})$

Time function: 1st d. BHW

f_{max}=30 GHz λ_{min}=10 mm

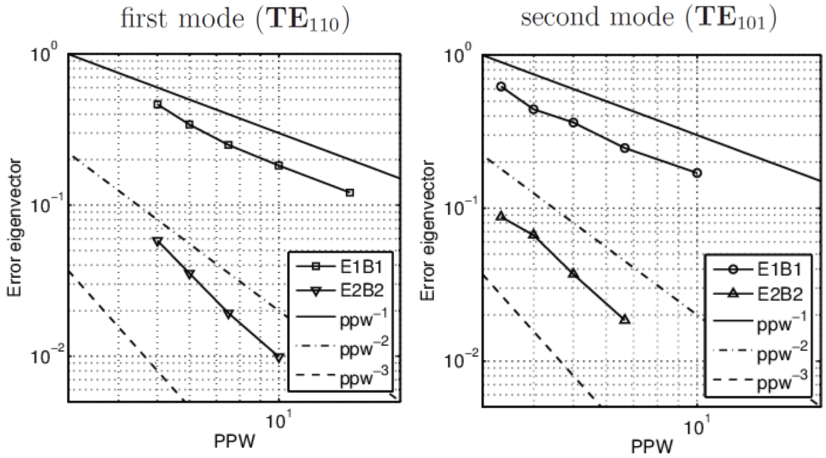

QHL/DGTD

DUKE EDMUND T. PRATT, JR. SCHOOL OF ENGINEERING

Transient solution, tetrahedral element

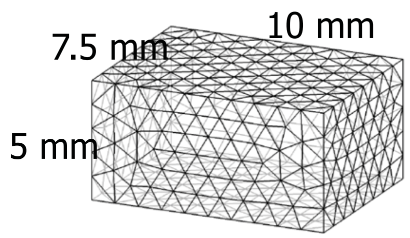

Source: $(\sqrt{2}\,\mathrm{mm}, \sqrt{2}\,\mathrm{mm}, \sqrt{2}\,\mathrm{mm})$

Receiver: $(6\sqrt{2}\,\mathrm{mm}, 4\sqrt{2}\,\mathrm{mm}, 2\sqrt{2}\,\mathrm{mm})$

Time function: 1st d. BHW

f_{max}=30 GHz λ_{min}=10 mm

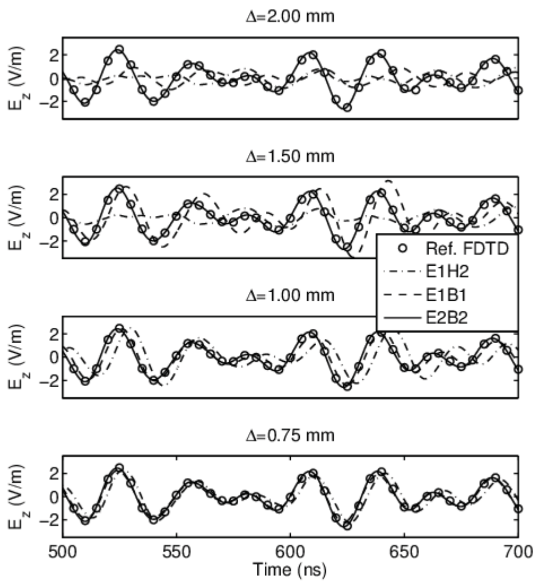

E1H2 is the most dispersive method

E2B2 is the most accurate method

Study of spectral prism element

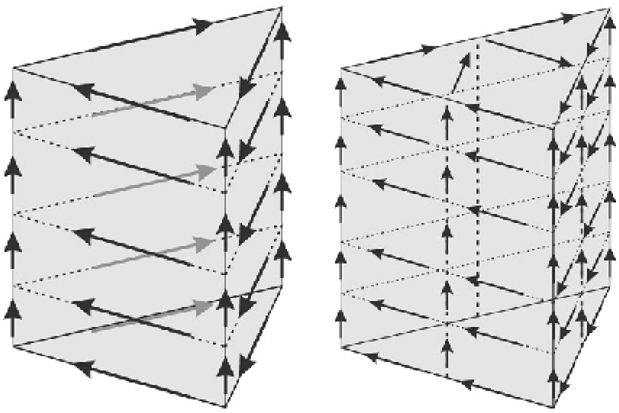

Algebraic and exponential convergence

h-refinement

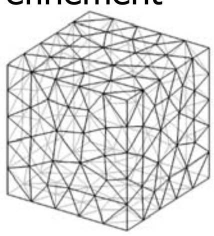

p-refinement

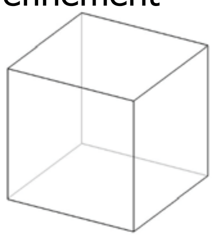

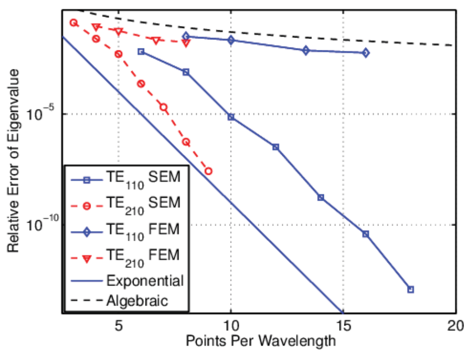

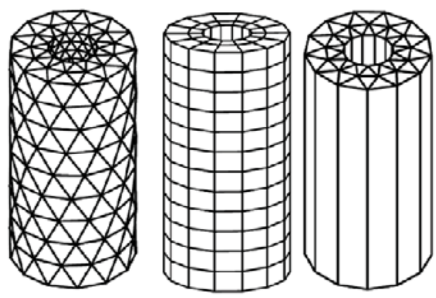

(a) (b) (c)

QHL/DGTD

Spectral prism element, convergence

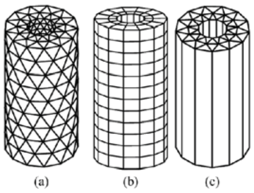

Mode	Frequency (GHz)
TEM_1	7.494811
TEM_2	14.989622
$\mathrm{TE}_{1,1,1}$	15.846394
$\mathrm{TE}_{1,1,2}$	20.490442
TEM_3	22.500000
$\mathrm{TE}_{1,1,3}$	26.478448
$\mathrm{TE}_{2,1,1}$	28.160966
TEM_4	29.979246

Algebraic

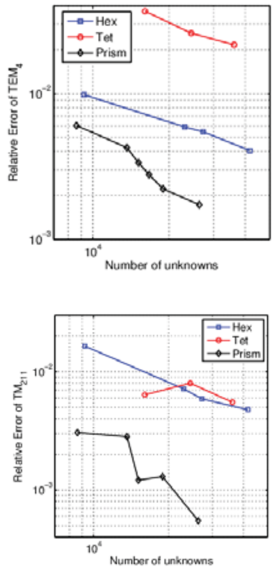

Exponential

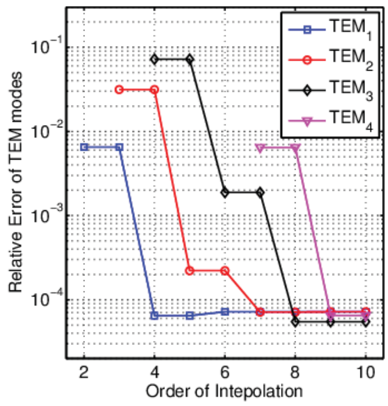

QHL/DGTD

EB Scheme Upwind Flux DG Formulation

Weak Forms of Maxwell's Equations with DG

$$\int_V \hat{\mathbf{\Phi}}^i\cdot\left(\varepsilon_r\frac{\partial\hat{\mathbf{E}}^i}{\partial t}+\frac{\sigma_e}{\varepsilon_0}\hat{\mathbf{E}}^i+\frac{\sqrt{\mu_0}}{\varepsilon_0}\mathbf{J}^i\right)dV = c_0\int_V \nabla\times\hat{\mathbf{\Phi}}^i\cdot\mu_r^{-1}\hat{\mathbf{B}}^i dV + c_0\int_S \hat{\mathbf{\Phi}}^i\cdot(\hat{\mathbf{n}}^i\times\mu_r^{-1}\hat{\mathbf{B}}^t)dS$$

$$\int_V \hat{\mathbf{\Psi}}^i\cdot\left(\frac{\partial\hat{\mathbf{B}}^i}{\partial t}+\frac{\sigma_m}{\mu}\hat{\mathbf{B}}^i+\frac{\mathbf{M}^i}{\sqrt{\varepsilon_0}}\right)dV = -c_0\int_V \hat{\mathbf{\Psi}}^i\cdot\nabla\times\hat{\mathbf{E}}^i dV + c_0\int_V \hat{\mathbf{\Psi}}^i\cdot(\hat{\mathbf{n}}^i\times\hat{\mathbf{E}}^i)dS - c_0\int_S \mathbf{\Psi}^i\cdot(\hat{\mathbf{n}}^i\times\hat{\mathbf{E}}^t)dS$$

$$\hat{\mathbf{E}} = \sqrt{\mu_0}\mathbf{E}$$

$$\hat{\mathbf{B}} = \mathbf{B}/\sqrt{\varepsilon_0}$$

EB Scheme Riemann Solver

$$(\hat{\mathbf{n}}^i\times\mathbf{E}^t) = \frac{\hat{\mathbf{n}}^i\times(Y^i\mathbf{E}^i+Y^j\mathbf{E}^j)}{Y^i+Y^j} - \frac{\hat{\mathbf{n}}^i\times\hat{\mathbf{n}}^i\times(\mu_j\mathbf{B}^i-\mu_i\mathbf{B}^j)}{\mu_i\mu_j(Y^i+Y^j)}$$

$$(\hat{\mathbf{n}}^i\times\mu^{-1}\mathbf{B}^t) = \frac{\hat{\mathbf{n}}^i\times(\mu_j Z^i\mathbf{B}^i+\mu_i Z^j\mathbf{B}^j)}{\mu_i\mu_j(Z^i+Z^j)} - \frac{\hat{\mathbf{n}}^i\times\hat{\mathbf{n}}^i\times(\mathbf{E}^i-\mathbf{E}^j)}{Z^i+Z^j}$$

Non-Conformal Mesh

Allow different kinds of elements

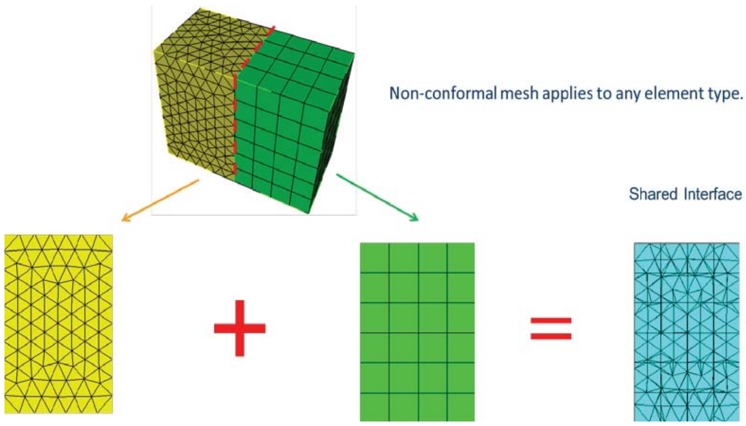

Allow a sharp change of element size

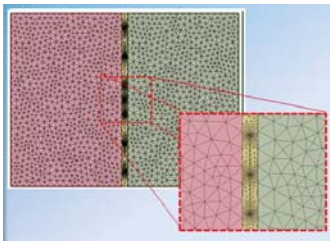

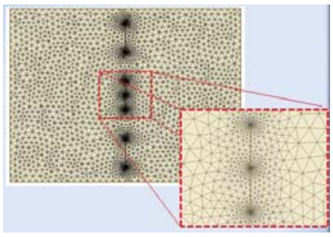

DGTD, EB scheme

$$\mathbf{M}_{ee}^{(i)}\frac{d\mathbf{e}^{(i)}}{dt} = \mathbf{K}_{eb}^{(i)}\mathbf{b}^{(i)} + \mathbf{C}_{ee}^{(i)}\mathbf{e}^{(i)} + \mathbf{j}^{(i)} + \sum_{j=1}^{N}\mathbf{L}_{eb}^{(ij)}\mathbf{b}^{(j)},\ i = 1, \dots N$$

$$\mathbf{M}_{bb}^{(i)}\frac{d\mathbf{b}^{(i)}}{dt} = \mathbf{K}_{be}^{(i)}\mathbf{e}^{(i)} + \mathbf{C}_{bb}^{(i)}\mathbf{b}^{(i)} + \mathbf{m}^{(i)} + \sum_{j=1}^{N}\mathbf{L}_{be}^{(ij)}\mathbf{e}^{(j)},\ i = 1, \dots N$$

$$(\mathbf{L}_{eb}^{(ij)})_{pq} = \frac{1}{2}\langle \mathbf{\Phi}_p^{E,(i)}, (\hat{\mathbf{n}}^{(i)} \times \frac{\mathbf{\Psi}_q^{B,(j)}}{\mu^{(j)}})\rangle_{S_{ij}}$$

$$(\mathbf{L}_{be}^{(ij)})_{pq} = \frac{1}{2}\langle \mathbf{\Psi}_p^{B,(i)}, (\hat{\mathbf{n}}^{(i)} \times \mathbf{\Phi}_q^{E,(j)})\rangle_{S_{ij}}$$

QHL/DGTD

DGTD, Cavity case

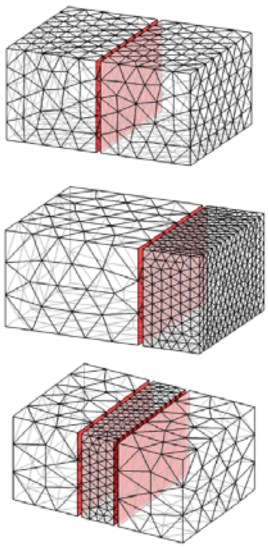

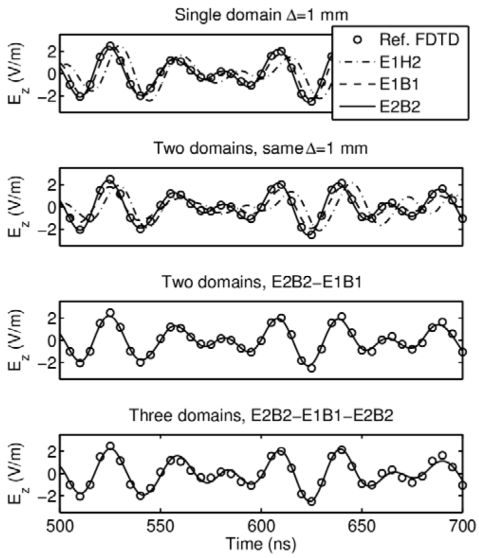

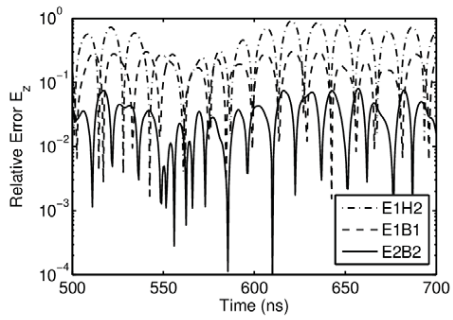

1. The EB scheme is more accurate than EH scheme.
2. Dispersion error in the E1H2 scheme is very high.
3. Numerical dispersion in the E2B2 scheme is the lowest.

QHL/DGTD

Maxwellian ODE Non-Convolutional PML

Coordinate Stretching

$$\partial\eta \rightarrow \left[1 + \frac{\omega_\eta(\eta)}{-j\omega}\right]\partial\eta \quad (\eta = x, y, z)$$

PML Profile

$$\omega_\eta = K_{max}\omega \frac{|\eta - \eta_b|^p}{d^p_{PML}} (\eta = x,\ y,\ z)$$

$$K_{max} = 5 - 12 \qquad p = 0 - 2$$

Auxiliary Equations

$$\tilde{\mathbf{B}} = \mathbf{B} + \Lambda_0\bar{\mathbf{B}} \qquad \tilde{\mathbf{E}} = \mathbf{E} + \Lambda_0\bar{\mathbf{E}} \qquad \bar{\mathbf{E}} = \int \mathbf{E}\, dt \qquad \bar{\mathbf{B}} = \int \mathbf{B}\, dt$$

$$\Lambda_0 = diag\{\omega_x, \omega_y, \omega_z\}$$

$$\Lambda_1 = diag\{(\omega_x - \omega_y)(\omega_x - \omega_z), (\omega_y - \omega_x)(\omega_y - \omega_z), (\omega_z - \omega_x)(\omega_z - \omega_y)\}$$

$$\Lambda_2 = diag\{(\omega_x - \omega_y)(\omega_x - \omega_z), (\omega_y - \omega_x)(\omega_y - \omega_z), (\omega_z - \omega_x)(\omega_z - \omega_y)\}$$

$$\mathbf{M}^i_{ee}\frac{d\tilde{\mathbf{e}}^i}{dt} = \mathbf{K}^i_{eb}\tilde{\mathbf{b}}^i + \mathbf{R}^i_{ee}\tilde{\mathbf{e}}^i + \mathbf{S}^i_{ee}\bar{\mathbf{e}}^i + \mathbf{j}^i + \sum_{j=1}^{N}\mathbf{L}^{ij}_{eb}\tilde{\mathbf{b}}^j + \sum_{j=1}^{N}\mathbf{L}^{ij}_{ee}\tilde{\mathbf{e}}^j$$

$$\mathbf{M}^i_{bb}\frac{d\tilde{\mathbf{b}}^i}{dt} = \mathbf{K}^i_{be}\tilde{\mathbf{e}}^i + \mathbf{R}^i_{bb}\tilde{\mathbf{b}}^i + \mathbf{S}^i_{bb}\bar{\mathbf{b}}^i + \mathbf{m}^i + \sum_{j=1}^{N}\mathbf{L}^{ij}_{be}\tilde{\mathbf{e}}^j + \sum_{j=1}^{N}\mathbf{L}^{ij}_{bb}\tilde{\mathbf{b}}^j$$

$$\mathbf{M}^i_{ee}\frac{d\bar{\mathbf{e}}^i}{dt} = \mathbf{M}^i_{ee}\tilde{\mathbf{e}}^i + \mathbf{T}^i_{ee}\bar{\mathbf{e}}^i \qquad \mathbf{M}^i_{bb}\frac{d\bar{\mathbf{b}}^i}{dt} = \mathbf{M}^i_{bb}\tilde{\mathbf{b}}^i + \mathbf{T}^i_{bb}\bar{\mathbf{b}}^i$$

Advantage

1. Unsplit, Maxwellian (FE, SE)
2. Non-convolutional
3. Long-time stability
4. Ordinary differential equations

18

QHL/DGTD

DG-TD, Time Stepping schemes

Rewritting previous DGTD equations

$$\mathbf{M}^{(i)}\frac{d\mathbf{v}^{(i)}}{dt}=\sum_{j=1}^{N}\mathbf{L}^{(i,j)}\mathbf{v}^{(j)}+\mathbf{f}^{(i)},\ i=1,\ldots N$$

	Accuracy	Stability	CPU time	Memory	Cases
ExRK	High	Conditional	Fast	Low	EH, EB, high order elements
ImExRK	Middle	Conditional	fast	Medium	EH, EB, multiscale structures
CN-GS	Low	Unconditional	Slow	Medium	EH, EB, small structures
CN-BT	High	Unconditional	Fast	High	EH, EB, sequential cases
CN-LDU	High	Unconditional	Fast	Medium	EH, sequential cases

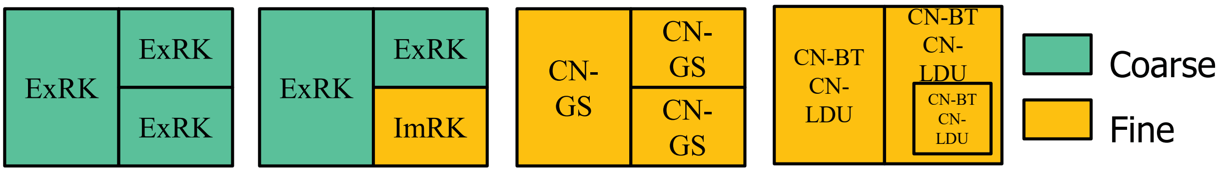

QHL/DGTD

DG-TD, ImEx Runge-Kutta

$$\mathbf{v}_{n+1}^{(i)}=\mathbf{v}_{n}^{(i)}+\Delta t\sum_{k=1}^{s}b_k\mathbf{u}_k^{(i)},\quad i=1,\cdots,N_{\text{im}}+N_{\text{ex}}$$

Explicit

$$\mathbf{M}^{(i)}\mathbf{u}_k^{(i)}=\sum_{j=N_{\text{im}}+1}^{N_{\text{im}}+N_{\text{ex}}}\mathbf{L}^{(ij)}\left(\mathbf{v}_n^{(j)}+\Delta t\sum_{l=1}^{k-1}a_{k,l}^{\text{ex}}\mathbf{u}_l^{(j)}\right)$$
$$+\sum_{j=1}^{N_{\text{im}}}\mathbf{L}^{(ij)}\left(\mathbf{v}_n^{(j)}+\Delta t\sum_{l=1}^{k}a_{k,l}^{\text{im}}\mathbf{u}_l^{(j)}\right)$$
$$+\mathbf{f}^{(i)}(t_n+c_k\Delta t)$$

Implicit

$$\left(\mathbf{M}^{(i)}-\Delta t a_{k,k}^{\text{im}}\mathbf{L}^{(ii)}\right)\mathbf{u}_k^{(i)}=\mathbf{f}^{(i)}(t_n+c_k\Delta t)$$
$$+\mathbf{L}^{(ii)}\left(\mathbf{v}_n^{(i)}+\Delta t\sum_{l=1}^{k-1}a_{k,l}^{\text{im}}\mathbf{u}_l^{(j)}\right)$$
$$+\sum_{j=N_{\text{im}}+1}^{N_{\text{im}}+N_{\text{ex}}}\mathbf{L}^{(ij)}\left(\mathbf{v}_n^{(j)}+\Delta t\sum_{l=1}^{k-1}a_{k,l}^{\text{ex}}\mathbf{u}_l^{(j)}\right)$$

$$\begin{array}{c|cccccc}
0 & 0 & 0 & \cdots & \cdots & 0\\
c_2 & a_{2,1}^{\text{ex}} & 0 & \ddots & \ddots & \vdots\\
c_3 & a_{3,1}^{\text{ex}} & a_{3,2}^{\text{ex}} & 0 & \ddots & \vdots\\
\vdots & \vdots & \vdots & \vdots & \ddots & 0\\
c_s & a_{s,1}^{\text{ex}} & a_{s,2}^{\text{ex}} & \cdots & a_{s,s-1}^{\text{ex}} & 0\\
\hline
 & b_1 & b_2 & b_3 & \cdots & b_s
\end{array}$$

$$\begin{array}{c|cccccc}
0 & a_{1,1}^{\text{im}} & 0 & \cdots & \cdots & 0\\
c_2 & a_{2,1}^{\text{im}} & a_{2,2}^{\text{im}} & 0 & \ddots & \vdots\\
c_3 & a_{3,1}^{\text{im}} & a_{3,2}^{\text{im}} & a_{3,3}^{\text{im}} & \ddots & \vdots\\
\vdots & \vdots & \vdots & \vdots & \ddots & 0\\
c_s & a_{s,1}^{\text{im}} & a_{s,2}^{\text{im}} & \cdots & a_{s,s-1}^{\text{im}} & a_{s,s}^{\text{im}}\\
\hline
 & b_1 & b_2 & b_3 & \cdots & b_s
\end{array}$$

QHL/DGTD

DGTD, Crank-Nicholson method

Sequential order of subdomains:

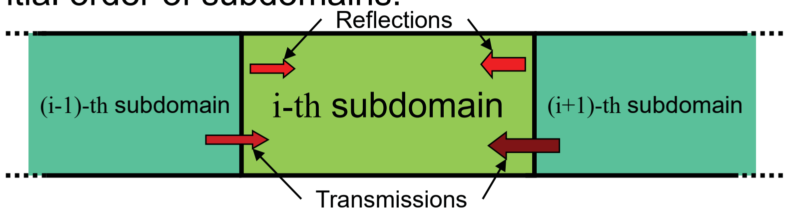

$$\mathbf{M}^{(i)}\frac{d\mathbf{v}^{(i)}}{dt} = \sum_{j=i-1}^{i+1} \mathbf{L}^{(i,j)}\mathbf{v}^{(j)} + \mathbf{f}^{(i)},\ i = 1, \dots M$$

Crank-Nicholson implicit method:

$$\left(\mathbf{M}^{(i)}\mathbf{v}^{(i)}_{n+1} - \frac{\Delta t}{2}\boxed{\sum_{j=i-1}^{i+1} \mathbf{L}^{(i,j)}}\mathbf{v}^{(j)}_{n+1}\right) = \left(\mathbf{M}^{(i)}\mathbf{v}^{(i)}_{n} + \frac{\Delta t}{2}\sum_{j=i-1}^{i+1} \mathbf{L}^{(i,j)}\mathbf{v}^{(j)}_{n}\right) + \mathbf{f}^{(i)}_{n+\frac{1}{2}} = \mathbf{q}^{(i)}$$

Block tridiagonal!!

QHL/DGTD

DGTD, LDU algorithm (1)

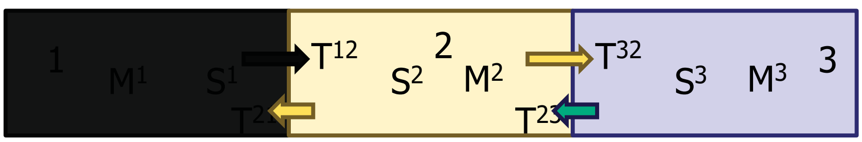

LDL decomposition

Volumes — Surface to volume — Volume

$$\begin{bmatrix} A^1_V & 0 & 0 & A^1_{VS+} & 0 & 0 & 0 \\ 0 & A^2_V & 0 & 0 & A^2_{VS-} & A^2_{VS+} & 0 \\ 0 & 0 & A^3_V & 0 & 0 & 0 & A^3_{VS-} \\ A^1_{S+V} & 0 & 0 & A^1_{S+} & B^1 & 0 & 0 \\ 0 & A^2_{S-V} & 0 & C^2 & A^2_{S-} & \boxed{A^2_{S-S+}} & 0 \\ 0 & A^2_{S+V} & 0 & 0 & \boxed{\mathcal{A}^2_{S+S-}} & A^2_{S+} & B^2 \\ 0 & 0 & A^3_{S-V} & 0 & 0 & C^3 & A^3_{S-} \end{bmatrix} \begin{bmatrix} u^1_V \\ u^2_V \\ u^3_V \\ u^1_{S+} \\ u^2_{S-} \\ u^2_{S+} \\ u^3_{S-} \end{bmatrix}$$

No Transpose

Volume to surface — Interfaces — Interface

Connection between interfaces in same domain.
Usually are zeros

QHL/DGTD

DGTD, LDU algorithm (2)

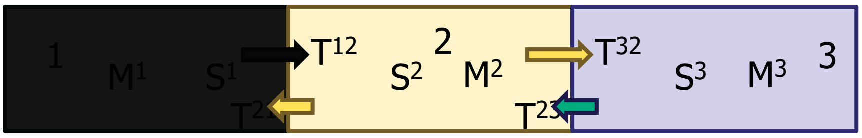

LDL-Block decomposition

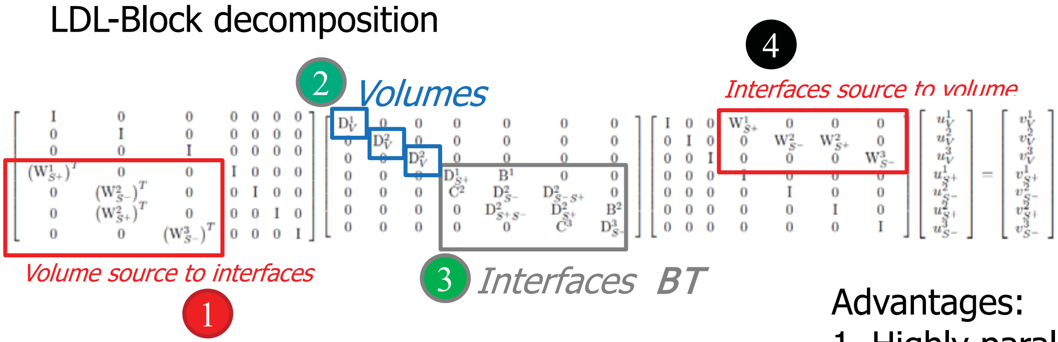

Advantages:

1. Highly parallelizable
2. Smaller matrices
3. Memory cost
4. CPU time

QHL/DGTD

DG-TD, LDU algorithm evaluation

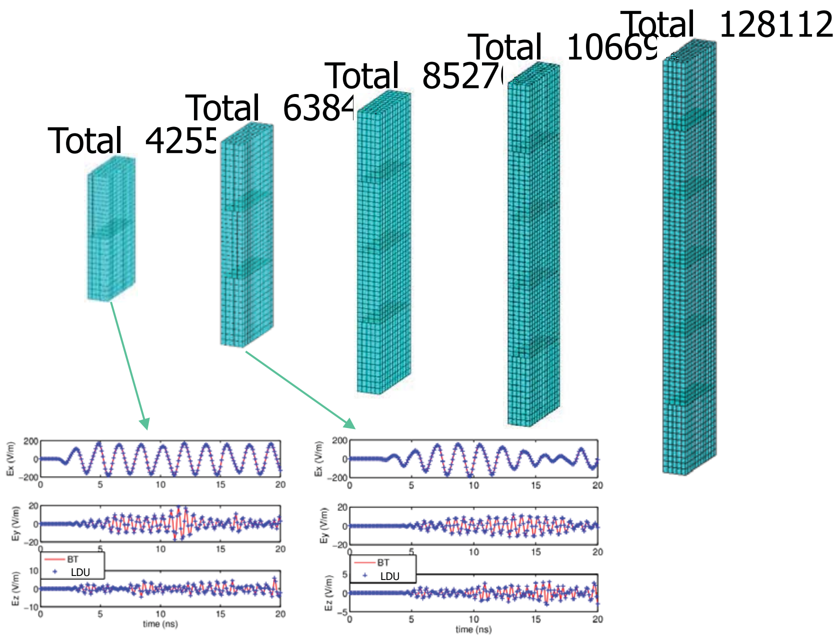

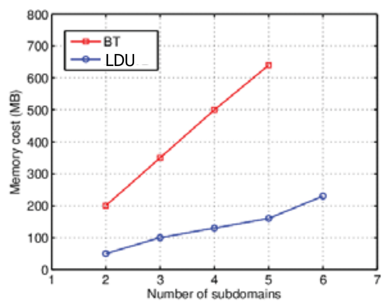

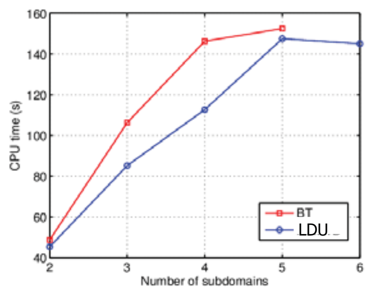

QHL/DGTD

EH scheme: Multilayer MW filter

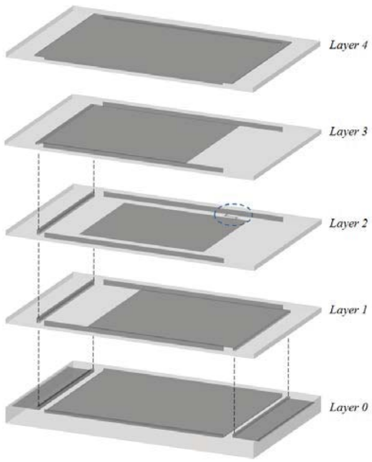

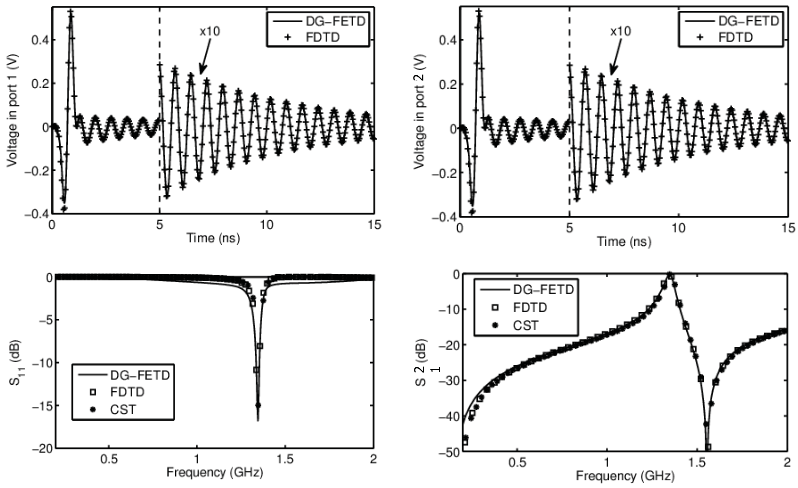

Thickness of plates
in layers 1, 2 and 3 is 6

Multiscale Factor $\frac{60mm}{6\mu m} = 10000$

	FDTD	CST	DG-FETD
Number of unknowns	3763200	13303453	221211
Memory (MB)	120	609	250
Δt	18.6 fs	55.5 fs	20 ps
CPU time (h)	5.9	10.2	0.4

Brick element
CN-GS

QHL/DGTD

EH scheme: Multilayer MW filter

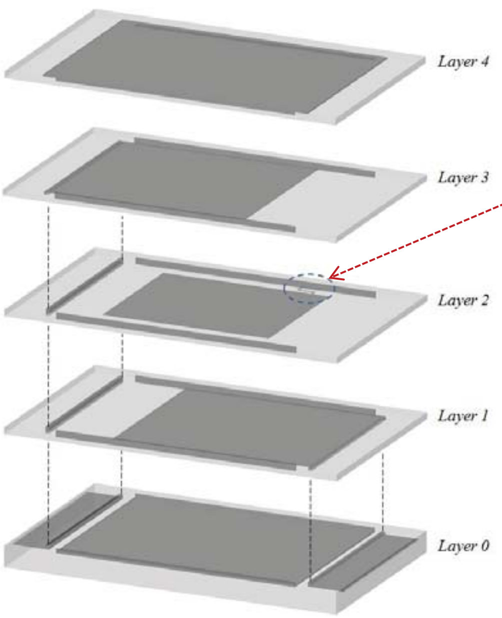

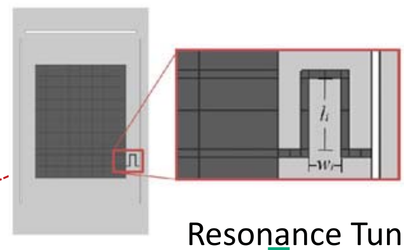

Resonance Tunning

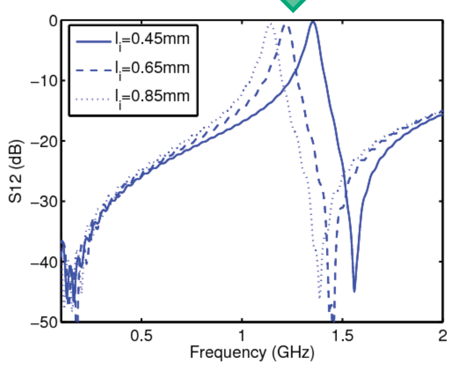

Resonant frequency

l_i	f_r
0.45mm	1.34GHz
0.65mm	1.22GHz
0.85mm	1.14GHz

This analysis takes less than 1.5 hours.

5.9 hours for one simulation using FDTD

QHL/DGTD

EH scheme: Packaging-to-Chip interconnect

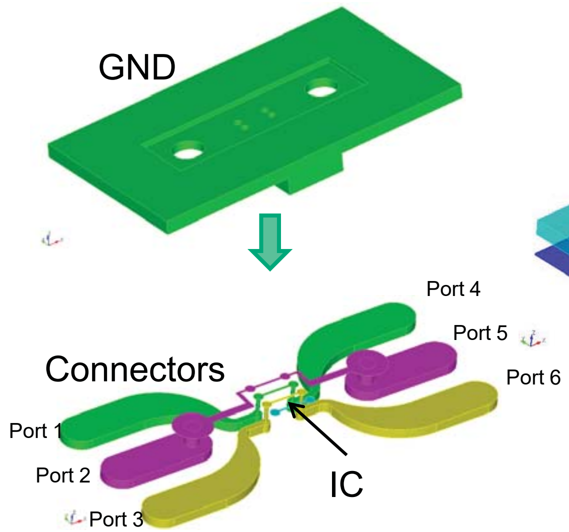

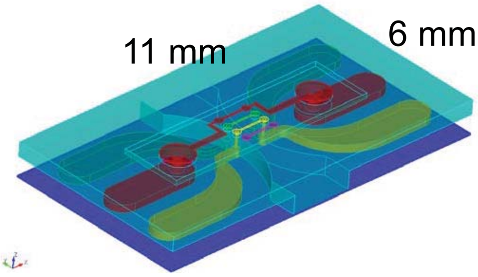

Active port: Port 1 (50 Ohms)
Passive port: Port 4 (50 Ohms)
V_s: BHW fc=2.6 GHz

QHL/DGTD

EH scheme: Packaging-to-Chip interconnect

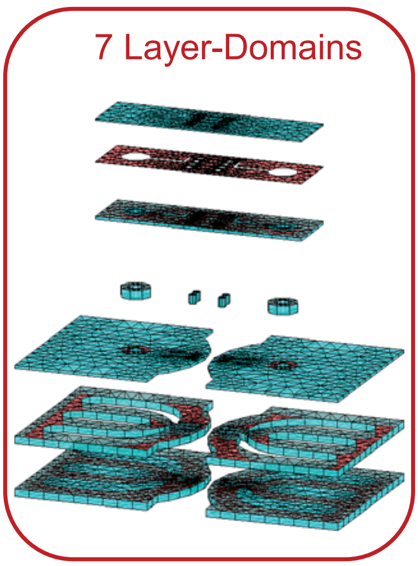

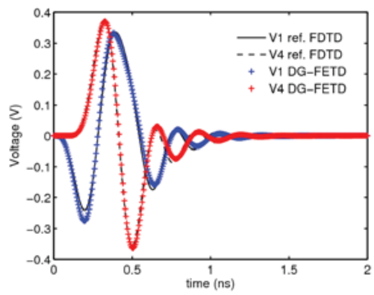

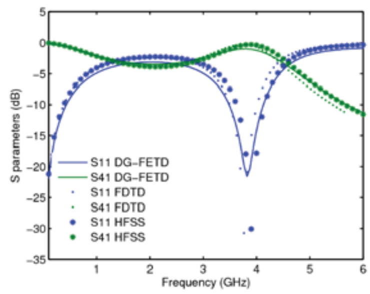

Method	Memory (MB)	CPU time (s)
Explicit FDTD	1.4	2160
HFSS	66	686
Prism DG-FETD	80	360

QHL/DGTD

EH scheme: Highly multiscale

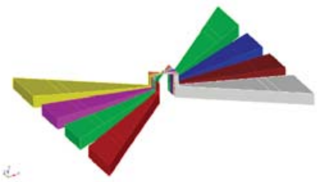

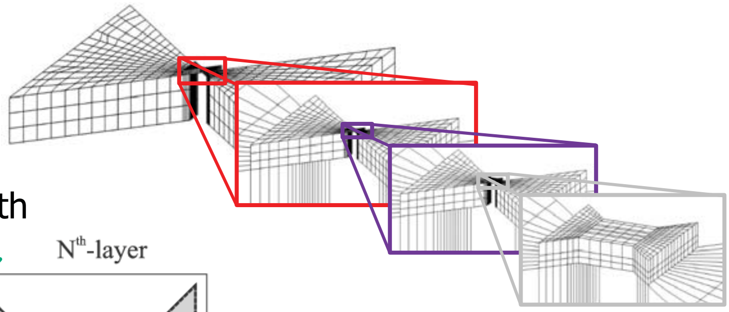

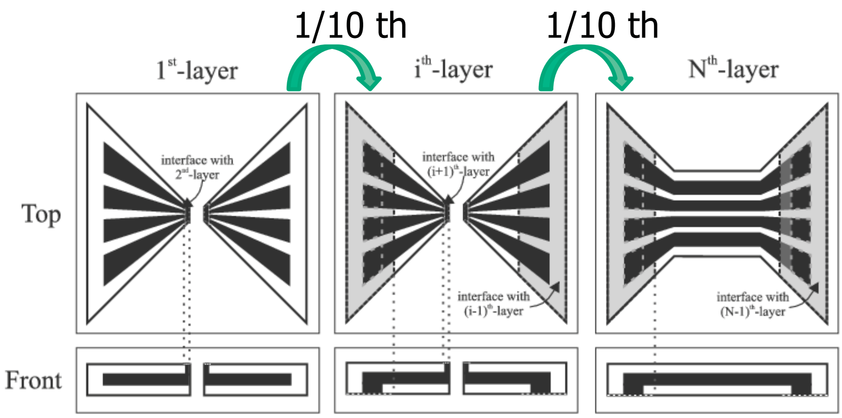

Multiscale factor = 1cm/0.15μm ≈ 67000

QHL/DGTD

EH scheme: Highly multiscale

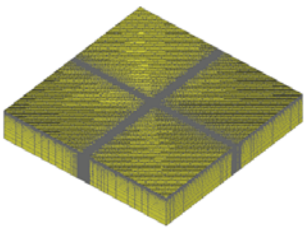

FDTD
Grid: 108 x 140 x 39

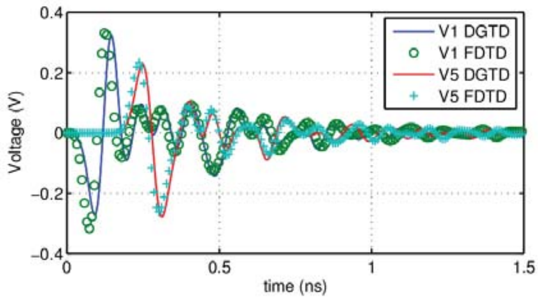

COMPUTATIONAL COSTS

	Explicit FDTD	Implicit DGTD	Gain
Number of unknowns	3.5 millions	138514	25
$\triangle t$	0.36 fs	2 ps	5700
Number of steps for 8 ns	22.8 millions	4000	5700
CPU time per time step (s)	0.0117	0.6	0.02
Total CPU time (s)	265712	2400	110
Memory (MB)	56	1340	0.04

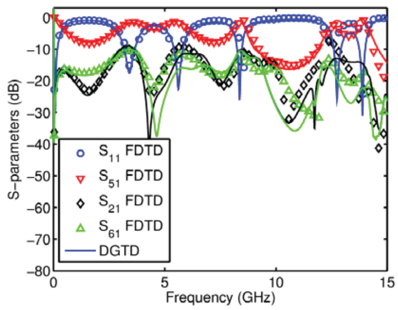

QHL/DGTD

EB scheme: Long MSL

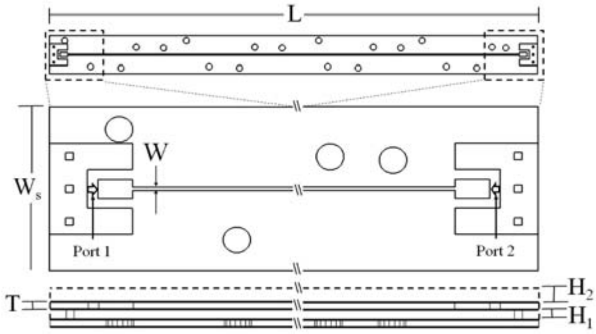

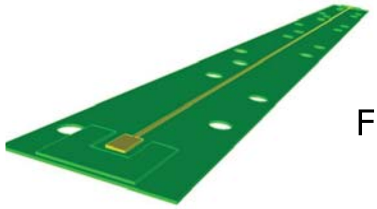

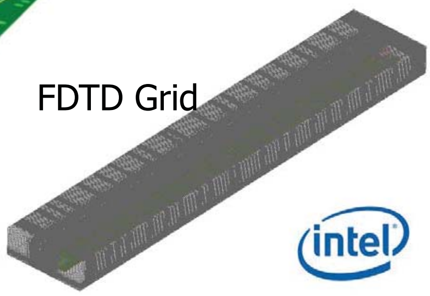

L=17 mm ≈ 3 x λ_{min}
W=0.06 mm ≈ (1/125) x λ_{min}
T=0.05 mm ≈ (1/125) x λ_{min}

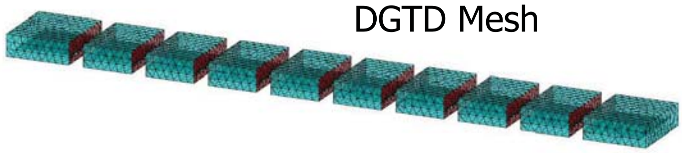

QHL/DGTD

EB scheme: Long MSL

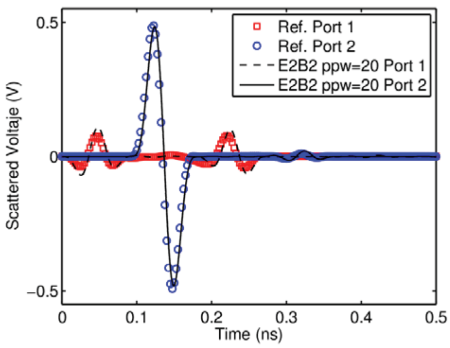

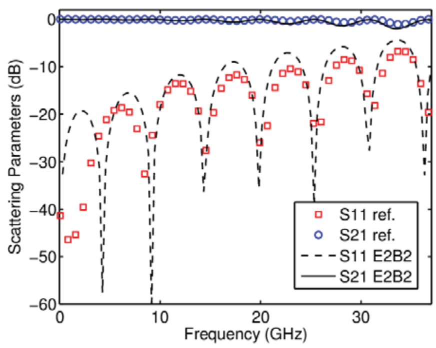

Table 2: Computional Cost, long MSL

	FDTD	DGTD	gain
Unknowns	6.9 MDoF	1 MDoF	6.9
Memory	284 MB	1.7 GB	0.17
$\triangle t$	0.5 fs	1 ps	2000
CPU time	10 h 21 m	1 h 2 m	10

CN-BT

QHL/DGTD

EB scheme: 3D IC

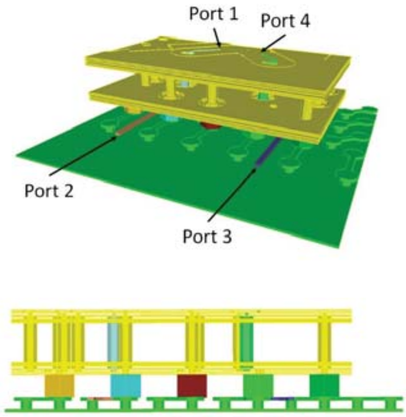

23 subdomains

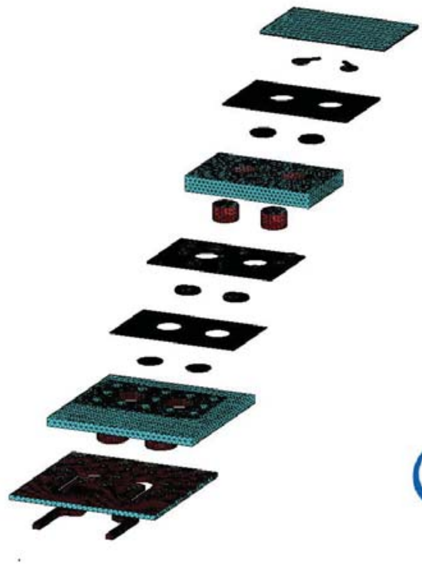

QHL/DGTD

EB scheme: 3D IC

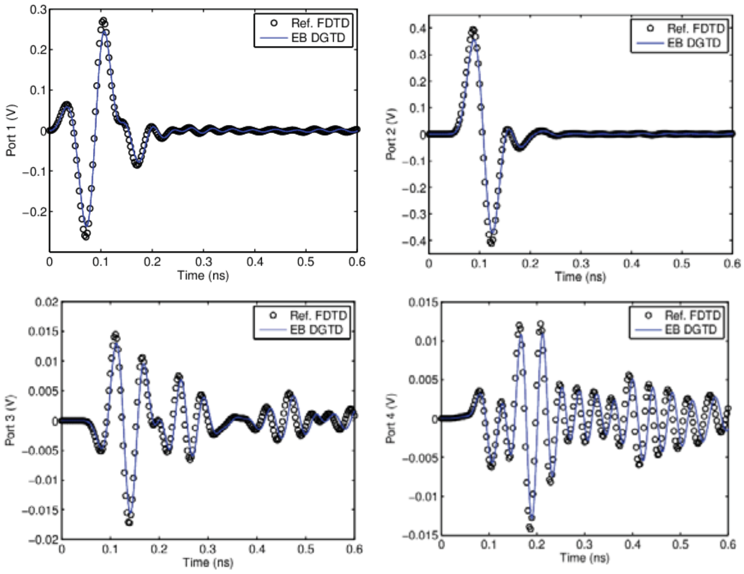

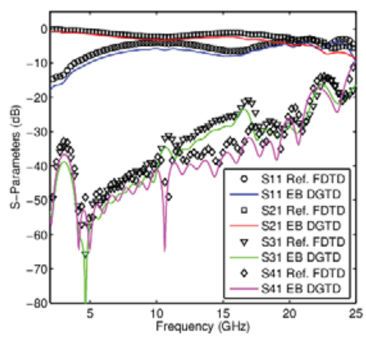

	FDTD	DGTD	gain
Unknowns	1.1 TDoF	1.6 MDoF	1e6
Memory	24 GB	9.5 GB	2.5
Δt	11 fs	25 fs	2.3
CPU time	10 d 13 h 4m	1 d 18 h 8 m	6

Anisotropic Media and Riemann Solver

Operator Splitting

$$\nabla = \frac{\partial}{\partial n}\hat{\mathbf{n}} + \nabla_S$$

Problem A

$$\frac{\partial \mathbf{H}}{\partial t} + \bar{\mu}^{-1}\frac{\partial}{\partial n} n\times\mathbf{E} = 0$$

$$\frac{\partial \mathbf{E}}{\partial t} - \bar{\varepsilon}^{-1}\frac{\partial}{\partial n} n\times\mathbf{H} = 0$$

$$\frac{\partial \mathbf{q}}{\partial t} = \mathbf{A}\frac{\partial \mathbf{q}}{\partial n}$$

$$\varepsilon' = \bar{\varepsilon}^{-1}$$

$$\mu' = \bar{\mu}^{-1}$$

$$\mathbf{A} = \begin{bmatrix} 0 & 0 & \mu'_{12} & -\mu'_{11} \\ 0 & 0 & \mu'_{22} & -\mu'_{21} \\ -\varepsilon'_{12} & \varepsilon'_{11} & 0 & 0 \\ -\varepsilon'_{22} & \varepsilon'_{21} & 0 & 0 \end{bmatrix} \qquad \mathbf{q} = [\mathbf{H}_{t1}, \mathbf{H}_{t2}, \mathbf{E}_{t1}, \mathbf{E}_{t2}]^T$$

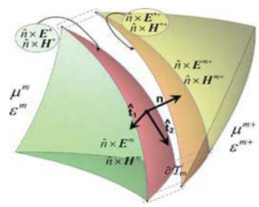

Alvarez, J., Luis D. Angulo, A. Rubio Bretones, and S. Gonzalez Garcia. "3D discontinuous Galerkin time domain method for anisotropic materials." IEEE Antennas and Wireless Propagation Letters 11 (2012): 1182-1185.

R. J. Leveque, Finite-Volume Methods for Hyperbolic Problems. Cambridge: Cambridge University Press, 2004.

Problem B

$$\frac{\partial \mathbf{H}}{\partial t} + \bar{\mu}^{-1}\nabla_S\times\mathbf{E} = 0$$

$$\frac{\partial \mathbf{E}}{\partial t} - \bar{\varepsilon}^{-1}\nabla_S\times\mathbf{H} = 0$$

EB Scheme Anisotropic Riemann Solver

$$(\hat{\mathbf{n}}^i\times\bar{\mu}^{-1}\mathbf{B}^t) = \mathbf{T}^{-1}(\mathbf{Z}^i+\mathbf{Z}^j)^{-1}[\mathbf{Z}^i\mathbf{T}(\hat{\mathbf{n}}^i\times(\bar{\mu}^i)^{-1}\mathbf{B}^i) + \mathbf{Z}^j\mathbf{T}(\hat{\mathbf{n}}^i\times(\bar{\mu}^j)^{-1}\mathbf{B}^j) - \mathbf{T}\hat{\mathbf{n}}^i\times\hat{\mathbf{n}}^i\times(\mathbf{E}^j-\mathbf{E}^i)]$$

$$(\hat{\mathbf{n}}^i\times\mathbf{E}^t) = \mathbf{T}^{-1}(\mathbf{Y}^i+\mathbf{Y}^j)^{-1}[\mathbf{Y}^i\mathbf{T}(\hat{\mathbf{n}}^i\times\mathbf{E}^i) + \mathbf{Y}^j\mathbf{T}(\hat{\mathbf{n}}^i\times\mathbf{E}^j) + \mathbf{T}\hat{\mathbf{n}}^i\times\hat{\mathbf{n}}^i\times((\bar{\mu}^j)^{-1}\mathbf{B}^j-(\bar{\mu}^i)^{-1}\mathbf{B}^i)]$$

Time Domain Anisotropic PML (1)

- Diagonal time-domain anisotropic PML

Wang, Shumin, Robert Lee, and Fernando L. Teixeira. "Anisotropic-medium PML for vector FETD with modified basis functions." *Antennas and Propagation, IEEE Transactions on* 54, no. 1 (2006): 20-27.

Gedney, Stephen D. "An anisotropic PML absorbing media for the FDTD simulation of fields in lossy and dispersive media." *Electromagnetics* 16, no. 4 (1996): 399-415.

Zhao, Li, and Andreas C. Cangellaris. "GT-PML: Generalized theory of perfectly matched layers and its application to the reflectionless truncation of finite-difference time-domain grids." *Microwave Theory and Techniques, IEEE Transactions on* 44, no. 12 (1996): 2555-2563.

$$\mathbf{\Lambda} = \begin{bmatrix} \frac{s_y s_z}{s_x} & 0 & 0 \\ 0 & \frac{s_z s_x}{s_y} & 0 \\ 0 & 0 & \frac{s_x s_y}{s_z} \end{bmatrix}$$

- Non-diagonal time-domain anisotropic PML

Garcia, S. González, R. Gomez Martin, and B. García Olmedo. "Extension of Berenger's absorbing boundary conditions to match dielectric anisotropic media." *Microwave and Guided Wave Letters, IEEE* 7, no. 9 (1997): 302-304.

Semi-analytical, not generalized

Split-field

Zhao, An Ping. "Generalized-material-independent PML absorbers used for the FDTD simulation of electromagnetic waves in 3-D arbitrary anisotropic dielectric and magnetic media." Microwave Theory and Techniques, IEEE Transactions on 46, no. 10 (1998): 1511-1513.

Liu, Qing Huo. "PML and PSTD algorithm for arbitrary lossy anisotropic media." *IEEE microwave and guided wave letters* 9, no. 2 (1999): 48-50

E H B D $\quad \sigma^{\mathbf{D}}\ \sigma^{\mathbf{B}}$

Split-field

QHL/DGTD

Time Domain Anisotropic PML (2)

A compact form of the governing equations for PML region:

$$\nabla\times\tilde{\mathbf{E}} = -\frac{\partial\tilde{\mathbf{B}}}{\partial t} - (\bar{\sigma}_m\bar{\mu}^{-1} + \mathbf{\Lambda}_1 + \bar{\mu}\mathbf{\Lambda}_0\mu^{-1})\tilde{\mathbf{B}} - \mathbf{\Lambda}_2\bar{\sigma}_m\bar{\mu}^{-1}\mathbf{B}^{(2)} - (\mathbf{\Lambda}_1\bar{\sigma}_m\bar{\mu}^{-1} - \bar{\sigma}_m\mathbf{\Lambda}_0\bar{\mu}^{-1} + \bar{\mu}\mathbf{\Lambda}_0^2\bar{\mu}^{-1} - \mathbf{\Lambda}_1\bar{\mu}\mathbf{\Lambda}_0\bar{\mu}^{-1} + \mathbf{\Lambda}_2)\mathbf{B}^{(1)}$$

$$\nabla\times\mu^{-1}\tilde{\mathbf{B}} = \frac{\partial\bar{\varepsilon}\tilde{\mathbf{E}}}{\partial t} + (\bar{\sigma}_e + \mathbf{\Lambda}_1\bar{\varepsilon} + \bar{\varepsilon}\mathbf{\Lambda}_0)\tilde{\mathbf{E}} + \mathbf{\Lambda}_2\bar{\sigma}_e\mathbf{E}^{(2)} + (\mathbf{\Lambda}_1\bar{\sigma}_e - \bar{\sigma}_e\mathbf{\Lambda}_0 + \bar{\varepsilon}\mathbf{\Lambda}_0^2 - \mathbf{\Lambda}_1\bar{\varepsilon}\mathbf{\Lambda}_0 + \mathbf{\Lambda}_2\bar{\varepsilon})\mathbf{E}^{(1)}$$

$$\frac{\partial\mathbf{E}^{(1)}}{\partial t} = \tilde{\mathbf{E}} - \mathbf{\Lambda}_0\mathbf{E}^{(1)} \qquad \frac{\partial\mathbf{E}^{(2)}}{\partial t} = \mathbf{E}^{(1)} \qquad \frac{\partial\mathbf{B}^{(1)}}{\partial t} = \tilde{\mathbf{B}} - \bar{\mu}\mathbf{\Lambda}_0\bar{\mu}^{-1}\mathbf{B}^{(1)} \qquad \frac{\partial\mathbf{B}^{(2)}}{\partial t} = \mathbf{B}^{(1)}$$

where $\mathbf{\Lambda}_1 = diag\{\omega_y+\omega_z, \omega_z+\omega_x, \omega_x+\omega_y\}$ $\quad \mathbf{\Lambda}_2 = diag\{\omega_y\omega_z, \omega_z\omega_x, \omega_x\omega_y\}$

1. Unsplit, Maxwellian (FE, SE)
2. Non-convolutional
3. Ordinary differential equations

QHL/DGTD

Anisotropic PEC Cavity

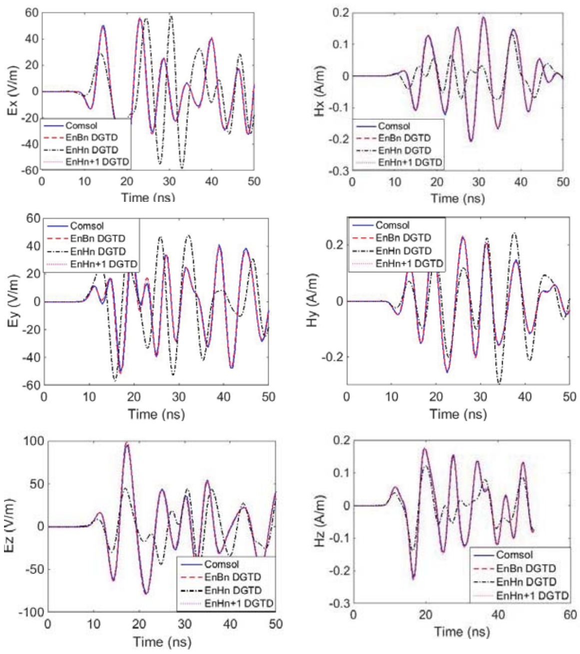

L=2 m

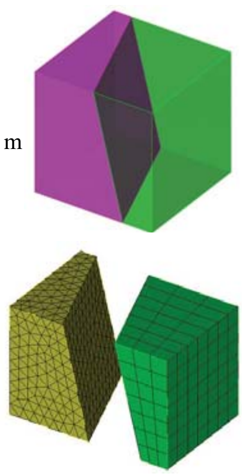

Blackman- Harris Window (BHW) pulse
f_ch=100 MHz

$$\varepsilon_{r,1} = \begin{bmatrix} 3.1253 & -0.8283 & 0.6657 \\ -0.8283 & 1.5524 & -0.7651 \\ 0.6657 & -0.7651 & 2.3223 \end{bmatrix}$$

$$\varepsilon_{r,2} = \begin{bmatrix} 1.0302 & -0.1099 & 0.1310 \\ -0.1099 & 3.1612 & 0.9997 \\ 0.1310 & 0.9997 & 2.8087 \end{bmatrix}$$

$$\mu_{r,1} = \begin{bmatrix} 2.3125 & -0.3750 & -0.7578 \\ -0.3750 & 2.2500 & 0.2165 \\ -0.7578 & -0.3750 & 1.4375 \end{bmatrix}$$

$$\mu_{r,2} = \begin{bmatrix} 1.2500 & 0.2165 & 0.3750 \\ 0.2165 & 2.6875 & -0.5413 \\ 0.3750 & -0.5413 & 2.0625 \end{bmatrix}$$

$$\sigma_1 = \begin{bmatrix} 0.0014 & -0.0005 & 0.0001 \\ -0.0005 & 0.0016 & -0.0001 \\ 0.0001 & -0.0001 & 0.0010 \end{bmatrix}$$

$$\sigma_2 = \begin{bmatrix} 0.0010 & 0 & 0 \\ 0 & 0.0011 & 0.0003 \\ 0 & 0.0003 & 0.0019 \end{bmatrix}$$

QHL/DGTD

DUKE

Anisotropic M-PML Case (1)

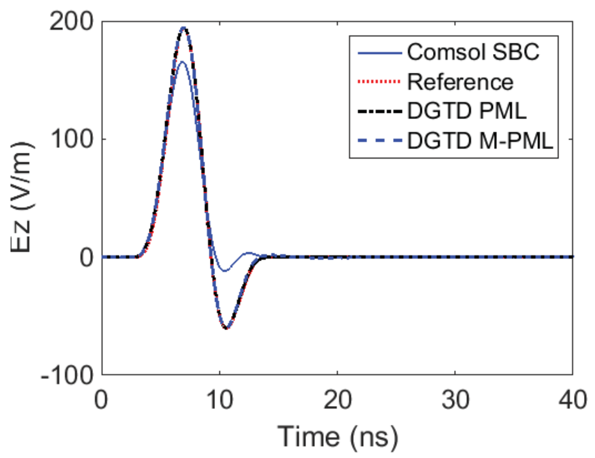

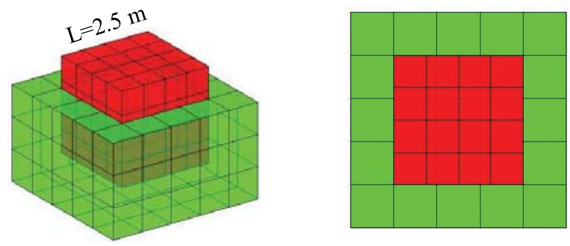

$$\varepsilon_r = \begin{bmatrix} 1.3750 & -0.0777 & -0.4779 \\ -0.0777 & 1.0161 & 0.0990 \\ -0.4779 & -0.0990 & 1.6089 \end{bmatrix} \quad \mu_r = \begin{bmatrix} 1.9375 & 0.2296 & 0.0765 \\ 0.2296 & 1.1562 & -0.2812 \\ 0.0765 & -0.2812 & 1.9062 \end{bmatrix}$$

Blackman- Harris Window (BHW) pulse

f_ch=89.5
MHz

QHL/DGTD

DUKE

Anisotropic M-PML Case (2)

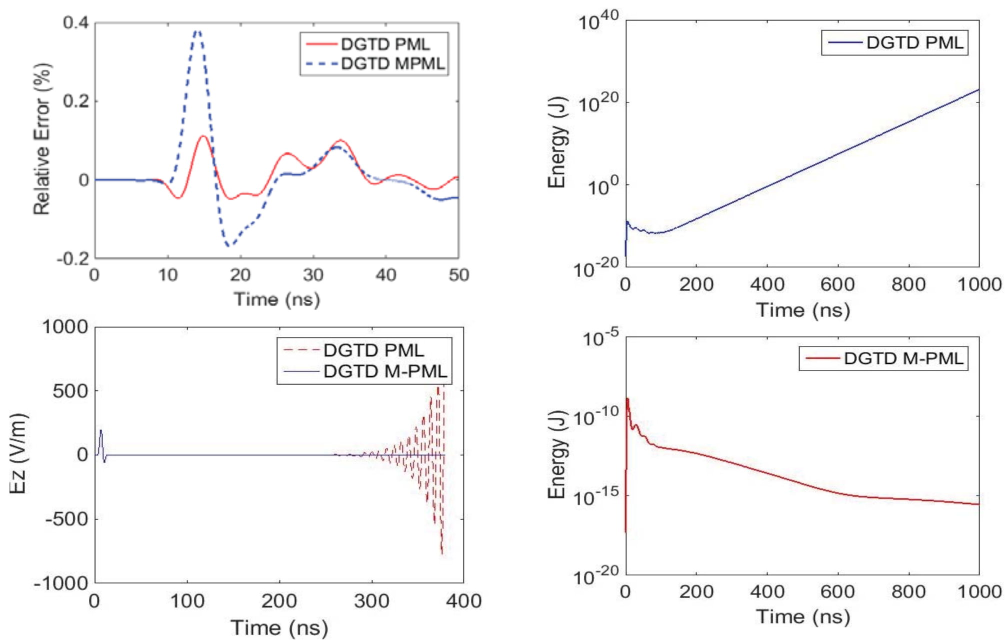

Relative larger error from M-PML than classical MPL, but long time stability.

$3e^5$steps stability

QHL/DGTD

Space-Time Separated Non-Conformal TF/SF BC for VBF (1)

$$e_{inc,p} = \langle \mathbf{E}_{inc}, \mathbf{\Phi}_{j,p} \rangle \qquad b_{inc,p} = \langle \mathbf{B}_{inc}, \mathbf{\Psi}_{j,p} \rangle$$

$$\mathbf{v}_{j,inc} = [e_{inc,1}, \ \cdots, \ e_{inc,k}, \ b_{inc,1}, \ \cdots, \ b_{inc,l}]^T$$

Time delay matrix

$$\mathbf{F}_i = \begin{bmatrix} f(t - \frac{r_{i,1}}{c}) & & & \\ & \cdot & & \\ & & \cdot & \\ & & & f(t - \frac{r_{i,m+n}}{c}) \end{bmatrix}$$

$$\mathbf{M}_i \frac{d\mathbf{v}_i}{dt} = \mathbf{L}_{ii}\mathbf{v}_i + \sum_j \mathbf{L}_{ij}\mathbf{v}_j + \mathbf{F}_i \sum_j \mathbf{L}_{ij}\mathbf{v}_{j,inc}$$

Advantages:
1. Space time separation
2. Multi-function of the TF/SF interface

TF/SF interface:
1. Non-conformal mesh connector
2. DG interface
3. Source surface

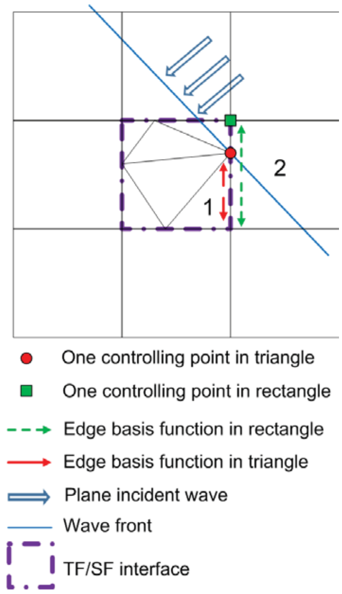

QHL/DGTD

Space-Time Separated Non-Conformal TF/SF BC for VBF (2)

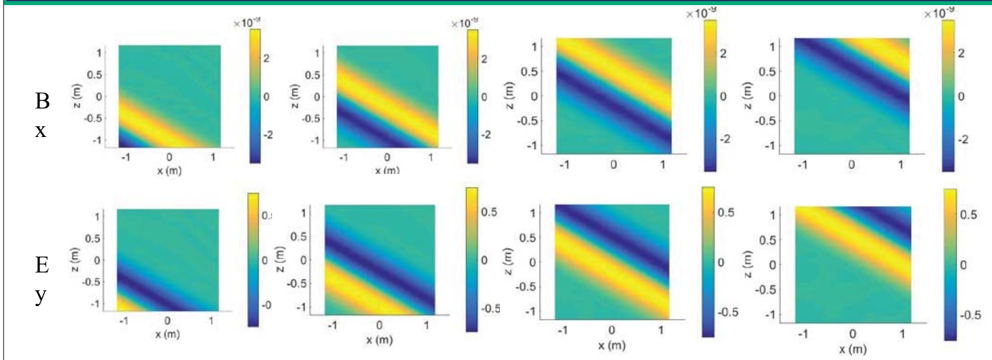

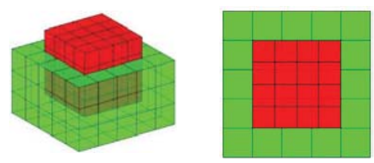

$$\varepsilon_r = \begin{bmatrix} 1.3750 & -0.0777 & -0.4779 \\ -0.0777 & 1.0161 & 0.0990 \\ -0.4779 & -0.0990 & 1.6089 \end{bmatrix}$$

$$\mu_r = \begin{bmatrix} 1.9375 & 0.2296 & 0.0765 \\ 0.2296 & 1.1562 & -0.2812 \\ 0.0765 & -0.2812 & 1.9062 \end{bmatrix}$$

Field records at the receiver

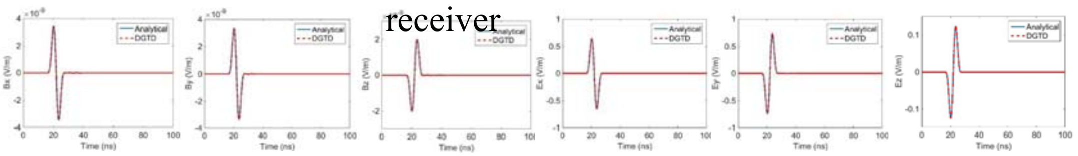

Blackman- Harris Window (BHW) pulse plane wave
f_ch=89.5 MHz

QHL/DGTD

DUKE

Negative Refraction (1)

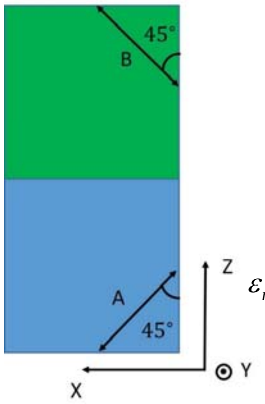

YVO_4 bicrystal

In principal axial $\varepsilon_r = \begin{bmatrix} 4.0671 & 0 & 0 \\ 0 & 4.0671 & 0 \\ 0 & 0 & 5.0661 \end{bmatrix}$ $\quad \mu_{r,A} = \begin{bmatrix} 1 & 0 & 0 \\ 0 & 1 & 0 \\ 0 & 0 & 1 \end{bmatrix}$

$$\varepsilon_{r,A} = \begin{bmatrix} 4.5666 & 0 & -0.4995 \\ 0 & 4.0671 & 0 \\ -0.4995 & 0 & 4.5666 \end{bmatrix} \quad \varepsilon_{r,B} = \begin{bmatrix} 4.5666 & 0 & 0.4995 \\ 0 & 4.0671 & 0 \\ 0.4995 & 0 & 4.5666 \end{bmatrix} \quad \mu_{r,B} = \begin{bmatrix} 1 & 0 & 0 \\ 0 & 1 & 0 \\ 0 & 0 & 1 \end{bmatrix}$$

C. M. Krowne and Y. Zhang, Physics of Negative Refraction and Negative Index Materials. Springer, 2007

QHL/DGTD

DUKE

Anisotropic Time Domain Half Space TF/SF Boundary Condition

Half Space TF/SF Boundary Condition

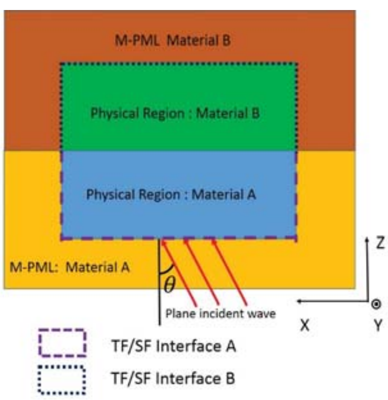

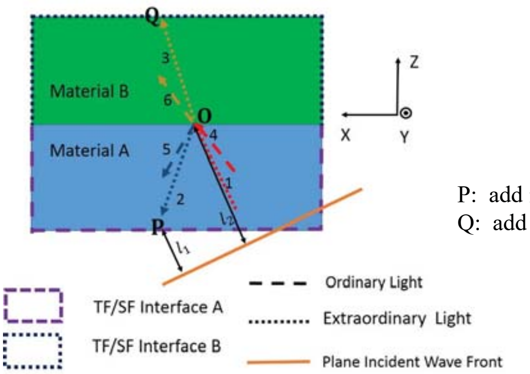

P: add incident and reflected waves
Q: add refracted wave

The M-PML is divided into two halves, each half has the same material as the physical domain it is matched for.

$$\mathbf{E}_P = f(t-t_1)\mathbf{E}_1 + f(t-t_2)\mathbf{E}_2 \qquad \mathbf{E}_Q = f(t-t_3)\mathbf{E}_3$$

$$t_1 = l_1 / \mathbf{v}_{p,A} \qquad t_2 = (l_2 + \overline{OP}) / \mathbf{v}_{p,A} \qquad t_3 = (l_2 + \overline{OQ}) / \mathbf{v}_{p,B}$$

The refracted and reflected angles, $\mathbf{v}_{p,A}$ and $\mathbf{v}_{p,B}$ can be calculated via the state-variable approach for layered media

QHL/DGTD

DUKE

Negative Refraction (2)

Normal Refraction 1

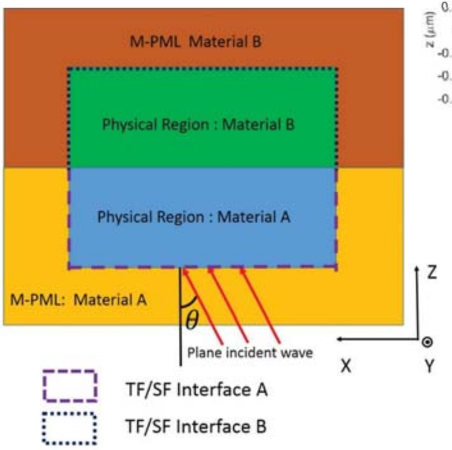

$\theta = -10^{\circ}$

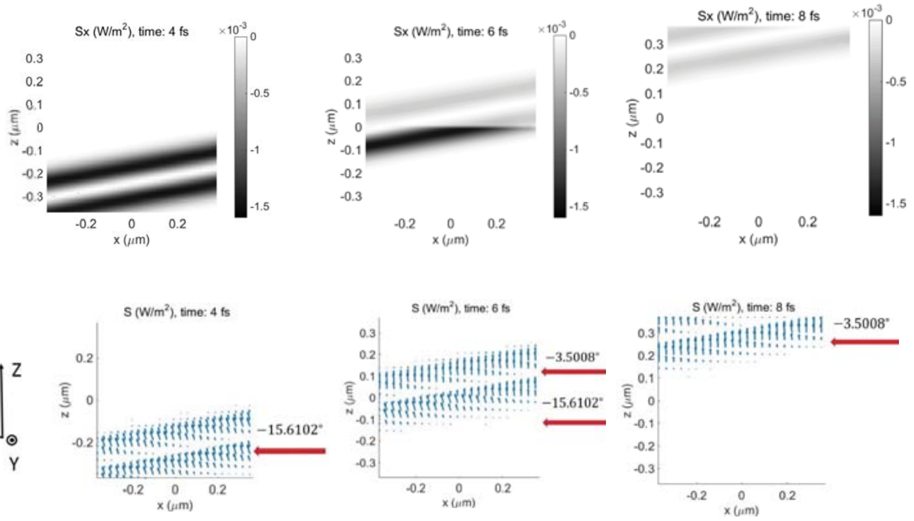

QHL/DGTD

DUKE

Negative Refraction (3)

Normal Refraction 2

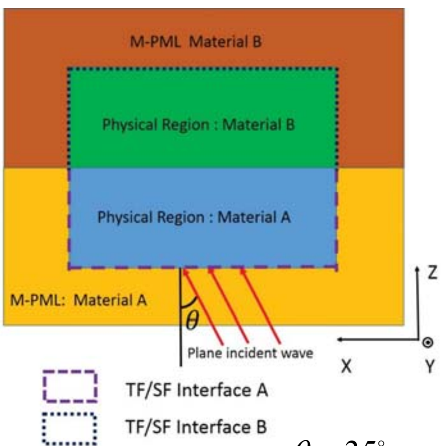

$\theta = 35^{\circ}$

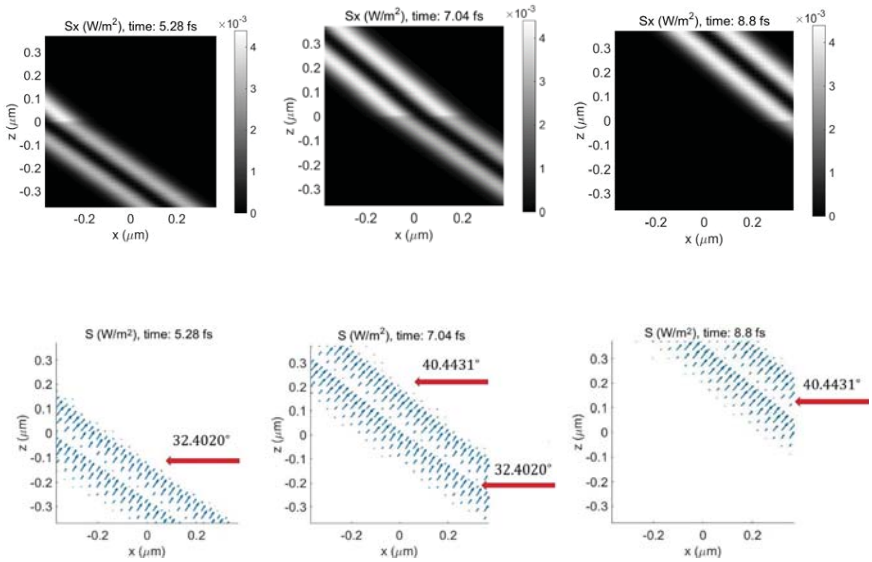

QHL/DGTD

DUKE

Negative Refraction (4)

Negative Refraction

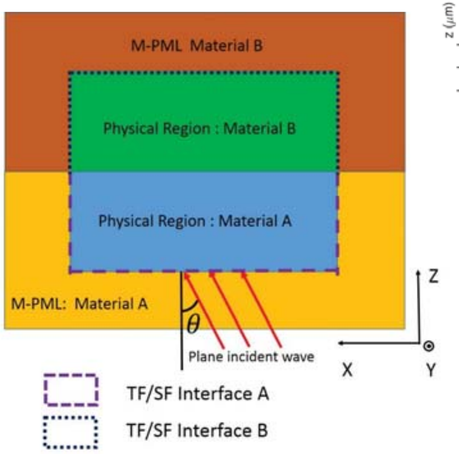

$\theta = 0^{\circ}$

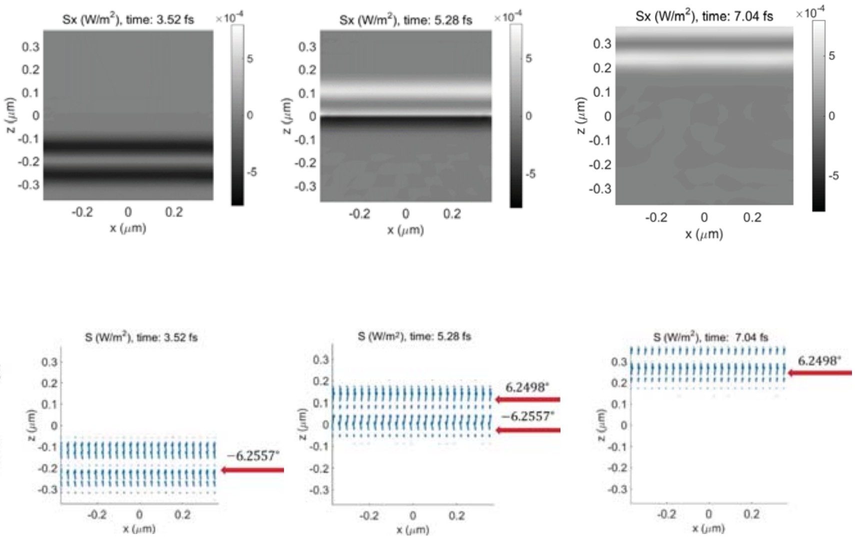

QHL/DGTD

DUKE

Negative Refraction (5)

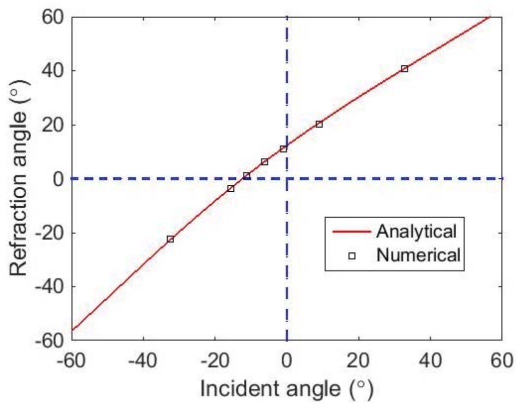

More cases are simulated.

They all agree with the analytical solution.

The relative errors of incidence and refraction angles (respect to energy) are all less than 1%.

QHL/DGTD

DUKE EDMUND T. PRATT, JR. SCHOOL OF ENGINEERING

3.4 Vector DGTD Method with the Wave Equation

- Vector (Subdomain) DGTD Method with the Wave Equation
  - Q. Sun, Q. Zhan, Q. Ren, and Q. H. Liu, "Wave Equation-Based Implicit Subdomain DGTD Method for Modeling of Electrically Small Problems", IEEE Trans. Microw. Theory Tech., vol. 65, no. 4, pp. 1111-1119, Apr. 2017.
  - Q. Sun, Discontinuous Galerkin Based Multi-Domain Multi-Solver Technique for Efficient Multiscale Electromagnetic Modeling, Ph.D. Dissertation, Duke University, 2017.
  - Q. Sun, R. Zhang, Q. Zhan, and Q. H. Liu, "A Novel Coupling Algorithm for Perfectly Matched Layer with Wave Equation Based Discontinuous Galerkin Time Domain Method", IEEE Trans. Antennas Propagat., vol. 66, no. 1, pp. 255-261, Jan. 2018.

- Slides in 5.4 - 5.6 are modified from Q. Sun's PhD defense.

QHL/DGTD

DUKE EDMUND T. PRATT, JR. SCHOOL OF ENGINEERING

The First-Order Maxwell's Curl Equations

- Governing equations (**EB**)

$$\epsilon\frac{\partial \mathbf{E}}{\partial t} = \nabla\times\mu^{-1}\mathbf{B} - \sigma_e\mathbf{E} - \mathbf{J}_i$$

$$\frac{\partial \mathbf{B}}{\partial t} = -\nabla\times\mathbf{E} - \sigma_m\mu^{-1}\mathbf{B} - \mathbf{M}_i$$

- Weak form

$$\int_{\Omega^{(i)}}\mathbf{\Phi}_p^{(i)}\cdot\epsilon^{(i)}\frac{\partial\mathbf{E}^{(i)}}{\partial t}dV = \int_{\Omega^{(i)}}\nabla\times\mathbf{\Phi}_p^{(i)}\cdot\mu^{(i)^{-1}}\mathbf{B}^{(i)}dV - \int_{\Omega^{(i)}}\mathbf{\Phi}_p^{(i)}\cdot\left(\sigma_e^{(i)}\mathbf{E}^{(i)}+\mathbf{J}_i^{(i)}\right)dV + \boxed{\oint_{\partial\Omega^{(i)}}\mathbf{\Phi}_p^{(i)}\cdot\left(\hat{n}^{(i)}\times\mu^{-1}\mathbf{B}^*\right)dS}$$

Numerical flux

$$\int_{\Omega^{(i)}}\mathbf{\Psi}_q^{(i)}\cdot\frac{\partial\mathbf{B}^{(i)}}{\partial t}dV \approx -\int_{\Omega^{(i)}}\mathbf{\Psi}_q^{(i)}\cdot(\nabla\times\mathbf{E}^{(i)})dV - \int_{\Omega^{(i)}}\mathbf{\Psi}_q^{(i)}\cdot\left(\sigma_m^{(i)}\mu^{(i)^{-1}}\mathbf{B}^{(i)}+\mathbf{M}_i^{(i)}\right)dV \boxed{- \oint_{\partial\Omega^{(i)}}\mathbf{\Psi}_q^{(i)}\cdot\left(\hat{n}^{(i)}\times\mathbf{E}^*\right)dS + \oint_{\partial\Omega^{(i)}}\mathbf{\Psi}_q^{(i)}\cdot\left(\hat{n}^{(i)}\times\mathbf{E}^{(i)}\right)dS}$$

- Riemann solver (upwind flux)

$$\hat{n}^{(i)}\times\mathbf{E}^* = \frac{\hat{n}^{(i)}\times\left(Y^{(i)}\mathbf{E}^{(i)}+Y^{(j)}\mathbf{E}^{(j)}\right)}{Y^{(i)}+Y^{(j)}} - \frac{\hat{n}^{(i)}\times\hat{n}^{(i)}\times\left(\mu^{(i)^{-1}}\mathbf{B}^{(i)}-\mu^{(j)^{-1}}\mathbf{B}^{(j)}\right)}{Y^{(i)}+Y^{(j)}}$$

$$\hat{n}^{(i)}\times\mu^{-1}\mathbf{B}^* = \frac{\hat{n}^{(i)}\times\left(Z^{(i)}\mu^{(i)^{-1}}\mathbf{B}^{(i)}+Z^{(j)}\mu^{(j)^{-1}}\mathbf{B}^{(j)}\right)}{Z^{(i)}+Z^{(j)}} + \frac{\hat{n}^{(i)}\times\hat{n}^{(i)}\times\left(\mathbf{E}^{(i)}-\mathbf{E}^{(j)}\right)}{Z^{(i)}+Z^{(j)}}$$

- Question: Can one use only E (or H) as an unknown field in a wave equation to reduce the unknowns?

QHL/DGTD

The Second-Order Wave Equation

- Governing equation (**EHs**)

$$\nabla \times (\mu^{-1} \nabla \times \mathbf{E}) + \epsilon \frac{\partial^2 \mathbf{E}}{\partial t^2} + \sigma_e \frac{\partial \mathbf{E}}{\partial t} = -\frac{\partial \mathbf{J}_i}{\partial t} - \nabla \times (\mu^{-1} \mathbf{M}_i)$$

Subject to: $\hat{n} \times (\nabla \times \mathbf{E}) = \sqrt{\epsilon\mu} \frac{\partial(\hat{n} \times \mathbf{E} \times \hat{n})}{\partial t}, \text{ on } \Gamma_{\text{ABC}}$

- Modified Riemann solver

$$\hat{n}^{(i)} \times \frac{\partial \mathbf{H}^*}{\partial t} = \frac{\hat{n}^{(i)} \times (Z^{(i)} \frac{\partial \mathbf{H}^{(i)}}{\partial t} + Z^{(j)} \frac{\partial \mathbf{H}^{(j)}}{\partial t})}{Z^{(i)} + Z^{(j)}} + \frac{\hat{n}^{(i)} \times \hat{n}^{(i)} \times \left(\frac{\partial \mathbf{E}^{(i)}}{\partial t} - \frac{\partial \mathbf{E}^{(j)}}{\partial t} \right)}{Z^{(i)} + Z^{(j)}}$$

$$\hat{n}^{(i)} \times \frac{\partial \mathbf{E}^*}{\partial t} = \frac{\hat{n}^{(i)} \times \left(Y^{(i)} \frac{\partial \mathbf{E}^{(i)}}{\partial t} + Y^{(j)} \frac{\partial \mathbf{E}^{(j)}}{\partial t} \right)}{Y^{(i)} + Y^{(j)}} - \frac{\hat{n}^{(i)} \times \hat{n}^{(i)} \times \left(\frac{\partial \mathbf{H}^{(i)}}{\partial t} - \frac{\partial \mathbf{H}^{(j)}}{\partial t} \right)}{Y^{(i)} + Y^{(j)}}$$

- Semi-discretized sub-systems

$$\mathbf{M}^{(i)} \frac{\partial^2 \mathbf{u}^{(i)}}{\partial t^2} + \sum_{j=1}^{N} \mathbf{L}^{(i,j)} \frac{\partial \mathbf{u}^{(j)}}{\partial t} + \mathbf{S}^{(i)} \mathbf{u}^{(i)} = \mathbf{q}^{(i)}.$$

- Weak form

$$\int_{\Omega^{(i)}} \nabla \times \mathbf{\Phi}^{(i)} \cdot {\mu^{(i)}}^{-1} \nabla \times \mathbf{E}^{(i)} dV + \int_{\Omega^{(i)}} \mathbf{\Phi}^{(i)} \cdot \epsilon^{(i)} \frac{\partial^2 \mathbf{E}^{(i)}}{\partial t^2} dV$$
$$+ \int_{\Omega^{(i)}} \mathbf{\Phi}^{(i)} \cdot {\sigma_e}^{(i)} \frac{\partial \mathbf{E}^{(i)}}{\partial t} dV - \boxed{\int_{\Gamma_{\text{ITF}}^{(i)}} \mathbf{\Phi}^{(i)} \cdot \hat{n}^{(i)} \times \frac{\partial \mathbf{H}^*}{\partial t} dS}$$
$$+ \int_{\Gamma_{\text{ABC}}^{(i)}} \mathbf{\Phi}^{(i)} \cdot \sqrt{\frac{\epsilon^{(i)}}{\mu^{(i)}}} \frac{\partial(\hat{n}^{(i)} \times \mathbf{E} \times \hat{n}^{(i)})}{\partial t} dS$$

Numerical flux

$$= -\int_{\Omega^{(i)}} \mathbf{\Phi}^{(i)} \cdot \frac{\partial \mathbf{J}_i^{(i)}}{\partial t} dV - \int_{\Omega^{(i)}} \nabla \times \mathbf{\Phi}^{(i)} \cdot {\mu^{(i)}}^{-1} {\mathbf{M}_i}^{(i)} dV$$

$$\int_{\Gamma_{\text{ITF}}^{(i)}} \mathbf{\Psi}^{(i)} \cdot \hat{n}^{(i)} \times \frac{\partial \mathbf{E}^{(i)}}{\partial t} dS = \int_{\Gamma_{\text{ITF}}^{(i)}} \mathbf{\Psi}^{(i)} \cdot \frac{\hat{n}^{(i)} \times \left(Y^{(i)} \frac{\partial \mathbf{E}^{(i)}}{\partial t} + Y^{(j)} \frac{\partial \mathbf{E}^{(j)}}{\partial t} \right)}{Y^{(i)} + Y^{(j)}} dS$$
$$- \int_{\Gamma_{\text{ITF}}^{(i)}} \mathbf{\Psi}^{(i)} \cdot \frac{\hat{n}^{(i)} \times \hat{n}^{(i)} \times \left(\frac{\partial \mathbf{H}^{(i)}}{\partial t} - \frac{\partial \mathbf{H}^{(j)}}{\partial t} \right)}{Y^{(i)} + Y^{(j)}} dS.$$

- For electrically fine domains, this equation is solved by the Newmark beta method.

QHL/DGTD

Coupling with PML

- The physical region (**EHs**)

$$\boxed{\nabla \times (\mu^{-1} \nabla \times \mathbf{E}) + \epsilon \frac{\partial^2 \mathbf{E}}{\partial t^2} + \sigma_e \frac{\partial \mathbf{E}}{\partial t} = -\frac{\partial \mathbf{J}_i}{\partial t} - \nabla \times (\mu^{-1} \mathbf{M}_i)}$$

$$\boxed{\mathbf{M}^{(i)} \frac{\partial^2 \mathbf{u}^{(i)}}{\partial t^2} + \sum_{j=1}^{N} \mathbf{L}^{(i,j)} \frac{\partial \mathbf{u}^{(j)}}{\partial t} + \mathbf{S}^{(i)} \mathbf{u}^{(i)} = \mathbf{q}^{(i)}, \quad i = 1, \ldots N_s}$$

- The PML region (**EB**)

$$\nabla \times \tilde{\mathbf{E}} = -\frac{\partial \tilde{\mathbf{B}}}{\partial t} - \mathbf{\Lambda}_1 \tilde{\mathbf{B}} - \mathbf{\Lambda}_2 \bar{\mathbf{B}}$$

$$\nabla \times \mu^{-1} \tilde{\mathbf{B}} = \epsilon \frac{\partial \tilde{\mathbf{E}}}{\partial t} + \epsilon \mathbf{\Lambda}_1 \tilde{\mathbf{E}} + \epsilon \mathbf{\Lambda}_2 \bar{\mathbf{E}}$$

$$\frac{\partial \bar{\mathbf{E}}}{\partial t} = \tilde{\mathbf{E}} - \mathbf{\Lambda}_0 \bar{\mathbf{E}} \qquad \frac{\partial \bar{\mathbf{B}}}{\partial t} = \tilde{\mathbf{B}} - \mathbf{\Lambda}_0 \bar{\mathbf{B}}$$

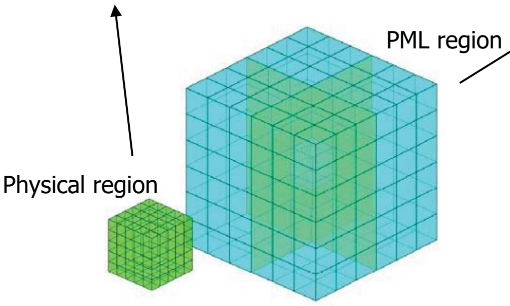

$$\mathbf{M}^{(i)} \frac{\partial \tilde{\mathbf{u}}^{(i)}}{\partial t} = \sum_{j=1}^{N} \mathbf{L}^{(i,j)} \tilde{\mathbf{u}}^{(j)} + \mathbf{S}^{(i)} \bar{\mathbf{u}}^{(i)} + \mathbf{q}^{(i)}, \quad i = N_s + 1, \ldots N$$
$$\mathbf{M}^{(i)} \frac{\partial \bar{\mathbf{u}}^{(i)}}{\partial t} = \mathbf{M}^{(i)} \tilde{\mathbf{u}}^{(i)} + \mathbf{T}^{(i)} \bar{\mathbf{u}}^{(i)}, \quad i = N_s + 1, \ldots N.$$

QHL/DGTD

Numerical Results, Resonant cavity

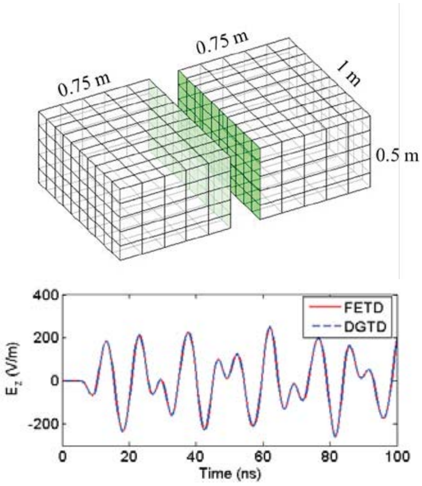

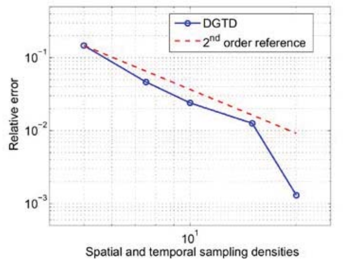

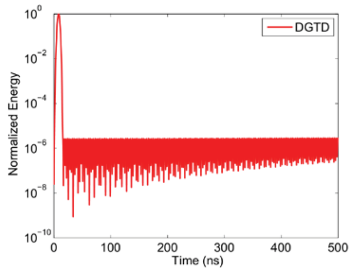

- The wave equation based DGTD method shows approximately the second-order convergence;
- The proposed method is unconditionally stable, and has no obvious numerical dissipation to physical fields.

QHL/DGTD

Numerical Results, Dipole radiation

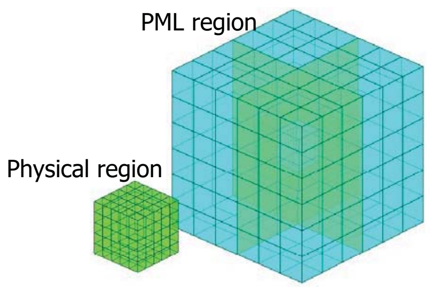

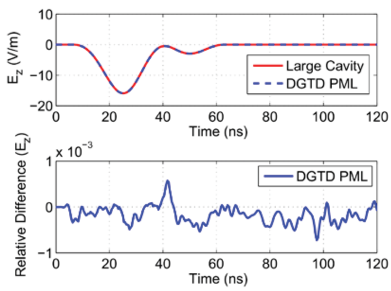

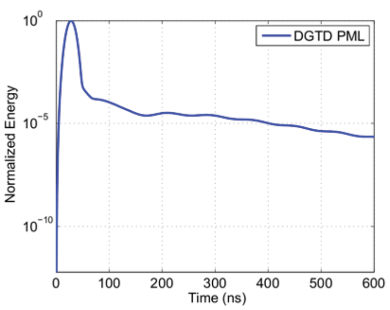

- The novel coupling method of PML with wave equation based DGTD shows good accuracy;
- Energy evolution for a long time window is observed, and no instability occurs, demonstrating that PML works properly in the novel coupling method.

QHL/DGTD

Numerical Results, Patch antenna radiation

DUKE EDMUND T. PRATT, JR. SCHOOL OF ENGINEERING

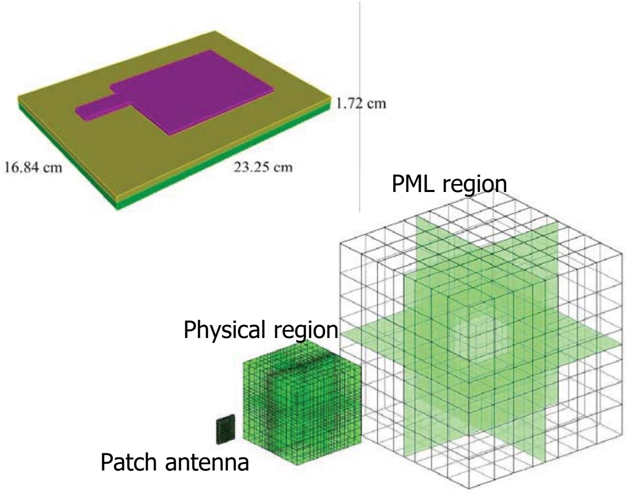

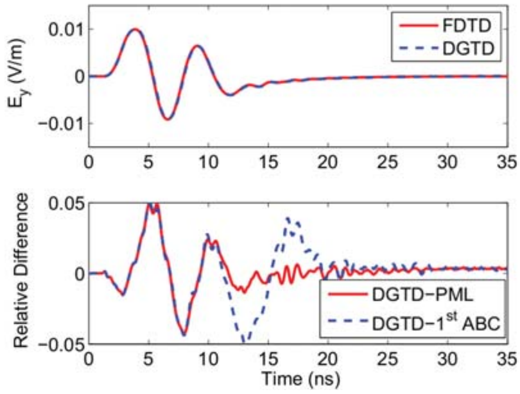

- The novel coupling method of PML with wave equation based DGTD shows good agreement;
- On the same mesh PML shows better accuracy than the first-order absorbing boundary condition.

QHL/DGTD

Numerical Results, Long microstrip line

DUKE EDMUND T. PRATT, JR. SCHOOL OF ENGINEERING

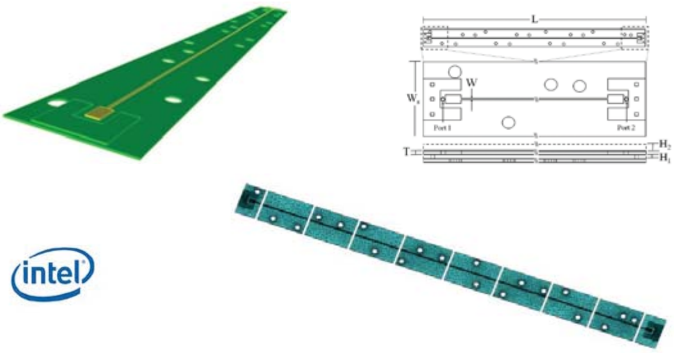

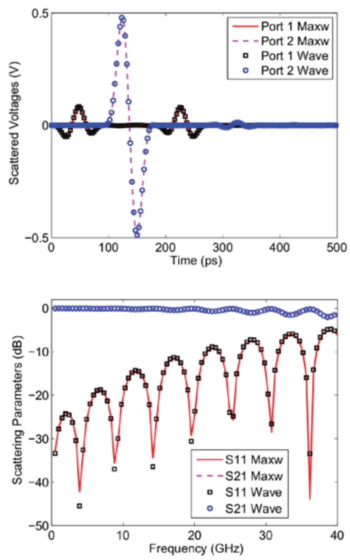

Table 2.3: Computational statistics of the long microstrip line model

Intel(R) Xeon(R) E5645 (2.40 GHz)	DGTD-Maxw (Implicit LDU)	DGTD-Wave (Implicit LDU)
DoFs (million)	1.0	0.43
Total CPU time (h.)	2.4	0.6
Memory (GB)	14.8	7.6

- The DGTD-Wave shows good agreement and lower computational overheads.

QHL/DGTD

Numerical Results, Interconnect package

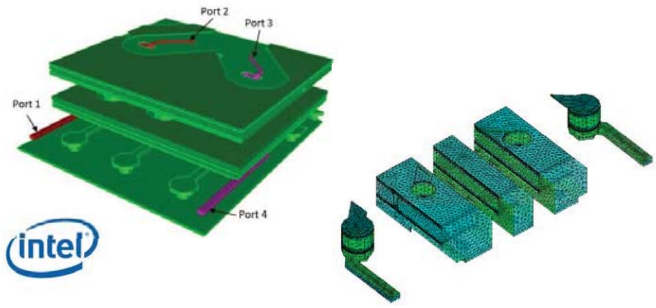

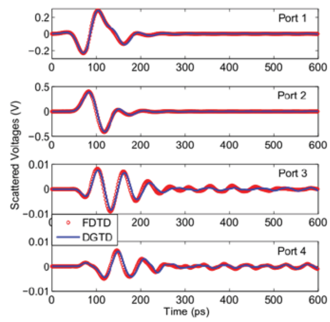

Table 2.4: Computational statistics of the integrated package model

Intel(R) Xeon(R) E5645 (2.40 GHz)	**DGTD-Maxw (Implicit GS)**	**DGTD-Wave (Implicit LDU)**
DoFs (million)	1.9	0.8
CPU time for preprocessing (min.)	4.1	200.5
CPU time per time step (s)	30.1	8.0
Total CPU time (h.)	13.0	6.8
Memory (GB)	18.7	27.2

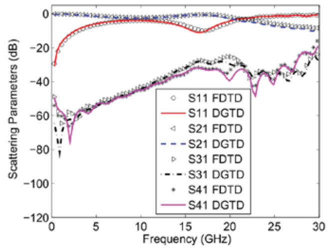

- The DGTD-Wave shows good agreement and smaller CPU time.

QHL/DGTD

Summary

✓ Propose a new DGTD method based on the second-order wave equation

- introduces a modified Riemann solver to evaluate the flux;
- has fewer DoFs for each subdomain with implicit time integration;
- shows better performance than the first-order Maxwell's curl equations based DGTD methods.

✓ Propose a novel coupling scheme of PML for the second-order wave equation based DGTD method

- physical and PML regions employ different governing equations;
- shows better accuracy than the first-order absorbing boundary condition.

3.5 Vector DGTD Method for Coupling SE, FE and FDTD Methods

- Vector (Subdomain) DGTD Method to couple SE, FE and FDTD methods
  - B. Zhu, J. Chen, W. Zhong, and Q. H. Liu, "A Hybrid FETD-FDTD Method with Nonconforming Meshes," Commun. Comput. Phys., vol. 9, no. 3, pp. 828-842, 2011. doi: 10.4208/cicp.230909.140410s.
  - B. Zhu, J. Chen, W. Zhong, and Q. H. Liu, "Analysis of photonic crystals using the hybrid finite element/finite-difference time domain technique based on the discontinuous Galerkin method," Intl. J. Numer. Methods Eng., vol. 92, no. 5, pp. 495-506, 2012.
  - B. Zhu, J. Chen, W. Zhong, and Q. H. Liu, "Hybrid finite-element/finite-difference method with an implicit-explicit time-stepping scheme for Maxwell's equations," Intl. J. Numer. Modelling-Electronic Networks Devices and Fields, vol. 25, no. 5-6, Special Issue, pp. 607-620, DOI: 10.1002/jnm.1853, 2012.
  - Q. Sun, Q. Ren, Q. Zhan, and Q. H. Liu, "3-D Domain Decomposition Based Hybrid Finite-Difference Time-Domain/Finite-Element Time-Domain Method with Nonconformal Meshes", IEEE Trans. Microw. Theory Tech., Vol. 65, no. 10, pp. 3682-3688, Oct. 2017.

Hybrid FDTD-SETD-FETD

Galerkin's Weak Form		Strong Form	Hybrid FDTD-SETD-FETD
FE (Tetrahedron)	SE (Hexahedron)	FD (Yee's grid)	
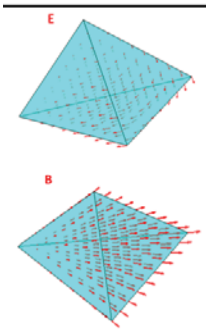	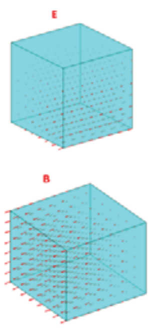	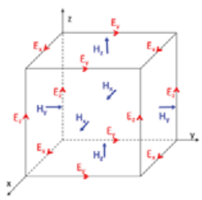	**Key advantages:** • FD: linear complexity • FE: simplex elements • SE: spectral accuracy **Key issues:** • meshing strategy • field coupling schemes • late time instability

QHL/DGTD

DUKE
EDMUND T. PRATT, JR.
SCHOOL OF ENGINEERING

Hybrid FDTD-SETD-FETD with a Buffer Zone

Typical approaches:

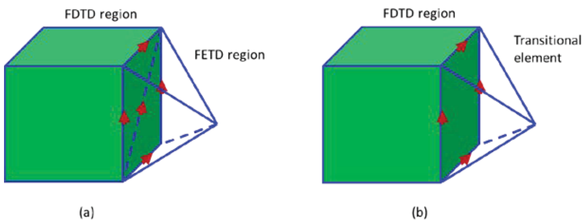

Limitations:

- Quasi-conformal mesh: interpolation approach, Nitsche's method;
- Conformal mesh: pyramid element;
- Meshing is not flexible.

Proposed scheme:

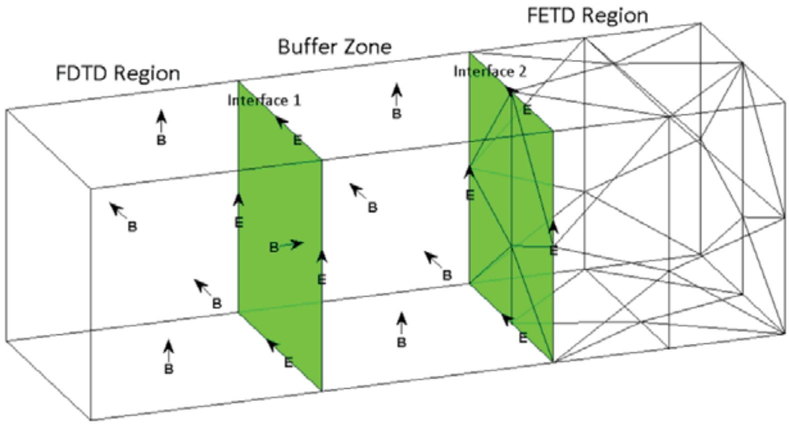

Three regions

- FDTD region: Cartesian grid, as conventional;
- Buffer zone: Cartesian grid, conformal with FDTD region;
- FETD region: tetrahedron element, non-conformal with Buffer zone.

QHL/DGTD

DUKE
EDMUND T. PRATT, JR.
SCHOOL OF ENGINEERING

Elements & Basis Functions

FETD region (Tetrahedron)

SETD/Buffer zone (Hexahedron, Brick)

FDTD region (Brick)

Curl-Conforming

Div-Conforming

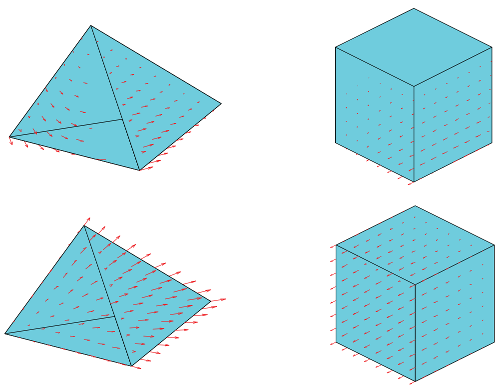

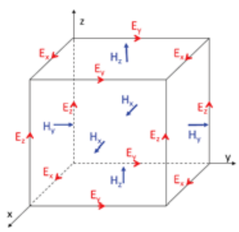

Staggered Yee's grid

- FETD region: tetrahedron element, high order basis;
- SETD region: hexahedron element, high order basis;
- Buffer zone: brick element, 1st order basis;
- FDTD region: brick element, staggered Yee's grid.

QHL/DGTD

Global Explicit Leapfrog Time Integration

DUKE EDMUND T. PRATT, JR. SCHOOL OF ENGINEERING

FDTD region

(1) $\mathbf{E}^{n-1/2}$ to $\mathbf{E}^{n+1/2}$

E^{n+1/2} at Interface 1 ← **B^n** in both FDTD and buffer;

(2) $\mathbf{B}^{n}$ to $\mathbf{B}^{n+1}$

B^{n+1} at Interface 1 ← **E^{n+1/2}** at Interface 1;

SETD/ FETD and buffer regions

(3) $\mathbf{E}^{n-1/2}$ to $\mathbf{E}^{n+1/2}$

$$\mathbf{M}_{ee}^{(i)}\frac{\mathbf{e}_{n+\frac{1}{2}}^{(i)}-\mathbf{e}_{n-\frac{1}{2}}^{(i)}}{\Delta t}=\sum_{j=1}^{N}(\mathbf{L}_{ee}^{(i,j)}\mathbf{e}_{n-\frac{1}{2}}^{(j)}+\mathbf{L}_{eb}^{(i,j)}\mathbf{b}_{n}^{(j)})+\mathbf{j}_{n}^{(i)}$$

(4) $\mathbf{B}^{n}$ to $\mathbf{B}^{n+1}$

$$\mathbf{M}_{bb}^{(i)}\frac{\mathbf{b}_{n+1}^{(i)}-\mathbf{b}_{n}^{(i)}}{\Delta t}=\sum_{j=1}^{N}(\mathbf{L}_{be}^{(i,j)}\mathbf{e}_{n+\frac{1}{2}}^{(j)}+\mathbf{L}_{bb}^{(i,j)}\mathbf{b}_{n}^{(j)})+\mathbf{m}_{n+\frac{1}{2}}^{(i)}$$

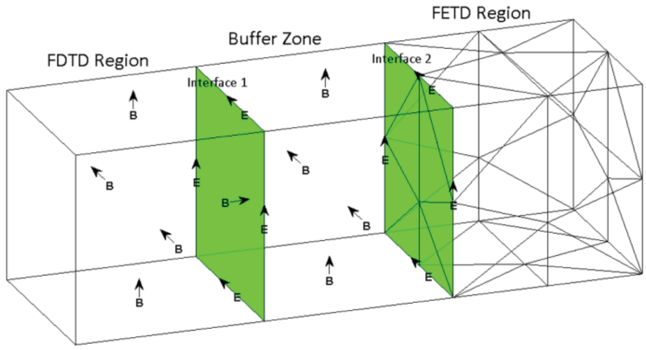

QHL/DGTD

Implicit-Explicit CN-LF Time Integration

DUKE EDMUND T. PRATT, JR. SCHOOL OF ENGINEERING

FDTD region (LF)

(1) $\mathbf{E}^{n-1/2}$ to $\mathbf{E}^{n+1/2}$

E^{n+1/2} at Interface 1 ← **B^n** in both FDTD and buffer;

(2) $\mathbf{B}^{n}$ to $\mathbf{B}^{n+1}$

B^{n+1} at Interface 1 ← **E^{n+1/2}** at Interface 1;

SETD/FETD and buffer regions

(3) Sub-step 1: pseudo-forward Euler (buffer zone)

$$\mathbf{M}_{ee}^{(i)}\frac{\mathbf{e}_{n+\frac{1}{2}}^{(i)}-\mathbf{e}_{n}^{(i)}}{\Delta t/2}=\sum_{j=1}^{N}(\mathbf{L}_{eb}^{(i,j)}\mathbf{b}_{n}^{(j)}+\mathbf{L}_{ee}^{(i,j)}\mathbf{e}_{n}^{(j)})+\mathbf{j}_{n+\frac{1}{4}}^{(i)};$$

$$\mathbf{M}_{bb}^{(i)}\frac{\mathbf{b}_{n+\frac{1}{2}}^{(i)}-\mathbf{b}_{n}^{(i)}}{\Delta t/2}=\sum_{j_{ex}}(\mathbf{L}_{bb}^{(i,j)}\mathbf{b}_{n}^{(j)}+\mathbf{L}_{be}^{(i,j)}\mathbf{e}_{n+\frac{1}{2}}^{(j)})+\sum_{j_{im}}(\mathbf{L}_{bb}^{(i,j)}\mathbf{b}_{n}^{(j)}+\mathbf{L}_{be}^{(i,j)}\mathbf{e}_{n}^{(j)})+\mathbf{m}_{n+\frac{1}{4}}^{(i)}$$

(4) Sub-step 2: Crank-Nicolson (SETD/FETD region)

$$\mathbf{M}^{(i)}\frac{\mathbf{u}_{n+1}^{(i)}-\mathbf{u}_{n}^{(i)}}{\Delta t}=\sum_{j_{ex}}\mathbf{L}^{(i,j)}\mathbf{u}_{n+\frac{1}{2}}^{(j)}+\sum_{j_{im}}\mathbf{L}^{(i,j)}\frac{\mathbf{u}_{n+1}^{(j)}+\mathbf{u}_{n}^{(j)}}{2}+\mathbf{q}_{n+\frac{1}{2}}$$

(5) Sub-step 3: reversed pseudo-forward Euler (buffer zone)

$$\mathbf{M}_{bb}^{(i)}\frac{\mathbf{b}_{n+1}^{(i)}-\mathbf{b}_{n+\frac{1}{2}}^{(i)}}{\Delta t/2}=\sum_{j_{ex}}(\mathbf{L}_{be}^{(i,j)}\mathbf{e}_{n+\frac{1}{2}}^{(j)}+\mathbf{L}_{bb}^{(i,j)}\mathbf{b}_{n+\frac{1}{2}}^{(j)})+\sum_{j_{im}}(\mathbf{L}_{be}^{(i,j)}\mathbf{e}_{n+1}^{(j)}+\mathbf{L}_{bb}^{(i,j)}\mathbf{b}_{n+1}^{(j)})+\mathbf{m}_{n+\frac{3}{4}}^{(i)}$$

$$\mathbf{M}_{ee}^{(i)}\frac{\mathbf{e}_{n+1}^{(i)}-\mathbf{e}_{n+\frac{1}{2}}^{(i)}}{\Delta t/2}=\sum_{j_{ex}}(\mathbf{L}_{ee}^{(i,j)}\mathbf{e}_{n+\frac{1}{2}}^{(j)}+\mathbf{L}_{eb}^{(i,j)}\mathbf{b}_{n+1}^{(j)})+\sum_{j_{im}}(\mathbf{L}_{ee}^{(i,j)}\mathbf{e}_{n+1}^{(j)}+\mathbf{L}_{eb}^{(i,j)}\mathbf{b}_{n+1}^{(j)})+\mathbf{j}_{n+\frac{3}{4}}^{(i)}$$

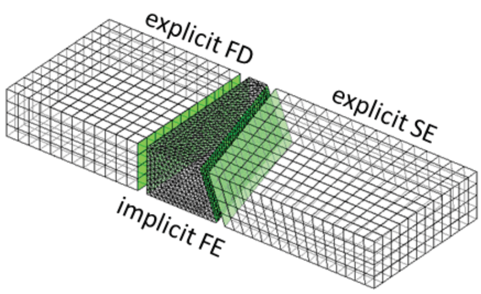

QHL/DGTD

Numerical Results, Resonant cavity

f_{ch} = 2.98 GHz (BHW pulse)

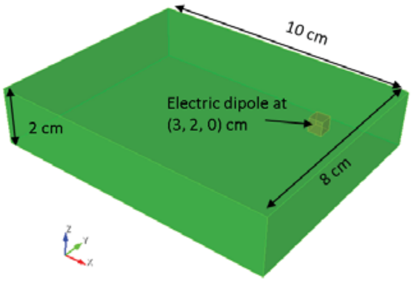

Model configuration
(the cavity centers at the origin)

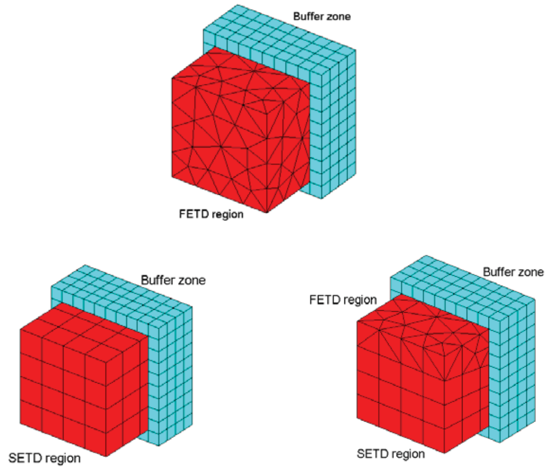

Non-conformal mesh

QHL/DGTD

Numerical Results, Resonant cavity

- Field comparison

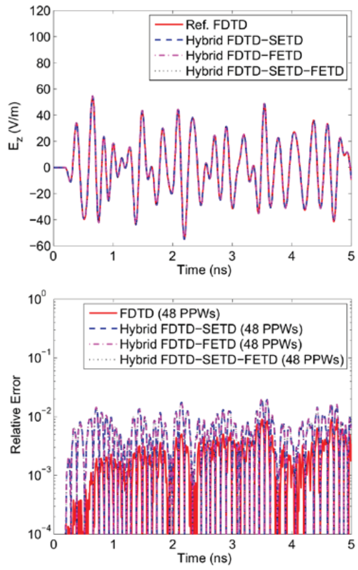

- Eigenspectrum comparison

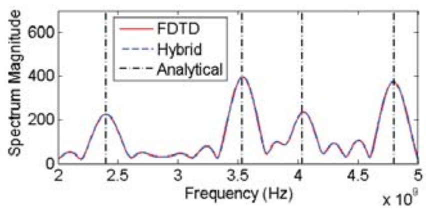

- Long time behavior

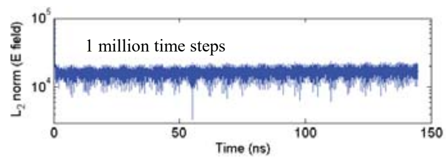

- The hybrid method shows good agreement with the references;
- The hybrid method shows long time stability.

QHL/DGTD

Numerical Results, PEC horn shell

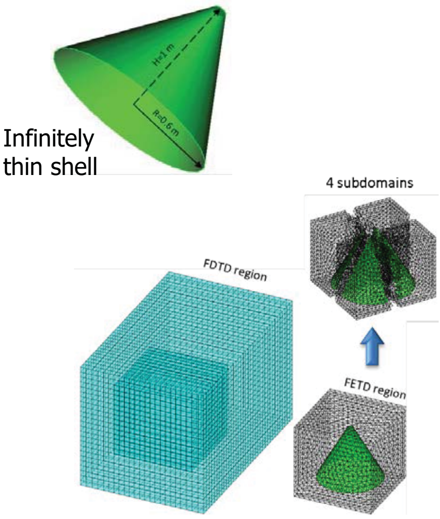

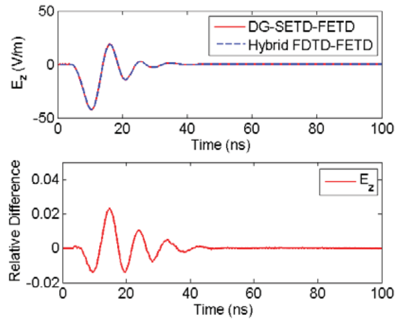

Table 3.1: Computational statistics for the PEC horn shell

Intel i5-2320 (3.0 GHz)	Hybrid SETD-FETD	Hybrid FDTD-FETD
DoFs	6.4×10^5	1.3×10^6
Δt (ps)	19.2	19.2
Total CPU time (h.)	5.6	0.35
Memory (GB)	3.8	0.61

- The hybrid FDTD-FETD shows good agreement with the reference;
- The hybrid FDTD-FETD consumes lower computational overheads than the reference.

QHL/DGTD

Numerical Results, Pseudo-elliptic waveguide filter

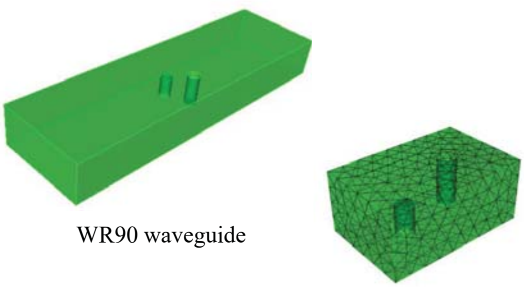

WR90 waveguide

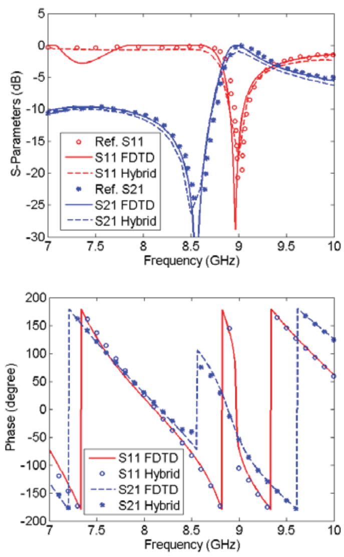

Table 3.2: Computational statistics for the waveguide filter

Intel i5-2320 (3.0 GHz)	FDTD	Hybrid FDTD-FETD
DoFs	1.0×10^7	1.6×10^5
Δt (ps)	0.26	0.38
Total CPU time (h.)	3.8	0.50
Memory (GB)	1.2	0.98

- The hybrid method shows good agreement with the reference;
- The hybrid method consumes lower computational overheads than FDTD.

QHL/DGTD

Numerical Results, CSEM example

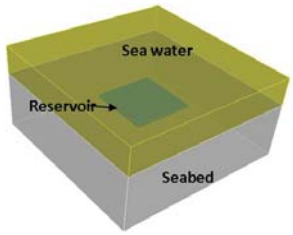

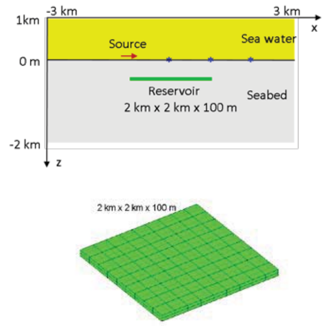

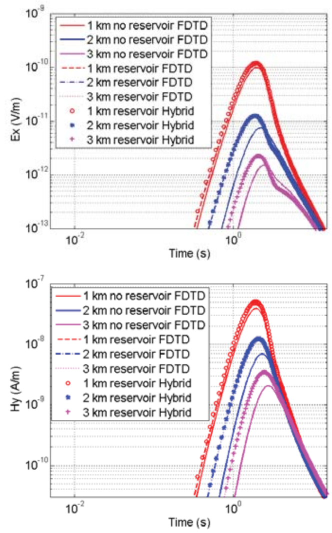

Table 3.3: Computational statistics for the CSEM example

Intel i5-2320 (3.0 GHz)	**FDTD**	**Hybrid FDTD-SETD**
Δt (ms)	0.19	1.59
Total CPU time (h.)	10.25	1.46
Memory (GB)	0.85	1.05

- The hybrid method shows good agreement with the reference;
- The hybrid method consumes smaller CPU time than FDTD with implicit-explicit time integration.

QHL/DGTD

Summary of the Hybrid FDTD-SETD-FETD

✓ Propose a hybrid FDTD-SETD-FETD method with buffer
- allows non-conformal mesh;
- introduces a buffer zone between SETD/FETD and FDTD;
- shows good accuracy and long time stability.

✓ Propose efficient time integration schemes
- introduces an explicit global leapfrog time integration;
- for practical application, introduce an implicit-explicit time integration scheme;
- shows better performance than FDTD.

✓ Propose an advanced hybrid FDTD-SETD-FETD method without buffer
- allows non-conformal mesh;
- shows similar accuracy but better performance w.r.t. the one with buffer.

QHL/DGTD

Summary

In this work we have reviewed the concepts, the formulations, and the implementation of discontinuous Galerkin time domain method for multiscale electromagnetic simulations. Several different DGTD schemes are discussed in a general DG framework.

- Spurious solutions
  - Non-physical modes with high values of wavenumber
  - Transient solutions with rapid spatial variations
- *p*-forms/FEM
  - Field intensities (E and H) are associated to 1-forms and curl-conforming basis func
  - Flux densities (D and B) are associated to 2-forms and div-conforming basis functi
  - Hodge Operator transform *p*-form in (*p+1*)-form, and vice versa.
- Dispersion analysis
  - Semidiscrete and modal dispersion analysis
  - Dispersive Hodge operator
  - Fields belonging to different p-form (e.g., E and B) uses basis functions with same order of interp
  - Different order of interpolation must be used if two fields belong to the same p-form (e.g., E and I
- Elements and Basis functions
  - New Spectral-Prism Element: DDM + Non-conforming triangular meshes +high-order in he
  - Tetrahedral elements: curl- and div-conforming basis functions
- DG-TD
  - DGTD works accurately and efficiently for highly multiscale EM systems.
  - CN-BT-DGTD and LDU-DGTD
  - EB-DGTD shows improvements in all numerical features: eigenvalues, eigenvectors, disper
  - EB-DGTD is a promising method to solve large, multiscale, and complex EM problems.